AD-A116 307 CASE WESTERN RESERVE UNIV CLEVELAND OH DEPT OF METAL--ETC F/G 11/6
INDIVIDUAL AND COMBINED EFFECTS OF SULFUR AND PHOSPHORUS ON THE--ETC(U)
MAY 82 E CHANG, J F WALLACE DAAG46-79-C-0094

UNCLASSIFIED AMMRC-TR-82-33 NL

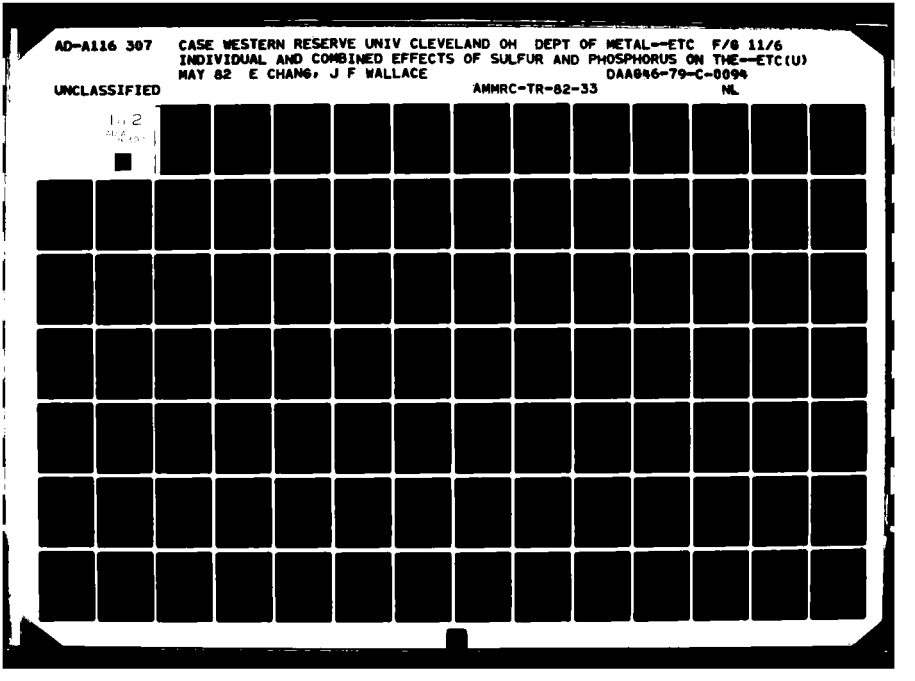

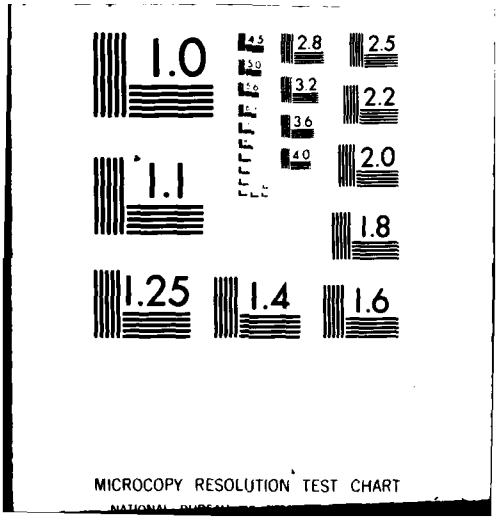
1.0
1.1
1.25
1.4
1.6
1.8
2.0
2.2
2.5
2.8
3.2
3.6
4.0
MICROCOPY RESOLUTION TEST CHART

AD

AMMRC TR 82-33

INDIVIDUAL AND COMBINED EFFECTS OF SULFUR AND PHOSPHORUS ON THE TOUGHNESS OF HIGH STRENGTH STEELS

May 1982

EDWARD CHANG and JOHN F. WALLACE
Case Western Reserve University
Dept. of Metallurgy and Materials Science
10900 Euclid Avenue
Cleveland, Ohio 44106

FINAL REPORT Contract No. DAAG46-79-C-0094

Prepared for

ARMY MATERIALS AND MECHANICS RESEARCH CENTER
Watertown, Massachusetts 02172

UNCLASSIFIED

SECURITY CLASSIFICATION OF THIS PAGE (When Data Entered)

REPORT DOCUMENTATION PAGE		READ INSTRUCTIONS BEFORE COMPLETING FORM
1. REPORT NUMBER AMMRC TR 82-33	2. GOVT ACCESSION NO. AD-A116307	3. RECIPIENT'S CATALOG NUMBER
4. TITLE (and Subtitle) INDIVIDUAL AND COMBINED EFFECTS OF SULFUR AND PHOSPHORUS ON THE TOUGHNESS OF HIGH STRENGTH STEELS		5. TYPE OF REPORT & PERIOD COVERED Final Report - November 1979-November 1981 6. PERFORMING ORG. REPORT NUMBER
7. AUTHOR(s) Edward Chang and John F. Wallace		8. CONTRACT OR GRANT NUMBER(s) DAAG46-79-C-0094
9. PERFORMING ORGANIZATION NAME AND ADDRESS Case Western Reserve University Dept. of Metallurgy and Materials Science 10900 Euclid Avenue Cleveland, Ohio 44106		10. PROGRAM ELEMENT, PROJECT, TASK AREA & WORK UNIT NUMBERS D/A Project: 1L162105AH84 AMCMS Code: 612105.H840011
11. CONTROLLING OFFICE NAME AND ADDRESS Army Materials and Mechanics Research Center ATTN: DRXMR-K Watertown, Massachusetts 02172		12. REPORT DATE May 1982 13. NUMBER OF PAGES 173
14. MONITORING AGENCY NAME & ADDRESS(if different from Controlling Office)		15. SECURITY CLASS. (of this report) Unclassified 15a. DECLASSIFICATION/DOWNGRADING SCHEDULE

16. DISTRIBUTION STATEMENT (of this Report)

Approved for public release; distribution unlimited.

17. DISTRIBUTION STATEMENT (of the abstract entered in Block 20, if different from Report)

18. SUPPLEMENTARY NOTES

19. KEY WORDS (Continue on reverse side if necessary and identify by block number)

Low alloy steels	Impurities	Toughness
Phosphorus	4340 steel	Embrittlement
Sulfur	Mechanical properties	Test temperatures

20. ABSTRACT (Continue on reverse side if necessary and identify by block number)

(SEE REVERSE SIDE)

DD FORM 1 JAN 73 1473 EDITION OF 1 NOV 65 IS OBSOLETE

UNCLASSIFIED

SECURITY CLASSIFICATION OF THIS PAGE (When Data Entered)

Block No. 20

ABSTRACT

This investigation was undertaken to determine the feasibility of specifying a maximum sum of phosphorus plus sulfur contents rather than a maximum for each element as related to the effects that these elements exert on the toughness of steel. First, a computer analysis of the literature was conducted on the data on the influence of phosphorus and sulfur in the toughness of steel. Then, an experimental program was undertaken to produce a series of 4340 cast steels with a matrix of phosphorus and sulfur contents including low, medium and high values of each. These steels were heat treated by oil quenching to martensite and tempering at 1100°F to a 150 ksi yield strength and at 400°F to a 220 ksi yield strength. The steels were then tested to determine the tensile properties, Charpy V-notch transition curves for regular and precracked specimens and the static fracture toughness properties.

The behavior of phosphorus and sulfur on the toughness of these steels is sufficiently different that it does not appear feasible to substitute the sum of the elements for maxima for each in specifications for steels requiring specific toughness properties. Phosphorus raises the transition temperature and embrittles the steel significantly, particularly at high strengths and in the presence of sharp notches. Phosphorus is in supersaturated solid solution in the steel and embrittles the steel because of the higher friction stress of the lattice for dislocation motion. Sulfur increases the number of sulfide inclusions and lowers the toughness by the decohesion of sulfide inclusions during the early stages of plastic deformation of the matrix. The low energy required for decohesion reduces the total energy required for crack propagation. Although both elements lower the toughness measurements, their effect on the toughness is sufficiently different so that similar toughness can only be expected under a few conditions.

The different influence of each element on the toughness results in an equal amount of both elements producing transition curves that cross over one another when plotted. The high phosphorus steels have higher fracture energy at higher temperatures and lower fracture energies at lower temperatures because increasing phosphorus raises the transition temperature. Increasing sulfur lowers the ductile shelf energy but has little influence on the transition temperatures for the medium strength steel and above room temperature for the high strength steel. The phosphorus plus sulfur contents only provide a predictable influence in the toughness valves under conditions at which these cross over temperatures occur. This temperature varies with notch acuity and composition.

Phosphorus increases the yield strength, the temperature dependence of the yield strength and the notch sensitivity of the steel. The fatigue crack growth rate is decreased to a small extent by higher phosphorus and sulfur contents for the medium strength steel. However, for the high strength steel, phosphorus greatly increases the fatigue crack growth rate but sulfur has no effect on this rate.

The computer analysis of data in the literature on the influence of phosphorus and sulfur on the toughness showed the individual the collective effects of these elements clearly. These results were confirmed by the experimental work.

TABLE OF CONTENTS

TABLE OF CONTENTS

... Continued ...

INTRODUCTION

A. Effect of Phosphorus and Sulfur on Mechanical Properties of Steels

The deleterious effect of phosphorus and sulfur on the mechanical properties of steel was recognized in the early days of steelmaking. In 1909, ASTM specified 0.04% max. P and 0.05% max. S for structural steel. (1) As early as 1919, there was so much concern about the behavior of phosphorus and sulfur in the steel that a special team called the "Joint Committee on Investigation of the Effect of Phosphorus and Sulfur in Steel" was formed by the joint action of 11 organizations. (2) The program of this committee was to investigate the individual effect of phosphorus and sulfur on plain carbon wrought and cast steels. The concept of the combined effect of both elements was not evaluated.

The effect of phosphorus on low carbon steel was thoroughly studied by Hopkins and Tipler. (3) Enzian (4) also made a similar study, but he investigated the simultaneous variations in phosphorus and nitrogen on the properties of low carbon steel. Phosphorus increases the tensile strength, (3,4) yield strength (3,4) impact transition temperature (3) and decreases the impact energy (4) of this material.

Sulfur, on the other hand, apparently does not increase the tensile or the yield strength of low to medium plain carbon steel. (5) Lowering the sulfur content from 0.06% to 0.02% results in some improvement in the ductility and toughness of low strength steel. (5)

The mechanisms of embrittlement of phosphorus and sulfur in steels is of considerable significance in determining their relative effects in steels. Phosphorus dissolves substitutionally in iron, and its solubility in α-Fe has been determined: 1000°C, 2.14%; 800°C, 1.01%; 600°C, 0.56%; and 400°C, 0.28%. (6) By extrapolating to lower temperatures, it is noted, as shown in Figure 1, that the solubility of P in α-Fe is about 0.015% at room temperature. (6,7) However, in the metastable state, Hopkins and Tipler found no evidence of second phase precipitation for Fe-0.31% P alloy, (3) apparently because of the very slow kinetics of phosphorus in α-iron at lower temperatures. In the presence of carbon and silicon, a phosphorus content of more than 0.12% in gray iron results in phosphide particles called steadite. (8) According to the Fe-S equilibrium phase diagram, sulfur is not soluble in α-iron. It is generally agreed that phosphorus strengthens the iron matrix by a solid solution strengthening mechanism. (9) Phosphorus embrittles the steel by either increasing the yield strength of the material (3) or preferentially segregating to the grain boundaries (10) and causing intergranular failures. (3,11,12) Sulfur forms nonmetallic inclusions with manganese (assuming the presence of sufficient manganese) in the liquid and solid. (13,14)

At low carbon and low strength levels, phosphorus significantly strengthens the iron matrix by solid solution hardening. The yield strength is proportionally increased and ductility and toughness decreased with an increase of phosphorus content (3,4) because of an increased friction stress

in shear (τ_i) and corresponding decreased plastic zone size (R) as shown subsequently in this paper. On the other hand, sulfur does not change the strength of low strength steel since the sulfide interparticle spacing is considered too large to operate as an Orowan strengthening mechanism. (15) The reduction in ductility and toughness results from the notch effect in the presence of sulfide particles. The notch effect promotes a stress concentration and microcrack nucleation ahead of the main propagating crack. (16) The result is a higher microcrack advancing velocity, smaller plastic zone size and decreased toughness with an increase of sulfur content.

At higher strength levels, the effect of phosphorus on the strength of steel is not well-documented. It is unclear whether embrittlement by matrix strengthening, which occurs in the case of low carbon steel, or embrittlement by enhanced phosphorus segregation or co-segregation with metallic elements to the grain boundaries, plays the major role in lowering the toughness of the steel.

As the strength of the steel increases, however, the sulfur is also observed to be deleterious in 0.26% C, 1.5% Mn steel. An increase of sulfur from 0.005% to 0.053% increases the yield point from 73.7 to 77.1 ksi and decreases RA and CVN at room temperature from 71.7% to 37.5% and 109 ft-lb to 10 ft-lb respectively. (17) In this example, the yield point increases 4.4% only, while the RA and CVN decrease 47.7% and 90.8%, respectively. In another 1% Ni, Cr, Mo cast steel, low and high sulfur steel exhibit virtually no difference in tensile properties. (18)

These results indicate that sulfur does not strengthen the iron crystal, and sulfide inclusions contribute very little in strengthening the steel by acting as a second phase. The deleterious effect of sulfur results from the notch effect or stress concentration effect produced by the sulfide inclusions. Sulfur may also segregate to the grain boundaries and thus embrittle the steel.

Typical reports of the effects of phosphorus and sulfur on the Charpy V-notch impact transition curve for alloyed steels are shown in Figures 2 (19) and 3 (18). Phosphorus and sulfur affect both the impact energy and impact transition temperature. Figure 2 indicates that the primary effect of small increases in phosphorus is to shift the transition curve to the right.

The effects of sulfur on the notch toughness of low alloy high strength 0.3 C, 2.5 Ni, 0.8 Cr, 0.45 Mo wrought steel were studied by Hodge et al. (20) No such systematic study of the sole effect of phosphorus on the notch toughness of low alloy wrought steels was found. This work indicates that:

1) The decrease in maximum (upper ductile shelf) Charpy V-notch impact energy value with sulfur content is more marked at lower sulfur than at higher levels as shown in Figure 4A. The Charpy V-notch impact energy increases sharply for sulfur contents below 0.04%. This is the basis for specifying a maximum sulfur content of 0.04% in low alloy steels.

2) Neither the fracture transition temperature, as indicated by the temperature at the midpoint of the steeply sloping portion of the curves

shown in Figure 4B, nor the ductility transition temperature, such as the temperature for an energy value of 15 ft-lb, is greatly affected by the sulfur content. This is an important point and will be discussed later.

The relative influence of phosphorus and sulfur in cast low alloy steel is also of interest. Zotos (21) studied the significance of reduced phosphorus and sulfur content on cast AISI 4325 low alloy steels. However, in reality, the phosphorus contents were kept virtually constant. The results of the relative % RA, Charpy V-notch impact energy at -20°F and % elongation correlate very well with the sulfur contents. For each 0.010% change in sulfur contents, % RA, Charpy V-notch energy and elongation change 9.75%, 7.82 ft-lb and 2.15%, respectively. The impact transition curve was not reported in the publication.

The effects of high phosphorus and high sulfur contents on the ductility transition behavior of cast AISI 8630 steel were reported by Breznyak and Wallace. (22) The influence of carbon, phosphorus and sulfur on the NDTT of normalized and tempered Cr-Mo steels was investigated by Dutcher et al. (23) Sigala (24) studied the effects of different chemical composition and heat treatment on the toughness of cast railroad component steel. The influence of chemical composition, including phosphorus and sulfur as variables on the toughness of high strength, low alloy cast steel is reported by Larson and Herlihy. (25) A similar experiment on medium carbon cast steels processed under controlled atmospheres has been presented by Wright and Quarrell. (17)

Birkle et al (26) have analyzed the fracture toughness of wrought 0.45 C, Ni, Cr, Mo steels with different sulfur contents. Kula and Anctil (27) suggest a correlation between fracture toughness and phosphorus plus sulfur for wrought SAE 4340 steel, as shown in Figure 5. Recently, Groves and Wallace (28) also found a similar correlation for cast AISI 4335 steel as shown in Figure 6.

So far, much has been presented about the effect of phosphorus and sulfur on the toughness of steel. However, as will be discussed in detail later, few of these investigations contain the proper type or amount of data to permit a statistical analysis of the relative influence of phosphorus and sulfur on the toughness of steel. Mickelson (29) studied the simultaneous variation of phosphorus and sulfur in various composition range on the toughness of AAR Grade B cast steel. A correlation between transition temperature and phosphorus + sulfur was proposed based on this work. (29)

B. The Toughness of Materials

Toughness is the capacity of a material to absorb energy by elastic or elastic-plastic deformation before fracture. The value of toughness depends on the composition, structure and processing of steel. The toughness also depends on the extrinsic variables or states to which it is subjected. Geometry (notch, size of specimen) and strain rate, among the extrinsic variables, are considered significant in the toughness of a material.

B.1. Effect of a Notch

The presence of a notch in a material raises the tensile stress in the region below the notch by the following ways: (16)

1) The notch raises the effective strain rate ($\dot{\varepsilon}_{eff}$) below the notch. For strain rate sensitive material, the yield stress increases with increasing strain rate and the yield stress of an unnotched specimen (σ_Y) will be increased to σ_Y^* below the notch.

2) The notch enhances strain hardening rate ($d\sigma/d\varepsilon_{eff}$) by concentrating plastic strain in the "tensile specimen" below the notch. This increases σ_Y^*.

3) The notch introduces a triaxial stress state below the notch. During local yielding at the notch of a nonstrain-hardening material, the tensile stress distribution (σ_{yy}) ahead of the notch is modified and increased to $\sigma_{yy} = \sigma_Y + \sigma_{xx} = K_{\sigma(p)}\sigma_Y$, where σ_{xx} is the tensile stress in crack advancing direction and $K_{\sigma(p)}$ is the plastic stress concentration factor.

B.2. Effect of Strain Rate

As a crack advances in a material, the dislocations move and join the moving crack and the crack-tip is relaxed plastically. This relaxation process depends on the number of mobile sources, multiplication process (Frank-Reed or cross slip) and the velocity of the gliding dislocations. As the strain rate increases, the velocity of the dislocations to join the crack becomes relatively slower, and the plastic zone size or the toughness of material is reduced accordingly.

For Frank-Reed source multiplication, assume that dislocation velocity (V) is related to local shear stress (τ_L), friction stress in shear (τ_i) and temperature (T) as:

$$V = V_o \exp - \left(\frac{A}{\left(\frac{\tau_L}{\tau_i}\right)^2 T} \right) \qquad (1)$$

where A is a constant and V_o is the velocity of dislocation as τ_L and T approach infinity. Following similar procedure as Tetelman and McEvily, (16) it can be shown that plastic zone size (R) can be expressed as:

$$R \sim \frac{G^2 b T}{9A\tau_i^2} \ell n \left(\frac{V_c}{V_o \cos\beta}\right), \text{ where } \frac{V_c}{V_o \cos\beta} \lesssim 1 \qquad (2)$$

where G is the modulus of elasticity in shear, b is Burgers vector, V_c is the advancing velocity of the microcrack and β is a constant.

From Eq. (2) it is noted that the toughness of a material increases with increasing temperature and with decreasing friction stress and strain rate. In addition, the effect of strain rate on the toughness of a material follows a logarithmic relation.

Increasing the loading rate also increases the friction stress or yield stress for BCC metals.

The effect of notch severity and strain rate on the plastic zone size (and hence toughness) and ductile-brittle transition behavior for low strength material is shown in Figure 7. Higher strain rate as shown in Figure 7A increases the yield strength from σ_Y to σ_Y^*. The tensile stress distribution ahead of the notch reaches a maximum $\sigma_{yy}^{max} = K_{\sigma(p)}^{max}\sigma_Y^*$ at elastic-plastic interface. Smaller notch radius or severer notch increases the stress level and therefore reduces the plastic zone size from R to R'. In Figure 7B, the brittleness transition temperature (T_D) of an unnotched specimen, the temperature at which the maximum tensile stress beneath the notch root reaches the cleavage fracture strength (σ_f^*) and induces fracture upon yielding, is raised to $T_{D(N)}$ for a notched specimen.

B.3. Load-Temperature Diagram Analysis

Figure 8 shows the typical variation of general yield load (P_{GY}), local yield load (P_{LY}), and fracture load (P_F) with temperature, for a low strength BCC Charpy specimen loaded in bending. (16,30) In region I, cleavage fracture occurs immediately upon local yielding when the first slip band forms near the notch root. In region II, fracture is caused by plastic constraint induced cleavage fracture as imposed by triaxial stress state. Cleavage fracture occurs at the elastic-plastic interface, where the maximum tensile stress σ_{yy}^{max} reaches the cleavage fracture strength (σ_f^*). In region III, fracture results from plastic constraint and strain hardening induced cleavage fracture. In region IV, above the initiation transition temperature ($T_{S(N)}$), fracture is initiated by fibrous tearing.

B.4. Development of Fracture Toughness Concept

Engineering materials have been known to fracture at a stress well below the theoretical strength by 10 to 100 times. To explain this discrepancy, Griffith, in 1921, postulated that flaws such as cracks, which are inherently present in structures, result in a stress concentration that initiates fracture at low stress levels. (31) Consider an infinite plate with a crack held between fixed grips, the crack propagates when the elastic energy release rate is faster than the rate of created surface energy of the system. Griffith then used a stress analysis that was developed by Inglis (32) to show that fracture stress (σ_F) is related to Young's Modulus (E), surface energy (γ_e), and crack length (2a) by the equation:

$$\sigma_F = \sqrt{\frac{E(2\gamma_e)}{\pi a}} \qquad (3)$$

Irwin (33) and later Orowan (34) suggested that the Griffith fracture criterion for ideally elastic solid could be modified and applied to brittle materials and metals by taking into account the plastic work (γ_p) in addition to elastic surface energy that is required for crack extension. Modern fracture mechanics was initiated by Irwin (35) who adopted the stress analysis by Westergaard (36) defined a term $K = \sigma\sqrt{\alpha\pi a}$ called stress intensity factor, where α is a parameter depending on specimen and crack geometry. This stress intensity factor is more appropriate in describing a local stress field near a notch. The Irwin's analysis of fracture assumes that crack extension occurs when stress intensity factor reaches a critical value called fracture toughness (K_c), while the energy release rate defined as $G = K^2/E$ (in plane stress) is equal to G_c, the critical strain-energy release rate. Thus,

$$\frac{K_c^2}{E} = G_c \tag{4}$$

And

$$\sigma_F = \sqrt{\frac{EG_c}{\alpha\pi a}} = \frac{K_c}{\sqrt{\alpha\pi a}} \tag{5}$$

With the development of a testing method for fracture toughness, it was recognized that the quantity of fracture toughness under condition of plane strain (K_{Ic}), as illustrated in Figure 9A, was a material constant independent of specimen size (37) and therefore a more valuable parameter of materials. To ensure that a plane strain condition is obtained, it has been determined that the crack length of specimen (a) and thickness (B) should be greater than the quantity $2.5(K_{Ic}/\sigma_Y)^2$. The details of the plane strain fracture toughness test method are specified in ASTM E399-78a.

Wells proposed that the crack-tip of a notched structure undergoes a displacement called crack-opening displacement (COD) when this structure is subjected to a tensile load. (38) It has been experimentally determined by Robinson and Tetelman (39) that COD is related to strain energy release rate (G) and yield strength (σ_Y) through the relationship for many materials:

$$G = \lambda\sigma_Y COD, \quad \lambda \simeq 1 \tag{6}$$

$$COD = \frac{K^2(1-\nu^2)}{E\sigma_Y} \text{ (in plane strain)} \tag{7}$$

where ν is Poisson's ratio.

Prior to the development of the plane strain fracture toughness (K_{Ic}) concept, other test methods such as Charpy impact test or dynamic tear test have been widely used for notch-toughness measurement. However, few or none of these test results can be used directly in fail-safe design

against fracture. Successful use of the data depends on extensive field experiences. The plane strain fracture toughness approach provides a quantitative relationship between maximum allowable stress for a given crack size or vice versa. This information can be directly applied to structural design.

B.5. Dynamic Fracture Toughness

It has been noted in Section B.2. that a high strain rate can reduce the toughness of a material. For some uses it may be more desirable to measure the "dynamic" plane strain fracture toughness (K_{Id}) at a much higher strain rate than those specified in "static" plane strain fracture toughness tests. Unfortunately the requirements of both test procedures are stringent and costly, especially for lower strength materials, (40,41) and therefore usually excluded for quality control or surveillance purposes.

In an attempt to circumvent this problem, an instrumented Charpy test has become available. (42) This test permits both the load time (or deflection) and consequently energy time information of the unprecracked or precracked Charpy specimen to be measured during the normal impact event. The instrumented fatigue-precracked Charpy test resembles the dynamic plane strain fracture toughness test in many ways except that specimen size is frequently too small for lower strength materials. An experiment comparing K_{Ic}, K_{Id}, and K_{Id} obtained from instrumented precracked Charpy impact test for ASTM A533B steel (σ_Y = 70 ksi) is illustrated in Figure 9B. (43)

B.6. Fracture Toughness of Elastic-Plastic Materials

In recent years, interest in linear elastic fracture mechanics (LEFM) has been extended to elastic-plastic fracture mechanics aiming at establishing the fracture criteria for elastic-plastic materials. Of the techniques suggested, Crack-Opening Displacement (COD), R-Curve Analysis, and J Integral are promising methods.

As suggested in Eq. 6, COD fracture criterion is equivalent to the LEFM criteria when LEFM applies. In contrast to LEFM, however, COD measurement can be made when considerable plastic flow occurs ahead of a crack for elastic-plastic materials. The British Standards Institution has established methods for COD testing. (44)

An R-Curve analysis is a plot of crack growth resistance (K_R) in a material under specific conditions of temperature, strain rate and plate thickness as a function of crack extension (Δa). Experimental method for R-Curve measurement is addressed in ASTM publications. (45-47)

The J-Integral, as proposed by Rice, is a method of characterizing the complicated elastic-plastic stress-strain field by taking an integration path far away from the crack tip. (48) Begley and Landes have used multiple specimens to calculate J and applied it as a fracture criterion. (49,50) The accuracy of estimating J by many techniques employing a single specimen was evaluated. (51,52) In addition, an experimental procedure to measure the critical J value (J_{Ic}) has been proposed. (53) J was related to COD

in a similar way to Eq. 6 as (54)

$$J = \lambda \sigma_Y COD, \quad \lambda \simeq 0.48 - 2.98 \tag{8}$$

In addition to the above techniques, an equivalent-energy concept developed by Witt enables the determination of K_{Ic} with small specimen by an empirical method. (55,56)

C. Objectives of this Investigation

The reduction in toughness of steels that occurs at higher sulfur and phosphorus levels has been well established, as indicated in the literature. Because of the loss in toughness, various specifications require maximum sulfur and phosphorus levels for steels. The presence of this requirement for both elements results in higher manufacturing costs because of the different melting conditions needed to remove phosphorus and sulfur from the steels. This investigation is primarily directed towards determining whether it is feasible to specify a total sulfur plus phosphorus content for the steels rather than maxima for the individual elements. This determination is to be made by using toughness as the criterion. The behavior of phosphorus and sulfur on the tensile properties of the steels will be studied to a minor extent and only when appropriate.

The project consists of two phases. First, a computer analysis of the available data from the literature employing a multiple regression technique is conducted to determine the individual and collective effect of phosphorus and sulfur on the toughness of steels. Then experimental work that determines this relationship will be conducted and compared to the results of the computer analysis.

II. COMPUTER ANALYSIS

A. Introduction

Although the reduction in toughness of steel that occurs at higher phosphorus and sulfur levels has been well known for a long time, most investigators consider only either element as a variable in their investigation. Therefore, the weight of individual contribution and combined effects of these two elements on the dynamic behavior of steel are less certain. Systematic studies with statistical significance on the effects of phosphorus and sulfur on the toughness of steel are rarely documented.

In an attempt to analyze the separate and collective effects of phosphorus and sulfur on the toughness of steel, a computer analysis based on the published literature using a multiple regression method (57,58) was undertaken. The significant question that it is desired to address is

whether the available literature on the influence of sulfur and phosphorus on the steel can be employed to predict, with sufficient accuracy, the effect of simultaneous variation in each on the toughness of steel. This information is desired to determine whether it is feasible to specify a maximum value for the sum of sulfur and phosphorus rather than individual maxima for each element as far as their effects on the toughness of steel is concerned.

B. Regression Analysis and Results

Since the toughness of steel depends on several variables, it is necessary to simplify the problem and to include only those significant variables in a multiple regression analysis. It would have been desirable to include as many variables as possible in regression equation; however, this is impractical since insufficient test results or samples are reported in the various papers. As will be seen later, even with only three variables, some unreasonable results were obtained.

The toughness (TF) of steel depends on its structure and the presence of defects such as non-metallic inclusion and porosity. The structure is related in a complicated manner to many variables such as compositional and impure elements (E), processing-solidification, welding and thermal-mechanical treatment (PR) for a specific geometry of specimen (D) tested at certain strain rate ($\dot{\varepsilon}$), and environment and temperature (ET). This relationship is mathematically described as follows:

$$TF = f\ (E,\ PR,\ D,\ \dot{\varepsilon},\ ET,.....) \qquad (9)$$

This relationship is complicated and should be simplified to find the correlation between toughness and phosphorus and sulfur desired in this work. To do this, only one type of steel will be considered at each time. This enables a consideration of variations in only one element such as carbon (C) instead of all compositional elements. Furthermore, consideration is restricted to only tempering temperature (T) in the thermal-mechanical treatment, and phosphorus and sulfur in the category of impurities. If all other factors are kept constant, Eq. (9) can be simplified to the form:

$$TF_i = f(C_i,\ T_i,\ P_i,\ S_i) + E_i$$

or

$$TF \simeq f(C,\ T,\ P,\ S) \qquad (10)$$

where $_i$'s are for specific values and E_i is unobservable random error. (59)

Including the variables of carbon and tempering temperature in Eq. (10) complicates the problem. However, in certain experiments in the published literature, carbon contents and tempering temperature are kept virtually invariant. For others, these variables can be normalized to some standard

values. In both cases, Eq. (10) may be rewritten as:

$$TF = f(P, S) \tag{11}$$

Obviously, the investigations with this characteristic are relatively few. More importantly, however, even when these data are available in the literature, multiple regression analysis will not automatically provide a meaningful result if the sampling of phosphorus and sulfur are not representative.

In general, TF can be expressed explicitly in terms of P and S as:

$$TF = Bo + B_1P + C_1P^2 + \text{-----} + B_2S + C_2S^2 + \text{-----}$$
$$+ D_1P.S + D_2P.S^2 + D_3P^2.S + \text{-----} \tag{12}$$

where B's, C's, and D's are constants. The coupling terms such as P.S, $P.S^2$, and $P^2.S$ will not be employed since it is believed that phosphorus and sulfur embrittle the steel independently as a result of different mechanisms.

$$TF = B_0 + B_1P + C_1P^2 + \text{-----} + B_2S + C_2S^2 + \text{-----} \tag{13}$$

Very often toughness can be adequately expressed as linear or exponential functions such as shown in Eq. (14) and Eq. (15), respectively:

$$TF = B_0 + B_1P + B_2S \tag{14}$$

$$TF = B_0e^{-(B_1P + B_2S)} \tag{15}$$

In the present study, the regression analyses were performed with the aid of a 1108 Univac digital computer. The standard multiple regression subprogram was provided by Chi Corporation and was available in the software items. (60) A typical program is indicated in Appendix A.

Seven regression analyses were made to determine the effect of phosphorus and sulfur on the toughness of cast and wrought, plain carbon and low alloy steels. The criteria used for toughness determination were Charpy V-notch or Izod impact energy (CVN, Izod), plane strain fracture toughness (K_{Ic}), nil ductility transition temperature (NDTT) and 15 ft-lb Charpy V-notch transition temperature. In each analysis, the regression analysis was undertaken to determine the separate or individual effect of phosphorus and sulfur on the toughness. The regression analysis was then performed to find the correlation between toughness and phosphorus and sulfur, with phosphorus and sulfur in the regression equation simultaneously. Lastly, phosphorus plus sulfur was employed as a single variable to determine whether it would fit better with the regression analysis.

In each regression analysis, correlation coefficient (R) and standard error of estimation (SEE) are automatically computed and furnished by the computer in addition to the regression coefficients (B's). In some cases, the experimental data were normalized to the same carbon content or tempering temperature before it was placed into the computer regression analysis program.

Tables 1, 2, and 3 show the results of the correlation between impact energy and phosphorus and sulfur from the works of Larson and Herlihy, (25) Wright and Quarrell, (17) and Zotos, (21) respectively. Table 4 shows the effect of phosphorus and sulfur on the fracture toughness of wrought 4340 steel based on Kula and Anctil's research. (27) The correlation between Charpy V-notch impact energy and fracture toughness of AISI 4335 cast steel and phosphorus and sulfur as reported by Groves and Wallace (28) is listed in Table 5. The deleterious effect of phosphorus and sulfur as obtained from Dutcher et al on the nil ductility transition temperature (23) and from Mickelson on Charpy V-notch transition temperature (29) is shown in Table 6 and Table 7, respectively. In Table 2 and Table 5, curvilinear equations are used to fit the data better, otherwise linear equations are used.

C. Discussion on Computer Analysis

As mentioned previously, insufficient test data can cause unreasonable results in regression analysis. Examples of this behavior are shown in Eqs. (16) and (17) from Tables 4 and 5 respectively.

$$K_{Ic}\ (400°F) = 53.41 + 193.4P - 1348.0S$$
$$K_{Ic}\ (700°F) = 77.23 + 1292.0P - 2362.0S \qquad (16)$$

$$CVN = 17.55e^{-(36.09P - 5.056S)} \qquad (17)$$

The first two cases indicate that phosphorus is beneficial to fracture toughness while the third indicates that sulfur is beneficial to Charpy V-notch impact energy; this, of course, is inaccurate as shown by many studies. (20,21,26-28)

One factor that requires consideration is whether the particular regression analysis conducted is significant or meaningful. The reliability of a regression analysis depends on unobservable random error, such as experimental error, and the number of samples. In this analysis, the errors from biased samples rather than random samples seems responsible for most of the unreasonable results. An example of this behavior is the correlation between CVN and phosphorus and sulfur simultaneously, as shown in Table 5 and graphically represented in Figure 10A. LMN is a surface representing the variation of CVN in accordance with phosphorus and sulfur. OH is a line equidistant from OP and OS, which represents the chemical composition when P = S. The phosphorus and sulfur contents of alloys are shown as dots on POS plane. The range of variation of CVN corresponding

to these alloys is depicted as the strip MX on the LMN surface. It is evident that the deviation of chemical composition away from OH is artifically small, which corresponds to the narrow strip MX. Essentially, the regression analysis is asked to predict a full surface LMN on the basis of narrow surface MX. The closer the values of P and S are to OH, the more difficult it becomes for the regression analysis to determine to what extent phosphorus or sulfur actually contribute to the variation of CVN. The error in this example is large and produces the ridiculous result of Eq. (17) or the corresponding graphical representation in Figure 10B.

This behavior is explained further in Figure 10C. This figure repreents a plane perpendicular to OH, such as along AB. The shaded area represents unobservable or experimental error and A'B' the exact change of CVN with the corresponding change in chemical compositions along AB. For a large deviation of composition from P = S, such as E, the predicted regression line is GH which is away from A'B' but at least has the same tendency. If the deviation of chemical composition from P = S is small, such as F, the predicted regression line IJ will be completely wrong in both size and direction.

Sampling near the OH line or when a P = S corresponds to a narrow strip MX on the LMN surface, as shown above. An additional analysis was performed by adding samples one by one away from OH to determine the effect on the regression analysis. When the samples are sufficient in number and cover a large area in the P - S plane, the predicted toughness should approach a stable value as the number of samples approaches infinity. Only when the toughness becomes stabilized during a sampling convergence test obtained by increasing the number of samples in the regression analysis would the result from the analysis become meaningful.

This sampling convergence test was employed for all seven regression analyses in this investigation to determine whether this test can serve to reject the unreasonable regression analysis results and confirm the reliable ones. The results of such tests are shown in Figures 11-17. In each figure, the chemical compositions are shown by dots in (A). The digit numbers represent the successive total number of cases in a regression analysis; 3 means samples 1, 2, and 3 are included in a regression analysis, and 4 means samples 1, 2, 3, and 4 are included, and so on. When analyzed in this manner, only Figure 17 demonstrates satisfactory results. All regression coefficients, B_0, B_1, and B_2, converge and the contributions from unobservable errors are overpowered and damped away as the number of samples increases. Some convergence was obtained for the data in Figures 11 and 12. Equations (16) and (17) were shown to be inaccurate by Figures 14 and 15, respectively.

If the sequence or order of adding samples to the regression equation is random, instead of as shown in Figure 17A, the sampling convergent test exhibits a similar result, as indicated in Figure 18. The minimum number of samples depends on the variation from the P = S line. When data are similar to that shown in Figure 19, fewer samples are needed than in cases where the data are closer to the P = S line.

The individual effect of phosphorus and sulfur on the toughness of steels is confirmed in this investigation. One typical example is shown in Figure 20. These plots can be examined to determine whether the correlation between toughness and phosphorus plus sulfur is closer than one between toughness and either phosphorus or sulfur. It has been determined that the correlation with the sum of these elements is closer than for the individual elements when there are sufficient samples that consist of a variety of heats of chemical compositions, as for the data in Tables 1 and 7. The correlation coefficient is higher when the sum is plotted as shown in Figure 21A compared with the individual element correlations in Figures 20A and 20B. However, this is not the case if the compositions are biased, the sum of the elements does not provide as good a result. This is the case in Table 2 where, in one series Alloy 17A-18C, the phosphorus contents are kept virtually constant and in another series Alloy 24B-24D the sulfur contents are kept constant. In this instance, the correlation coefficient -0.6608 appears to be only an average of -0.1133 and -0.9621 for the individual correlation with phosphorus and sulfur, respectively. A correlation between toughness and phosphorus and sulfur simultaneously will always produce a better fit for the experimental results in terms of the correlation coefficient as shown in Tables 1 through 7. However, the multiple regression analysis will not necessarily provide more useful information unless the significance of analysis is verified.

The variation of transition temperature (15 ft-lbs criterion) with a simultaneous change in phosphorus and sulfur contents for AAR Grade B cast steel (29) can be depicted in the two-dimensional representation using P + 0.7S as a single parameter as shown in Figure 21B in the light of the following equations rewritten from Table 7:

$$\text{Tran. Temp. } (°F) = -26.08 + 701.6P + 495.5S \tag{18}$$

or

$$\text{Tran. Temp. } (°F) \approx -26.08 + 701.6\,(P + 0.7S) \tag{19}$$

Phosphorus as shown in Eqs. (18) and (19) is more potent compared to sulfur in raising the transition temperature of Grade B cast steel. For this steel the specification for chemical composition is 0.05% max. P and 0.05% max. S. The transition temperature corresponds to 0.05% P and 0.05% S, by Eq. (19), is 23.56°F. By inserting this value into Eq. (19) we obtain:

$$P + 0.7S \leq 0.085 \tag{20}$$

Equation (20) actually represents a specification equivalent to the one of $P \leq 0.05\%$ and $S \leq 0.05\%$. The advantages of the proposed specification suggested in Eq. (20) are:

1) The parameter P + 0.7S is highly correlated with the transition temperature of the Grade B steel, while phosphorus or sulfur content individually only suggests a loose correlation with this property.

2) The range of the chemical composition allowed by the specification is extended to $0 \leq P \leq 0.085$ and $0 \leq S \leq 0.12$ as long as Eq. (20) is obeyed. This provides more leeway for compositional variations in steel making, and

3) Since the parameter $P + 0.7S$ is highly correlated to the toughness of this steel, it is a more accurate quality control value.

Alternatively a specification, as shown in Eq. (21), is also justified for the similar arguments.

$$P + S \leq 0.10 \tag{21}$$

Again the prediction of toughness in terms of transition temperature is much improved by using P + S as a single parameter instead of P or S individually. In Eq. (21) we have assumed that phosphorus and sulfur are interchangeable, purely additive, and equally potent in lowering the toughness of the steel. However, it has been suggested by Eq. (19) that phosphorus is actually more deleterious than sulfur. Taking this into consideration for the steel with very high phosphorus contents, a modification of Eq. (21) to Eq. (22) can be employed for all chemical compositions of phosphorus and sulfur:

$$P + S \leq 0.09 \tag{22}$$

The primary consideration of toughness thus far in this discussion has been in terms of the criterion of transition temperature. The toughness as evaluated by the Charpy V-notch impact energy is also important. The work conducted by Larson and Herlihy (25) as shown in Table 1 and Figure 11 suggested that sulfur is more influential in lowering the room temperature Izod impact energy for AISI 4335 cast steel as expressed in the following equations:

$$\text{Izod (ft-lb)} = 28.00 - 177.9P - 241.2S \tag{23}$$

or

$$\text{Izod (ft-lb)} \approx 28.00 - 177.9\,(P + 1.3S) \tag{24}$$

These equations indicate that sulfur is about 30% more effective in lowering the room temperature Izod impact energy. If P + S together are taken as a single parameter to determine the effect on the toughness of this steel, the result is represented by Eq. (25):

$$\text{Izod (ft-lb)} \_ 27.83 - 211.1\,(P + S) \tag{25}$$

The correlations are improved by employing either P + 1.3S or P + S over the correlations using P or S content individually as shown by comparing the correlation coefficients in Table 1. Assuming that the phosphorus and sulfur specifications for AISI 4335 steel are 0.035% max. and 0.040% max., respectively, the proposed corresponding specifications considering room temperature Charpy V-notch impact energy as the criterion are indicated in either Eq. (26) or Eq. (27):

$$P + 1.3S \leq 0.09 \tag{26}$$

$$P + S \leq 0.075 \tag{27}$$

Equation (26) provides a slightly better fit with the experimental results. If very high sulfur heats are considered, a slight modification of Eq. (27) to Eq. (28) is indicated:

$$P + S \leq 0.07 \tag{28}$$

Additional support for the position that sulfur is more detrimental to the steel based on the room temperature impact energy is provided by Wright and Quarrell's work on plain carbon cast steel shown in Table 2. (17) The alloys investigated in Wright and Quarrell's experiments contain an exceptionally high 0.22-0.32% aluminum content and therefore the regression analysis from Table 2 may be subject to some question. However, a comparison of three heats from their experiments is shown below:

ALLOY	P(%)	S(%)	CVN(ft-lb)
17A	0.009	0.021	55.0
17D	0.009	0.053	10.0
24D	0.077	0.021	30.5

At 0.009% phosphorus the CVN is decreased 14.06 ft-lb for every 0.01% increase in sulfur; on the other hand, at 0.021% sulfur level, CVN is decreased 3.60 ft-lb for every 0.01% increase in phosphorus.

It is noted that a systematic statistically significant study on the effects of phosphorus and sulfur on the toughness of steel has not been conducted. Accordingly, the relative effect of phosphorus and sulfur on the room temperature Charpy V-notch impact energy and transition temperature for the same steel is not available. It is postulated, by comparing Eq. (19) with Eq. (24) for different types of cast steels, that the role of phosphorus in steel is mainly one of shifting transition temperature and the role of sulfur is in shifting the impact energy. This behavior of phosphorus and sulfur in steel is schematically represented in Figure 22. Equation (19), Eq. (24), Table 2, Figure 2, and Figure 4B indicate that this behavior is possible.

D. Conclusions from the Computer Analysis

A computer analysis by the regression analysis technique was undertaken to determine the individual and combined effects of phosphorus and sulfur on the toughness of carbon, low and medium alloy steels. The toughness, as expressed by impact energy from Charpy V-notch and Izod tests, plane strain fracture toughness, nil ductility transition temperature and 15 ft-lb transition temperature in the Charpy V-notch test, has been correlated to phosphorus and sulfur separately, phosphorus and sulfur simultaneously, and phosphorus plus sulfur as a single variable for several steels using the data available in the technical literature. The results allow the following conclusions.

1) The correlation between toughness and phosphorus plus sulfur is closer than one between toughness and either phosphorus or sulfur when there are sufficient sample that consist of a variety of variations in both sulfur and phosphorus.

2) A sampling convergence test was employed in the multiple regression analysis for the case of three variables in the equation, namely toughness, phosphorus and sulfur. This test was successful in determining the significance or meaningfulness of a multiple regression analysis.

3) Higher sulfur and phosphorus contents reduce the toughness of carbon, low and medium alloy steels. Higher phosphorus contents in steel appear mainly to raise the transition temperature; increasing sulfur content lowers impact energy.

4) It seems possible to consider some modification of the maximum values of phosphorus and sulfur contents in steel based on these results. These modifications should be to require a maximum sulfur plus phosphorus value in place of individual sulfur and phosphorus maxima.

III. MATERIALS AND PROCEDURES

A. Melting and Casting Practice

The steel selected for this investigation was AISI 4340 steel of the following nominal composition:

%C	%Mn	%Si	%Ni	%Cr	%Mo
0.38/0.43	0.60/0.80	0.35/0.45	1.65/2.00	0.70/0.90	0.20/0.30

Two one-thousand-pound heats of this steel have been cast and processed. The charge materials and their compositions are listed in Table 8. The steels were air melted in a basic-lined high frequency induction furnace.

The melting practice for both heats consisted of the following:

1) Cold charge electrolytic iron, electrolytic nickel, and low carbon steel scrap.

2) When molten, deslag and add FeMo.

3) Heat to 2850°F and boil for five minutes with pig iron.

4) Heat to 2900°F and block with FeSi and FeMn.

5) Add FeCr.

6) Tap into a preheated ladle at 3000°F and deoxidize with 0.07%Al and 0.05%CaSi.

7) Compensating additions of silicon and manganese were made to the ladle along with the deoxidizer as needed to maintain the desired levels of silicon and manganese during the holding of the heat.

8) Variations in phosphorus and sulfur were made by adding these elements as FeP and FeS to the ladle with the deoxidizer and compensating additions.

9) Pour into sand molds at about 2900°F.

Each tap was cast into a green sand mold to produce a casting of the dimensions shown in Figure 23. This casting was designed with an adequate riser and taper and no evidence of microshrinkage occurred in any casting.

The first heat was tapped and poured into seven castings designated I, E, N, O, M, A, and P; the second heat was tapped and poured into nine castings designated J, F, K, B, L, G, C, H, and D.

B. Sectioning, Machining and Heat Treatment

All of the cast blocks were sectioned, machined and heat treated in accordance with the procedures as described below:

Remove riser

600°F x 24 hr. A.C.

1800°F x 4 hr. A.C.

1200°F x 2 hr. A.C.

Section and machine test pieces to 0.020 inch oversize

1550°F x 1 hr. O.Q.

1100°F x 2 hr. O.Q. or 400°F x 2 hr. A.C.

Finish machine

The casting design is shown in Figure 23. The layout of tensile, Charpy impact and plane strain fracture toughness test specimens is indicated in Figure 24. For each cast block, half of the specimens were tempered at 1100°F and the other half at 400°F to provide two strength levels for the steels.

C. Hardness and Tensile Tests

The tensile test specimen used in this study had a 0.500 inch diameter test section with a 2.0 inch long gauge length per ASTM A370-77. Tensile tests were conducted at room temperature on a 60,000 lb capacity BALDWIN testing machine at crosshead speed of 0.005 in/min or an equivalent strain rate of 0.25%/min. Load versus elongation was provided by the outputs of a mechanical load device and an LVDT extensometer that were fed into an X-Y recorder. The Rockwell C hardness measurements were conducted on the finish machined Charpy impact specimens.

D. Charpy Impact Tests--Conventional, Instrumented and Instrumented Precracked

The conventional Charpy impact test was conducted on a Wiedemann-Baldwin machine using a maximum energy capacity of 100 ft-lbs with a striking velocity of 10.9 ft/sec. Standard V-notch specimens were tested over the temperature range -320°F to 320°F per ASTM E23-72 and A370-77.

Instrumented precracked Charpy impact test was performed with similar procedures on the same machine instrumented with Dynatup Model 500 manufactured by Effects Technology, Inc. The instrumentation package has been fully described elsewhere. (42,61,62) Precracking of the Charpy impact specimens was conducted on a standard ManLab precracker. The sample was fatigue precracked using tension-zero loading. The a/W ratios obtained ranged from 0.33 to 0.37 (where a = crack length = notch + precrack depth, and W = 0.394 inch).

Both elastic and elastic-plastic fractures were obtained in this investigation. Load-time and energy-time traces were obtained for all precracked specimens tested. Measurements of the crack length were made at the following three positions: at the center of the crack front and at two other locations between the center and edge. The average of these three measurements of crack lengths is used to calculate dynamic fracture toughness, K_{Id}. The calculation of K_{Id} values was straightforward for elastic fractures with the help of the linear elastic fracture mechanics relationship for the three point bending specimen. However, for elastic-plastic fracture no standard method exists for the calculation of fracture toughness. Equivalent energy concept as proposed by Witt was used in this investigation. The procedure to calculate K_{Id} values is presented in Appendix B.

Instrumented Charpy V-notch impact test was performed in a similar way on specimens M, A, and P only to measure the effect of high sulfur and phosphorus on the load or yield strength versus temperature under the conditions of high strain rate loading and plastic constraint as imposed by the impact loading.

E. Plane Strain Fracture Toughness Test

A compact tension specimen of ASTM E399-78a was chosen for the K_{Ic} test. The specimen dimensions were: thickness (B) = 1.000 inch; depth (W) = 2.000 inch; crack length (a) = $0.958 \leq a \leq 1.060$ inch. An MTS Model 632.01 clip-on gauge with displacement working range 0.150 inch (0.475-0.625 inch) was attached to the specimen. The crack (a) consists of three sections, a 1/8 inch wide slot, a 0.003 inch wide EDM slot, and a sharp fatigue precrack. The fatigue precrack length was longer than 0.05a or 0.05 inch, and maximum stress intensity factor, K_f, of the fatigue load was less than 60% of the "K_Q" in accordance with ASTM E399-78a.

The compact tension specimen was fractured at room temperature on an MTS 810 machine. During the test, signal of load and displacement across the notch, as measured from a 50,000 lb load cell and a clip-on gauge, was fed into MTS recorder as load (Y) and strain (X), respectively. Loading rate was 0.0125 in/min or approximately 90,000 psi $\sqrt{\text{in}}$/min within the range of ASTM requirement. Following testing, the crack length was measured in a similar way, as described for instrumented precracked Charpy impact specimen, and the load-displacement curve analyzed per ASTM requirements.

F. Fatigue Crack Propagation Test

The fatigue crack propagation rate was measured on all compact tension specimens prepared for the fracture toughness test prior to fracture. The test was conducted in air at room temperature on the same machine used for K_{Ic} test. A stroke control was chosen to prevent a possible open-loop condition. (63) A load fluctuation range at 5 Hz frequency was maintained as a constant by adjusting the span of the MTS control system and calibrated on the ocilloscope. The stress intensity factor range (ΔK_I) was 40.0 ksi$\sqrt{\text{in}}$ and 20.0 ksi$\sqrt{\text{in}}$ for 1100°F and 400°F tempered steels, respectively. In both cases, a stress ratio $R = K_{Imin}/K_{Imax} = 0.1$ was used. A Gaertner microscope mounted in a micrometer slide was employed to measure the fatigue crack extension. The micrometer slide was accurate to 0.001 mm. To determine the effect of high sulfur and high phosphorus on the behavior of fatigue crack propagation at different stress intensity factor ranges, additional tests also conducted on M, A, and P specimens.

G. Metallography and Fractography

Metallographic specimens were prepared from center of the casting using standard technique. The volume fraction of nonmetallic inclusions was measured by point count method per JISG0555. (64) Fracture surfaces of selected Charpy V-notch specimens were examined using a Cambridge Stereoscan S4-10 Scanning Electron Microscope.

IV. RESULTS AND DISCUSSION

A. Chemical Composition of Materials

The chemical analyses of the steels cast in the two heats are listed in Table 9. The analyses of all elements in the 4340 type steel are within the specified range and reasonably close to each other except for the deliberate variation of sulfur and phosphorus contents. The matrix of phosphorus and sulfur contents produced by the various analyses on these two heats is shown in Figure 25.

B. Microstructure

The microstructures of the castings tempered at both 400°F and 1100°F were examined. In unetched specimens, both Type II and Type III sulfide inclusions occurred and were generally segregated to the interdendritic regions. The non-metallic inclusion content for all the castings produced is reported in Table 10. Etching the specimens revealed a typical quenched and tempered martensitic structure. No difference in microstructure can be detected as affected by either sulfur or phosphorus, except for higher sulfide inclusion content of the higher sulfur steels.

C. Effect of P and S on Hardness and Tensile Properties

The hardness and tensile properties of the steels studied are summarized in Tables 11 and 12. The matrices in Figures 26 and 27 show the variation in Rockwell C hardness and yield strength, respectively, as affected by phosphorus and sulfur for medium strength (tempered at 1100°F) and high strength (tempered at 400°F) 4340 cast steels. As indicated in these figures, phosphorus very slightly increases the hardness and yield strength of both strength level steels, whereas sulfur has a negligible effect. From Tables 11 and 12, it is noted that the ultimate tensile strength is also insensitive to the variations of phosphorus and sulfur. The true fracture strength and tensile reduction of area are, however, much affected by these two elements, as shown in Figures 28 and 29.

The effect of phosphorus and sulfur on the tensile properties of 4340 cast steel is summarized as follows.

1) Phosphorus very slightly increases the hardness and yield strength, whereas sulfur has a negligible effect.

2) The ultimate tensile strength is not sensitive to the variation of phosphorus and sulfur.

3) Both the true fracture strength and tensile ductility are significantly reduced by phosphorus and sulfur. Sulfur is slightly more potent than phosphorus in reducing the true fracture strength and tensile ductility for both strength level steels.

D. Effect of P and S on Charpy V-Notch Impact Properties

D.1. Charpy Impact Transition Curves

The Charpy impact properties of all the steels studied are summarized in Tables 13 through 19. The influence of increasing phosphorus at various sulfur levels on the Charpy V-notch impact properties from -320°F to +320°F is listed in Figures 30-1 through 30-4 for the steels tempered at 1100°F. These figures indicate the fracture energy, percent fibrosity in the fracture, and lateral expansion as a function of testing temperature. The steels A, B, C, and D in Figure 30-1 show effect of increasing phosphorus at high sulfur (0.050%S) levels, the sulfur levels gradually drop for E, F, G, and H (0.035%S) in Figure 30-2, for I, J, K, and L (0.025%S) in Figure 30-3, and for low sulfur (0.010%S) in the M, N, O, and P steels in Figure 30-4. It is noted that the fracture energy and lateral expansion increase as the sulfur content decreases.

Similar data showing the Charpy V-notch transition temperature curve over the -320°F to +320°F range are demonstrated in Figures 31-1 to 31-4 for these steels tempered at 400°F to the higher hardness. The fracture energy and lateral expansion data are plotted. No distinct fibrosity transition was observed. Steels A, B, C, and D in Figure 31-1 show the effect of increasing phosphorus levels at the high sulfur 0.050%S levels; steels E, F, G, and H in Figure 31-2 show the same effects at a lower sulfur of 0.035%S; steels I, J. K, and L in Figure 31-3 show the transition curves for increasing phosphorus with a 0.025%S content; and steels M, N, O, and P in Figure 31-4 demonstrate the transition curves for increasing phosphorus at the lowest 0.010%S level.

The combined effects of phosphorus and sulfur contents on the Charpy V-notch transition curves over a range of -320°F to +320°F are plotted in Figure 32. The curves at the top in "A" show the transition curves for those steels tempered at 1100°F and the curves in the bottom, Figure 32B, indicate the transition curves after tempering at 400°F. The transition curves plotted in this figure combine the lowest, intermediate and highest sulfur and phosphorus contents for each steel.

The Charpy V-notch transition curves plotted in Figures 33-1 through 33-4 indicate the effect of increasing phosphorus with a constant sulfur level in the top of "A" plots and increasing sulfur contents with a constant phosphorus level in the bottom or "B" plots. The lowest sulfur and phosphorus levels are held constant in Figure 33-1; intermediate sulfur and phosphorus levels are held constant in Figures 33-2 and 33-3; and the highest sulfur and phosphorus levels are constant in Figure 33-4. All these steels in Figure 33 are tempered at 1100°F. A dashed line has been plotted on each figure in Figure 33. The data along this line indicate the maximum variation in Charpy V-notch impact fracture energy among the four curves at each testing temperature. This curve is the locus of points showing the difference in impact energy between the highest and lowest level at each temperature.

The Charpy V-notch fracture energy transition curves plotted in Figures 34-1 through 34-4 show the same type of curves with constant sulfur

and constant phosphorus levels and increasing amounts of the other element for the steels tempered at 400°F. The lowest level of the constant elements is in Figure 34-1, intermediate levels in Figures 34-2 and 34-3 and highest level in Figure 34-4. A dashed curve showing the maximum difference in impact energy at each testing temperature also appears on each plot in this figure.

Examination of the curves in Figures 33 and 34 indicates that increasing phosphorus levels move the transition curves to the right or higher temperatures. The change in the level of fibrous energy on the upper shelf fracture energy is relatively small. The increasing sulfur levels, however, have little effect on the transition temperature of the curves. The level of fibrous fracture energy or the upper shelf energy is significantly decreased by increasing sulfur levels. This difference in the relative effects of the two impurity elements produces different shapes of the dashed curves showing the difference between the maximum and minimum energy at each temperature. These dashed curves for the plots with increasing sulfur levels are similar in shape to transition curves but depressed to lower levels of fracture energy. The similar curves for the plots with increasing phosphorus have maximum values in the transition temperature range and minimum values at the highest and lowest testing temperatures where the fractures are either all ductile or brittle.

The Charpy V-notch impact energy transition curves plotted in Figure 35 show the relative transition temperature behavior of phosphorus and sulfur. Each plot compares the two steels with counterpart combinations of these elements at both the 1100°F and 400°F tempering temperature level. The plot in Figure 35-1A is for the highest phosphorus, lowest sulfur steel plotted against the highest sulfur, lowest phosphorus level. Figure 35-1B is the second highest phosphorus and second lowest sulfur steel versus the second highest sulfur, second lowest phosphorus steel. In a similar manner the other plots in Figure 35 compare the following steels:

Figure 35-2A	Highest phosphorus, second lowest sulfur vs. highest sulfur, second lowest phosphorus.
Figure 35-2B	Second highest phosphorus, lowest sulfur vs. second highest sulfur, lowest phosphorus.
Figure 35-3A	Highest phosphorus, second highest sulfur vs. highest sulfur, second highest phosphorus.
Figure 35-3B	Second lowest phosphorus, lowest sulfur vs. second lowest sulfur, lowest phosphorus.

Since higher sulfur lowers the fracture energy in the ductile fracture region but has little effect on the transition temperature and higher phosphorus raises the transition temperature but has less effect on the fibrous fracture energy levels, the two transition curves for the equal amount of these impurity elements cross or intersect as indicated on Figure 35-1. This intercept point averages -115°F for the steels tempered at 1100°F and +150°F for the steels tempered at 400°F. This is considered to be the testing temperature at which sulfur and phosphorus are exerting equivalent

effects on the impact fracture energy.

Figure 35-4 contains the Charpy V-notch transition curves for the lowest sulfur, lowest phosphorus steel versus both the lowest sulfur, highest phosphorus and lowest phosphorus, highest sulfur steel. In this figure, the curves for the 1100°F temper are plotted at the top figure and for the 400°F temper in the bottom figure. This plot demonstrates the decrease in fibrous impact energy levels with the higher sulfur content, and higher transition temperature with the higher phosphorus content.

D.2. Fracture Energy Correlations and Transition Temperature of 1100°F Tempered Steels

The effect of phosphorus content on the fracture energy of the Charpy V-notch specimens broken at -115°F (ave. cross over temperature in Figure 35) at various sulfur levels is shown in Figure 36A. The influence of sulfur level on this -115°F fracture energy is shown at different phosphorus levels in Figure 36B. These data are for steels tempered at 1100°F. It is observed that the slope or rate of decrease of fracture energy with increasing phosphorus (Figure 36A) is comparable to that with increasing sulfur (Figure 36B) at the cross over temperature. The effect of combined sulfur and phosphorus contents on the fracture energy at this temperature is plotted in Figure 36C. The equally, and therefore additively, detrimental effect of sulfur and phosphorus at -115°F is reflected in a fairly good correlation between fracture energy and P + S as a parameter in Figure 36C.

Similar results to Figure 36 on both sides of -115°F, namely -150°F and 80°F or room temperature, are plotted in Figures 37 and 38. Below the cross over temperature at -150°F, phosphorus is slightly more deleterious than sulfur in lowering the fracture energy, as indicated by comparing the slopes in Figures 37A and 37B. However, the combined phosphorus plus sulfur plots versus fracture energy at this temperature as shown in Figure 37C are smooth and decrease uniformly from high to low energy levels with increasing total phosphorus plus sulfur contents.

When these plots of increasing phosphorus, increasing sulfur and increasing phosphorus plus sulfur are compared at the higher, room temperature testing temperature (Figure 38), it is noted that the slope or rate of decrease of fracture energy versus sulfur content is considerably greater than versus the phosphorus content because of a larger effect of sulfur on the upper shelf fracture energy. The combined phosphorus plus sulfur content versus fracture energy curve exhibits much more scatter. This suggests a poor additive nature of P + S as a single parameter in measuring the toughness of steels fractured much above the ductility transition temperature.

The effect of phosphorus on the transition temperature is clearly illustrated in Figure 39 where the percent fibrosity in the fracture is plotted against the testing temperature for steels of increasing phosphorus levels tempered at 1100°F. Higher phosphorus contents with base sulfurs of 0.010%S (Figure 39-1A), 0.025%S (Figure 39-1B), 0.035%S (Figure 39-2A) and 0.050%S (Figure 39-2B) all indicate steadily higher transition temperatures at higher phosphorus levels.

Similar plots of percent fibrosity versus testing temperature for increasing sulfur levels at constant phosphorus contents in Figure 40 demonstrate practically no effect of sulfur on the transition temperature at all constant phosphorus levels. All of these steels were tempered at 1100°F.

Plots of the 50% fibrosity transition temperature versus % phosphorus content, percent sulfur content, and percent combined phosphorus and sulfur contents in Figure 41 show a direct increase in transition temperature with phosphorus, no effect of sulfur, and a definite trend of increasing the temperature with combined higher phosphorus and sulfur content. However, the combined element plot exhibits significantly more scatter. Plots of the 50% energy transition temperature versus the phosphorus, sulfur, and combined phosphorus and sulfur contents in Figure 42 show a similar influence of the elements on this transition.

D. 3. Fracture Energy Correlations and Transition Temperature of 400°F Tempered Steels

Similar plots that were made for the steels tempered at 400°F are shown in Figures 43-46 for the higher strength steels tempered at 400°F. In this steel the average cross over temperature between the higher phosphorus and sulfur steels in Figure 35 occurred at +150°F. For this reason the effect of increasing phosphorus and sulfur levels on the fracture energy were compared at +150°F in Figure 43, -20°F in Figure 44, and +320°F testing temperature in Figure 45. These plots indicate a similar amount of decreasing fracture energy with increasing phosphorus or sulfur at -150°F in Figures 43A and 43B. The correlation with combined sulfur and phosphorus contents (Figure 43C) is fairly close for all steels. The lower testing temperature of -20°F for these steels tempered at 400°F demonstrates a slightly steeper slope in Figure 44A than that in Figure 44B. This indicates a similarity to those steels tempered at 1100°F that phosphorus is slightly more harmful than sulfur to the steel below the cross over temperature. The correlation between the combined phosphorus plus sulfur contents and the fracture energy at this testing temperature is fairly good, although more erratic than at +150°F.

At the higher testing temperature of +320°F, increasing phosphorus content has only a small influence on the fracture energy as shown in Figure 45A. Some decrease in this energy is apparent at the lowest sulfur level but this effect has just about disappeared at the higher sulfur contents. Increasing sulfur content. However, reduces the fracture energy sharply as shown in Figure 45B. The fracture energy is also reduced by increasing sulfur plus phosphorus, as indicated in Figure 45, but considerable scatter occurs.

The effects of the phosphorus, sulfur, and combined phosphorus and sulfur contents on the 50% energy transition temperature are plotted for the steels tempered at 400°F (Figure 46). This 50% energy transition temperature increases steadily with limited scatter at increasing phosphorus content in Figure 46A. Increasing sulfur content has no effect on the transition temperature as shown in Figure 46B. While the 50% transition temperature does

increase with combined phosphorus and sulfur contents as indicated in Figure 46C, the data exhibit a large amount of scatter. This larger scatter, compared with the 50% transition temperature of 1100°F tempered steels, is partly due to the slope of transition curve of 400°F tempered steel which is much flatter in the transition temperature range; and, for the same quantity of experimental error in CVN energy measurement, the corresponding error of 50% transition temperature measurement is much larger.

E. Effect of P and S on Plane Strain Fracture Toughness

The load displacement plots of the K_{Ic} test for the medium strength 4340 steel tempered at 1100°F exhibited distinct pop-ins which were taken as the critical loads. For high strength steel tempered at 400°F the critical load was defined at 5% load offset since no evident pop-in can be detected. The results of K_{Ic} tests are listed in Table 20 and 21. All of the tests of 400°F tempered steels met the ASTM E399-78a requirement and, therefore, the K_{Ic} values are valid. For most of the 1100°F tempered steels, however, the specimen thicknesses are undersized, the tests are invalid and, therefore, the conditional fracture toughness K_Q's are assigned.

Individual and combined effects of phosphorus and sulfur on the room temperature plane strain fracture toughness of the medium strength steels are shown in Figure 47. The result agrees fairly well with its counterpart Charpy V-notch test (Figure 38). Sulfur is more deleterious than phosphorus for medium strength 4340 steel tested at room temperature.

The Charpy tests conducted at room temperature for high strength steel have indicated that both phosphorus and sulfur reduce the toughness substantially. However, the K_{Ic} test as shown in Figure 48 for the same steel also tested at room temperature indicates that phosphorus has a pronounced effect, whereas sulfur has little effect on the plane strain fracture toughness of this high strength steel. The reason for this behavior is explained in Sec. A.2., Chapter V.

The plots as indicated in Figures 47C and 48C correlating K_Q and K_{Ic} with P + S for both strength level steels show significant scatter. Those steels that contain approximately equal amounts of phosphorus and sulfur provide a fairly good correlation, as shown by the solid circles in the same figures. This is in agreement with the results of Groves and Wallace. (28)

F. Effect of P and S on Dynamic Fracture Toughness

The dynamic fracture toughness properties of all the steels investigated are summarized in Tables 22 and 23. The combined effects of phosphorus and sulfur contents on the dynamic fracture toughness curves over a range of -320°F to 320°F or 400°F are plotted in Figure 49. The curves in Figure 49A at the top show the transition curves for those steels tempered at 1100°F and the curves at the bottom (Figure 49B) indicate the transition curves after tempering at 400°F. The curves in this figure combine the lowest, intermediate, and highest sulfur and phosphorus contents for each steel.

The transition curves plotted in Figure 50 show the individual and combined effect of phosphorus and sulfur on the dynamic fracture toughness behavior. This plot contains the K_{Id} transition curves for the lowest phosphorus and lowest sulfur, highest phosphorus and lowest sulfur, lowest phosphorus and highest sulfur, and highest phosphorus and highest sulfur steels.

As occurred with the Charpy tests, higher sulfur contents lower the fracture energy in the ductile fracture region but have little effect on the transition temperature. Higher phosphorus contents raise the transition temperature but have less effect on the upper shelf toughness. The two transition curves, namely high phosphorus and low sulfur versus low phosphorus and high sulfur, also cross or intersect in Figure 50 for both strength levels. This intercept point averages -110°F for steels tempered at 1100°F and 230°F for the steels tempered at 400°F compared to -115°F and 150°F for the counterpart Charpy V-notch tests. Dynamic fracture toughness had little influence on the cross over temperature for the steel tempered at 1100°F but significantly raised the temperature for the steel tempered at 400°F. This suggests an effect of phosphorus and sulfur on the notch sensitivity at the two different strength level steels, and this will be discussed later.

Figure 51 shows the effect of phosphorus plus sulfur contents on the dynamic fracture toughness of the medium strength steels tested at -150°F, -110°F, and 80°F, corresponding to below, at, and above the cross over temperature. A similar plot for higher strength steels tested at 80°F, 230°F, and 400°F is illustrated in Figure 52. It is noted that a high degree of correlation between K_{Id} and P + S exists only at the cross over temperatures, which are -100°F for the medium strength steel and 230°F for the high strength steel. Below the cross over temperature, for both strength level steels, phosphorus is more deleterious in lowering the fracture toughness and therefore the fracture toughness of high phosphorus specimens is scattered to the lower bound of the curves in Figures 51A and 52A. On the other hand above the cross over temperature, for both steels, sulfur is more deleterious in lowering the fracture toughness and therefore the fracture toughness of high sulfur specimens is scattered to the lower bound of the curves in Figures 51C and 52C.

G. Effect of P and S on Fatigue Crack Propagation

The results of fatigue crack propagation test are listed in Tables 24 and 25. The variation of fatigue crack growth rate with stress intensity factor, as affected by phosphorus and sulfur for medium and high strength 4340 cast steels, is shown in Figure 53. Examination of this figure indicates the following.

1) The 200 ksi yield strength steel has a higher fatigue crack growth rate than the 150 ksi yield strength steel at the same stress intensity factor range. In contrast, Imhof and Barsom report no difference between the different strength levels for wrought 4340 steel. (65)

2) Both phosphorus and sulfur increase the fatigue crack growth rate of the 150 ksi yield strength steel slightly.

3) Phosphorus sharply raises the fatigue crack growth rate of the 220 ksi yield strength steel, whereas sulfur has virtually no effect at this strength level.

4) The fatigue crack growth rate is correlated to the fracture toughness in all the steels studied. An increase in fracture toughness decreases the fatigue crack growth rate.

5) At a stress intensity factor range well below the critical fracture toughness, fatigue properties are not significantly affected by phosphorus and sulfur. The effect of phosphorus and sulfur on fatigue approaches their effect on the fracture toughness as the stress intensity factor range of a material approaches its critical fracture toughness.

Metallographic examination of the fatigue growth paths in these steels has yielded the following observations.

1) The fatigue crack paths may detour from the straight line to join inclusions.

2) The fatigue crack paths of the high strength steel is straighter than for medium strength, presumably because the plastic deformation is less extensive and the plastic zone size is smaller at the crack-tip of the high strength steel. This suggests that sulfide inclusions, and therefore sulfur, have less effect on the fatigue propagation property of high strength steel because less sulfide inclusions are encountered in the fatigue crack paths, this confirming the experimental results.

V. MECHANISM OF EMBRITTLEMENT

A. Effect of P and S on Strain Rate and Notch Sensitivities of 4340 Medium and High Strength Steels

A.1. Strain Rate Sensitivity as Affected by P and S

The rate of increase of the stress intensity factor (K_I) for both static and dynamic fracture toughness can be estimated by dividing the stress intensity factor by the time needed to reach this value. The values of K_{Ic} and K_{Id} are calculated to be $\sim$1.5 ksi$\sqrt{in}$/sec and $\sim$6.0 X 10^5 ksi$\sqrt{in}$/sec, respectively. The ratio of rate of increase of stress intensity factor for dynamic fracture toughness test versus static fracture toughness test, $\dot{K}_{Id}/\dot{K}_{Ic}$, is therefore $\sim$ 4 x 10^5 times.

Figure 54 plots the dynamic fracture toughness (K_{Id}) versus plane strain fracture toughness (K_{Ic}) of both 400°F and 1100°F tempered steels tested at room temperature. It is observed that the discrepancies in fracture toughness as measured by static and dynamic test methods are small. Based on this, it appears that both the medium and high strength steels are strain

rate insensitive. No evidence was found that phosphorus and sulfur could affect the strain rate sensitivity of the steels studied. One possible explanation of the strain rate insensitivity of this material is that its tempered martensite structure contains a high density of dislocations. Similar results were observed for 300 Maraging steel. (66)

A.2. Notch Sensitivity as Affected by P and S

It has been acknowledged in Sec. E, Chapter IV that for 400°F tempered high strength steel, sulfur exhibits a substantial detrimental effect on the toughness as measured by the Charpy V-notch test, but exerts little influence on the results of the plane strain fracture toughness test. It was also suggested earlier that phosphorus and sulfur might influence the notch sensitivity of medium and high strength 4340 steels.

Figure 55 contains both the impact and dynamic fracture toughness transition curves for both strength levels of this 4340 steel. To exhibit the maximum effect of phosphorus versus sulfur, two steels are compared, with one containing high phosphorus and low sulfur and the other, low phosphorus and high sulfur. The CVN specimen has a notch radium of 0.01 inch as compared with 0 radius for dynamic fracture toughness specimen.

For the steel tempered at 1100°F, a reduction in notch radius from 0.01 inch to 0 inch shifts the cross over temperature from -120°F to -110°F, or a small difference. However, for the high strength steel tempered at 400°F, a reduction in notch radius of the same amount raises the cross over temperature substantially or from 150°F to 270°F. These shifts are attributed to the relative shifting of high phosphorus and low sulfur steel transition curve versus low phosphorus and high sulfur steel transition curve associated with a change in notch radius. In other words, phosphorus and sulfur exert a different notch sensitivity effect on the materials investigated. This hypothesis is presented below.

The sensitivity of the impact energy of a specimen to the severity of a notch is defined, for the purpose of this experiment, as notch toughness sensitivity ratio (NTSR):

$$\text{NTSR} = \frac{\text{Impact energy per unit area of } \rho=0 \text{ Charpy specimen}}{\text{Impact energy per unit area of } \rho=0.01\text{" CVN specimen}} \qquad (29)$$

where ρ denotes radius of a notch. NTSR is a measurement of sensitivity of impact fracture energy to the severity of a notch and is therefore distinguished from the notch sensitivity of tensile strength to a notch.

The notch toughness sensitivity ratios as measured by comparing the fracture energy per unit area of precracked Charpy V-notch specimen versus conventional Charpy V-notch specimen for both 1100°F and 400°F tempered steels are presented in Tables 26 and 27.

The effect of phosphorus and sulfur on the notch toughness sensitivity ratio of medium and high strength 4340 cast steel is shown in Figure 56.

The steel with a lower NTSR value indicates that this steel is more susceptible to a reduction of toughness in the presence of a notch. It is noted that phosphorus increases the notch toughness sensitivity (decreases the NTSR) of the medium strength steel and sulfur reduces this sensitivity of the high strength and probably also the medium strength steel. It is also noted in the same figure that those steels having higher strength or lower strength but tested at low temperature are more sensitive to the severity of notch in reducing the impact fracture energy.

The effect of notch severity on the cross over temperature in Figure 55 can be understood in the light of Figure 56. In Figure 55A for the steel tempered at 1100°F, as the notch radius decreases from 0.01 inch to 0, the fracture toughness transition curve of the high sulfur steel is raised upward or remained unchanged relative to its CVN transition curve. However, the fracture toughness transition curve of the high phosphorus steel is depressed downward relative to its CVN transition curve; this occurs because the toughness of the high phosphorus, medium strength steel is notch toughness sensitive. The result is a shift of cross over temperature to higher temperatures. Similar arguments also apply to Figure 55B for 400°F tempered high strength steel. In this case the fracture toughness transition curve of high sulfur steel is raised upward relative to that of the high phosphorus steel because the toughness of the high sulfur, high strength steel is relatively notch insensitive.

A smaller shift of cross over temperature to the right in Figure 55A as compared with Figure 55B is because the slope of the curve near the cross over temperature of Figure 55A is much steeper and, for the same quantity of deviation in fracture toughness, the shift in cross over temperature is proportionally smaller.

B. Effect of P and S on Dynamic Tensile Properties

B.1. Tensile Strength as Affected by P and S

The load-deflection and load-temperature curves from the instrumented Charpy V-notch impact tests permit the determination of the effect of phosphorus and sulfur on the dynamic tensile behavior of medium and high strength 4340 cast steels tempered at 1100°F and 400°F, respectively.

The experimental results of pre-general yield fracture load (P_F), general yield load (P_{GY}), and maximum load after general yield (P_M) are shown in Tables 28 and 29 for medium and high strength steels, respectively. Since the load-deflection curve of all the steels studied exhibited the round house type of curve, the general yield load was determined as shown in Figure 57. Figure 58 plots the variation of load and CVN impact energy with temperature for low phosphorus and low sulfur, low phosphorus and high sulfur, and high phosphorus and low sulfur, medium strength 4340 cast steels.

In Figure 58, $T_{D(N)}$ denotes the brittleness transition temperature for a notched specimen in which fracture occurs upon general yielding, and $T_{S(N)}$, the initiation transition temperature which is the lowest temperature at which fracture is initiated by fibrous tearing. It is noted that an increase in temperature from $T_{D(N)}$ to $T_{S(N)}$ for the 0.010%P,).011%S, and the 0.050%P,

0.012%S medium strength steels shown in Figure 58 corresponds to the temperature range in which the fracture load rises sharply beyond the general yield load. The impact energy also increases sharply and the fracture changes from essentially all cleavage to fibrous tearing in this temperature range. For the 0.007%P and 0.049%S steel, however, the fracture load is depressed to a lower value compared to the higher fracture load for the other steels in the same temperature range between $T_{D(N)}$ and $T_{S(N)}$. An increase in phosphorus, while maintaining sulfur constant, produces the following effects on medium strength 4340 cast steel.

1) Phosphorus increases the yield strength at all temperatures and the temperature dependence of yield strength more noticeably at lower temperatures. The yield strength (σ_Y) of high phosphorus steel is related to friction stress (σ_i) and grain size (d) through the Hall-Petch relation:

$$\sigma_Y(x_p,T) = \sigma_i(x_p,T) + K_y(x_p,T)d^{-\frac{1}{2}}(x_p) \tag{30}$$

where x_p is % phosphorus content, T is temperature, and K_y is temperature dependence of grain size. K_y is assumed to be independent of temperature since twinning is not believed to be a mode of deformation even at very low temperature because of the high density of precipitates, dislocations, and other substructures for the materials studied. Therefore,

$$K_y(x_p,T) = K_y(x_p) \tag{31}$$

and

$$\sigma_Y(x_p,T) = \sigma_i(x_p,T) + K_y(x_p)d^{-\frac{1}{2}}(x_p) \tag{32}$$

The derivatives of the above equation become:

$$\frac{\partial\sigma_Y(x_p,T)}{\partial T} = \frac{\partial\sigma_i(x_p,T)}{\partial T} \tag{33}$$

$$\frac{\partial}{\partial x_p}\left(\frac{\partial\sigma_Y}{\partial T}\right) = \frac{\partial}{\partial x_p}\left(\frac{\partial\sigma_i}{\partial T}\right) \tag{34}$$

Phosphorus, in 4340 medium strength steel, increases the friction stress which in turn increases the yield strength of the lower phosphorus steel. The effect that phosphorus content exerts on the temperature dependence of friction stress, and hence the yield strength, is presumably caused by the decrease in solubility of phosphorus and the increase in degree of supersaturation with the decrease in temperature shown in Figure 1.

2) Phosphorus slightly increases the strain hardening rate which is responsible for a higher fracture load of 0.050%P and 0.012%S steel as compared with that of 0.010%P and 0.011%S steel between 0°F to -150°F, although the latter steel has a higher fracture strain at all temperatures.

3) An increase in phosphorus from 0.010% to 0.050% decreases the cleavage fracture strength (σ_f^*) from 440.2 ksi to 410.0 ksi as calculated in Appendix C.

4) An increase in phosphorus from 0.010% to 0.050% increases the brittleness transition temperature by 72°F (from -266°F to -194°F), the initiation transition temperature by 90°F (from -110°F to -20°F) and the 50% fibrosity transition temperature by 71°F (from -194°F to -123°F). The effect of phosphorus in shifting the ductile-brittle transition temperature is explained in Figure 59. Phosphorus increases the yield strength, the temperature dependence of yield strength, and decreases the cleavage fracture strength. Together these raise the brittleness transition temperature from $T_{D(N)}$ to $T'_{D(N)}$.

A similar plot showing the variation of load and CVN impact energy with temperature for low phosphorus and low sulfur, low phosphorus and high sulfur, and high phosphorus and low sulfur, high strength 4340 cast steels is exhibited in Figure 60. One significant characteristic in Figure 60 is that, above the brittleness transition temperature ($T_{D(N)}$), the fracture load follows almost immediately upon general yielding for the 0.010%P, 0.011%S, and the 0.050%P, 0.012%S high strength 4340 cast steels. This is in contrast to the case in Figure 58 for medium strength steels. Since a sharp rise in the fracture load and the corresponding fracture toughness beyond $T_{D(N)}$ is believed to be caused by a relaxation of the triaxial stress state (a decrease in $K_{\sigma(p)}{}^{max}$), the absence of this behavior is an indication which explains the failure of the high strength steel to undergo a distinct ductile to brittle transition. A high sulfur content in the high strength steel also causes a depression of the whole load-temperature curve in the entire temperature range studied. The fracture load, however, does not reach the general yield load of the low sulfur steels.

An increase in phosphorus produces the following effects on high strength 4340 cast steel:

1) Phosphorus increases the yield strength at all temperatures. Whether phosphorus also increases the temperature dependence of yield strength at lower temperature cannot be determined because of a major uncertainty in extrapolating the general yield load of 0.050%P, 0.012%S steel to lower temperatures.

2) An increase in phosphorus from 0.010% to 0.050% decreases the cleavage fracture strength (σ_f*) from 524.9 ksi to 509.3 ksi as calculated in Appendix C.

3) An increase in phosphorus from 0.010% to 0.050% raises the brittleness transition temperature greatly by 344°F (from -44°F to +300°F).

B.2. Plane Strain Ductility as Affected by P and S

Plane strain ductility is an important property of a material. It measures the ductility of this material under a plane-strain plastic strain state. (67) It is therefore reasonable that the fracture toughness of a material should correlate with the plane strain ductility rather than the axisymmetric ductility.

The deflection at maximum load (d_M) from a Charpy impact test is a measurement of ductility in a notched condition. A relation between de-

flection of a Charpy V-notch specimen loaded in three-point bending and the true strain was established by Wilshaw and was taken as the true fracture strain in the Charpy V-notch specimen: (68)

$$\varepsilon_{f,CVN} = \ell n(1 + 8d_M) \tag{35}$$

where d_M is in inches. The results of deflection at maximum load and true fracture strain in Charpy V-notch specimen for 0.012%P and 0.011%S, 0.007%P and 0.049%S, and 0.050%P and 0.012%S 4340 medium and high strength cast steels are listed in Tables 28 and 29. Clausing has shown that $\varepsilon_{f,CVN}$ is a measure of plane strain ductility. (67)

The critical crack-opening displacement (COD_{Id}) is a measurement of crack tip displacement under plane strain dynamic conditions prior to crack propagation. The COD_{Id} results at various test temperatures for 0.012%P and 0.011%S, 0.007%P and 0.049%S, and 0.050%P and 0.012%S medium and high strength 4340 cast steels as listed in Tables 30 and 31 are calculated from Eq. (7):

$$COD_{Id}(T) = \frac{K_{Id}^2(T)(1 - \nu^2)}{E(T)\sigma_Y(T)} \tag{7}$$

where K_{Id} was taken from the dynamic fracture toughness tests at various temperatures. The modulus of elasticity (E) of 4340 steel at 80°F was measured at 29.0×10^6 psi from the tensile test. Variation of E with temperature was estimated in accordance with: (69)

$$E(T) = (29.48 - 0.006T) \times 10^6 \text{ psi, where T in °F} \tag{36}$$

The variation of yield strength (σ_Y) with temperature was estimated from the general yield load at various temperatures as measured in Figures 58 and 60 in accordance with:

$$\sigma_Y(T) = 31.6\ F_{GY}(T) \text{ psi, for medium strength 4340 steel}$$
$$\sigma_Y(T) = 35.0\ F_{GY}(T) \text{ psi, for high strength 4340 steel} \tag{37}$$

This relationship was demonstrated in Appendix C.

The effects of phosphorus and sulfur at various temperatures on the critical crack-opening displacement (COD_{Id}) and true fracture strain in CVN specimen ($\varepsilon_{f,CVN}$) of medium and high strength 4340 cast steels are shown in Figures 61 and 62. Similar to the transition curves of CVN impact energy and dynamic fracture toughness, cross over temperatures associated with high phosphorus, low sulfur and low phosphorus, high sulfur 4340 cast steels also occurred for each case in Figures 61 and 62.

It is noted from fracture mechanics, as shown in Eq. (7) that $K_{Id} \sim (\sigma_Y COD_{Id})^{1/2}$. Comparing K_{Id} in Figure 50, σ_Y in Figures 58 and 60, and COD_{Id} in Figures 61A and 62A shows that the general shape of K_{Id} transition curve is

mainly determined by COD_{Id} rather than σ_Y. This occurs because the percentage variation of COD_{Id} with temperature is much larger than for σ_Y. The yield strength, however, modifies the shape of the COD_{Id} transition curve to obtain the K_{Id} transition curve.

The crack-tip geometry of a propagating crack is defined by the radius and the crack-opening displacement which is dependent on the true fracture strain at the crack tip. A relation between critical crack-opening displacement and true fracture strain in the CVN specimen for medium and high strength 4340 cast steels is shown in Figure 63.

Figure 64 shows the normalized COD_{Id} and $\varepsilon_{f,CVN}$ of the 0.007%P and 0.049%S, 0.050%P and 0.012%S steels compared to the 0.012%P and 0.011%S steel at both medium and high strength levels. The result clearly indicates that phosphorus embrittles the steel at low temperature. Some recovery in the normalized COD_{Id} value of the 0.050%P steel below -200°F occurs when the reference 0.012%P and 0.011%S steel also becomes brittle. This confirms the results shown in Figures 33A and 34A, where the variation in Charpy V-notch impact energy (dashed line) passes through a maximum in each case. Enzian also observed a similar effect of phosphorus on the work-embrittleness behavior of low carbon steel. The maximum detrimental effect of phosphorus occurs at intermediate amount of cold work. (4) Sulfur reduces the ductility and therefore toughness of the steel at higher temperatures as indicated in Figure 64. At the cross over temperature, phosphorus and sulfur equally embrittle the steel.

Figure 65 is a similar plot to Figure 64. The effect of the strength level of high sulfur steel on the normalized critical crack-opening displacement is shown in Figure 65A, and that of high phosphorus steel on the normalized critical crack-opening displacement is indicated in Figure 65B. It is noted that phosphorus is more detrimental to the COD_{Id} and therefore the fracture toughness of 4340 cast steel at the higher strength level over a wide temperature range. Sulfur reduces the COD_{Id} at all temperatures. This reduction is more pronounced for lower strength steel.

C. Fractographs of Fractures

C.1. Mode of Fracture as Affected by P and S

Examination of the fracture surfaces of the Charpy V-notch specimens for the high phosphorus versus high sulfur steels at both strength levels shows a distinct fibrosity transition for the lower strength steel. The high strength steel has a brittle fracture at low temperature that becomes only somewhat more ductile at high temperature. Examination of the fracture of medium strength steel under the scanning electron microscope indicates the following.

1) Below the cross over temperature, -200°F, the fracture of 0.049%S high sulfur steel consists of mixed quasicleavage facets and dimples interconnected by tear ridges; the large dimples are nucleated by sulfide inclusions. The fracture of 0.050%P high phosphorus steel is characterized by quasicleavage features.

2) Above the cross over temperature, 80°F, the fracture of 0.049%S high sulfur steel exhibits ductile dimples. Whereas the fracture of 0.050%P high phosphorus steel is characterized by mainly ductile dimples and small percentage of quasicleavage.

Scanning electron microscope examination of the fracture of high strength steels demonstrates the following characteristics.

1) Below the cross over temperature, -20°F, the fracture of 0.049%S high sulfur steel consists of mainly shallow dimples together with few quasicleavage facets. The fracture of 0.050%P high phosphorus steel is characterized by quasicleavage facets connected by tear ridges.

2) Above the cross over temperature, 320°F, the fracture of 0.049%S high sulfur steel shows a mix of ductile and shallow dimples. The fracture of 0.050%P high phosphorus steel exhibits a mix of mainly dimples and a small percentage of quasicleavage features.

It is apparent from the above discussion that phosphorus embrittles the steel by changing the mode of fracture from dimple to a quasicleavage mechanism at all temperatures; however, this deleterious effect becomes more pronounced at lower temperatures. Since no intergranular fractures were found in even the high phosphorus, medium and high strength steels, it is concluded that phosphorus embrittles the steels studied only through increasing the friction stress.

Sulfur is more deleterious at high temperatures. More dimples are produced by decohesion of sulfide inclusion from the matrix in the medium and high strength steels broken at 320°F than for the same steels broken at -320°F. Since decohesion of sulfide inclusion from the matrix involves plastic deformation, the reduced plastic deformation and quasicleavage at low temperatures provide less chance of an encounter between the crack path and sulfide inclusions.

C.2. Mode of Fracture as Affected by Strength Level

It has been noted that the medium strength 4340 steel undergoes a distinct fibrosity transition, while the high strength 4340 steel does not. It also has been suggested in Sec. B.1., Chapter V that the failure for a relaxation of triaxial stress state to occur above the brittleness transition temperature of the high strength 4340 steel may be responsible for a lack of fibrosity transition of this steel.

At very low temperature, the fractures of both medium and high strength 4340 cast steels exhibit quasicleavage features. Examination of fractures broken at room temperature, which is above the brittleness transition temperature, shows the following.

1) The fracture of medium strength steel consists of ductile dimples on a rolling fracture surface.

2) The fracture surface of high strength steel is comprised of shallow dimples connected by tear ridges on a fairly flat fracture surface. The

tear ridge is a ligament broken behind the main crack front and is a sign of localized plane stress state fracture. This difference is considered responsible for a large difference in the measured lateral expansion between medium and high strength 4340 cast steels.

VI. CONCLUSIONS

1. Although increasing content of both phosphorus and sulfur lowers the toughness of steel, the effect of these individual elements varies significantly. The toughness was reduced by larger amounts of each element whether measured by Charpy V-notch transition curves for regular or precracked notches, or by fracture toughness measurements. Higher phosphorus raises the transition temperature of the Charpy curves and lowers the static, room temperature, fracture toughness of the medium and high strength steels. However, higher sulfur content has little effect on the transition temperature but lowers the ductile shelf energy and insignificantly reduces the static fracture toughness of the high strength steel. Because of this different behavior of the two elements, utilizing the sum of the two in preference to individual maxima could fail to provide the same relative toughness under various stress conditions.

2. The reason that phosphorus and sulfur affect the toughness differently is because of the diverse mechanisms by which this toughness is lowered. Phosphorus is present in supersaturated solid solution below about 200°F and increases the friction stress for dislocation motion through the lattice, thereby embrittling the steel. The sulfur has no solubility in the steel and forms sulfide inclusions that reduce the cohesive strength between the inclusion and matrix interface of the steel, thereby facilitating fracture but without the embrittling influence of phosphorus.

3. For equal amounts of phosphorus and sulfur, their different effects on the transition curves result in a cross over temperature for the two steels. Above the cross over temperature, the higher phosphorus steel has higher fracture energy and below this temperature, the higher sulfur steel has higher energy. This cross over temperature occurs at relatively low temperatures (about -115°F) for the medium strength (150 ksi yield strength) steel and at higher temperature (about 150°F) for the high strength (220 ksi yield strength) steel. These cross over temperatures are raised for the sharper notch obtained with the precracked Charpy tests. This cross over temperature behavior is consistent with the effect of these elements on the measured toughness and the mechanism by which each lowers the toughness. Good correlation between the toughness and the phosphorus plus sulfur only occurs at these cross over temperatures.

4. In addition to the primary objective of this study discussed in the above conclusions, several other behavioral characteristics of phosphorus and sulfur were observed during the testing.

(a) Phosphorus increases the notch toughness sensitivity of the steel but sulfur decreases this sensitivity.

(b) The fatigue crack growth rate correlates with the fracture toughness. Phosphorus and sulfur have a small deleterious effect on the fatigue crack growth rate of 150 ksi yield strength steel. However at the 220 ksi yield strength level, phosphorus sharply increases the fatigue crack growth rate while sulfur has virtually no effect.

(c) Phosphorus increases the tensile yield strength, the temperature dependence of yield strength, and decreases cleavage fracture strength; these factors raise the ductile to brittle transition temperature and promote the quasicleavage mode of fracture.

(d) The medium strength 4340 steel undergoes a distinct fibrosity transition, while the high strength 4340 steel does not. This is attributed to a lack of relaxation in triaxial stress state above the brittleness transition temperature.

5. A computer analysis undertaken to determine the individual and collective effect of phosphorus and sulfur on the toughness of steels was successfully employed to show the influence of each element and their sum. The results of computer analysis were confirmed by the subsequent systematic experiments.

VII. REFERENCES

1. Webster, W.R., "Standard Specifications for Structural Steel for Bridges, Proc. ASTM, 1909, p. 37.

2. Burgess, G.K., "Progress Report of the Joint Committee on Investigation of the Effect of Phosphorus and Sulfur in Steel", Proc. ASTM, vol. 28, Part I, 1928, p. 95.

3. Hopkins, B.E. and Tipler, H.R., "The Effect of Phosphorus on the Tensile and Notch-impact Properties of High Purity Iron and Iron-Carbon Alloys", J.I.S.I., March 1958, pp. 218-237.

4. Enzian, G.H., "Effects of Phosphorus and Nitrogen on the Properties of Low Carbon Steel", Journal of Metals, February 1950, pp. 346-353.

5. Sims, C.E. and Dahle, F.B., "Effect of Aluminum on the Properties of Medium Carbon Cast Steel", Trans. American Foundryman's Association, vol. 46, 1938, pp. 65-103.

6. Elliott, R.P., Constitution of Binary Alloys, First Supplement, McGraw-Hill, New York, 1965, p. 424.

7 Hansen, M., Constitution of Binary Alloys, 2nd Ed., McGraw-Hill, New York, 1958

8. Gray and Ductile Iron Castings Handbook, Gray and Ductile Iron Founders' Society Inc., Cleveland, 1973, p. 112.

9. Poole, S.W. and Franklin, J.E., "High-Strength Structural and High-Strength Low-Alloy Steels, Metals Handbook, ASM, vol. 1, 9th Ed., 1978, p. 411.

10. Hondros, E.D. and Seah, M.P., "Grain Boundary Activity Measurement by Auger Electron Spectroscopy", Scripta Metall., vol. 6, 1972, pp. 1007-1012.

11. Briant, C.L. and Banerji, S.K., "Intergranular Failure in Steel: the Role of Grainboundary Composition", International Metals Reviews, No. 4, 1978, pp. 164-199.

12. McMahon, C.J., Cignelli, A.K. and Feng, H.C., "The Influence of Mo on P-Induced Temper Embrittlement in Ni-Cr Steel", Metall. Trans. A, vol. 8A, July 1977, pp. 1055-1057.

13. Yarwood, J.C., Flemings, M.C. and Elliott, J.F., "Inclusion Formation in the Fe-O-S System", Metall. Trans., vol. 2, 1971, pp. 2573-2588.

14. Flemings, M.C., Solidification Processing, McGraw-Hill Book Company, Inc., New York, 1974.

15. Brown, L.M. and Ham, R.K., "Dislocation - Particle Interactions", Ed. by Kelley, A. and Nicholson, R.B., Strengthening Methods in Crystals, 1971.

16. Tetelman, A.S. and McEvily, A.J., Fracture of Structural Materials, John Wiley & Sons, Inc., New York, 1967.

17. Wrights, J.A. and Quarrell, A.G., "The Effect of Chemical Composition on the Occurrence of Intergranular Fracture in Steel Castings Containing Aluminum and Nitrogen", J.I.S.I., vol. 200, April 1962, pp. 299-307.

18. Jackson, W.J., "QT 35 Cast Steels", Iron and Steel, vol. 44, April 1971, pp. 115-123.

19. Gill, G.M. Sweeney, B. and Bradshaw, J., "Factor Affecting the Properties of Cast 13% Cr Steels", British Foundryman, vol. 59, November 1966, pp. 463-473.

20. Hodge, J.M., Frazier, R.H. and Boulger, F.W., "The Effects of Sulfur on the Notch Toughness of Heat Treated Steels", Trans. AIME, vol. 215, October 1959, pp. 745-753.

21. Zotos, J., "Cast Low Alloy Steels Ductility and Toughness", Trans. AFS, vol. 67, 1959, pp. 698-704.

22. Breznyak, E. and Wallace, J.F., "The Effect of Sulfur and Phosphorus on the Dynamic Properties of Cast Steels", Steel Founders' Society Research Report No. 71, October 1968.

23. Dutcher, D., Byers, D. and Wieser, P., "The Nil Ductility Transition Temperature of Cast Steels", SFSA Report No. 75, August 1971.

24. Sigala, P.C., "The Influence of Chemical Composition and Heat Treatment on the Toughness of Cast Railroad Component Steel", Master Thesis, Case Western Reserve University, Cleveland, 1977.

25. Larson, H.R. and Herlihy, F.B., "Development of Low Alloy Steel Compositions Suitable for High Strength Steel Castings", Trans. AFS, vol. 67, 1959, pp. 718-731.

26. Birkle, A.J., Wei, R.P. and Pellissier, C.E., "Analysis of Plane-Strain Fracture in a Series of 0.45C-Ni-Cr-Mo Steels with Different Sulfur Contents", Trans. ASM, vol. 59, 1966, pp. 981-990.

27. Kula, E.B. and Anctil, A.A., "Tempered Martensite Embrittlement and Fracture Toughness in SAE 4340 Steel", Journal of Materials, vol. 4, December 1969, pp. 817-841.

28. Groves, M.T. and Wallace, J.F., "Plane Strain Fracture Toughness of Cast Steel", Journal of Steel Castings Research, No. 74, March 1976, pp. 1-15.

29. Mickelson, C.G., "How Do Sulfur and Phosphorus Affect Cast Steel?", Metal Progress, January 1964, pp. 84-86.

30. Wullaert, R.A., "Applications of the Instrumented Charpy Impact Test", ASTM STP 466, ASTM, 1970, pp. 148-164.

31. Griffith, A.A., "The Phenomena of Rupture and Flaw in Solids", Trans. Royal Society of London, A-221, 1920.

32. Inglis, C.E., "Stresses in a Plate Due to the Presence of Cracks and Sharp Corners", Proc. Institute of Naval Architects, 1913.

33. Irwin, G.R., "Fracture Dynamics", in Fracturing of Metals, ASM, Cleveland, 1948.

34. Orowan, E., "Fracture Strength of Solids", in Report on Progress in Physics, vol. 12, Physical Society of London, 1949.

35. Irwin, G.R., "Analysis of Stresses and Strains Near the End of a Crack Traversing a Plate", Trans. ASME, J. of Applied Mechanics, vol. 24, 1957.

36. Westergaard, H.M., "Bearing Pressures and Cracks", Trans. ASME, J. of Applied Mechanics, 1939.

37. Stephens, R.I., "Linear Elastic Fracture Mechanics and Its Application to Fatigue", SAE Paper No. 740220, 1974.

38. Wells, A.A., "Unstable Crack Propagation in Metals - Cleavage and Fast Fracture", Proc. of the Crack Propagation Symposium, The College of Aeronautics, Cranfield, England, 1961, pp. 210-230.

39. Robinson, J.N. and Tetelman, A.S., in Fracture Toughness and Slow - Stable Cracking, ASTM STP 559, ASTM, 1974.

40. Shabbits, W.O., Pryle, W.H. and Wessel, E.T., "Heavy Section Fracture Toughness Properties of A533 Grade B Class 1 Steel Plate and Submerged Arc Weldment", HSSTP-TR-6, 1969.

41. Shabbits, W.O., "Dynamic Fracture Toughness Properties of Heavy Section A533 Grade B Class 1 Steel Plate", HSSTP-TR-13, 1970 (WLAP-7623).

42. Server, W.L., Ireland, D.R. and Wullaert, R.A., "Strength and Toughness Evaluations from an Instrumented Impact Test", Effects Technology, Inc., TR 74-29, 1974.

43. Server, W.L. and Tetelman, A.S., "The Use of Pre-Cracked Charpy Specimens to Determine Dynamic Fracture Toughness", Engineering Fracture Mechanics, Vol. 4, 1972, pp. 367-375.

44. "Methods for Crack Opening Displacement (COD) Testing", British Standards Institution Draft for Development 19, London, 1972.

45. "Fracture Toughness Evaluation by R-Curve Methods", ASTM STP 527, ASTM, 1973.

46. Novak, S.R., "Resistance to Plane-Stress Fracture (R-Curve Behavior) of A572 Structural Steel", ASTM STP 591, ASTM, 1976.

47. "Recommended Practice for R-Curve Determination", ASTM Annual Book of Standards, Part 10, ASTM, 1975.

48. Rice, J.R., "A Path Independent Integral and the Approximate Analysis of Strain Concentration by Notches and Cracks", J. of Applied Mechanics, Trans. ASME, 1968.

49. Begley, J.A. and Landes, J.D., "The J-Integral as a Fracture Criterion", ASTM STP 514, ASTM, 1972, pp. 1-20.

50. Landes, J.D. and Begley, J.A., "The Effect of Specimen Geometry on J_{Ic}", ASTM STP 514, ASTM, 1972, pp. 24-39.

51. Landes, J.D., Walker, H. and Clarke, G.A., "Evaluation of Estimation Procedures Used in J-Integral Testing", Elastic-Plastic Fracture, ASTM STP 668, ASTM, 1979, pp. 266-287.

52. Berger, C., Keller, H.P. and Munz, D., "Determination of Fracture Toughness with Linear-Elastic and Elastic-Plastic Methods", Elastic-Plastic Fracture, ASTM STP 668, ASTM, 1979, pp. 378-405.

53. Landes, J.D. and Begley, J.A., "Test Results from J-Integral Studies--An Attempt to Establish J_{Ic} Testing Procedures", ASTM STP 560, 1974, pp. 170-186.

54. Paranjpe, S.A. and Banerjee, S., "Interrelation of Crack Opening Displacement and J-Integral", Engineering Fracture Mechanics, Vol. 11, 1979, pp. 43-53.

55. Witt, F.J., "Equivalent Energy Procedures for Predicting Gross Plastic Fracture", Fourth National Symposium on Fracture Mechanics, Carnegie Mellon University, August 1970.

56. Witt, F.J. and Mager, T.R., "A Procedure for Determining Bounding Values on Fracture Toughness, K_{Ic} at Any Temperature", Fifth National Symposium on Fracture Mechanics, University of Illinois, September 1971.

57. Ezekiel, M. and Fox, K.A., Methods of Correlation and Regression Analysis, Linear and Currilinear, 3rd Ed., John Wiley & Sons, Inc., New York, 1959.

58. Kerlinger, F.N. and Pedhazur, E.J., Multiple Regression in Behavioral Research, Holt, Rinehart and Winston, Inc., 1973.

59. Yamane, T., Statistics--An Introductory Analysis, Harper & Row Company, 1964.

60. Nie, N.H., Bent, D.H., and Hull, C.H., Statistical Package for the Social Sciences, 2nd Ed., McGraw-Hill Book Co., Inc., 1975.

61. Ireland, D.R. and Server, W.L., Utilization of Dynatup Velocometer, Effects Technology, Inc., TR72-16, 1972.

62. Dynatup Technical Literature, Effects, Technology, Inc., Bulletin D102, 1980.

63. Operator's Manual, Automated Materials Test System, No. 914.80, MTS System Corp., Minneapolis, Minnesota.

64. JIS Hand Book--Ferrous Materials and Metallurgy, Japanese Standards Association, 1974, Tokyo, Japan.

65. Imhof, E.J. and Barsom, J.M., "Fatigue and Corrosion Fatigue Crack Growth of 4340 Steel at Various Yield Strength", ASTM STP 536, ASTM, 1973, pp. 182-205.

66. Bertolo, R.B., Fracture Toughness of Aluminum Die Casting Die Steels, Ph.D. Thesis, Case Western Reserve University, Cleveland, 1976.

67. Clausing, D.P., "Effect of Plastic Strain State on Ductility and Toughness", International Journal of Fracture Mechanics, Vol. 6, No. 1, 1970.

68. Wilshaw, T.R., "The Deformation and Fracture of Mild Steel Charpy Specimens", SU-DMS Report No. 66-6, Stanford University January 1966.

69. Briggs, C.W., Ed., Steel Castings Handbook, 4th Ed., Steel Founders Society of America, 1974, pp. 419-421.

TABLE 1. REGRESSION ANALYSIS of the CORRELATION BETWEEN IZOD IMPACT ENERGY at ROOM TEMPERATURE and PHOSPHORUS and SULFUR CONTENTS for AISI 4335 CAST STEELS. DATA from LARSON and HERLIHY.(25)

Alloy	C(%)	P(%)	S(%)	Tempering Temp. (F°)	Izod (ft-lb)	Izod Normal. for Carbon* (ft-lb)	Izod Normal. for Tempering Temp.** (ft-lb)	Izod Normal. (ft-lb)
57-306	0.36	0.013	0.027	975	16.3 (Av.)	+0.5	--	16.8
58-386	0.35	0.012	0.024	975	18.4 (Av.)	+0.2	--	18.6
58-064-1	0.34	0.014	0.025	975	18.0	--	--	18.0
58-069-1	0.34	0.016	0.029	975	22.3	--	--	22.3
58-069-2	0.33	0.028	0.027	975	21.0	-0.2	--	20.8
58-071-2	0.36	0.022	0.028	975	17.3	+0.5	--	17.8
58-077-1	0.34	0.014	0.024	975	19.3	--	--	19.3
58-077-2	0.34	0.015	0.026	975	18.3	--	--	18.3
58-080-1	0.35	0.016	0.023	975	20.4	+0.2	--	20.6
58-080-2	0.34	0.019	0.023	975	15.1 (Av.)	--	--	15.1
58-082-1	0.33	0.016	0.026	975	19.0	-0.2	--	18.8
58-082-2	0.33	0.016	0.025	975	16.3	-0.2	--	16.1
58-049-2	0.35	0.025	0.030	975	15.3	+0.2	--	15.5
58-ARC-114	0.34	0.013	0.010	975	20.0	--	--	20.0
57-293	0.25	0.005	0.008	850	26.3	-1.9	+5.0	29.4
57-355	0.25	0.022	0.016	850	18.2	-1.9	+5.0	21.3
57-296	0.28	0.007	0.028	850	18.7	-1.2	+5.0	22.5

* Izod Impact Energy normalized to 0.34%C based on Figure 12.(25)

** Izod Impact Energy normalized to Tempering Temp. at 975°F based on Figure 17.(25)

TABLE 1. (continued)

$Izod = B_0 + B_1P + B_2S$	R	STD ERROR B_0	STD ERROR B_1	STD ERROR B_2
Izod = 23.97 - 279.7P	-0.4848	3.058	130.3	--
Izod = 26.68 - 306.5S	-0.5699	2.873	--	114.1
Izod = 28.00 - 177.9P - 241.2S	-0.6365	2.791	129.3	120.6

$Izod = B_0 + B_1 (P + S)$	R	STD ERROR B_0	STD ERROR B_1
Izod = 27.83 - 211.1 (P + S)	-0.6334	2.705	60.60

TABLE 2. REGRESSION ANALYSIS of the CORRELATION BETWEEN CHARPY V-NOTCH IMPACT ENERGY and PHOSPHORUS and SULFUR CONTENTS for MEDIUM CARBON CAST STEELS. DATA from WRIGHT and QUARRELL.(17)

ALLOY	P(%)	S(%)	CVN (ft-lb)
17A	0.009	0.021	55.0
17B	0.008	0.030	25.5
17C	0.008	0.041	15.0
17D	0.009	0.053	10.0
18A	0.010	0.005	109.0
18B	0.010	0.008	104.0
18C	0.006	0.011	104.0
24B	0.022	0.017	42.0
24C	0.037	0.020	41.5
24D	0.077	0.021	30.5

$CVN = B_0 e^{-(B_1 P + B_2 S)}$	R	STD ERROR B_0	STD ERROR B_1	STD ERROR B_2
$CVN = 44.42e^{-4.182P}$	-0.1133	2.380	12.97	---
$CVN = 135.9e^{-52.86S}$	-0.9621	1.269	---	5.297
$CVN = 161.9e^{-(7.663P + 53.95S)}$	-0.9840	1.181	2.497	3.714

$CVN = B_0 e^{-B_1 (P + S)}$	R	STD ERROR B_0	STD ERROR B_1
$CVN = 100.4e^{-21.22(P + S)}$	-0.6608	1.925	8.521

TABLE 3. REGRESSION ANALYSIS of the CORRELATION BETWEEN CHARPY V-NOTCH IMPACT ENERGY at -20°F and PHOSPHORUS and SULFUR CONTENTS for AISI 4325 CAST STEELS. DATA from ZOTOS.(21)

ALLOY	P(%)	S(%)	CVN (ft-lb)
A	0.010	0.037	14.2
B	0.009	0.032	18.4
C	0.010	0.028	23.5
D	0.008	0.024	34.2
E	0.012	0.017	35.6
F	0.009	0.014	36.5
G	0.012	0.010	34.1
H	0.009	0.008	38.6
I	0.010	0.007	38.8

$CVN = B_0 + B_1P + B_2S$	R	STD ERROR B_0	STD ERROR B_1	STD ERROR B_2
$CVN = 25.16 + 532.8P$	0.0786	9.856	2554.0	---
$CVN = 45.76 - 779.5S$	-0.9281	3.681	---	118.2
$CVN = 56.29 - 1006.0P - 808.9S$	-0.9393	3.665	977.5	121.1

$CVN = B_0 + B_1(P + S)$	R	STD ERROR B_0	STD ERROR B_1
$CVN = 54.26 - 806.0(P + S)$	-0.9388	3.406	111.8

TABLE 4. REGRESSION ANALYSIS of the CORRELATION BETWEEN FRACTURE TOUGHNESS and PHOSPHORUS and SULFUR CONTENTS for AISI 4340 WROUGHT STEELS TEMPERED at 700°F and 400°F. DATA from KULA and ANCTIL.(27)

ALLOY	P(%)	S(%)	K_{Ic}(400°F)* (KSI $\sqrt{IN}$)	K_{Ic}(700°F)* (KSI $\sqrt{IN}$)
21	0.006	0.005	55.0	73.0
20	0.010	0.005	48.0	79.5
22	0.009	0.008	40.5	63.5
--	0.015	0.009	45.0	76.0
18	0.012	0.015	28.0	65.0
22	0.019	0.026	26.0	37.5

* Estimate from Figure 13.(27)

K_{Ic} (400°F) = $B_0 + B_1P + B_2S$	R	STD ERROR B_0	STD ERROR B_1	STD ERROR B_2
K_{Ic} (400°F) = 61.47 - 1779.0P	-0.7196	8.874	858.6	---
K_{Ic} (400°F) = 54.64 - 1255.0S	-0.8858	5.931	---	328.8
K_{Ic} (400°F) = 53.41 + 193.4P - 1348.0S	-0.8868	6.819	1211.0	694.0

K_{Ic} (400°F) = $B_0 + B_1(P + S)$	R	STD ERROR B_0	STD ERROR B_1
K_{Ic} (400°F) = 59.03 - 803.4(P + S)	-0.8579	6.566	240.6

TABLE 4. (continued)

K_{Ic} (700°F) = $B_0 + B_1P + B_2S$	R	STD ERROR B_0	STD ERROR B_1	STD ERROR B_2
K_{Ic} (700°F) = 91.36 - 2165.0P	-0.6596	12.75	1233.0	---
K_{Ic} (700°F) = 85.49 - 1741.0S	-0.9260	6.402	---	354.9
K_{Ic} (700°F) = 77.23 + 1292.0P - 2362.0S	-0.9505	6.083	1080.0	619.0

K_{Ic} (700°F) = $B_0 + B_1(P + S)$	R	STD ERROR B_0	STD ERROR B_1
K_{Ic} (700°F) = 90.56 - 1071.0(P + S)	-0.8618	8.602	315.2

TABLE 5. REGRESSION ANALYSIS of the CORRELATION BETWEEN CHARPY V-NOTCH IMPACT ENERGY and FRACTURE TOUGHNESS at ROOM TEMPERATURE and PHOSPHORUS and SULFUR CONTENTS for AISI 4335 CAST STEELS. DATA from GROVES and WALLACE.(28)

ALLOY	P(%)	(S%)	CVN (ft-lb)	K_{Ic} (KSI $\sqrt{IN}$)
25	0.012	0.019	25.5	105.4
31	0.044	0.040	6.0	60.6
32	0.066	0.066	3.0	47.7
33	0.023	0.029	6.0	84.1
39	0.046	0.025	3.5	66.9
40	0.056	0.050	2.0	55.5
41	0.013	0.026	8.5	81.5
43	0.015	0.024	11.0	96.0

$CVN = B_0 e^{-(B_1 P + B_2 S)}$	R	STD ERROR B_0	STD ERROR B_1	STD ERROR B_2
$CVN = 18.68e^{-32.78P}$	-0.8626	1.554	7.848	---
$CVN = 21.47e^{-36.30S}$	-0.7223	1.827	---	14.19
$CVN = 17.55e^{-(36.09P - 5.056S)}$	-0.8641	1.617	17.13	22.66

$CVN = B_0 e^{-B_1 (P + S)}$	R	STD ERROR B_0	STD ERROR B_1
$CVN = 21.91e^{-18.58(P + S)}$	-0.8298	1.627	5.100

TABLE 5. (continued)

$K_{Ic} = B_0 e^{-(B_1 P + B_2 S)}$	R	STD ERROR B_0	STD ERROR B_1	STD ERROR B_2
$K_{Ic} = 111.3e^{-12.57P}$	-0.9611	1.086	1.474	---
$K_{Ic} = 124.4e^{-15.57S}$	-0.9003	1.139	---	3.073
$K_{Ic} = 118.0e^{-(9.493P + 4.690S)}$	-0.9706	1.082	2.817	3.727

$K_{Ic} = B_0 e^{-B_1 (P + S)}$	R	STD ERROR B_0	STD ERROR B_1
$K_{Ic} = 121.1e^{-7.449(P + S)}$	-0.9672	2.143	0.7991

TABLE 6. REGRESSION ANALYSIS of the CORRELATION BETWEEN NIL DUCTILITY TRANSITION TEMPERATURE and PHOSPHORUS and SULFUR CONTENTS for Cr-Mo CAST STEELS. DATA from DUTCHER et al.(23)

ALLOY	P(%)	S(%)	NDTT (°F)
64	0.020	0.028	160
63	0.030	0.018	90
66	0.017	0.020	40
67	0.019	0.020	20
68	0.010	0.011	20
62	0.030	0.027	10
65	0.010	0.018	0

$NDTT = B_0 + B_1P + B_2S$	R	STD ERROR B_0	STD ERROR B_1	STD ERROR B_2
$NDTT = -20.10 + 3726.0P$	0.4613	55.67	3205.0	---
$NDTT = -41.35 + 4433.0S$	0.4484	56.09	---	3952.0
$NDTT = -59.43 + 2609.0P + 2954.0S$	0.5320	59.40	3858.0	4722.0

$NDTT = B_0 + B_1(P + S)$	R	STD ERROR B_0	STD ERROR B_1
$NDTT = -58.20 + 2758.0\ (P + S)$	0.5316	53.15	1965.0

TABLE 7. REGRESSION ANALYSIS of the CORRELATION BETWEEN 15 ft-lb TRANSITION TEMPERATURE and PHOSPHORUS and SULFUR CONTENTS for AAR GRADE B CAST STEELS. DATA from MICKELSON.(29)

ALLOY	P(%)	S(%)	TRANSITION TEMP (°F)
1	0.005	0.016	-15.0
2	0.010	0.016	-15.0
3	0.017	0.028	-10.0
4	0.010	0.027	- 7.0
5	0.009	0.037	- 5.0
6	0.026	0.020	0.0
7	0.032	0.010	0.0
8	0.016	0.023	0.0
9	0.037	0.010	5.0
10	0.028	0.031	5.0
11	0.021	0.015	6.0
12	0.039	0.032	7.0
13	0.038	0.027	11.0
14	0.035	0.019	15.0
15	0.029	0.040	18.0
16	0.038	0.042	20.0
17	0.024	0.039	26.0

TABLE 7. (continued)

TRANS. TEMP. = $B_0 + B_1P + B_2S$	R	STD ERROR B_0	STD ERROR B_1	STD ERROR B_2
TRANS. TEMP. = - 14.59 + 746.2P	0.7176	8.598	187.0	---
TRANS. TEMP. = - 10.97 + 572.7S	0.4982	10.70	---	257.3
TRANS. TEMP. = - 26.08 + 701.6P + 495.5S	0.8360	7.012	153.3	169.4

TRANS. TEMP. = $B_0 + B_1(P + S)$	R	STD ERROR B_0	STD ERROR B_1
TRANS. TEMP. = - 26.66 + 607.9 (P + S)	0.8264	6.952	107.0

TABLE 8. CHEMICAL ANALYSIS of CHARGING MATERIALS.

Electrolytic Nickel	Ni	99.9%								
H.C. Ferromolybdenum	C	3%*,	Mo	65%						
L.C. Ferrochromium	Cr	65%								
Electrolytic Manganese	Mn	99.9%								
Metallic Silicon	Si	98%								
Electrolytic Iron	Fe	99.9%,	C	0.003%,	Mn	0.004%,	P	0.001%,	S	0.002%
L.C. Steel Scrap	C	0.01%,	Mn	0.26%,	Si	0.04%,	P	0.01%,	S	0.01%
Pig Iron	C	4.03%,	Mn	0.76%,	Si	2.37%,	P	0.02%,	S	0.003%
Ferrophosphorus	P	24%								
Ferrosulfide	S	36.5%								

* Estimation

TABLE 9. CHEMICAL ANALYSIS of CASTINGS PRODUCED.

CASTING NO.	C	Mn	Si	Ni	Cr	Mo	P	S	Al (Total)	P + S
A	.37	.85	.38	1.86	.85	.29	.007	.049	.062	.056
B	.38	.72	.38	1.90	.85	.28	.022	.051	.075	.073
C	.39	.70	.38	1.88	.86	.29	.037	.051	.075	.088
D	.39	.68	.38	1.88	.86	.29	.054	.052	.085	.106
E	.37	.87	.42	1.85	.84	.29	.011	.036	.061	.047
F	.38	.74	.39	1.90	.85	.28	.025	.038	.086	.063
G	.39	.70	.39	1.89	.86	.29	.036	.036	.073	.072
H	.39	.69	.36	1.88	.86	.29	.053	.040	.077	.093
I	.37	.84	.42	1.85	.84	.29	.009	.027	.064	.036
J	.38	.74	.36	1.90	.85	.28	.023	.022	.073	.045
K	.38	.73	.39	1.90	.85	.28	.037	.023	.082	.060
L	.39	.71	.39	1.89	.85	.28	.050	.025	.082	.075
M	.38	.82	.34	1.86	.85	.29	.012	.011	.064	.023
N	.38	.83	.37	1.85	.84	.29	.025	.011	.058	.036
O	.38	.84	.37	1.86	.85	.29	.042	.011	.060	.053
P	.37	.80	.30	1.86	.85	.29	.050	.012	.060	.062

TABLE 10. EFFECT of SULFUR CONTENT on the VOLUME FRACTION (V%) of NON-METALLIC INCLUSIONS.

CASTING	S (wt. %)	SULFIDE (V%)	OXIDE PLUS MICROPOROSITY (V%)	TOTAL INCLUSION (V%)
A	0.049	0.29	0.42	0.71
B	0.051	0.31	0.22	0.53
C	0.051	0.32	0.37	0.69
D	0.052	0.34	0.23	0.57
E	0.036	0.18	0.29	0.47
F	0.038	0.24	0.21	0.45
G	0.036	0.20	0.25	0.55
H	0.040	0.20	0.30	0.50
I	0.027	0.13	0.21	0.34
J	0.022	0.13	0.27	0.40
K	0.023	0.15	0.17	0.32
L	0.025	0.14	0.23	0.37
M	0.011	0.07	0.20	0.27
N	0.011	0.06	0.22	0.28
O	0.011	0.06	0.26	0.32
P	0.012	0.08	0.17	0.25

TABLE 11. TENSILE PROPERTIES of 1100°F TEMPERED STEELS.

CASTING	HARDNESS (R_c)	0.2% Y.S. (ksi)	U.T.S. (ksi)	σ_f (ksi)	% EL.	% R.A.
A	34.9	147.8	152.0	180.4	8.5	16.6
B	35.0	149.4	152.4	171.9	6.6	14.0
C	35.0	149.5	154.7	178.8	7.8	15.7
D	35.5	150.2	152.2	170.1	5.5	12.6
E	34.6	147.3	156.4	191.6	10.1	19.9
F	35.0	146.0	155.3	182.8	8.0	17.5
G	35.1	149.9	152.7	175.7	6.5	15.5
H	35.1	147.6	153.8	177.4	8.0	16.4
I	35.2	145.6	158.9	201.8	12.0	23.6
J	35.0	145.6	155.2	185.7	9.0	18.8
K	34.6	152.6	159.6	191.3	9.0	19.1
L	35.0	152.7	156.1	181.6	7.0	16.3
M	34.9	144.8	161.3	213.5	13.5	28.1
N	35.1	146.6	159.4	204.3	12.0	24.8
O	34.8	151.2	157.1	187.2	10.5	18.4
P	35.2	149.5	156.5	189.5	9.4	19.8

TABLE 12. TENSILE PROPERTIES of 400°F TEMPERED STEELS.

CASTING	HARDNESS (R_C)	0.2% Y.S. (ksi)	U.T.S. (ksi)	σ_f (ksi)	% EL.	% R.A.
A	52.4	219.7	252.5	263.4	3.2	5.0
B	52.8	221.9	255.2	266.3	3.5	6.1
C	52.3	219.2	247.6	257.2	3.0	4.5
D	53.0	223.0	245.7	255.4	2.7	4.0
E	52.3	220.4	258.9	270.9	4.0	5.9
F	52.3	219.2	259.3	272.9	4.0	5.3
G	52.8	225.4	256.4	269.7	3.6	5.7
H	52.7	220.7	252.8	266.0	3.5	5.0
I	52.7	222.4	267.2	283.5	4.8	7.2
J	52.6	221.3	265.0	280.7	4.7	6.1
K	52.9	216.7	253.1	267.3	3.5	6.5
L	53.6	226.7	256.5	264.3	3.2	4.5
M	52.4	220.1	272.4	298.8	7.4	10.2
N	52.7	219.6	266.1	285.2	5.2	7.4
O	53.1	222.8	262.2	277.0	4.1	6.3
P	52.6	221.6	260.0	273.1	3.8	5.6

TABLE 13. IMPACT ENERGY (ft-lbs) of 1100°F TEMPERED 4340 CAST STEEL from CHARPY V-NOTCH IMPACT TEST.

	TEST TEMPERATURE, °F							
CASTING	-320	-200	-150	-110	-20	80	212	320
A	5.6	10.4	13.1	14.6	16.1	16.4	16.9	17.6
B	4.5	8.0	10.3	11.0	14.0	14.0	16.0	14.0
C	4.2	6.2	8.7	10.6	12.5	13.5	15.7	13.8
D	3.0	5.2	5.6	10.3	10.6	12.7	13.7	13.7
E	6.1	11.1	17.5	20.0	22.0	24.8	25.9	26.0
F	5.0	8.0	13.4	14.6	17.8	21.4	21.5	20.3
G	5.7	7.0	10.3	14.3	17.0	20.3	19.8	16.4
H	4.2	5.4	7.5	11.6	14.7	18.0	20.2	19.1
I	7.7	13.0	20.7	26.2	28.2	32.2	33.0	33.0
J	5.3	11.9	14.8	20.2	24.6	29.7	29.0	28.8
K	4.6	8.8	12.5	16.0	21.4	26.1	27.7	28.1
L	3.0	5.2	5.8	9.7	15.2	18.4	20.6	22.0
M	6.6	15.9	23.5	30.0	33.7	36.0	36.2	36.3
N	6.5	13.3	19.3	29.0	34.0	36.2	36.9	37.5
O	4.2	8.5	13.6	16.0	27.0	27.7	29.7	33.2
P	4.8	6.3	10.5	15.8	24.3	26.0	28.5	30.7

TABLE 14. LATERAL EXPANSION (mils) of 1100°F TEMPERED 4340 CAST STEEL FROM CHARP' V-NOTCH IMPACT TEST.

	TEST TEMPERATURE, °F							
CASTING	-320	-200	-150	-110	-20	80	212	320
A	0	4.0	7.4	7.8	9.7	9.9	12.0	12.9
B	0	0.8	4.2	6.2	7.7	8.5	9.7	10.0
C	0	0.3	3.4	5.3	6.8	7.7	8.5	9.3
D	0	0.3	0.6	4.7	5.6	6.2	8.6	8.7
E	0.3	3.1	9.6	9.9	13.7	16.9	18.6	18.6
F	0.1	3.2	6.0	8.0	11.0	13.8	12.6	15.5
G	0	2.0	5.6	6.3	9.5	12.7	13.7	13.8
H	0	1.4	2.6	4.9	8.5	11.9	11.5	11.2
I	1.4	5.6	10.7	13.5	15.6	18.0	20.6	23.6
J	0.2	5.6	8.1	9.8	15.1	18.2	17.7	22.7
K	0	1.2	5.3	6.6	12.7	16.5	17.9	18.4
L	0	0	1.3	5.6	7.8	7.3	11.2	14.8
M	0.3	8.5	12.2	18.2	20.2	19.0	23.4	29.4
N	1.6	5.5	10.8	15.6	18.0	20.5	22.3	27.2
O	0.5	1.7	6.3	8.4	17.4	15.0	19.9	24.7
P	0	0.4	5.5	8.1	13.4	17.0	18.7	23.9

TABLE 15. % SHEAR FRACTURE of 1100°F TEMPERED 4340 CAST STEEL from CHARPY V-NOTCH IMPACT TEST.

	TEST TEMPERATURE, °F							
CASTING	-320	-200	-150	-110	-20	80	212	320
A	3	50	90	100	100	100	100	100
B	2	20	50	80	100	100	100	100
C	2	10	40	70	100	100	100	100
D	1	5	25	60	100	100	100	100
E	3	30	80	100	100	100	100	100
F	2	25	60	80	100	100	100	100
G	3	20	40	70	100	100	100	100
H	1	10	20	50	100	100	100	100
I	5	30	80	100	100	100	100	100
J	2	25	60	90	100	100	100	100
K	1	10	40	80	100	100	100	100
L	1	5	20	50	100	100	100	100
M	3	45	80	100	100	100	100	100
N	3	30	60	80	100	100	100	100
O	1	20	40	70	100	100	100	100
P	2	10	30	60	100	100	100	100

TABLE 16. SUMMARY of CHARPY V-NOTCH IMPACT TEST RESULTS of 1100°F TEMPERED 4340 CAST STEEL.

CASTING	ROOM TEMP. ENERGY (ft-lbs)	UPPER SHELF ENERGY (ft-lbs)	LOWER SHELF ENERGY (ft-lbs)	50% ENERGY* (ft-lbs)	50% FIBROSITY TRAN. TEMP. (°F)	50% ENERGY TRAN. TEMP. (°F)
A	16.4	17.6	5.6	11.6	-200	-177
B	14.0	16.0	4.5	10.3	-150	-135
C	13.5	15.7	4.2	10.0	-140	-114
D	12.7	13.7	3.0	8.4	-123	-101
E	24.8	26.0	6.1	16.1	-180	-158
F	21.4	21.5	5.0	13.3	-166	-131
G	20.3	20.3	5.7	13.0	-135	-113
H	18.0	20.2	4.2	12.2	-110	- 92
I	32.2	33.0	7.7	20.4	-182	-151
J	29.7	29.7	5.3	17.5	-165	-130
K	26.1	28.1	4.6	16.4	-142	-106
L	18.4	22.0	3.0	12.5	-110	- 70
M	36.0	36.3	6.6	21.5	-194	-160
N	36.2	37.5	6.5	22.0	-166	-140
O	27.7	33.2	4.2	18.7	-138	- 92
P	26.0	30.7	4.8	17.8	-123	- 86

* Defined as Lower Shelf Energy + 1/2(Upper Shelf Energy - Lower Shelf Energy)

TABLE 17. IMPACT ENERGY (ft-lbs) of 400°F TEMPERED 4340 CAST STEEL FROM CHARPY V-NOTCH IMPACT TEST.

	TEST TEMPERATURE, °F							
CASTING	-320	-200	-150	-110	-20	80	212	320
A	4.6	4.7	5.5	6.3	6.3	6.8	7.3	6.1
B	4.2	4.5	4.6	4.4	5.7	6.0	6.4	5.6
C	3.5	3.5	4.1	4.3	4.6	5.0	6.3	5.3
D	2.1	2.6	3.8	3.4	3.5	4.5	4.6	5.4
E	4.9	5.0	4.8	6.3	7.1	8.5	9.3	7.3
F	4.2	4.6	4.9	5.3	6.5	7.8	7.9	6.8
G	3.8	4.0	5.0	5.0	6.0	6.9	8.1	7.7
H	2.3	3.5	3.5	3.8	4.5	5.8	7.2	6.6
I	4.8	5.0	7.9	7.9	11.1	12.8	12.0	10.5
J	4.6	5.7	6.6	5.7	7.3	9.8	9.5	8.7
K	3.6	4.2	4.9	5.2	5.7	7.2	8.5	7.8
L	2.0	2.6	2.8	3.2	3.5	4.8	6.2	6.9
M	4.7	7.3	7.5	8.1	11.5	13.5	14.0	13.7
N	3.8	5.6	6.8	6.8	8.7	12.3	13.5	13.1
O	2.7	4.2	4.5	4.2	5.5	7.7	10.7	11.3
P	2.6	3.5	3.9	4.2	4.5	6.4	8.0	9.2

TABLE 18. LATERAL EXPANSION (mils) of 400°F TEMPERED 4340 CAST STEEL from CHARPY V-NOTCH IMPACT TEST.

	TEST TEMPERATURE, °F							
CASTING	-320	-200	-150	-110	-20	80	212	320
A	0.2	0.3	0.1	0.6	0.8	1.1	1.5	1.4
B	0.1	0.1	0.8	0.4	0.5	0.8	1.9	1.1
C	0.1	0.2	0.4	0.4	0.3	0.5	1.0	0.7
D	0	0	0.1	0	0.2	0.4	1.1	0.6
E	0.2	0.5	0.4	1.2	1.4	1.5	1.9	2.6
F	0.3	0.3	0.1	0.3	0.5	2.4	1.8	2.2
G	0.2	0.6	0.2	0.5	0.2	0.9	1.5	1.7
H	0	0	0.4	0.2	0.2	0.5	1.2	0.9
I	0.3	0.2	0.5	0.2	1.0	3.6	3.9	3.6
J	0.2	0.2	0.3	0.2	1.2	3.0	3.6	2.8
K	0	0.2	0.2	0.2	0.8	2.3	2.5	2.2
L	0	0	0	0.2	0.5	1.4	2.2	2.5
M	0.2	0.3	0.2	0.7	1.9	4.0	4.2	3.4
N	0.2	0	0.4	0.5	0.6	2.6	3.2	3.4
O	0.1	0.3	0.3	0.5	2.0	1.5	2.0	2.9
P	0	0	0.1	0.2	0.4	0.7	2.8	2.9

TABLE 19. SUMMARY of CHARPY V-NOTCH IMPACT TEST RESULTS of 400°F TEMPERED 4340 CAST STEEL.

CASTING	ROOM TEMP. ENERGY (ft-lbs)	UPPER SHELF ENERGY (ft-lbs)	LOWER SHELF ENERGY (ft-lbs)	50% ENERGY* (ft-lbs)	50% ENERGY TRAN. TEMP. (°F)
A	6.8	7.3	4.6	6.0	-100
B	6.0	6.4	4.2	5.3	- 45
C	5.0	6.3	3.5	4.9	- 10
D	4.5	5.4	2.1	3.8	0
E	8.0	9.3	4.9	7.1	- 40
F	7.8	7.9	4.2	6.1	- 65
G	6.9	8.1	3.8	6.0	- 40
H	5.8	7.2	2.3	4.8	0
I	12.8	12.8	4.8	8.8	-100
J	9.8	9.8	4.6	7.2	- 55
K	7.2	8.5	3.6	6.1	- 10
L	4.8	6.9	2.0	4.5	60
M	13.5	14.0	4.7	9.4	- 90
N	12.3	13.5	3.8	8.7	- 40
O	7.7	11.3	2.7	7.0	45
P	6.4	9.2	2.6	5.9	45

* Defined as Lower Shelf Energy + 1/2(Upper Shelf Energy - Lower Shelf Energy)

TABLE 20. PLANE STRAIN FRACTURE TOUGHNESS of 1100°F TEMPERED 4340 CAST STEEL.

CASTING	a/W	P_Q (lbs)	$2.5(\frac{K_Q}{\sigma_Y})^2$ (in)	K_Q (ksi$\sqrt{in}$)
A	0.530	12,875	1.08	97.0
B	0.520	12,365	0.91	90.0
C	0.519	11,400	0.77	82.7
D	0.523	11,200	0.75	82.5
E	0.516	15,250	1.38	109.5
F	0.524	14,375	1.32	105.9
G	0.516	14,000	1.12	100.5
H	0.528	12,870	1.06	96.1
I	0.523	17,200	1.88	126.2
J	0.520	16,300	1.66	118.6
K	0.522	15,450	1.37	113.1
L	0.523	15,130	1.32	111.1
M	0.520	17,750	1.99	129.2
N	0.521	17,950	2.00	131.0
O	0.524	16,200	1.56	119.4
P	0.522	15,625	1.46	114.4

TABLE 21. PLANE STRAIN FRACTURE TOUGHNESS of 400°F TEMPERED 4340 CAST STEEL.

CASTING	a/W	P_Q (lbs)	$2.5(\frac{K_{Ic}}{\sigma_{Ys}})^2$ (in)	K_{Ic} (ksi$\sqrt{in}$)
A	0.482	8,800	0.168	57.0
B	0.504	7,610	0.141	52.6
C	0.498	6,490	0.101	44.1
D	0.505	5,540	0.074	38.4
E	0.493	8,725	0.175	58.3
F	0.508	7,500	0.143	52.5
G	0.502	6,260	0.091	43.0
H	0.492	6,000	0.082	39.9
I	0.489	8,950	0.177	59.1
J	0.511	7,150	0.134	51.2
K	0.508	6,400	0.107	44.8
L	0.488	5,850	0.072	38.5
M	0.506	8,780	0.192	61.0
N	0.479	9,030	0.173	57.8
O	0.520	6,410	0.111	46.9
P	0.503	5,850	0.083	40.3

TABLE 22. DYNAMIC FRACTURE TOUGHNESS (K_{Id} in ksi$\sqrt{in}$) DATA for 1100°F TEMPERED STEELS.

	TEST TEMPERATURE, °F							
CASTING	-320	-200	-150	-110	-20	80	212	320
A	60.8	75.1	94.4	94.9	96.6	96.9	97.8	96.0
B	54.0	71.7	82.3	86.9	92.0	92.2	90.9	90.1
C	42.4	56.4	74.4	77.0	85.0	83.6	90.5	82.5
D	36.8	47.4	57.2	71.4	76.5	75.4	79.1	76.3
E	52.2	83.2	96.0	106.1	109.7	111.0	104.7	107.7
F	43.2	66.3	82.6	94.2	99.6	102.8	98.9	107.0
G	41.5	58.2	73.7	93.7	106.9	105.3	101.4	103.3
H	41.2	53.5	70.9	80.6	98.8	96.1	95.8	88.7
I	55.7	88.0	108.5	120.9	126.4	126.0	121.4	124.5
J	50.9	75.4	97.7	114.2	118.1	118.5	112.9	116.6
K	42.2	54.2	84.7	98.2	111.3	116.8	107.4	112.8
L	36.4	49.5	69.8	88.8	97.2	102.8	103.7	96.3
M	58.1	96.3	123.1	124.0	133.9	133.5	131.3	130.7
N	48.2	82.6	109.7	125.5	135.6	133.0	130.4	135.2
O	40.6	53.5	82.5	98.8	123.5	121.1	129.0	122.9
P	40.3	55.8	73.8	96.5	110.6	114.6	113.2	115.3

TABLE 23. DYNAMIC FRACTURE TOUGHNESS (K_{Id} in ksi$\sqrt{in}$) DATA for 400°F TEMPERED STEELS.

	TEST TEMPERATURE, °F						
CASTING	-320	-110	-20	80	212	320	400
A	26.5	47.5	53.4	59.4	60.6	55.1	59.6
B	23.8	36.7	50.4	51.4	54.0	49.0	51.8
C	24.9	30.5	40.5	45.5	47.6	50.1	48.2
D	20.5	30.1	33.2	39.4	47.9	49.0	47.6
E	25.2	40.0	54.2	61.8	58.1	62.2	60.6
F	21.1	32.4	42.9	50.2	56.0	57.8	56.7
G	24.0	29.5	41.3	49.4	57.8	59.8	58.3
H	22.9	29.3	40.1	45.3	48.9	51.9	49.1
I	22.0	36.8	52.8	62.4	66.1	67.0	68.2
J	22.8	34.1	50.5	52.7	62.2	65.3	63.9
K	20.5	27.8	40.6	46.6	63.7	57.1	62.6
L	21.0	28.6	39.0	38.1	48.3	50.6	60.1
M	26.3	49.3	60.0	68.3	73.6	72.9	68.6
N	21.6	35.8	49.1	56.6	66.6	73.3	74.1
O	21.2	30.0	42.3	43.9	61.2	68.8	67.0
P	20.3	30.3	37.9	45.3	55.1	64.1	68.3

TABLE 24. FATIGUE CRACK GROWTH RATE (10^{-6} in/cycle) of 1100°F TEMPERED 4340 CAST STEEL.

	STRESS INTENSITY FACTOR RANGE, ΔK, ksi$\sqrt{in}$				
CASTING	30	35	40	50	60
A	6.6	11.0	14.6	33.0	57.0
B			13.0		
C			14.8		
D			14.6		
E			12.3		
F			13.3		
G			13.4		
H			14.5		
I			11.8		
J			13.2		
K			12.1		
L			13.8		
M	6.6	10.8	11.7	25.5	44.0
N			12.3		
O			12.7		
P	6.8	11.0	13.2	30.0	46.0

TABLE 25. FATIGUE CRACK GROWTH RATE (10^{-6} in/cycle) of 400°F TEMPERED 4340 CAST STEEL.

	STRESS INTENSITY FACTOR RANGE, ΔK, ksi$\sqrt{in}$				
CASTING	15	20	25	30	35
A	2.1	4.7	7.6	10.6	17.0
B		5.0			
C		8.0			
D		9.6			
E		4.7			
F		4.8			
G		6.8			
H		9.0			
I		4.4			
J		4.7			
K		5.6			
L		7.9			
M	2.3	4.2	7.4	10.4	16.5
N		4.7			
O		5.9			
P	2.8	7.4	10.5	22.0	37.5

TABLE 26. EFFECT of CHEMICAL COMPOSITIONS and TEST TEMPERATURE on the NOTCH TOUGHNESS SENSITIVITY RATIO of 1100°F TEMPERED 4340 CAST STEEL.

	TEST TEMPERATURE, °F							
CASTING	-320	-200	-150	-110	-20	80	212	320
A	0.497	0.671	0.856	0.805	0.810	0.850	0.856	0.876
B	0.578	0.711	0.812	0.865	0.800	0.886	0.775	0.844
C	0.457	0.614	0.785	0.697	0.712	0.698	0.673	0.758
D	0.570	0.493	0.578	0.584	0.722	0.618	0.712	0.767
E	0.401	0.653	0.747	0.711	0.799	0.729	0.718	0.785
F	0.379	0.632	0.640	0.698	0.737	0.682	0.761	0.895
G	0.330	0.696	0.798	0.648	0.853	0.807	0.763	0.895
H	0.451	0.543	0.841	0.700	0.883	0.755	0.733	0.692
I	0.336	0.628	0.873	0.804	0.792	0.803	0.801	0.786
J	0.409	0.492	0.790	0.842	0.835	0.834	0.830	0.832
K	0.423	0.431	0.577	0.628	0.831	0.785	0.739	0.784
L	0.637	0.515	0.780	0.890	0.813	0.800	0.783	0.884
M	0.430	0.569	0.762	0.824	0.790	0.809	0.883	0.761
N	0.345	0.443	0.712	0.827	0.815	0.843	0.867	0.882
O	0.458	0.481	0.691	0.886	0.727	0.841	0.800	0.734
P	0.323	0.439	0.683	0.727	0.739	0.824	0.790	0.739

TABLE 27. EFFECT of CHEMICAL COMPOSITIONS and TEST TEMPERATURE on the NOTCH TOUGHNESS SENSITIVITY RATIO of 400°F TEMPERED 4340 CAST STEEL.

	TEST TEMPERATURE, °F					
CASTING	-320	-110	-20	80	212	320
A	0.344	0.541	0.584	0.628	0.583	0.770
B	0.320	0.461	0.523	0.552	0.602	0.602
C	0.349	0.442	0.522	0.550	0.439	0.762
D	0.422	0.416	0.515	0.446	0.653	0.595
E	0.265	0.382	0.538	0.587	0.476	0.555
F	0.252	0.382	0.441	0.425	0.547	0.642
G	0.289	0.384	0.348	0.484	0.538	0.589
H	0.326	0.475	0.511	0.406	0.478	0.594
I	0.275	0.271	0.341	0.407	0.463	0.623
J	0.237	0.376	0.421	0.412	0.560	0.630
K	0.266	0.345	0.404	0.422	0.602	0.556
L	0.383	0.392	0.499	0.490	0.522	0.620
M	0.418	0.365	0.446	0.521	0.569	0.603
N	0.280	0.316	0.358	0.389	0.492	0.570
O	0.370	0.442	0.392	0.404	0.477	0.516
P	0.402	0.426	0.468	0.403	0.549	0.593

TABLE 28A. INSTRUMENTED UNPRECRACKED CHARPY V-NOTCH IMPACT PROPERTIES of 0.010%P, 0.011%S MEDIUM STRENGTH 4340 CAST STEEL.

TESTING TEMP, °F	LOAD, LB			DEFL., IN	STRAIN	LAT. EXP.	ENERGY
	P_F	P_{GY}	P_M	d_M	$\varepsilon_{f,CVN}$	mil	W_T, ft-lb
-320	5300	-	-	0.0239	0.175	1.2	6.9
-260		5700	5800	-	-	3.0	8.9
-200		5500	6100	0.0270	0.195	7.4	14.2
-150		5300	5950	0.0287	0.206	12.4	22.6
-110		5200	5800	0.0291	0.209	17.4	27.8
- 20		4850	5350	0.0297	0.213	19.4	31.0
80		4500	5100	0.0313	0.223	20.2	33.8
212		4150	4920	0.0341	0.241	22.8	34.5
320		4050	4650	0.0333	0.236	26.5	34.4

NOTE: $d_M = \overline{V} \times t_{max} = 1/2[1 + (1 - \frac{E_i}{E_o})^{1/2}]V_o \times t_{max}$. (42)

$\varepsilon_{f,CVN} = \ln(1 + 8d_M)$. (68)

TABLE 28B. INSTRUMENTED UNPRECRACKED CHARPY V-NOTCH IMPACT PROPERTIES of 0.007%P, 0.049%S MEDIUM STRENGTH 4340 CAST STEEL.

TESTING TEMP, °F	LOAD, LB			DEFL., IN	STRAIN	LAT. EXP.	ENERGY
	P_F	P_{GY}	P_M	d_M	$\varepsilon_{f,CVN}$	mil	W_T, ft-lb
-320	3800	-	-	0.0189	0.141	0	4.8
-260	5000	-	-	-	-	1.0	6.1
-200		5500	5550	0.0208	0.154	3.0	9.5
-150		5300	5400	0.0235	0.172	7.3	12.7
-110		5100	5250	0.0235	0.172	7.4	13.3
- 20		4800	5300	0.0259	0.188	9.7	15.9
80		4600	5000	0.0268	0.194	11.8	17.1
212		4200	4700	0.0260	0.189	12.4	18.1
320		3950	4250	0.0247	0.180	12.9	16.7

TABLE 28C. INSTRUMENTED UNPRECRACKED CHARPY V-NOTCH IMPACT PROPERTIES of 0.050%P, 0.012%S MEDIUM STRENGTH 4340 CAST STEEL.

TESTING TEMP, °F	LOAD, LB			DEFL., IN	STRAIN	LAT. EXP.	ENERGY
	P_F	P_{GY}	P_M	d_M	$\varepsilon_{f,CVN}$	mil	W_T, ft-lb
-320	3400	-	-	0.0165	0.124	0	4.0
-260	4350	-	-	-	-	0	4.0
-200	5100	-	-	0.0184	0.137	1.1	6.4
-150		5550	6050	0.0208	0.154	4.3	10.7
-110		5350	5900	0.0259	0.188	8.1	14.5
- 20		4900	5420	0.0278	0.201	13.6	23.5
80		4700	5100	0.0290	0.209	16.9	25.4
212		4350	4800	0.0321	0.229	18.7	28.4
320		4100	4450	0.0300	0.215	21.8	28.9

TABLE 29A. INSTRUMENTED UNPRECRACKED CHARPY V-NOTCH IMPACT PROPERTIES of 0.010%P, 0.011%S HIGH STRENGTH 4340 CAST STEEL.

TESTING TEMP, °F	LOAD, LB			DEFL., IN	STRAIN	LAT. EXP.	ENERGY
	P_F	P_{GY}	P_M	d_M	$\varepsilon_{f,CVN}$	mil	W_T, ft-lb
-320	4000	-	-	0.0168	0.126	0.1	4.7
-110	5750	-	-	0.0189	0.141	0.6	8.2
- 20		6500	6600	0.0224	0.165	1.0	10.8
80		6100	6150	0.0218	0.161	2.7	12.0
212		6000	6100	0.0229	0.168	2.8	12.8
320		5800	5900	0.0232	0.170	3.2	12.9
400		5700	5750	0.0226	0.166	3.0	12.1

TABLE 29B. INSTRUMENTED UNPRECRACKED CHARPY V-NOTCH IMPACT PROPERTIES of 0.007%P, 0.049%S HIGH STRENGTH 4340 CAST STEEL.

TESTING TEMP, °F	LOAD, LB			DEFL., IN	STRAIN	LAT. EXP.	ENERGY
	P_F	P_{GY}	P_M	d_M	$\varepsilon_{f,CVN}$	mil	W_T, ft-lb
-320	3750	-	-	0.0150	0.113	0	4.0
-110	4900	-	-	0.0166	0.125	0.5	6.2
- 20	4750	-	-	0.0176	0.132	1.3	5.6
80	5000	-	-	0.0181	0.135	1.0	6.4
212	4300	-	-	0.0178	0.133	1.5	6.0
320	4600	-	-	0.0188	0.140	1.2	6.3
400	4200	-	-	0.0166	0.125	2.0	6.5

TABLE 29C. INSTRUMENTED UNPRECRACKED CHARPY V-NOTCH IMPACT PROPERTIES of 0.050%P, 0.012%S HIGH STRENGTH 4340 CAST STEEL.

TESTING TEMP, °F	LOAD, LB			DEFL., IN	STRAIN	LAT. EXP.	ENERGY
	P_F	P_{GY}	P_M	d_M	$\varepsilon_{f,CVN}$	mil	W_T, ft-lb
-320	1900	-	-	0.0092	0.071	0	2.0
-110	3300	-	-	0.0139	0.106	0.2	3.7
- 20	3600	-	-	0.0126	0.096	0.6	4.6
80	4700	-	-	0.0165	0.124	0.7	6.0
212	4800	-	-	0.0174	0.130	2.0	7.2
320		6000	6050	0.0206	0.153	2.4	9.3
400		5900	5950	0.0219	0.161	2.7	9.6

TABLE 30. CRACK OPENING DISPLACEMENT (COD in inch) versus TEMPERATURE for M, A, and P SPECIMENS TEMPERED at 1100°F.

SPECIMEN	-320°F	-200°F	-150°F	-110°F	-20°F	80 °F	212°F	320°F
M	0.00052	0.00158	0.00271	0.00285	0.00356	0.00385	0.00414	0.00446
A	0.00057	0.00096	0.00159	0.00167	0.00185	0.00203	0.00230	0.00241
P	0.00022	0.00050	0.00092	0.00166	0.00239	0.00280	0.00303	0.00341

TABLE 31. CRACK OPENING DISPLACEMENT (COD in inch) versus TEMPERATURE for M, A, and P SPECIMENS TEMPERED AT 400°F.

SPECIMEN	-320°F	-110°F	-20°F	80°F	212°F	320°F	400°F
M	0.00009	0.00031	0.00049	0.00066	0.00083	0.00086	0.00082
A	0.00009	0.00028	0.00039	0.00050	0.00056	0.00049	0.00060
P	0.00006	0.00011	0.00019	0.00029	0.00046	0.00065	0.00076

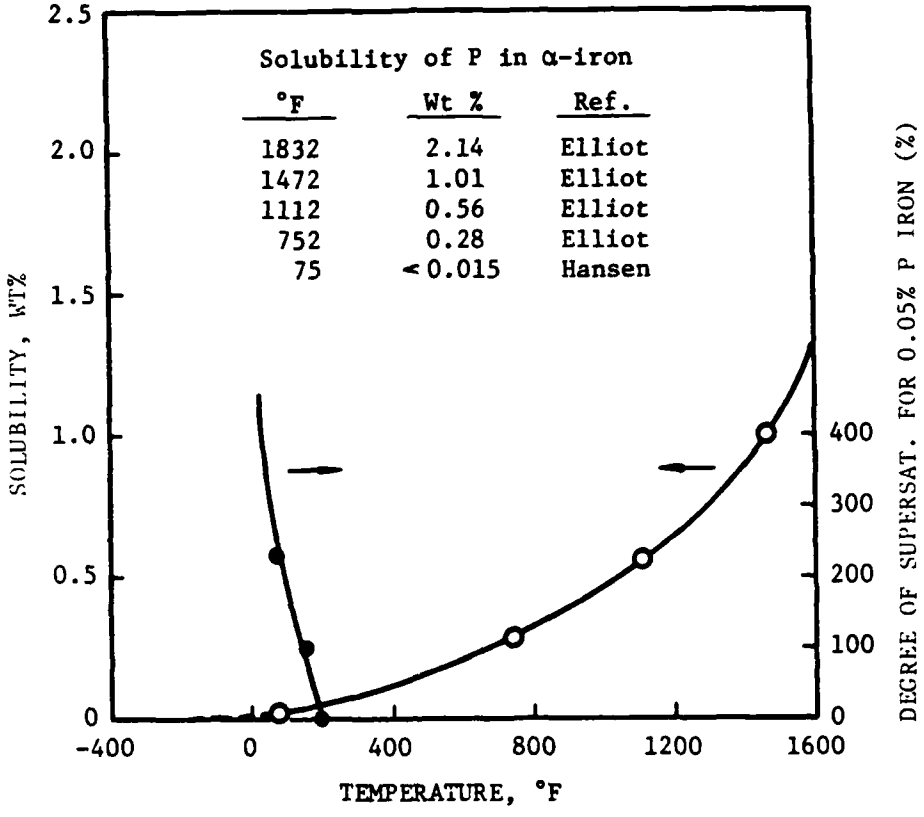

Note : Degree of Supersaturation for 0.05% P iron is defined as : [(0.05 - sol.)/sol.] x 100%.

FIGURE 1. SOLUBILITY OF PHOSPHORUS IN α-IRON AND DEGREE OF SUPERSATURATION OF AN IRON CONTAINING 0.05% P. (6,7)

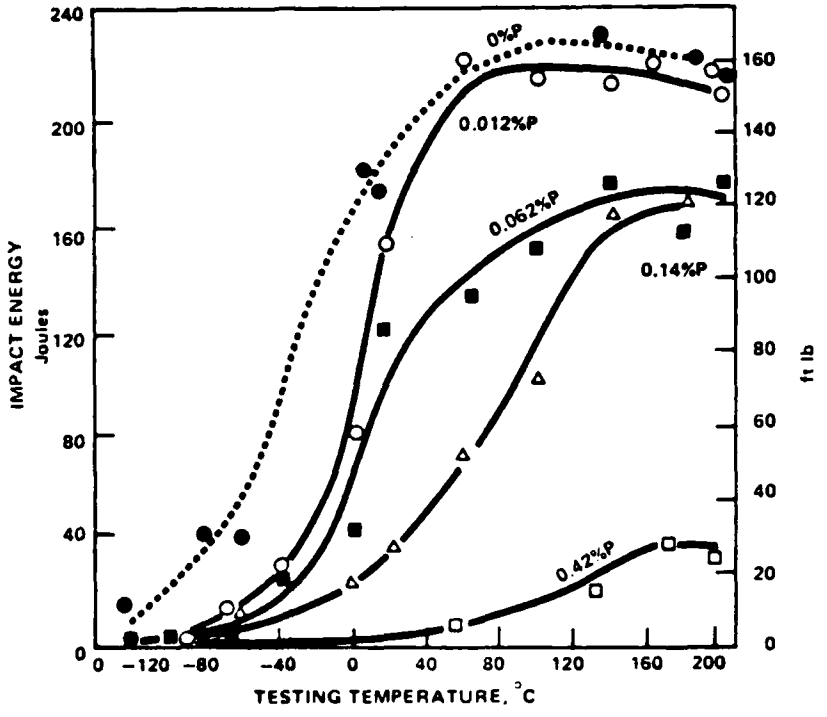

FIGURE 2. EFFECT OF PHOSPHORUS CONTENT ON THE CHARPY V-NOTCH TRANSITION CURVE FOR A HARDENED AND TEMPERED 13% Cr STEEL. (19)

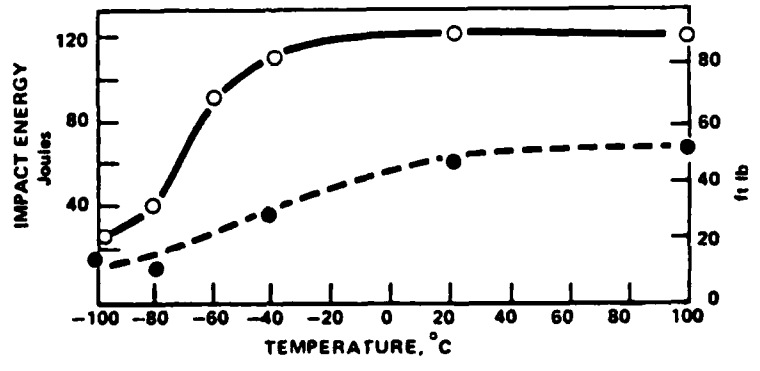

FIGURE 3. EFFECT OF SULFUR CONTENT ON THE CHARPY V-NOTCH TRANSITION CURVE FOR A LOW CARBON 1-1/2% Ni-Cr -Mo QUENCHED AND TEMPERED STEEL. (18)

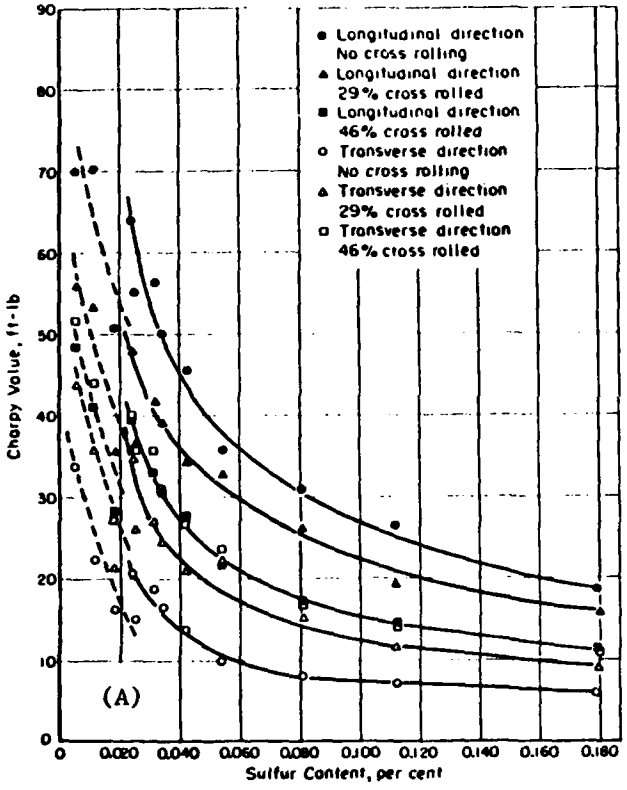

FIGURE 4A. EFFECT OF SULFUR CONTENT ON V-NOTCH CHARPY VALUE OF 0.3%C, NiCrMo STEEL HEAT TREATED TO 30 R_c AND TESTED AT -40°F. (20)

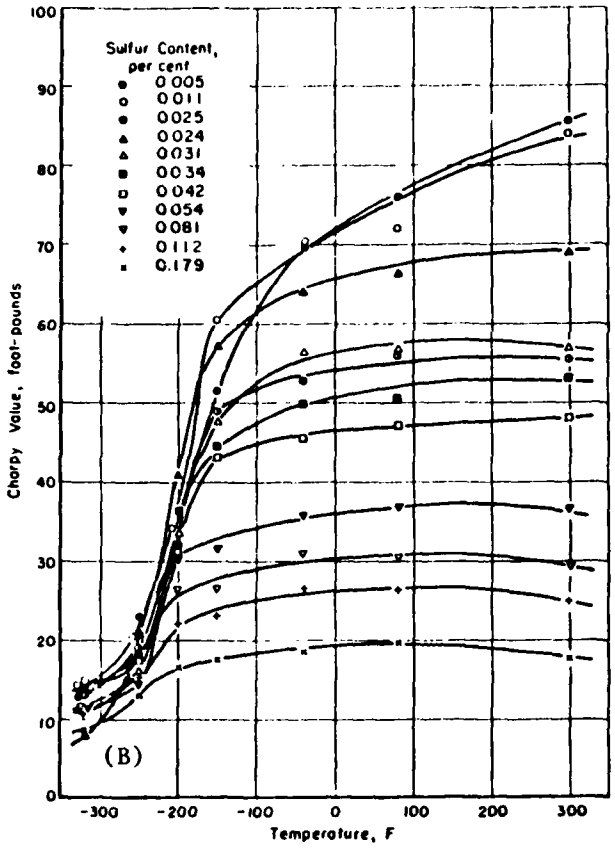

FIGURE 4B. TRANSITION CURVES OF 0.3%C, NiCrMo STEEL HEAT TREATED TO 30 R_c HARDNESS. (20)

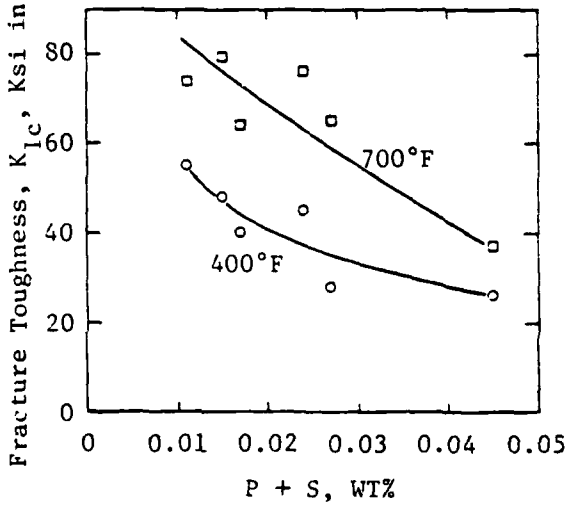

FIGURE 5. VARIATION OF FRACTURE TOUGHNESS WITH SULFUR PLUS PHOSPHORUS CONTENT FOR 400 AND 700°F TEMPERED 4340 WROUGHT STEELS. (27)

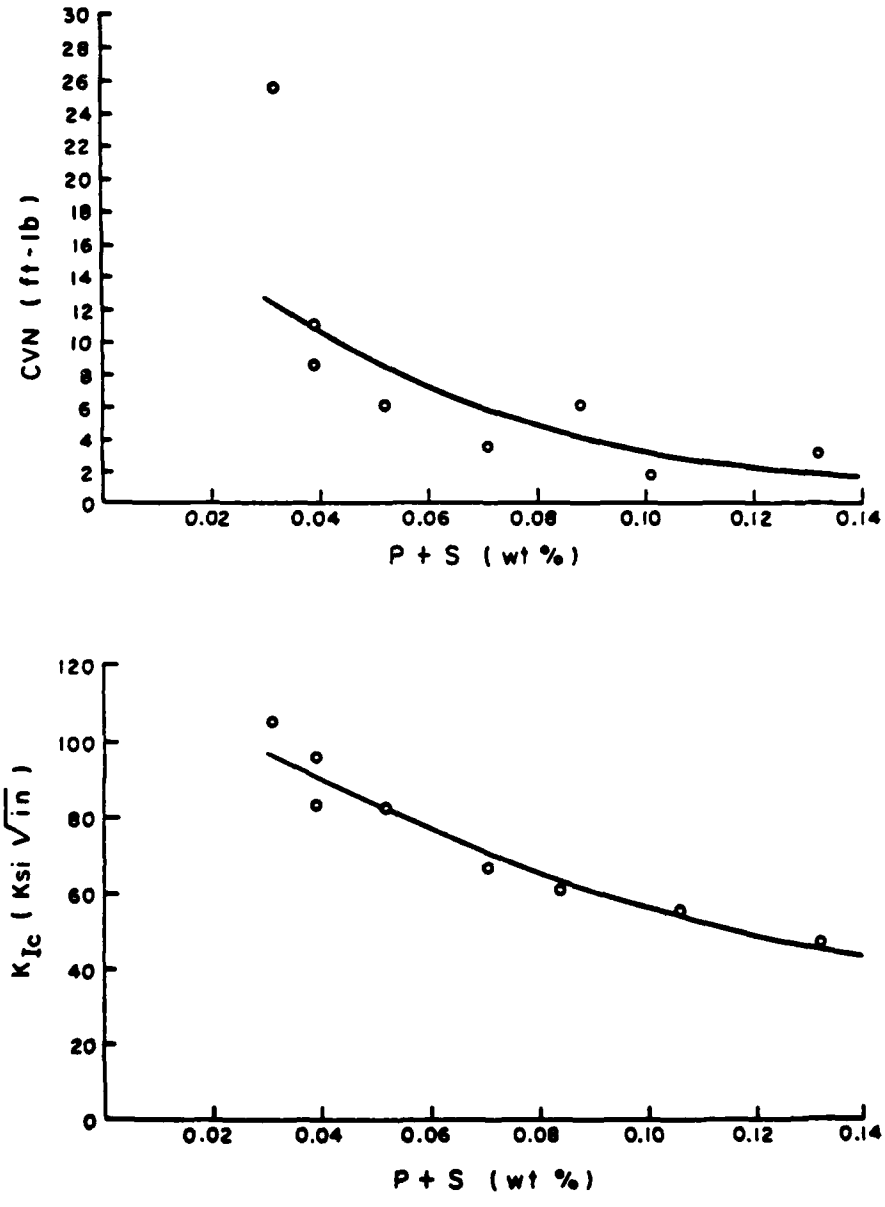

FIGURE 6. EFFECT OF PHOSPHORUS AND SULFUR CONTENT ON (A) CVN, AND (B) K_{Ic} IN 4335 CAST STEEL. (28)

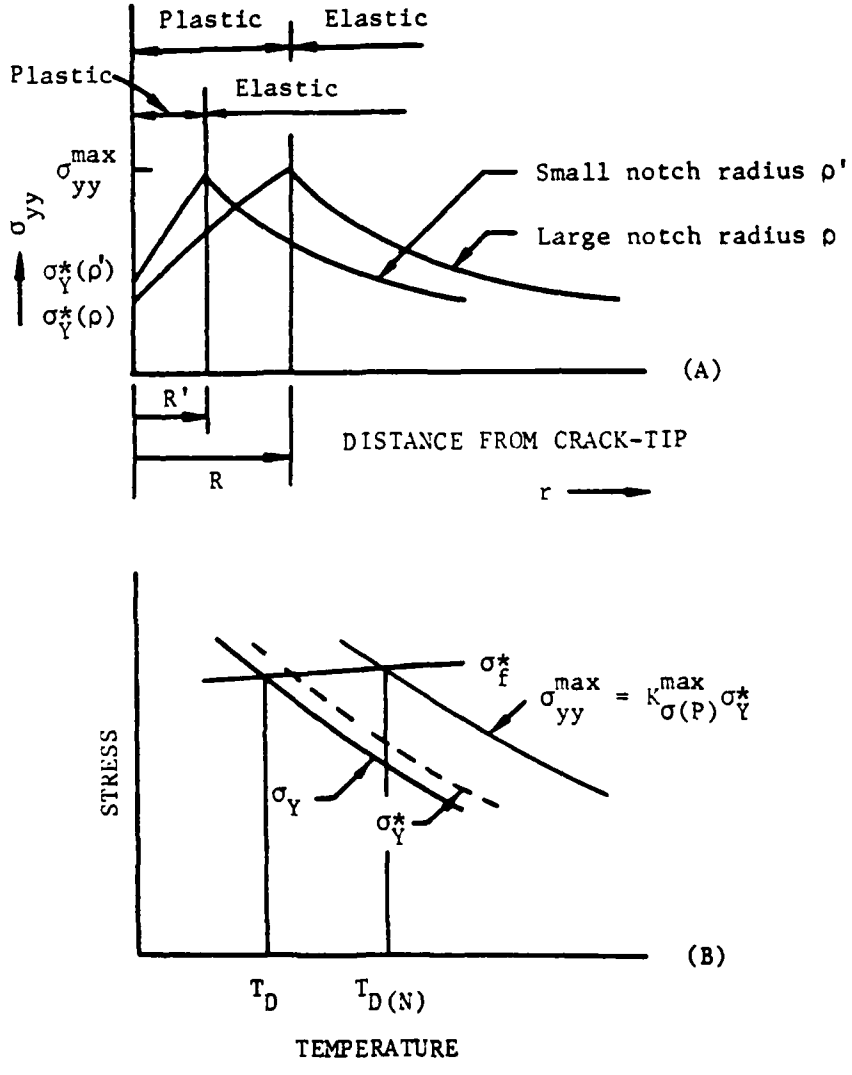

FIGURE 7. EFFECT OF NOTCH SEVERITY AND STRAIN RATE ON THE (A) PLASTIC ZONE SIZE (R), AND (B) BRITTLENESS TRANSITION TEMPERATURE (T_D).

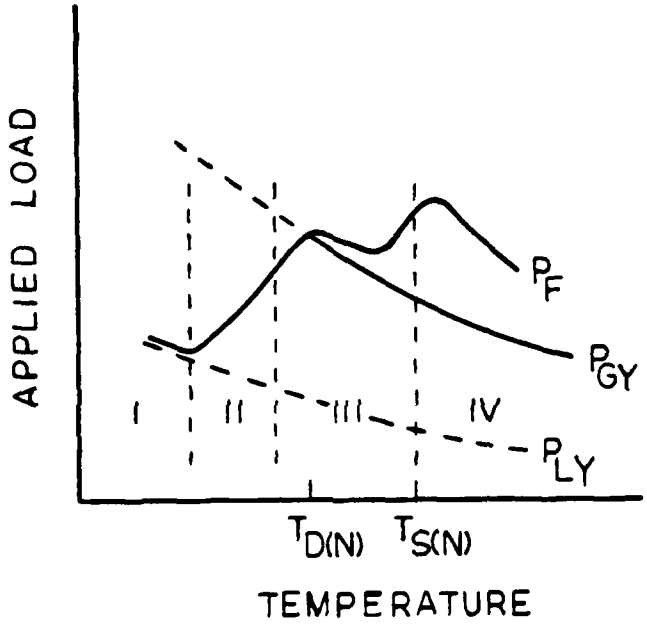

FIGURE 8. SCHEMATIC VARIATION OF GENERAL YIELD LOAD (P_{GY}), LOCAL YIELD LOAD (P_{LY}), FRACTURE LOAD (P_F) WITH TEMPERATURE FOR CHARPY SPECIMEN LOADED IN BENDING.

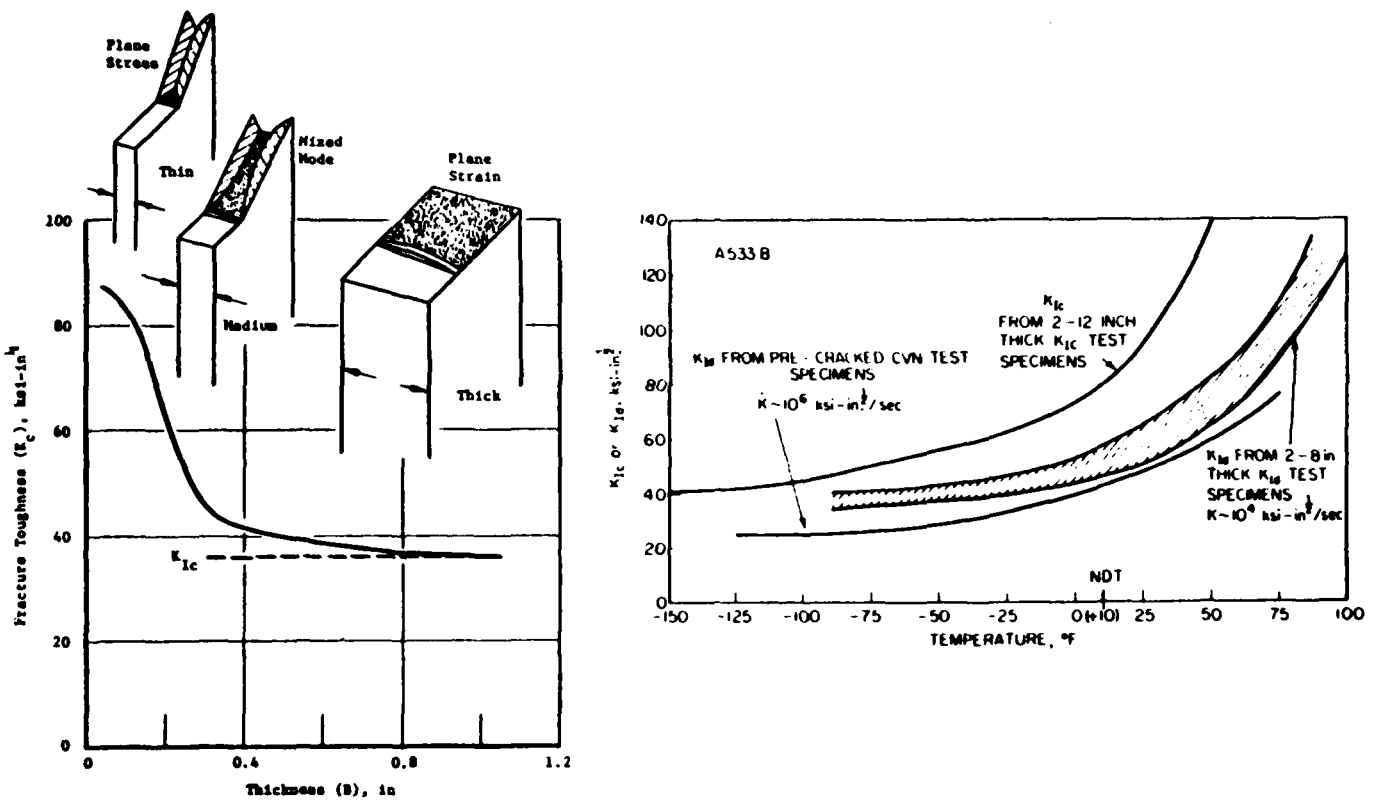

FIGURE 9. EFFECT OF (A) SPECIMEN THICKNESS (37), AND (B) STRAIN RATE (43) ON THE FRACTURE TOUGHNESS OF MATERIALS.

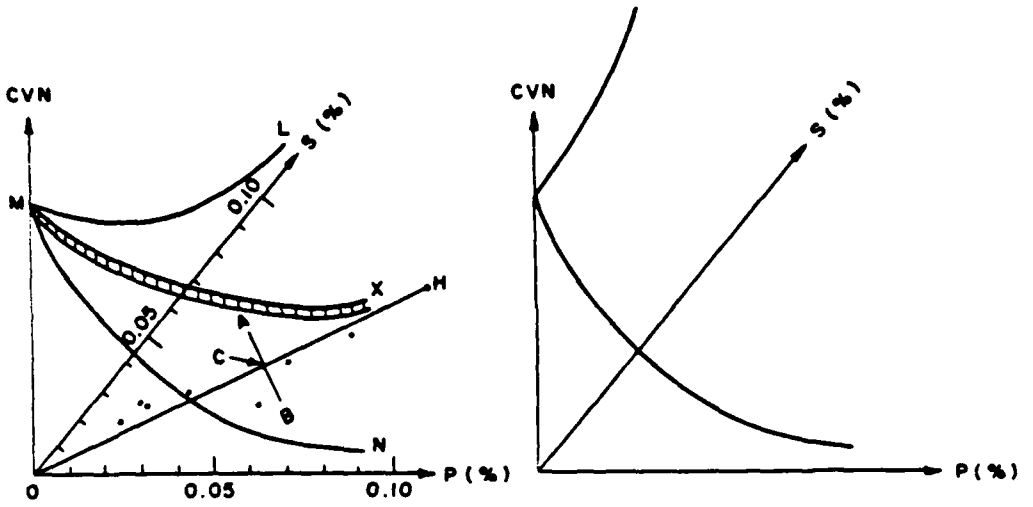

(A)

(B)

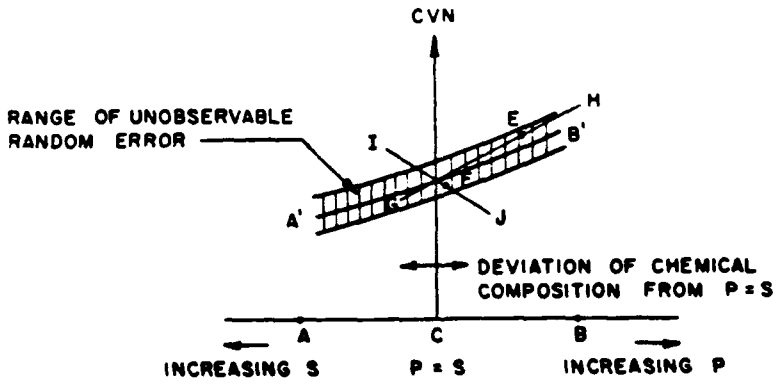

(C)

FIGURE 10. SCHEMATIC REPRESENTATION TO EXPLAIN THE UNREASONABLE REGRESSION RESULT CAUSED BY INAPPROPRIATE SAMPLING: (A) THREE DIMENSIONAL RELATIONSHIP AMONG CVN AND P,S, (B) GRAPHICAL REPRESENTATION OF EQU. (17), AND (C) A PLANE PERPENDICULAR TO OH AND PARALLEL TO OM IN (A).

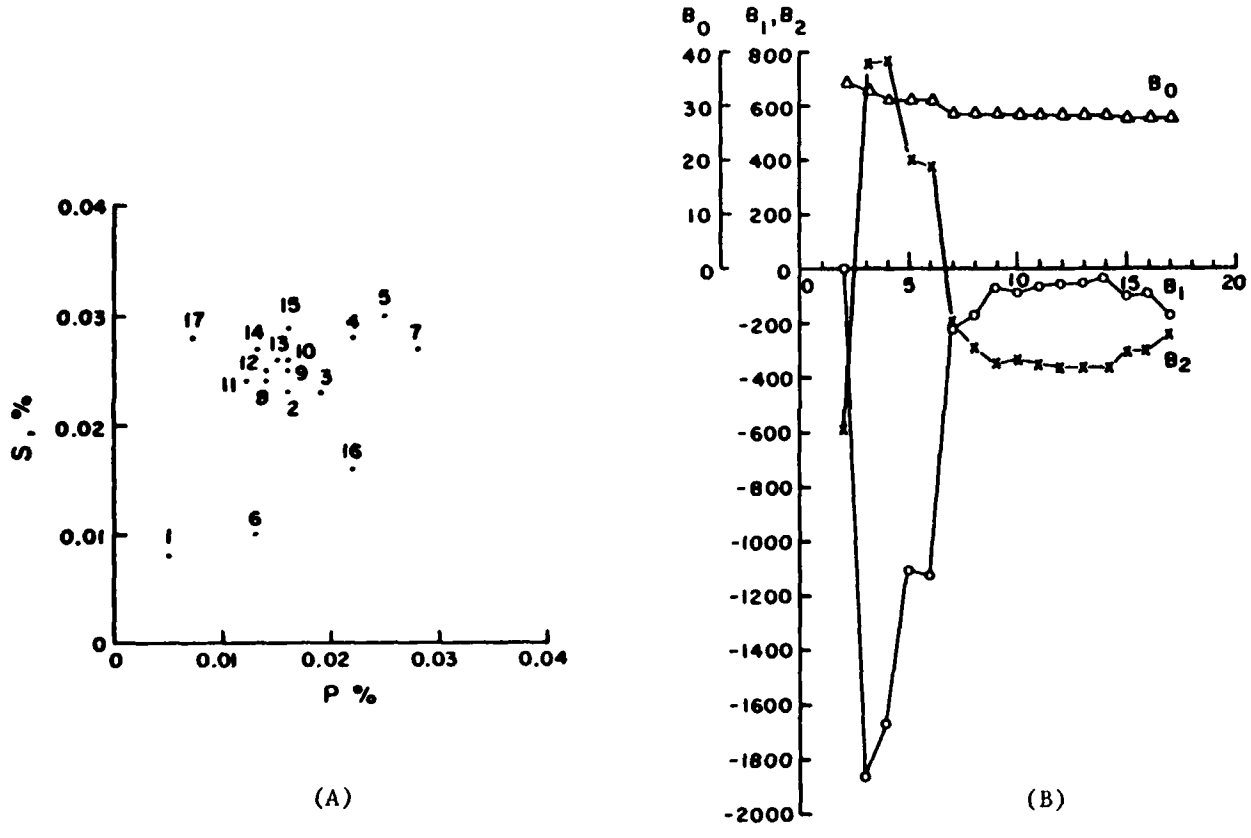

FIGURE 11. (A) CHEMICAL COMPOSITIONS DISTRIBUTION, AND (B) SAMPLING CONVERGENCE TEST OF THE DATA IN TABLE I FROM LARSON AND HERLIHY. (25)

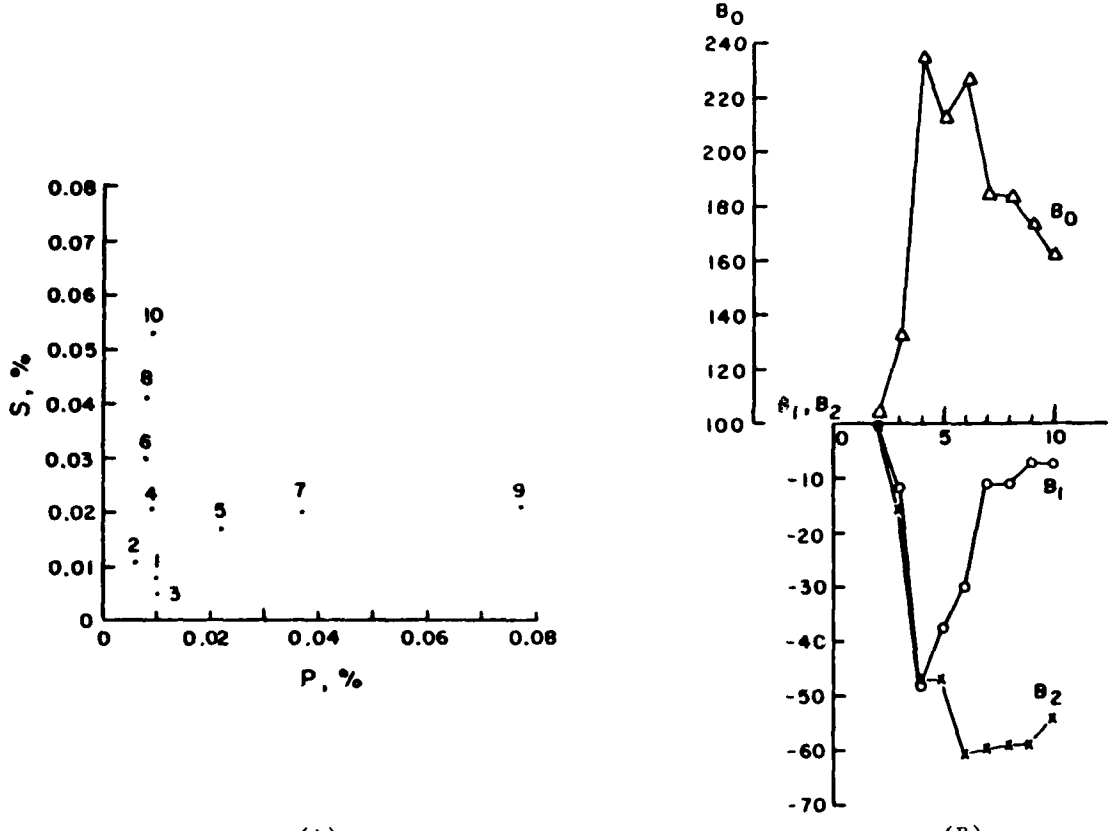

(A) (B)

FIGURE 12. (A) CHEMICAL COMPOSITIONS DISTRIBUTION, AND (B) SAMPLING CONVERGENCE TEST OF THE DATA IN TABLE 2 FROM WRIGHT AND QUARREL. (17)

AD-A116 307 CASE WESTERN RESERVE UNIV CLEVELAND OH DEPT OF METAL--ETC F/G 11/6
INDIVIDUAL AND COMBINED EFFECTS OF SULFUR AND PHOSPHORUS ON THE--ETC(U)
MAY 82 E CHANG, J F WALLACE DAAG46-79-C-0094

UNCLASSIFIED AMMRC-TR-82-33 NL

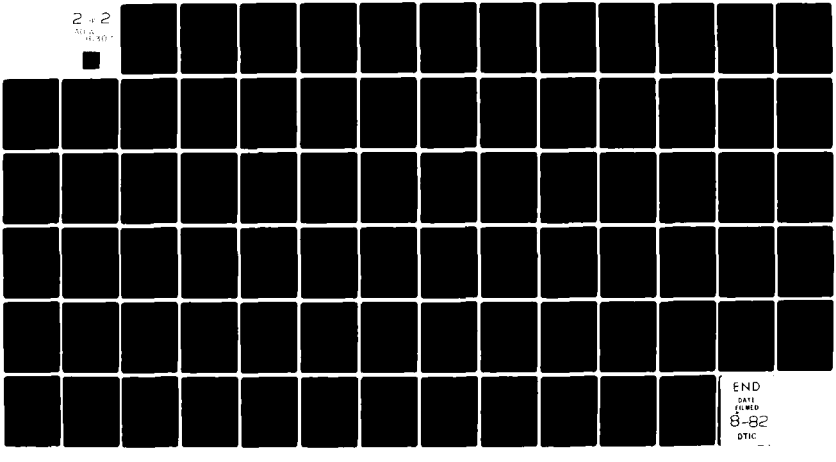

END
DATE FILMED
8-82
DTIC

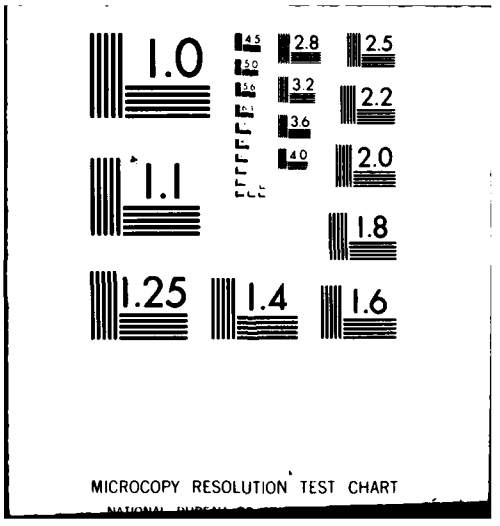
1.0
1.1
1.25
1.4
1.6
1.8
2.0
2.2
2.5
2.8
3.2
3.6
4.0
4.5
5.0
5.6
MICROCOPY RESOLUTION TEST CHART

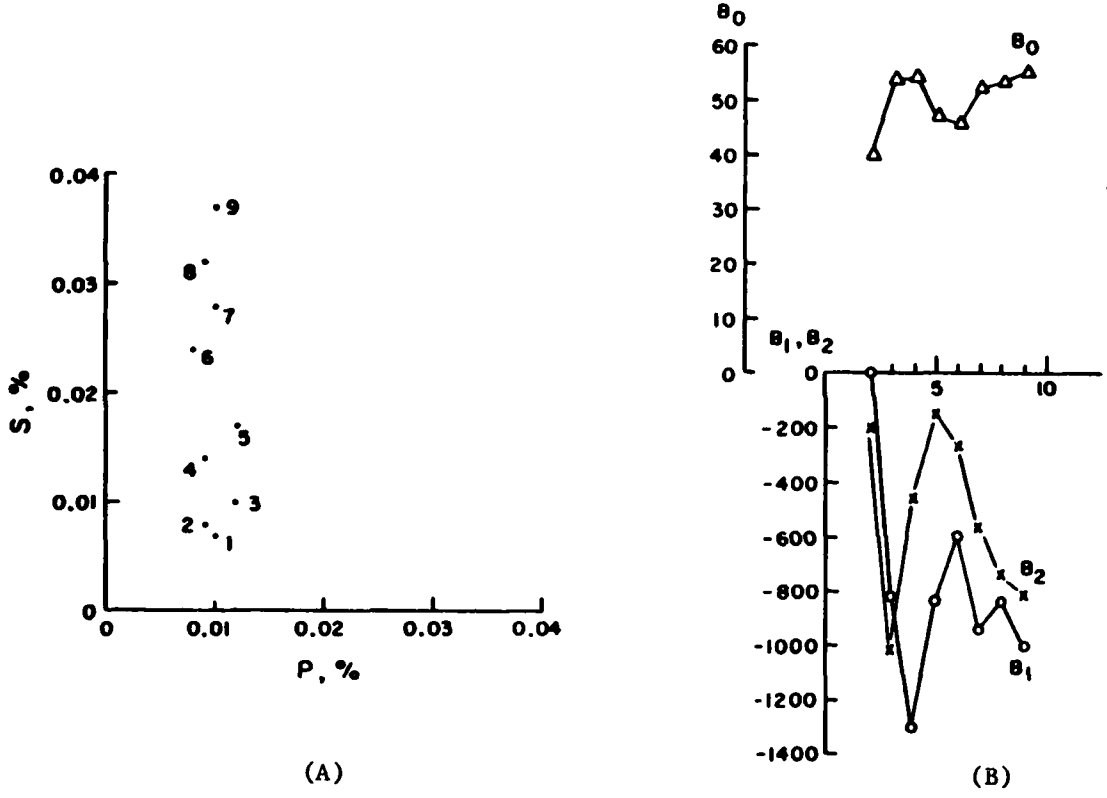

FIGURE 13. (A) CHEMICAL COMPOSITIONS DISTRIBUTION, AND (B) SAMPLING CONVERGENCE TEST OF THE DATA IN TABLE 3 FROM ZOTOS. (21)

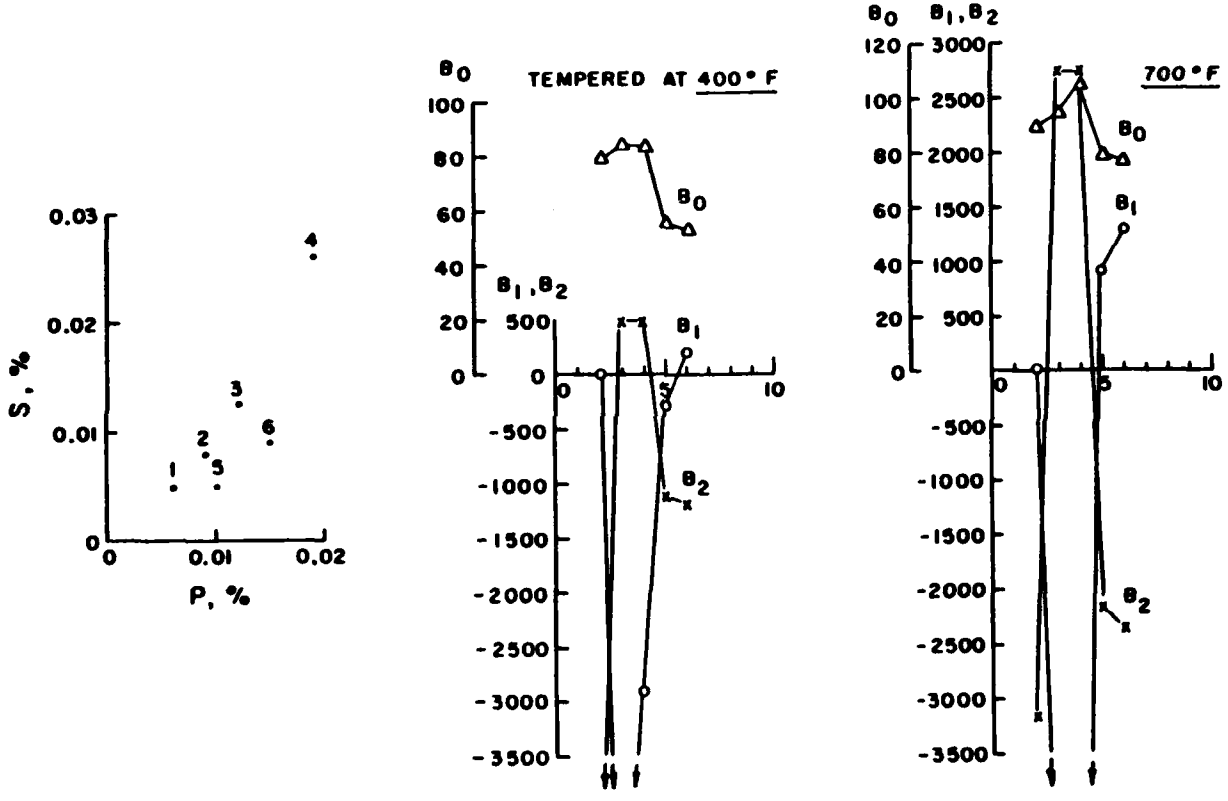

FIGURE 14. (A) CHEMICAL COMPOSITIONS DISTRIBUTION, AND (B) SAMPLING CONVERGENCE TEST OF THE DATA IN TABLE 4 FROM KULA AND ANCIL. (27)

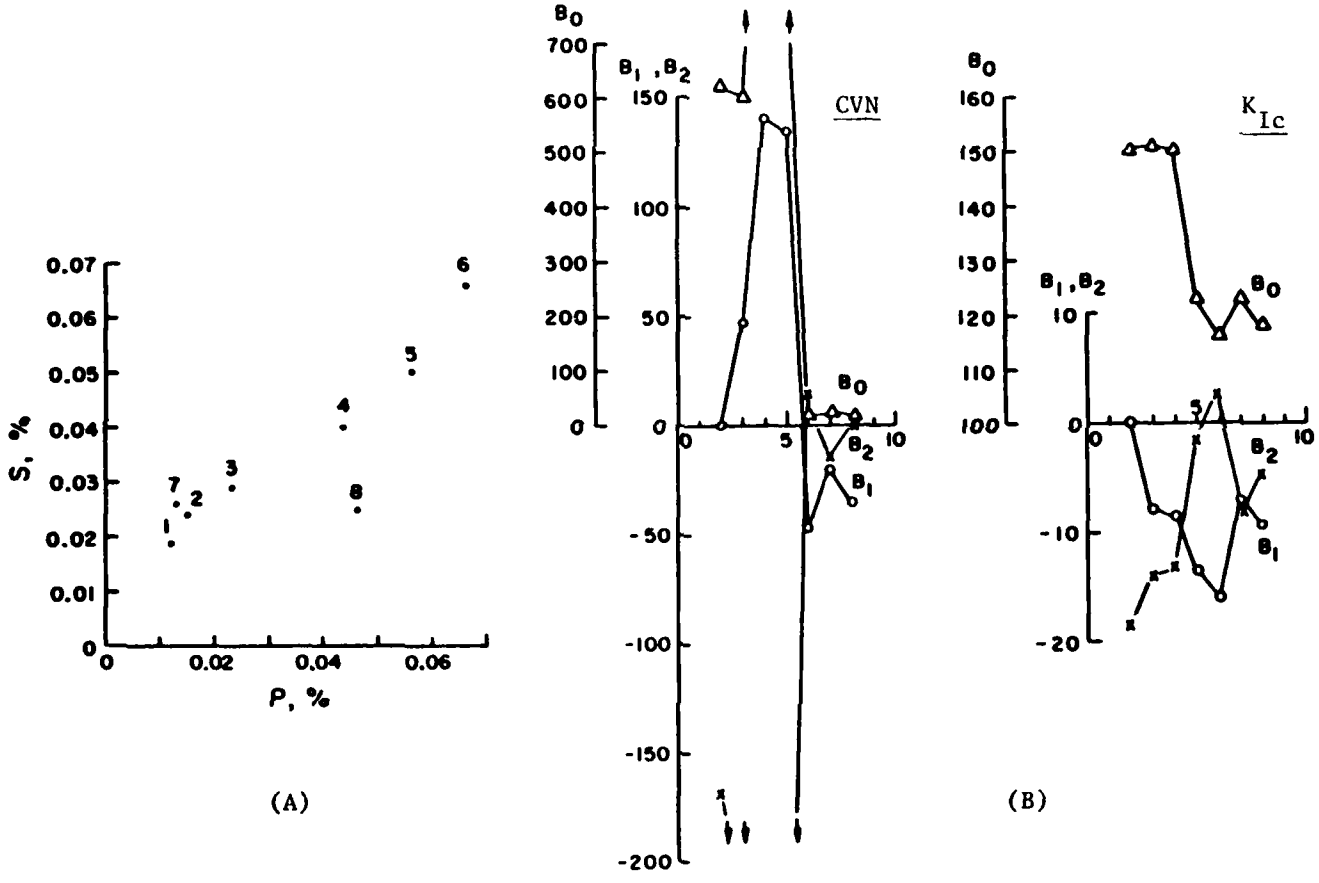

FIGURE 15. (A) CHEMICAL COMPOSITIONS DISTRIBUTION, AND (B) SAMPLING CONVERGENCE TEST OF THE DATA IN TABLE 5 FROM GROVES AND WALLACE. (28)

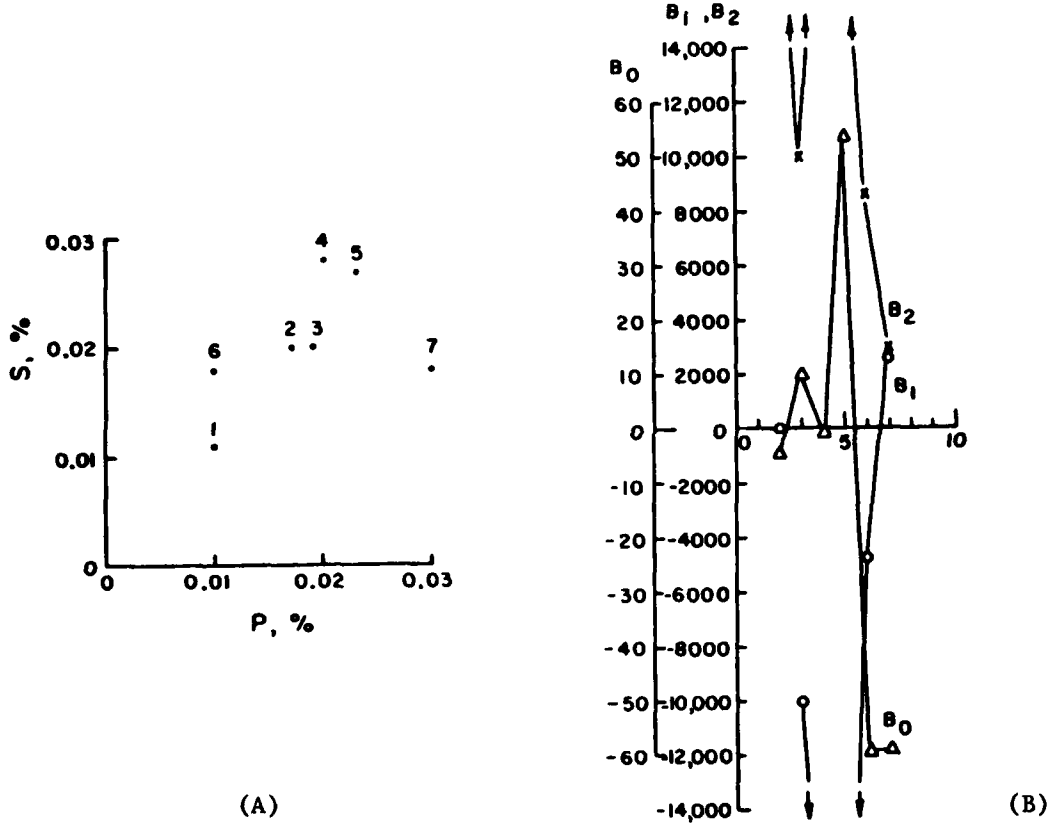

FIGURE 16. (A) CHEMICAL COMPOSITIONS DISTRIBUTION, AND (B) SAMPLING CONVERGENCE TEST OF THE DATA IN TABLE 6 FROM DUTCHER ET AL. (23)

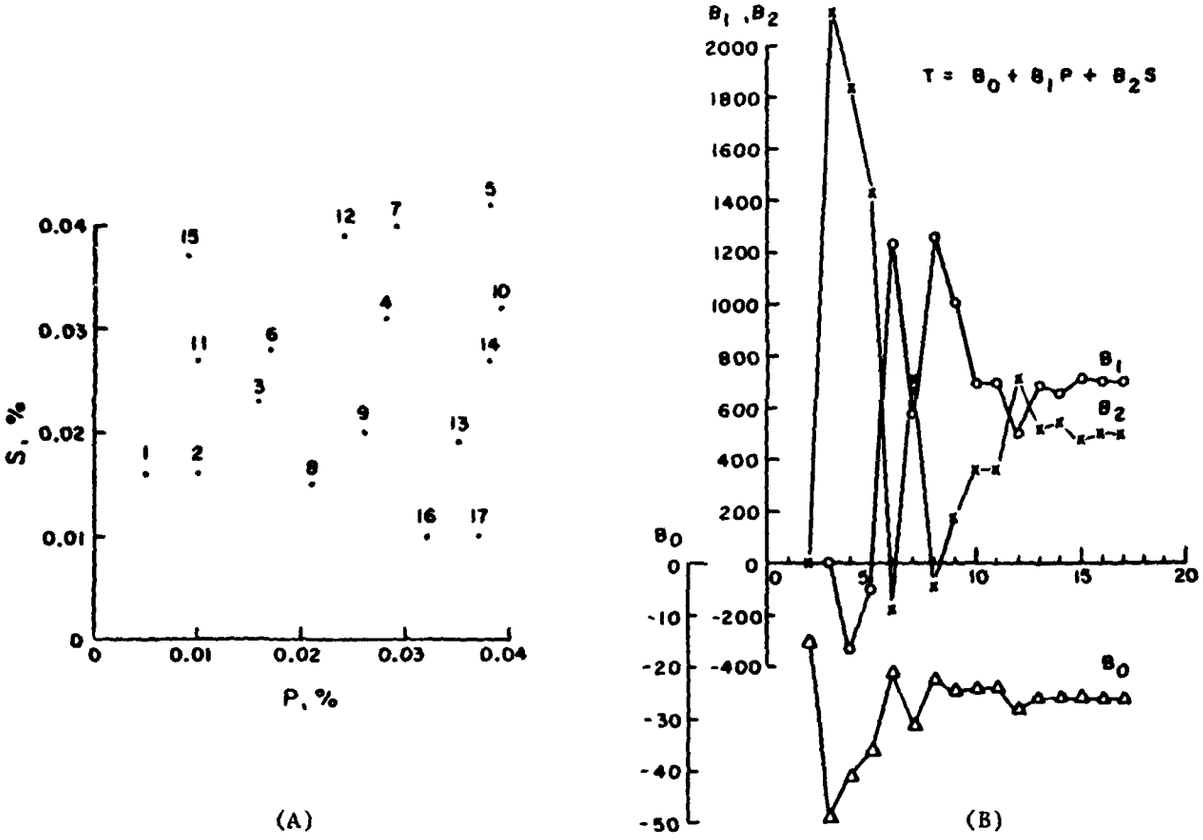

FIGURE 17. (A) CHEMICAL COMPOSITIONS DISTRIBUTION, AND (B) SAMPLING CONVERGENCE TEST OF THE DATA IN TABLE 7 FROM MICKELSON. (29)

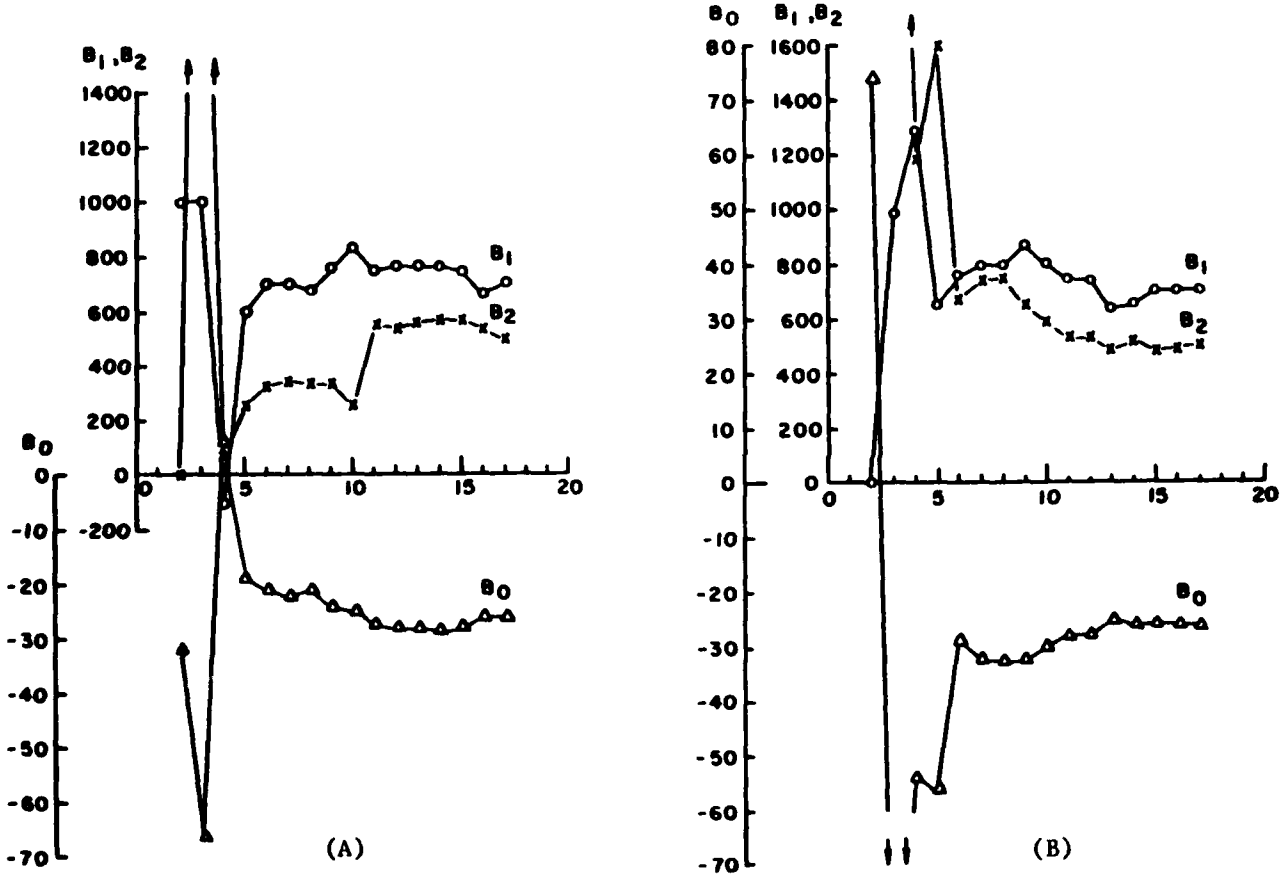

FIGURE 18. TWO EXAMPLES OF SPECIAL SAMPLING CONVERGENCE TEST IN WHICH SAMPLES ARE FED INTO THE REGRESSION EQUATION SUCCESSIVELY AND RANDOMLY. DATA FROM MICKELSON. (29)

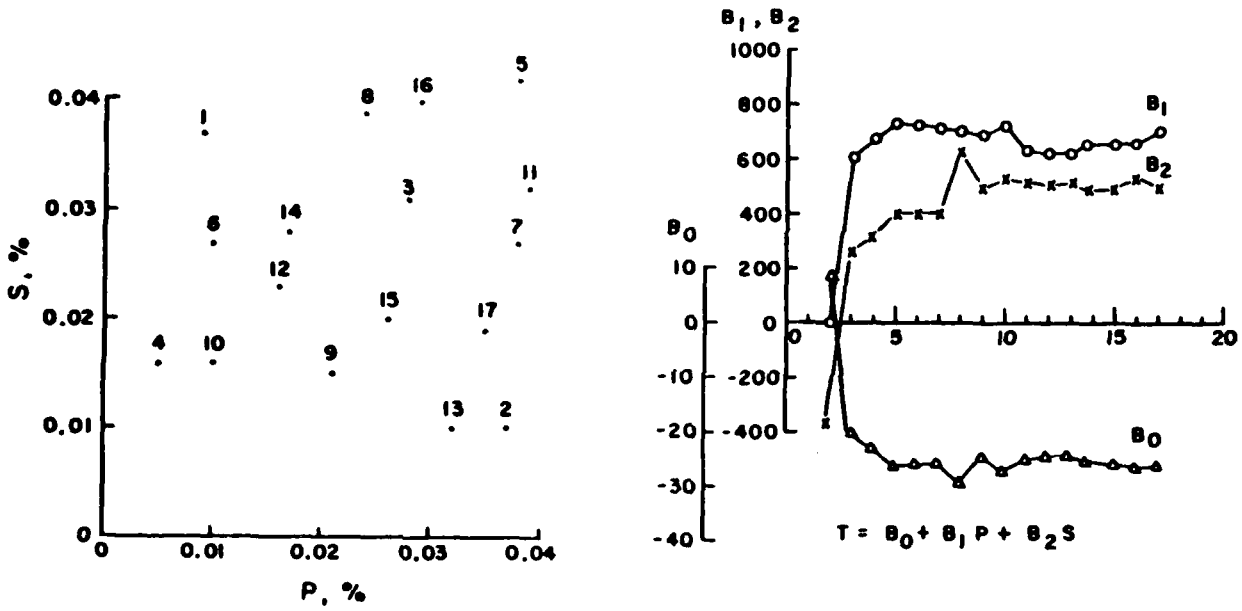

(A) (B)

FIGURE 19. SAMPLING CONVERGENCE TEST TO TEST THE MINIMUM SAMPLES NEEDED FOR MEANINGFUL REGRESSION ANALYSIS. DATA FROM MICKELSON. (29)

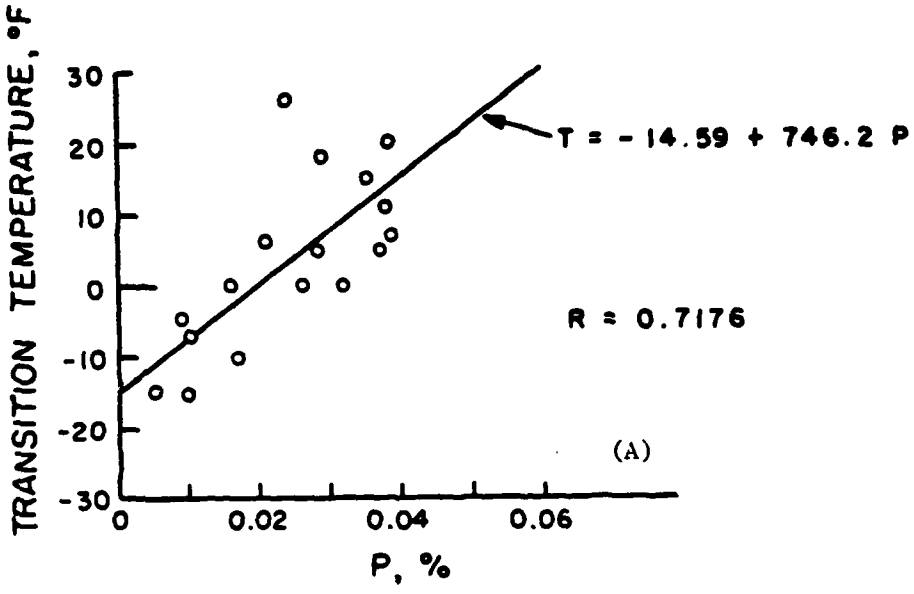

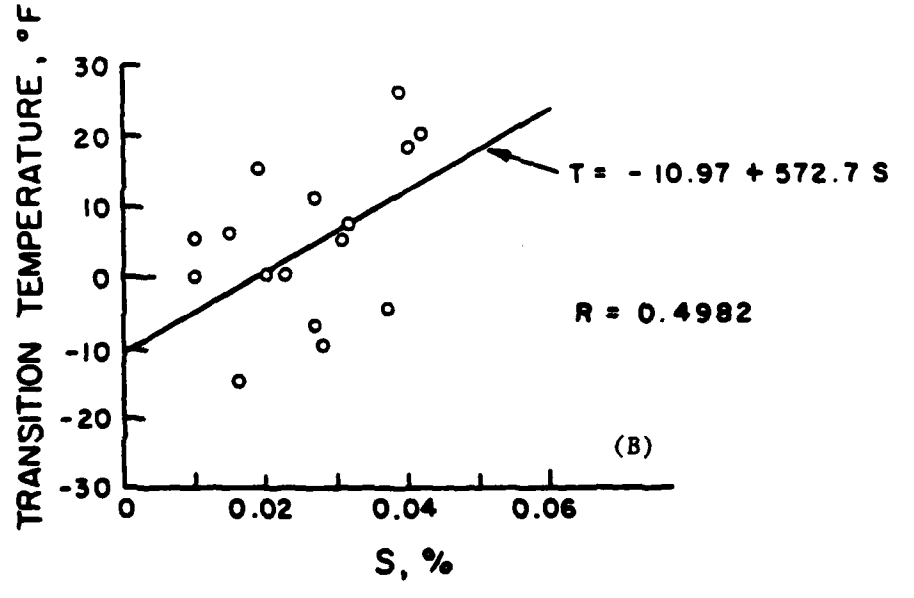

FIGURE 20. INDIVIDUAL EFFECT OF (A) PHOSPHORUS AND (B) SULFUR CONTENT ON THE 15 FT-LB CHARPY V-NOTCH IMPACT TRANSITION TEMPERATURE.

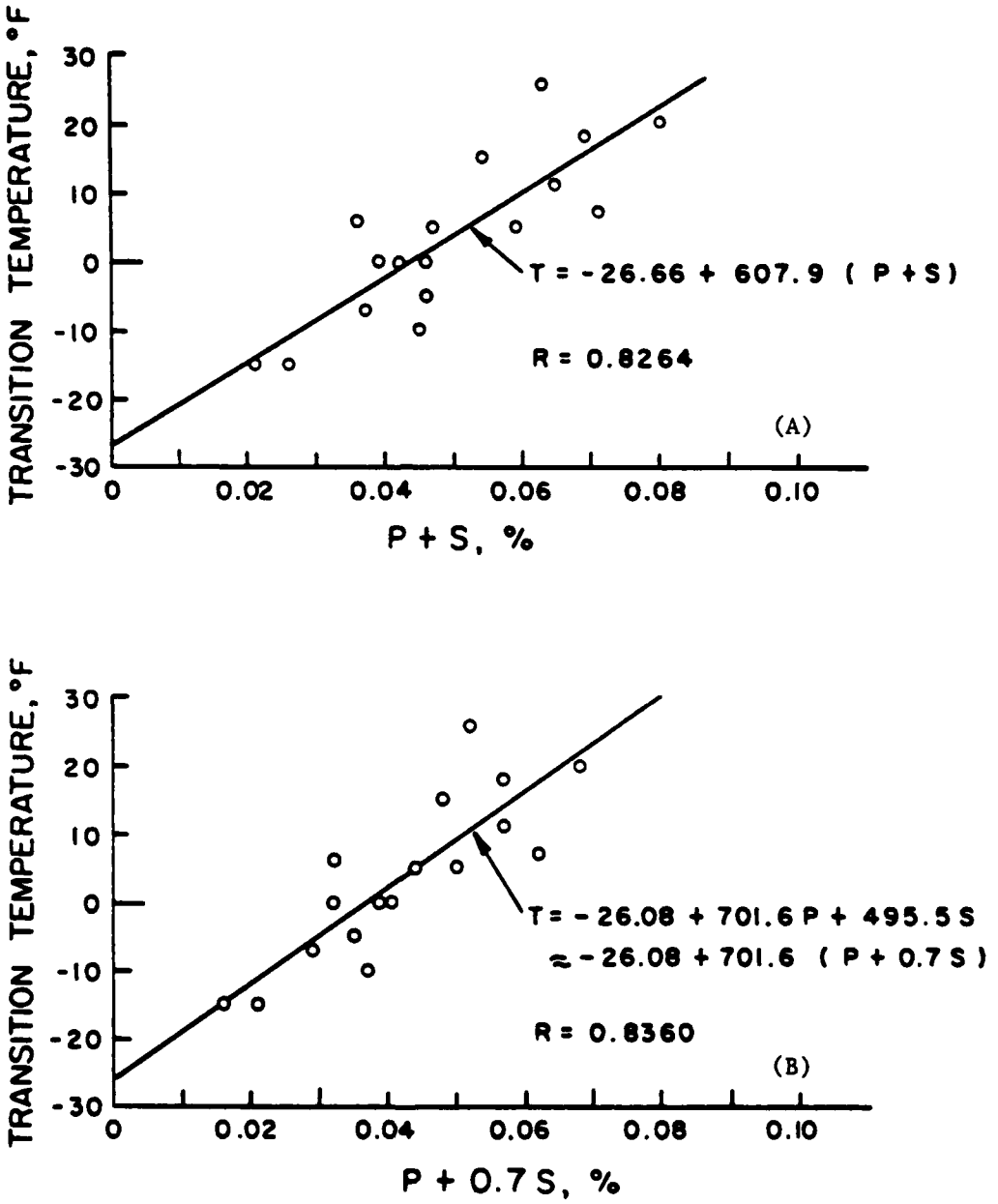

FIGURE 21. COMBINED EFFECT OF PHOSPHORUS AND SULFUR CONTENT ON THE 15 FT-LB CHARPY V-NOTCH IMPACT TRANSITION TEMPERATURE: (A) USING P + S AS A PARAMETER, AND (B) USING P + 0.7S AS A PARAMETER.

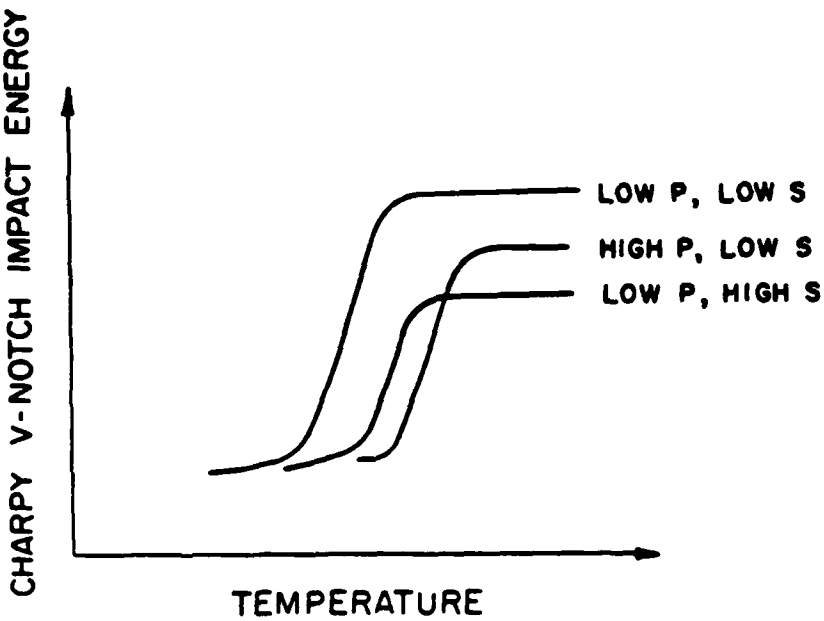

FIGURE 22. SCHEMATIC REPRESENTATION OF THE POSTULATED RELATIVE EFFECT OF PHOSPHORUS AND SULFUR ON THE IMPACT TRANSITION BEHAVIOR OF STEEL.

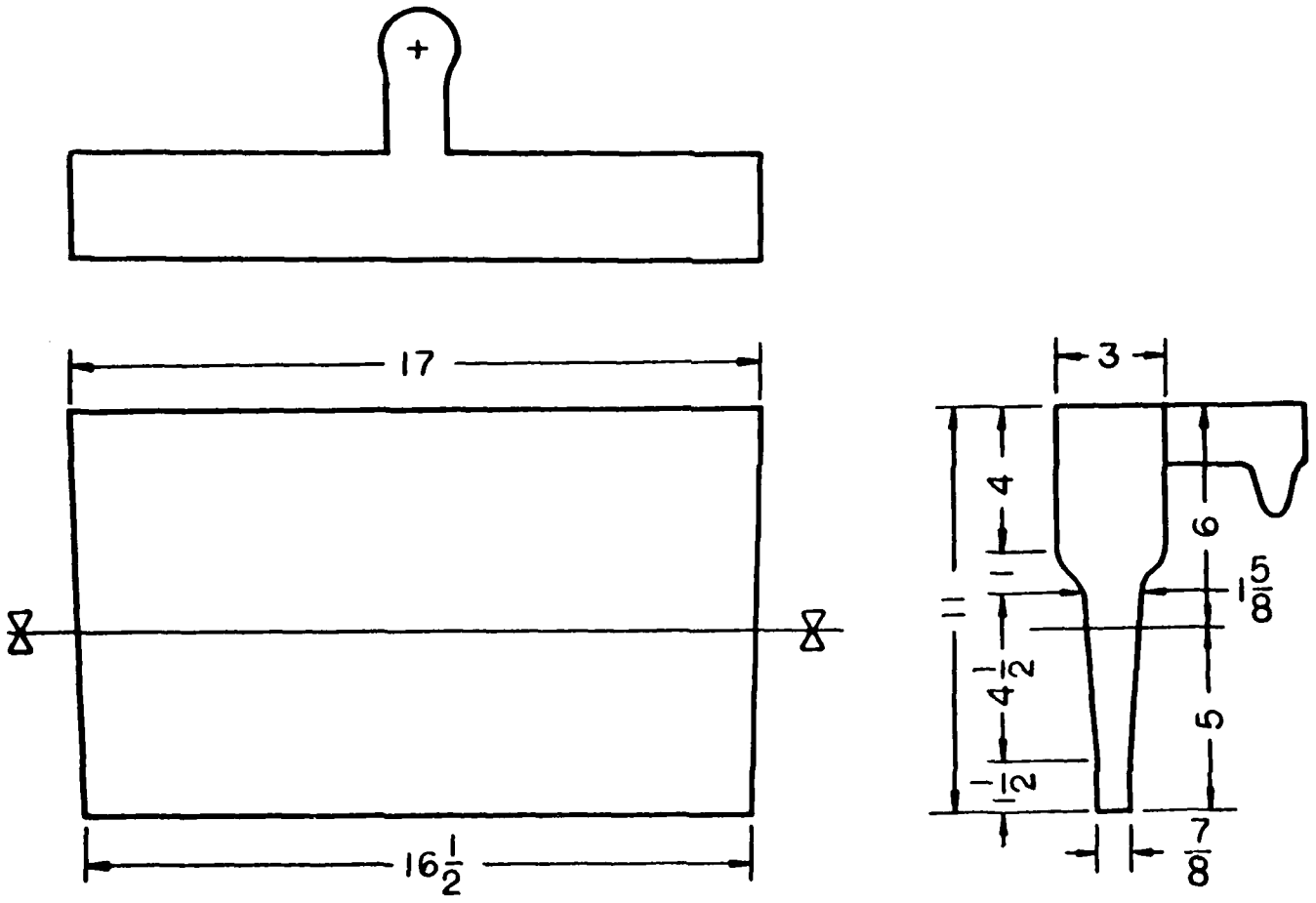

FIGURE 23. CASTING DESIGN (INCH).

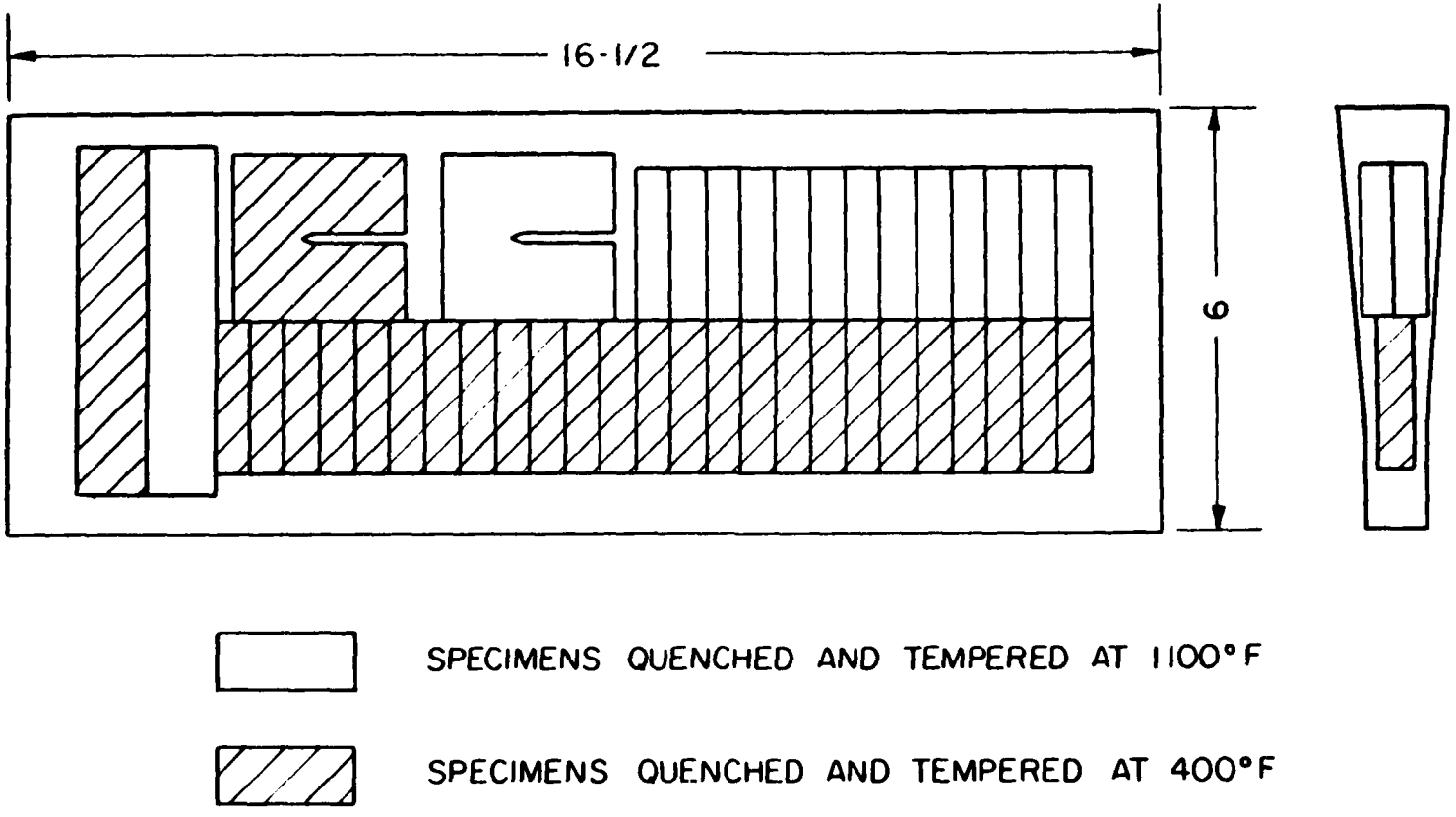

FIGURE 24. LAYOUT OF TENSILE, CHARPY V-NOTCH IMPACT AND PLANE STRAIN FRACTURE TOUGHNESS TEST SPECIMENS.

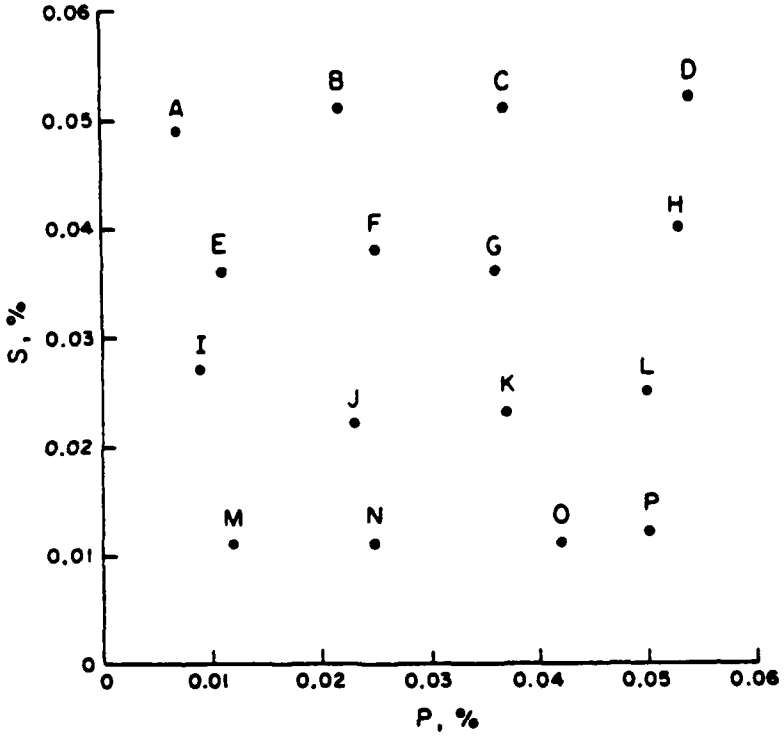

FIGURE 25. CHEMICAL COMPOSITION DISTRIBUTION OF PHOSPHORUS AND SULFUR FOR CASTINGS FROM A TO P.

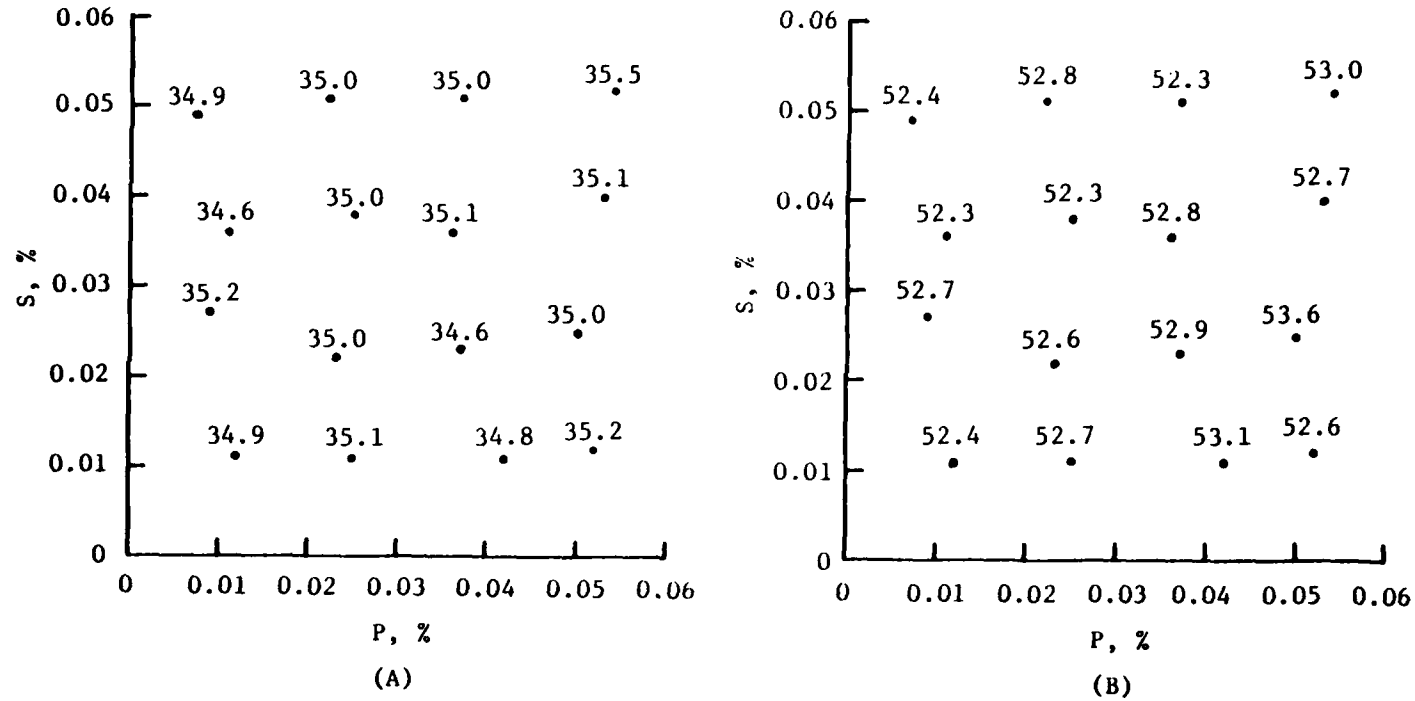

FIGURE 26. EFFECT OF PHOSPHORUS AND SULFUR ON THE HARDNESS OF (A) 1100°F AND (B) 400°F TEMPERED 4340 CAST STEEL.

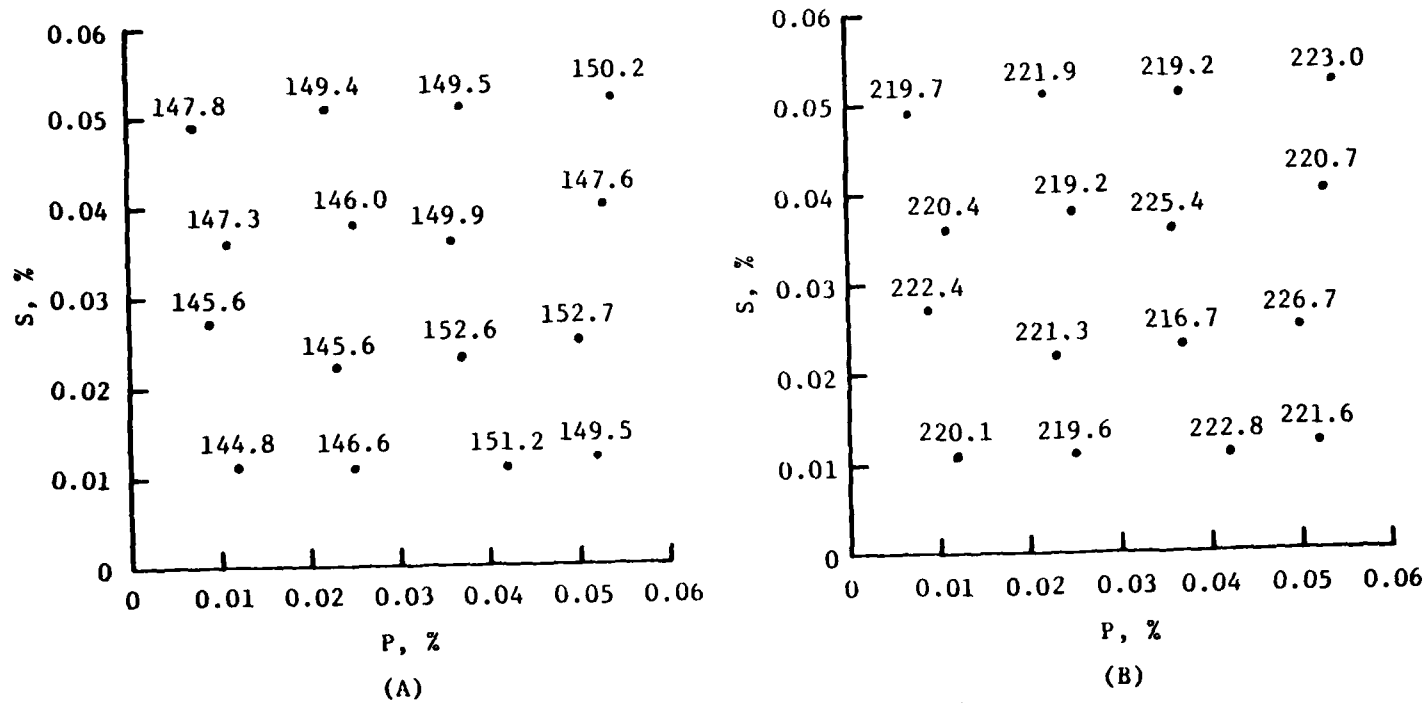

FIGURE 27. EFFECT OF PHOSPHORUS AND SULFUR ON THE YIELD STRENGTH OF (A) 1100°F AND (B) 400°F TEMPERED 4340 CAST STEEL.

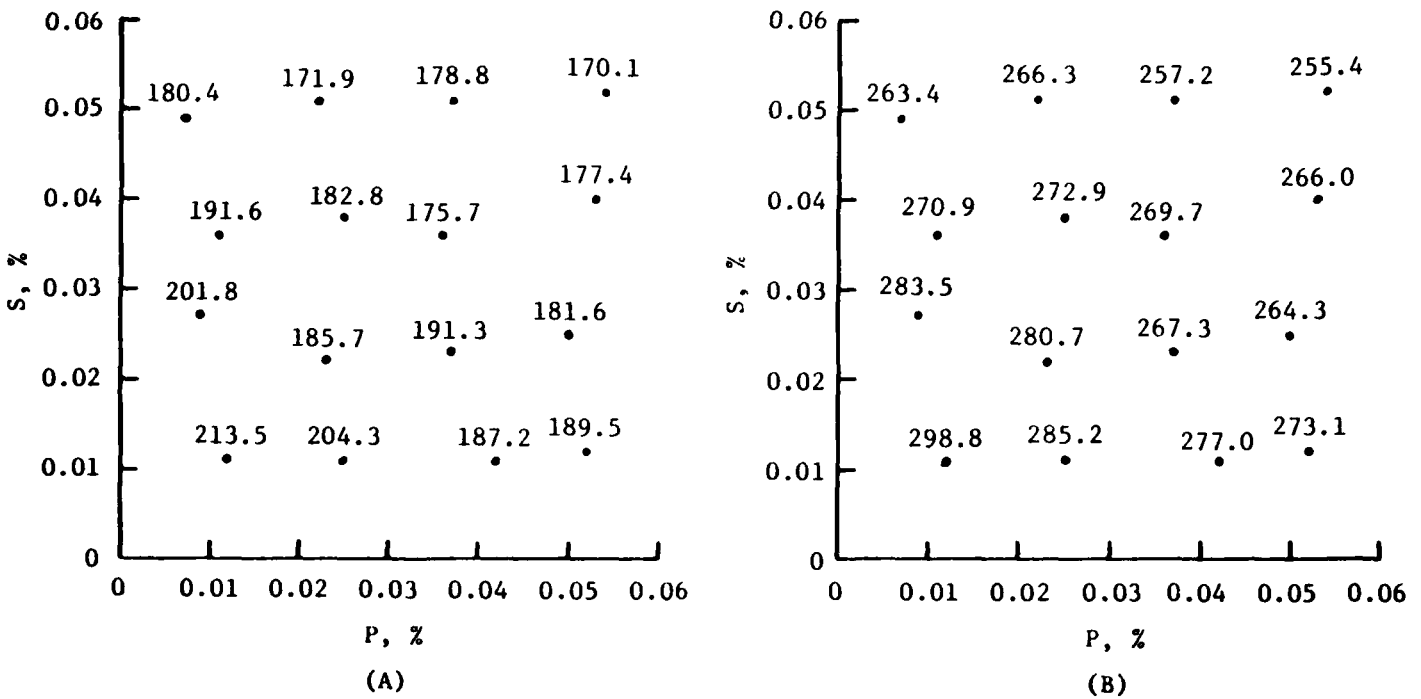

FIGURE 28. EFFECT OF PHOSPHORUS AND SULFUR ON THE TRUE FRACTURE STRESS OF (A) 1100°F AND (B) 400°F TEMPERED 4340 CAST STEEL.

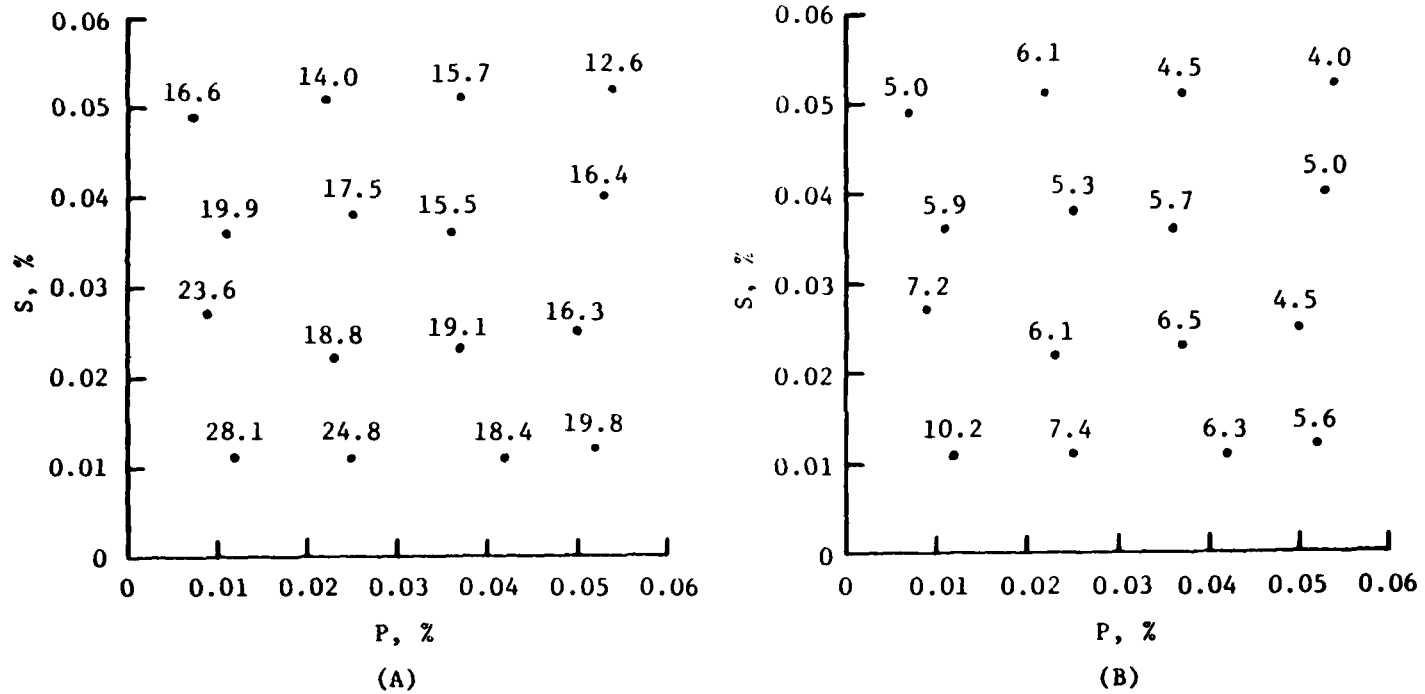

FIGURE 29. EFFECT OF PHOSPHORUS AND SULFUR ON THE REDUCTION OF AREA OF (A) 1100°F AND (B) 400°F TEMPERED 4340 CAST STEEL.

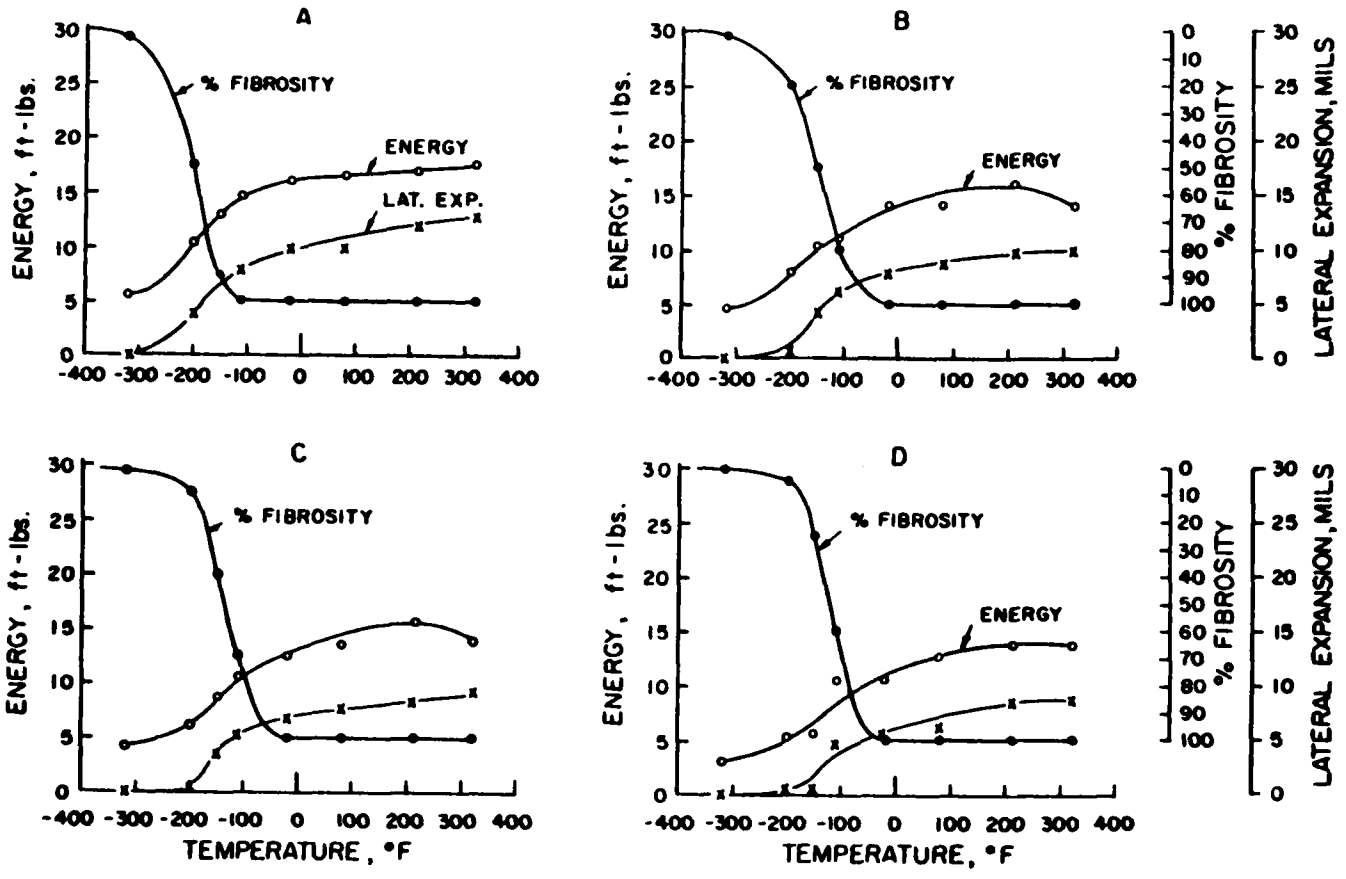

FIGURE 30-1. CHARPY IMPACT TOUGHNESS OF CASTINGS A, B, C AND D TEMPERED AT 1100°F.

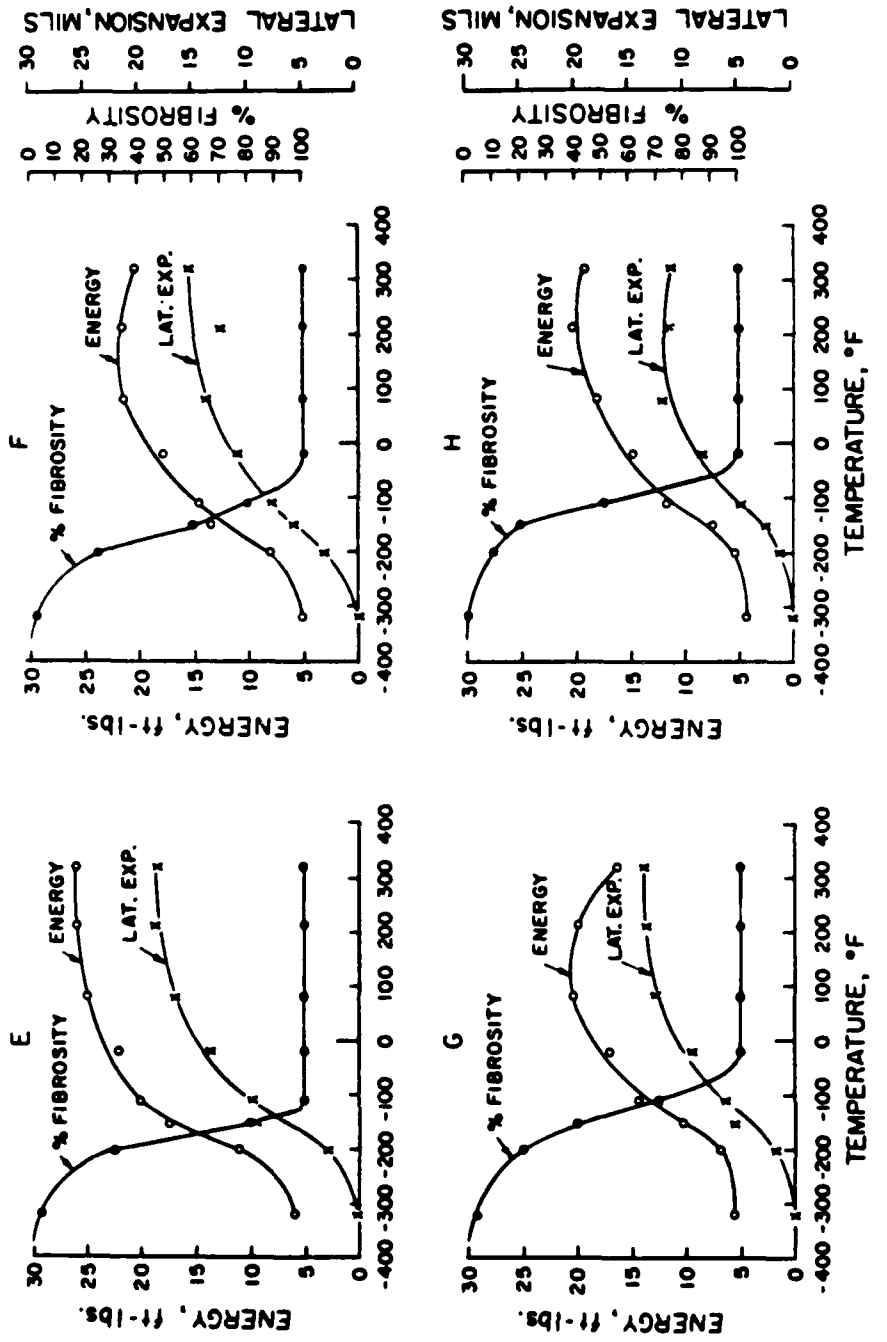

FIGURE 30-2. CHARPY IMPACT TOUGHNESS OF CASTINGS E, F, G AND H TEMPERED AT 1100°F.

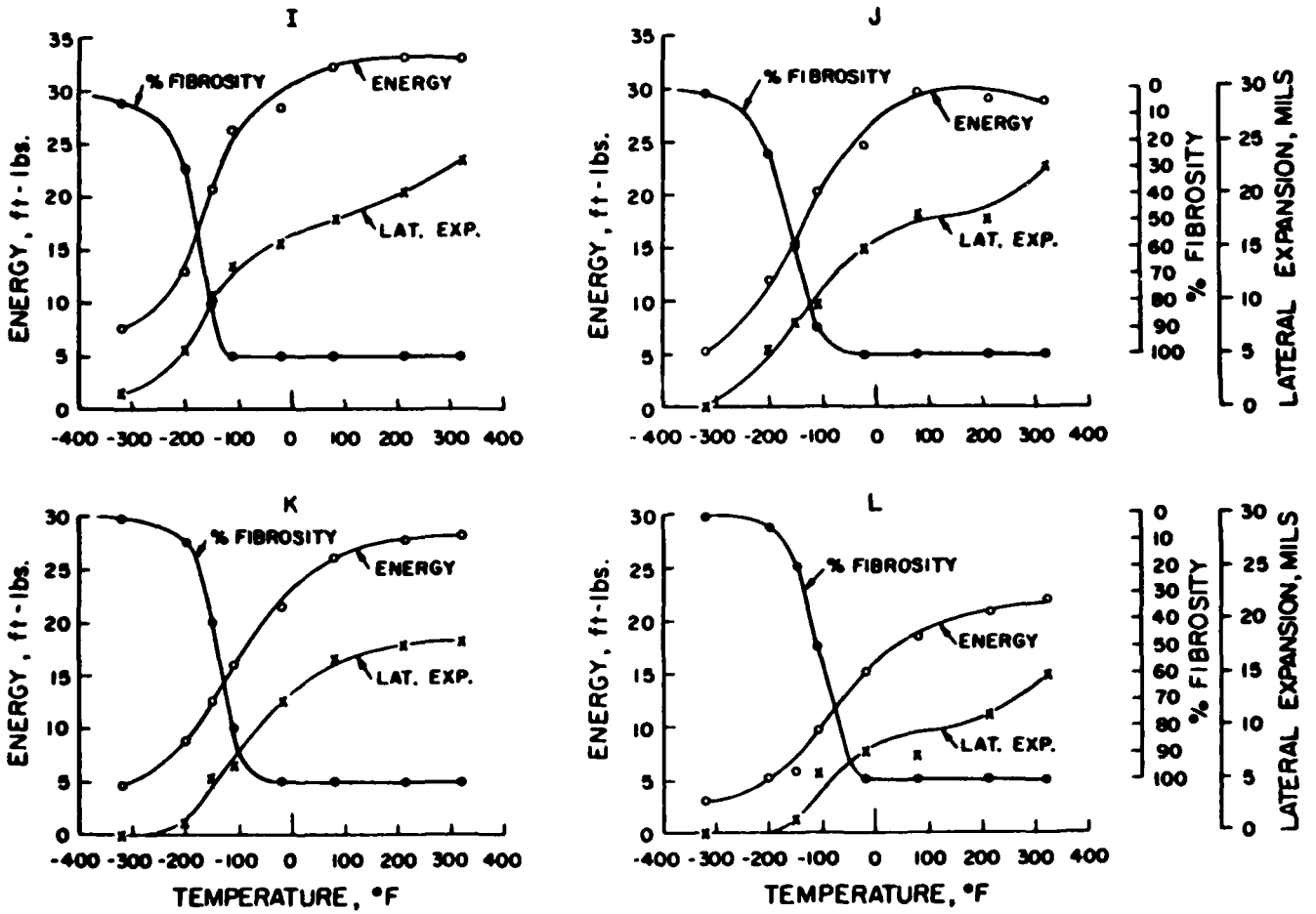

FIGURE 30-3. CHARPY IMPACT TOUGHNESS OF CASTINGS I, J, K AND L TEMPERED AT 1100°F.

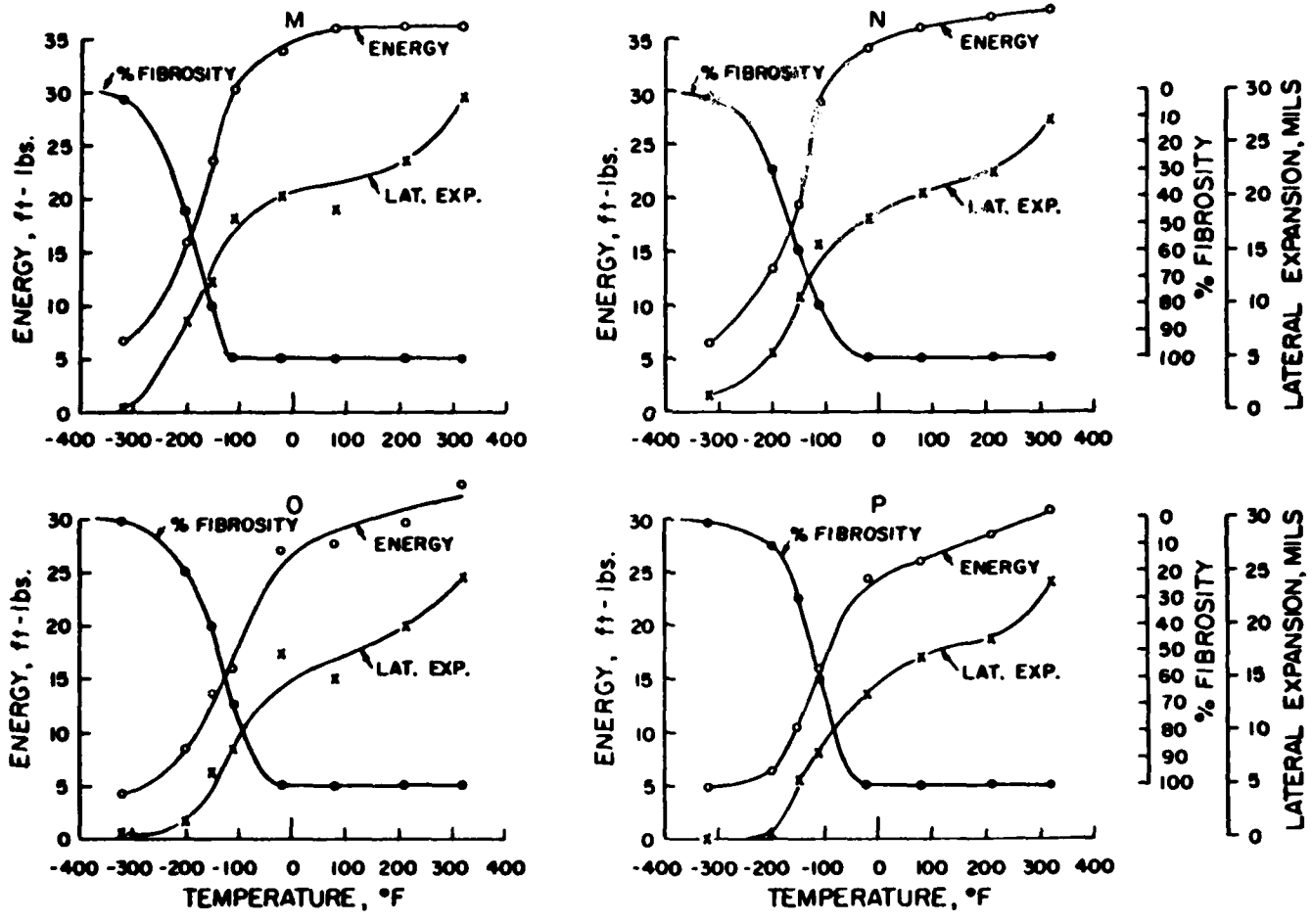

FIGURE 30-4. CHARPY IMPACT TOUGHNESS OF CASTINGS M, N, O AND P TEMPERED AT 1100°F.

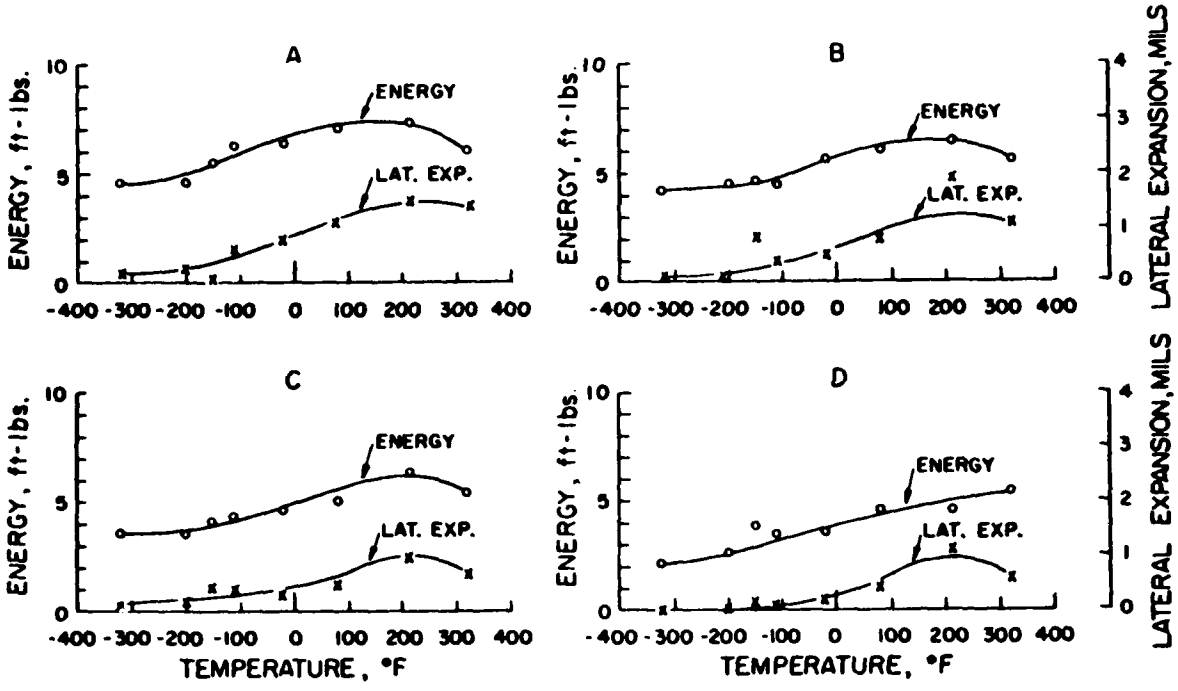

FIGURE 31-1. CHARPY IMPACT TOUGHNESS OF CASTINGS A, B, C AND D TEMPERED AT 400°F.

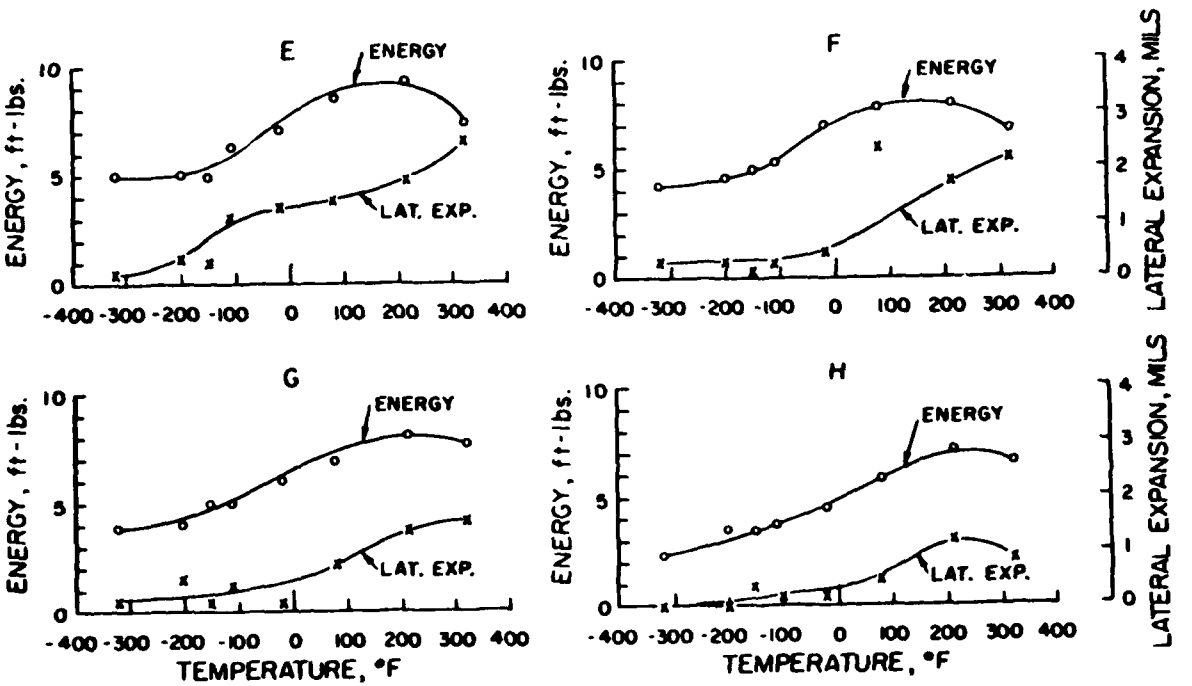

FIGURE 31-2. CHARPY IMPACT TOUGHNESS OF CASTINGS E, F, G AND H TEMPERED AT 400°F.

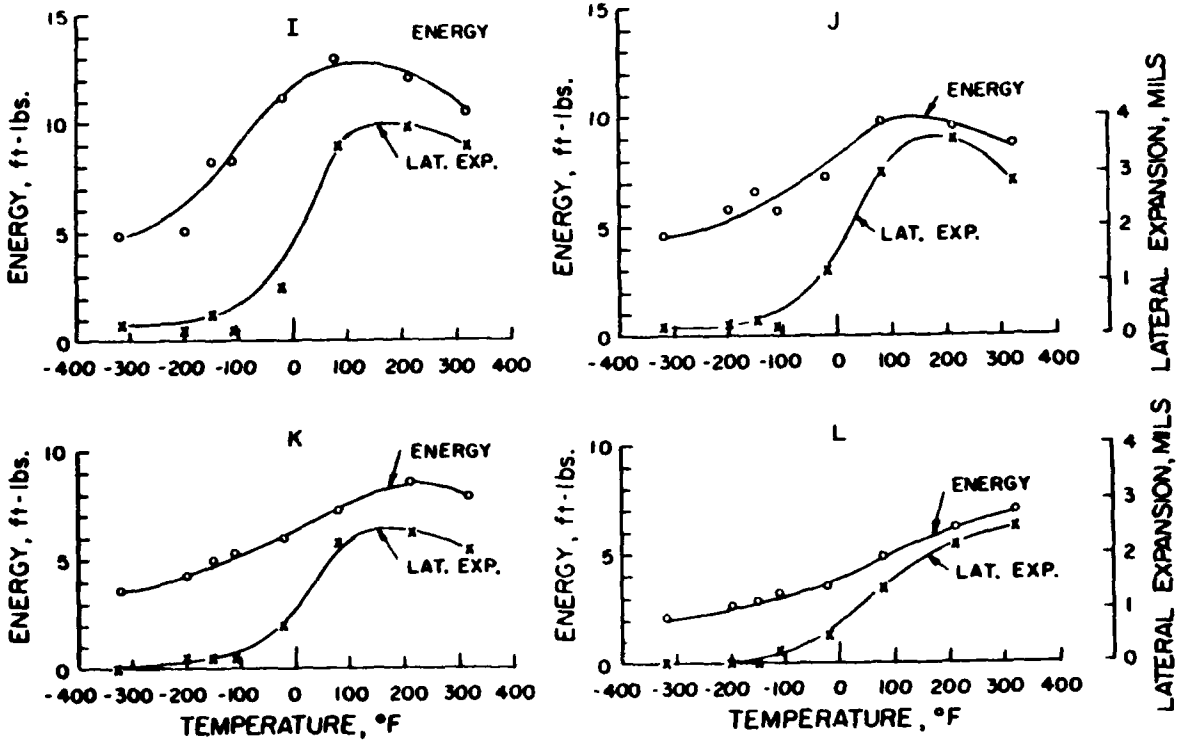

FIGURE 31-3. CHARPY IMPACT TOUGHNESS OF CASTINGS I, J, K AND L TEMPERED AT 400°F.

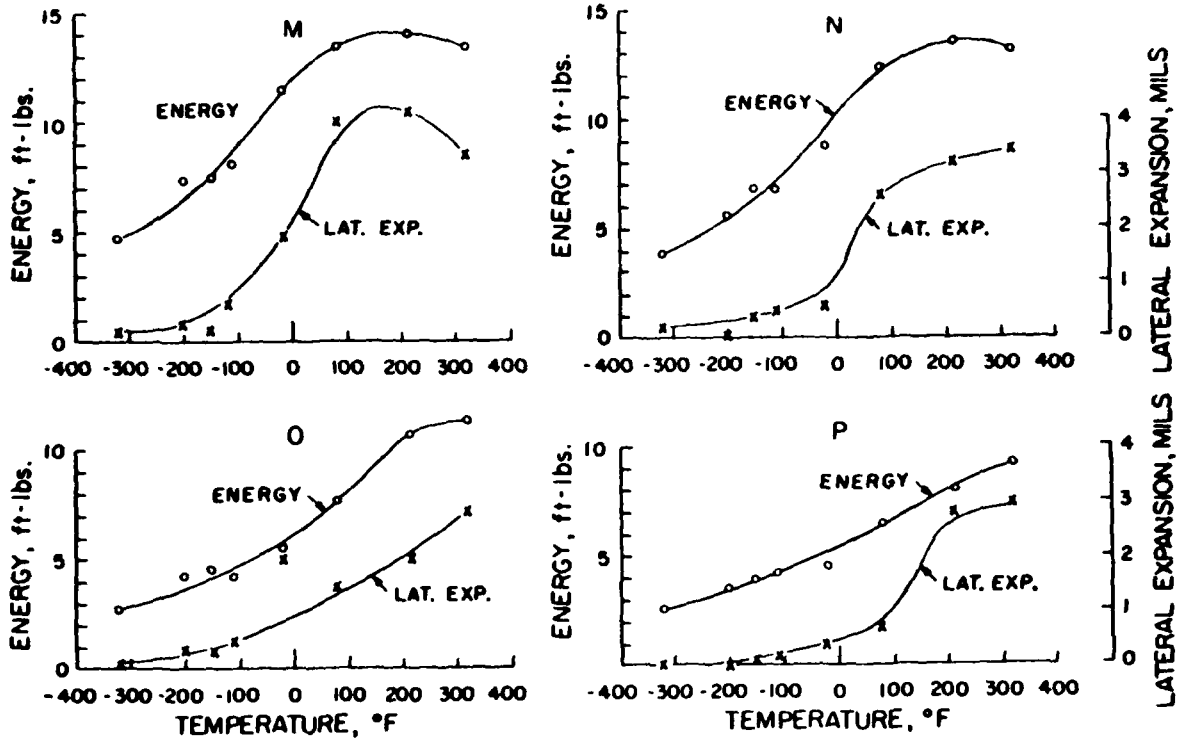

FIGURE 31-4. CHARPY IMPACT TOUGHNESS OF CASTINGS M, N, O AND P TEMPERED AT 400°F.

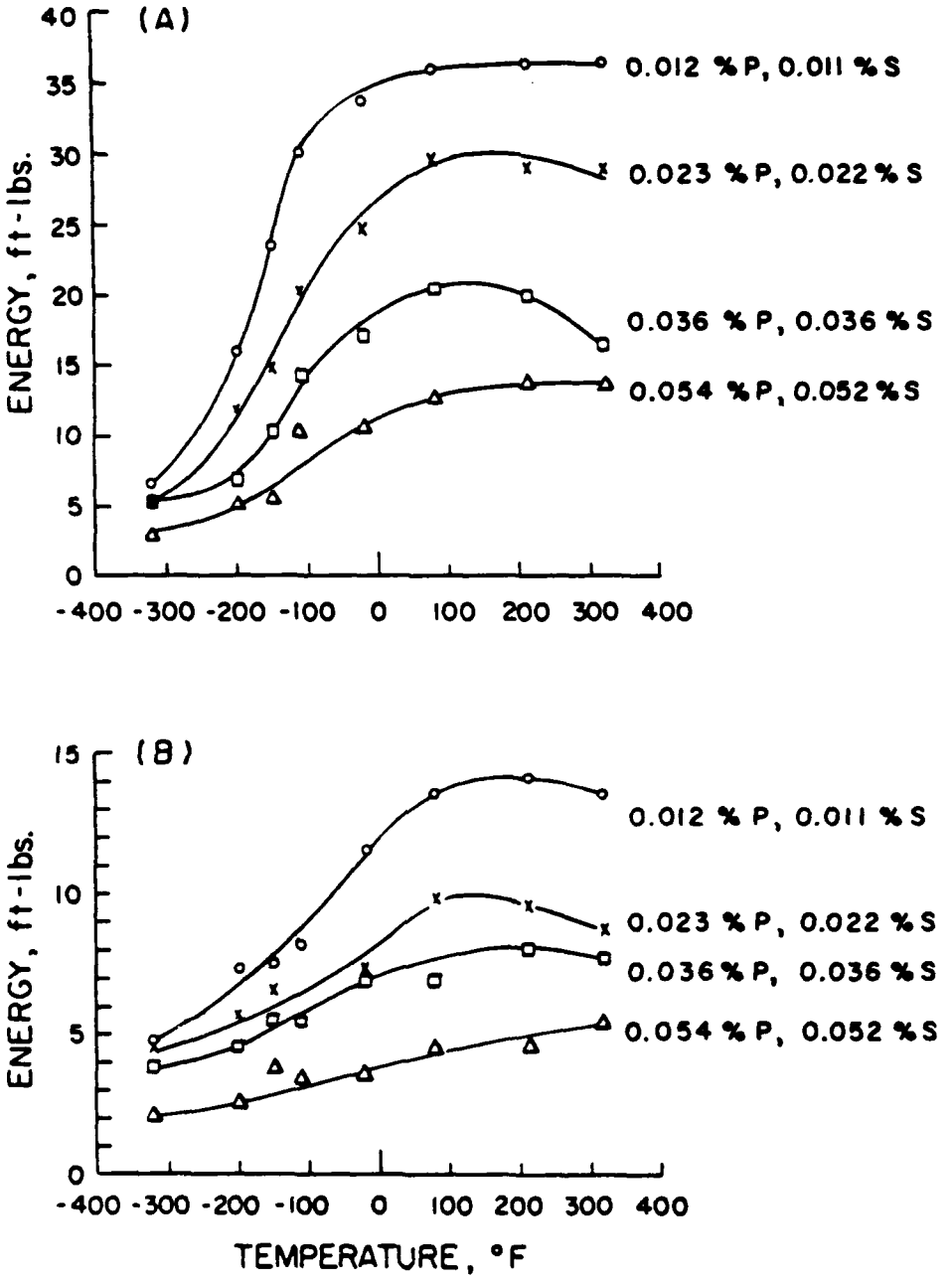

FIGURE 32. COMBINED EFFECT OF PHOSPHORUS AND SULFUR ON THE CHARPY IMPACT TOUGHNESS OF (A) 1100°F, AND (B) 400°F TEMPERED 4340 CAST STEEL.

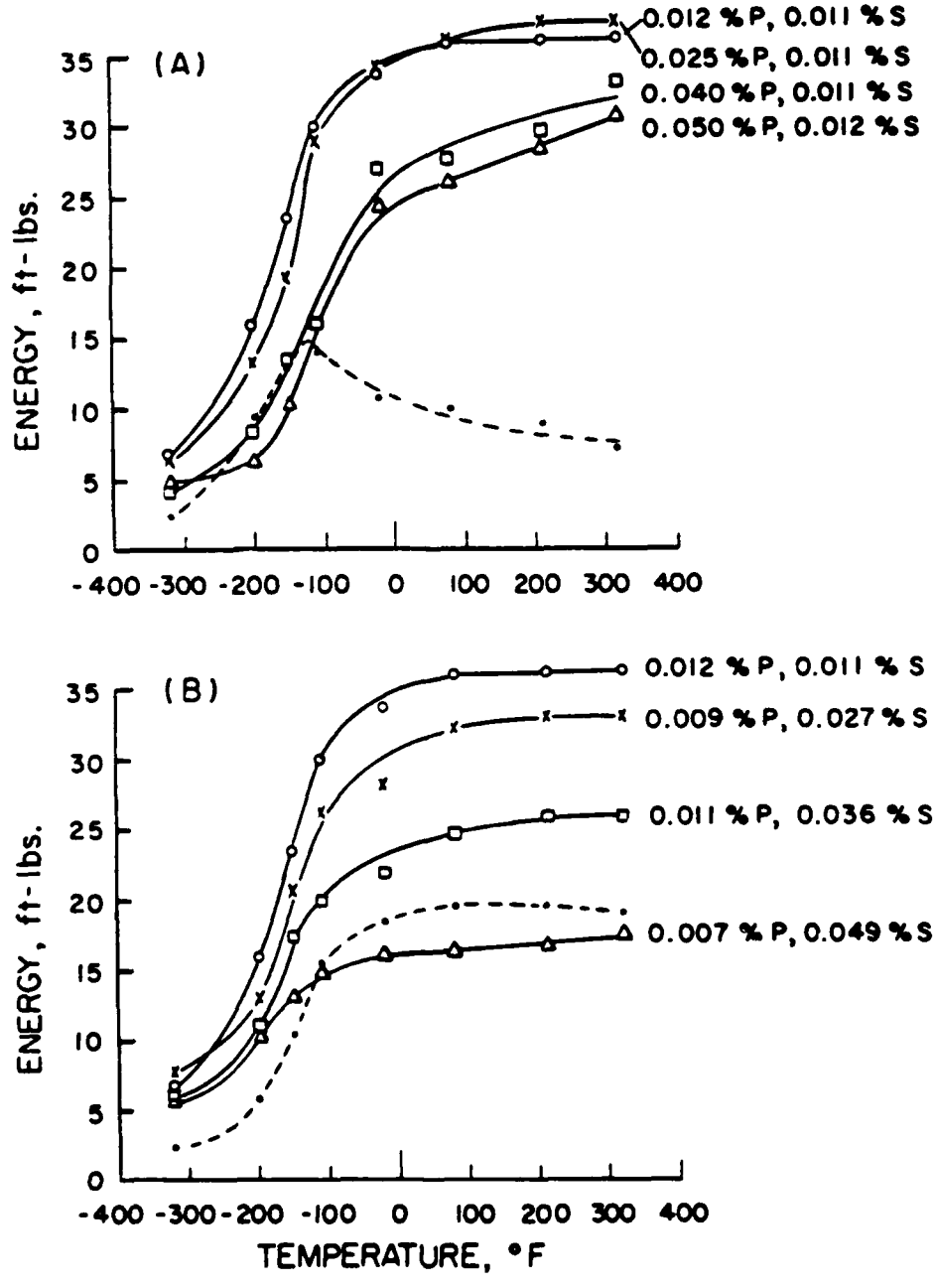

FIGURE 33-1. EFFECT OF INCREASING (A) PHOSPHORUS AT NOMINAL 0.010%S, AND (B) SULFUR AT NOMINAL 0.010%P ON THE CHARPY IMPACT TOUGHNESS OF 1100°F TEMPERED 4340 CAST STEEL.

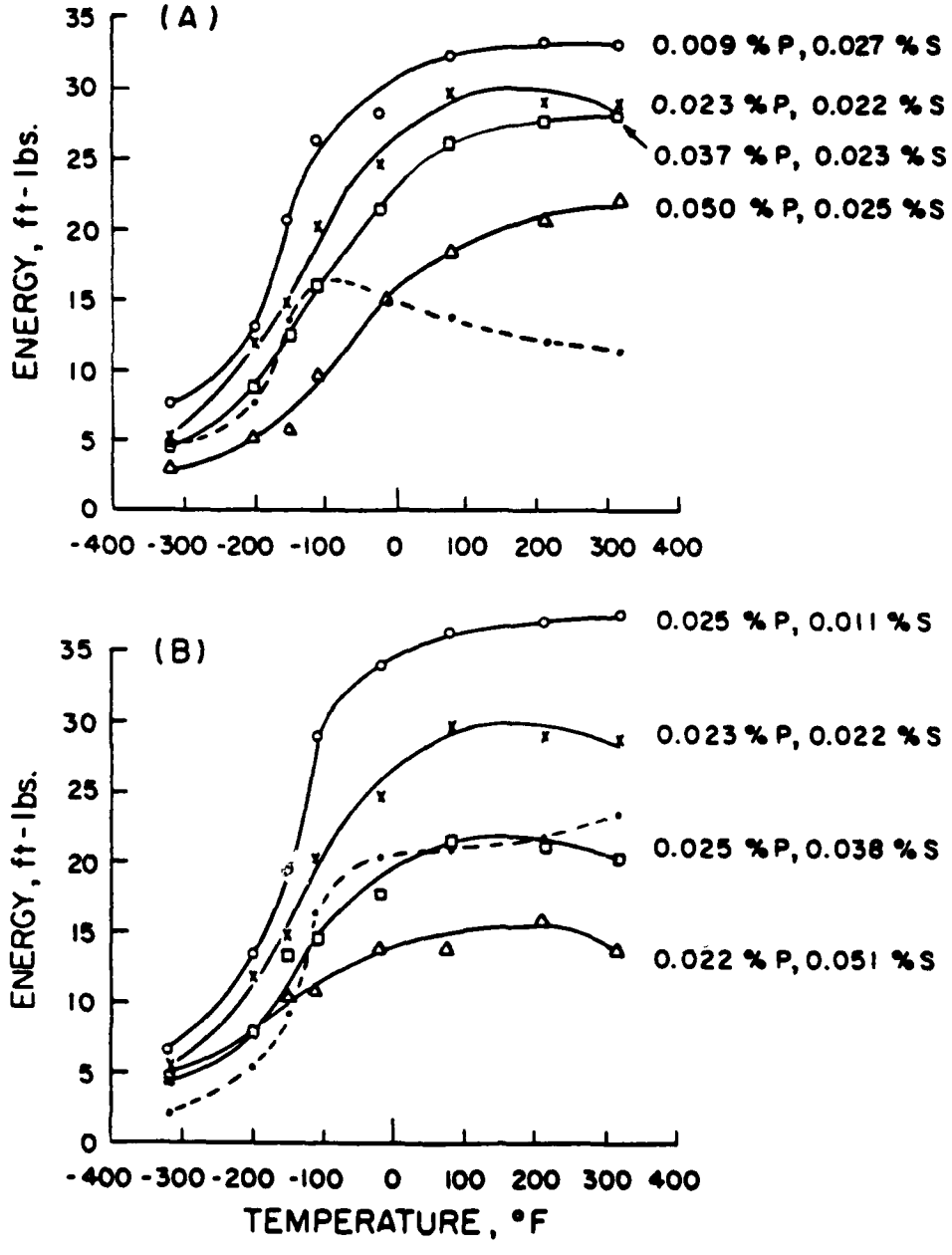

FIGURE 33-2. EFFECT OF INCREASING (A) PHOSPHORUS AT NOMINAL 0.025%S, AND (B) SULFUR AT NOMINAL 0.025%P ON THE CHARPY IMPACT TOUGHNESS OF 1100°F TEMPERED 4340 CAST STEEL.

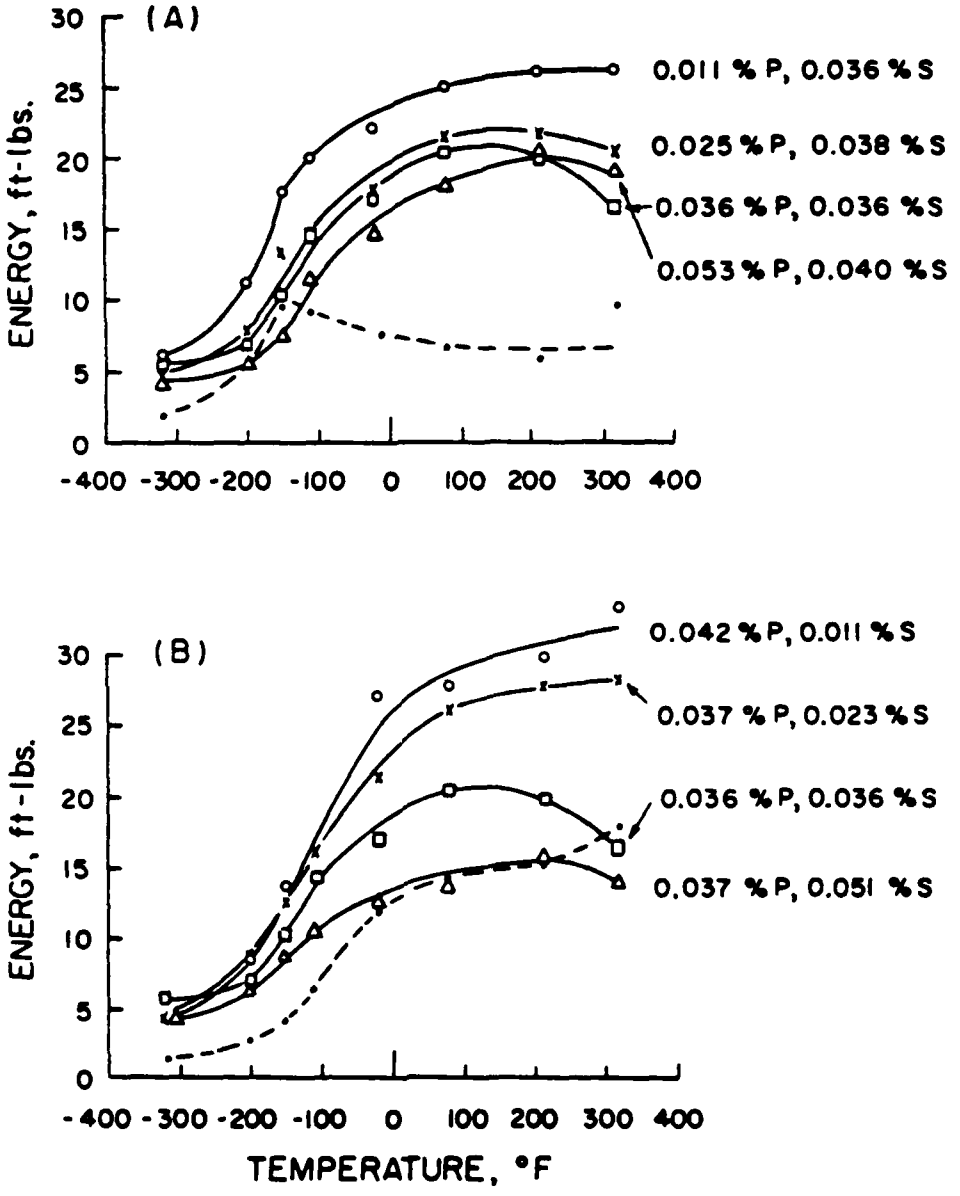

FIGURE 33-3. EFFECT OF INCREASING (A) PHOSPHORUS AT NOMINAL 0.035%S, AND (B) SULFUR AT NOMINAL 0.035%P ON THE CHARPY IMPACT TOUGHNESS OF 1100°F TEMPERED 4340 CAST STEEL.

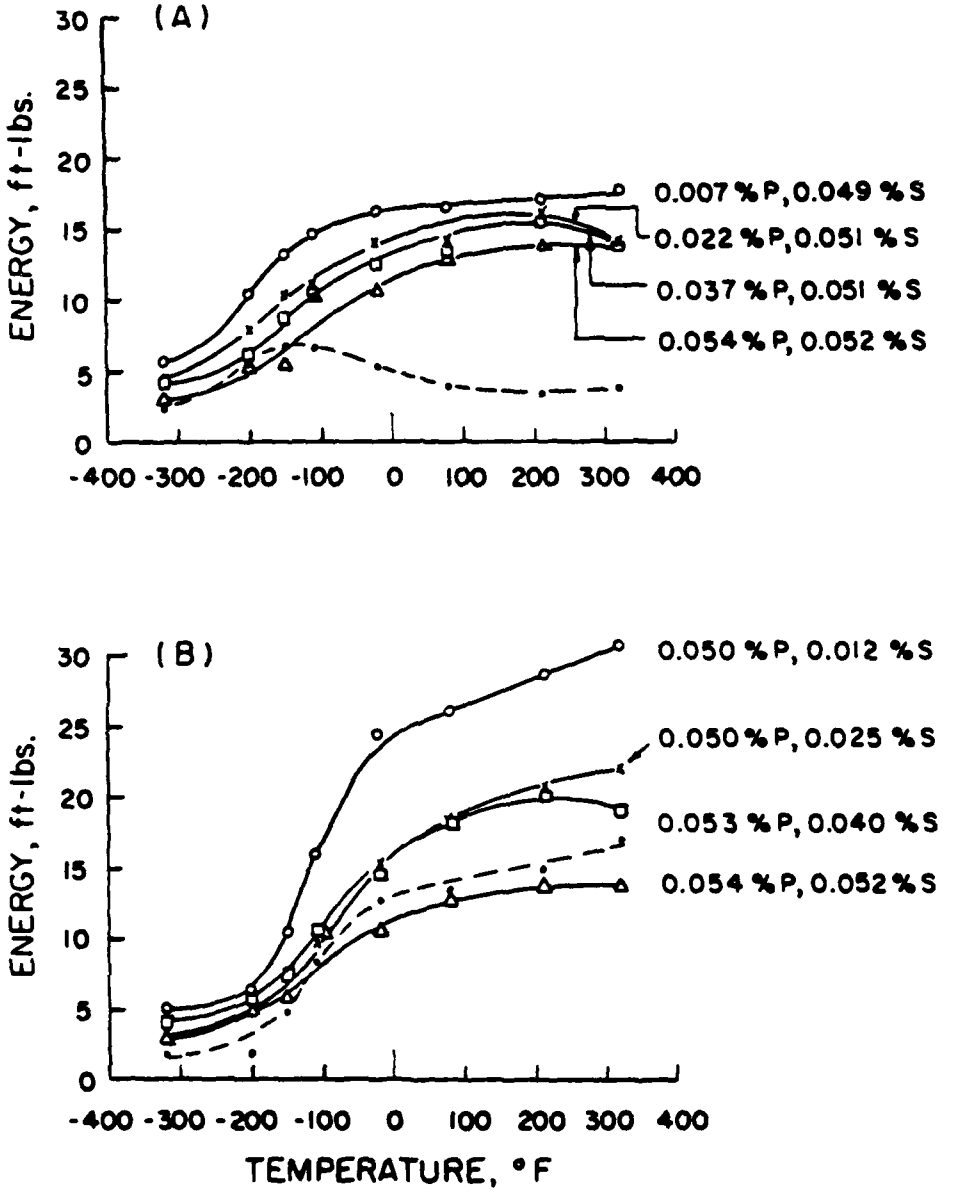

FIGURE 33-4. EFFECT OF INCREASING (A) PHOSPHORUS AT NOMINAL 0.050%S, AND (B) SULFUR AT NOMINAL 0.050%P ON THE CHARPY IMPACT TOUGHNESS OF 1100°F TEMPERED 4340 CAST STEEL.

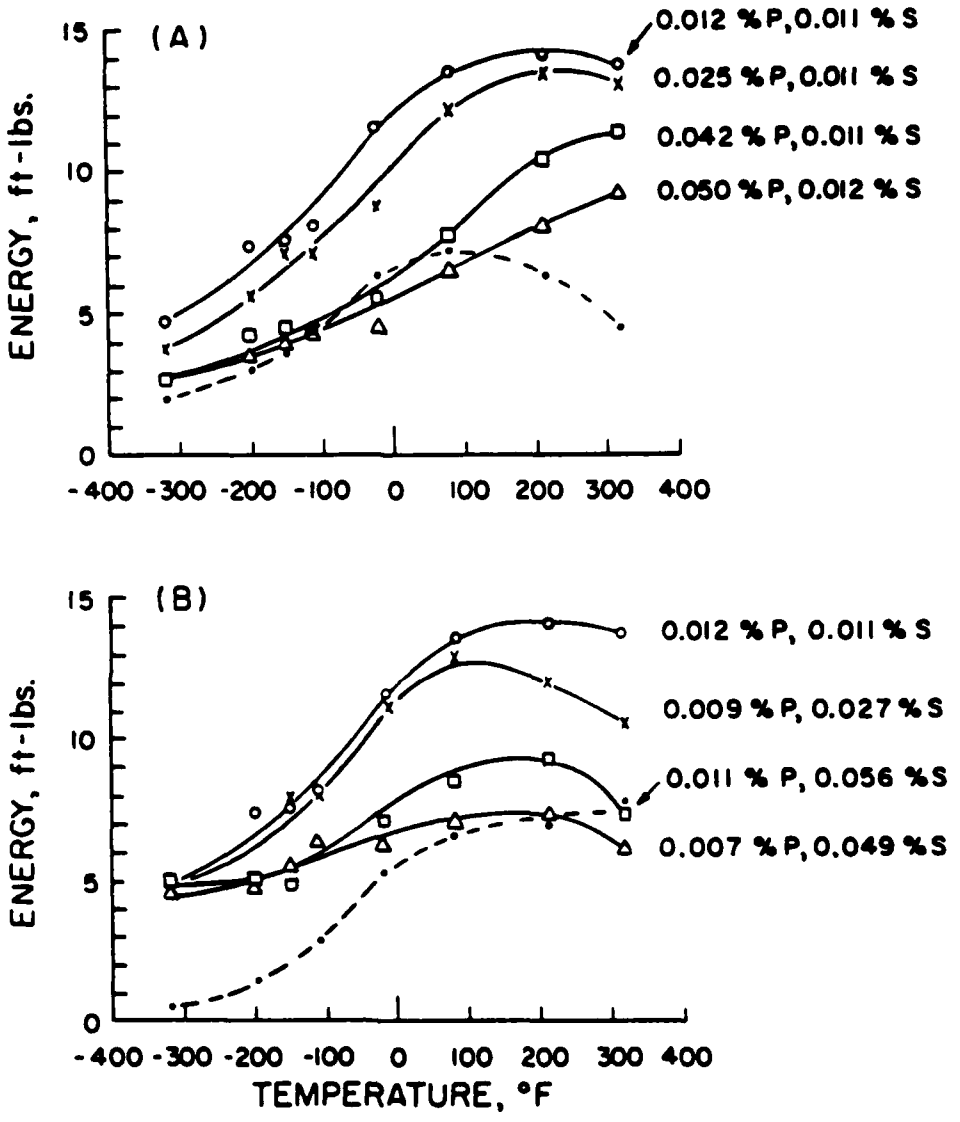

FIGURE 34-1. EFFECT OF INCREASING (A) PHOSPHORUS AT NOMINAL 0.010%S, AND (B) SULFUR AT NOMINAL 0.010%P ON THE CHARPY IMPACT TOUGHNESS OF 400°F TEMPERED 4340 CAST STEEL.

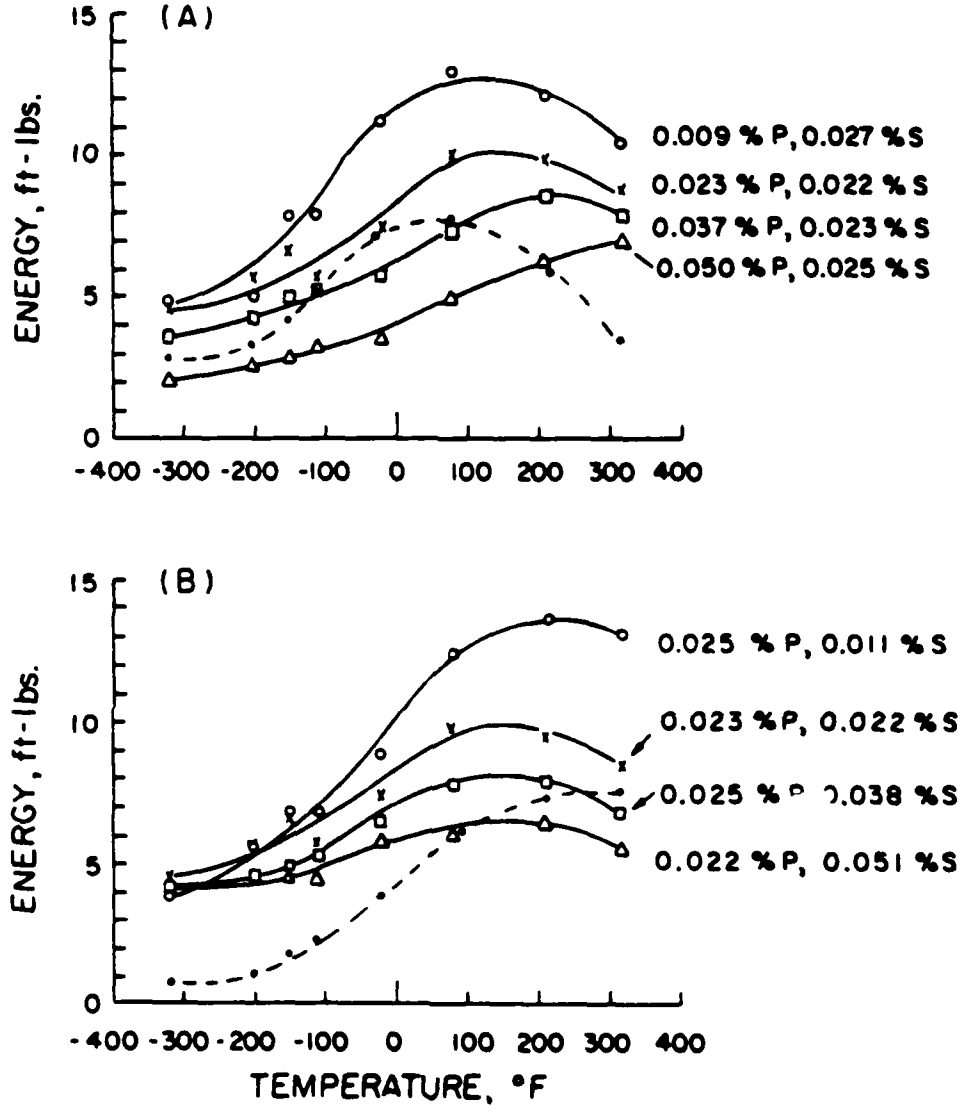

FIGURE 34-2. EFFECT OF INCREASING (A) PHOSPHORUS AT NOMINAL 0.025%S, AND (B) SULFUR AT NOMINAL 0.025%P ON THE CHARPY IMPACT TOUGHNESS OF 400°F TEMPERED 4340 CAST STEEL.

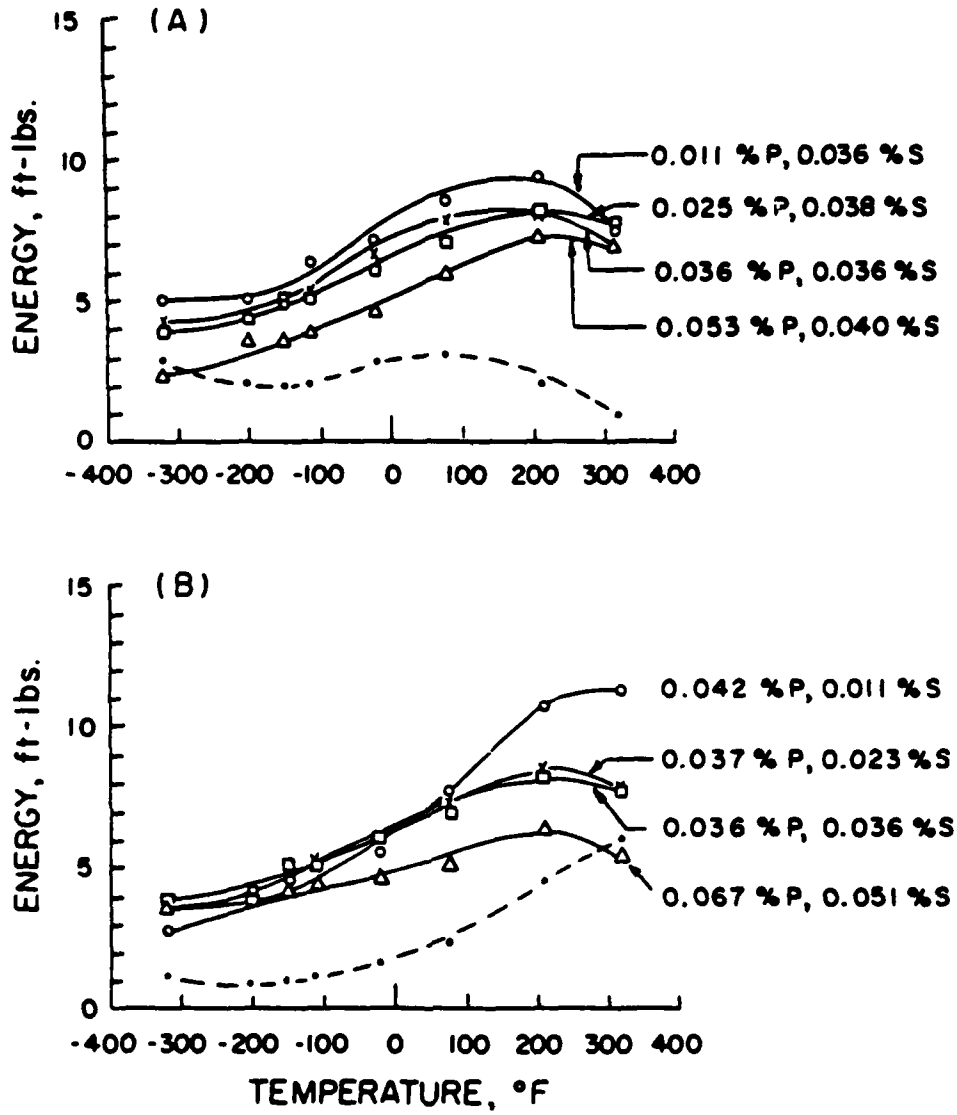

FIGURE 34-3. EFFECT OF INCREASING (A) PHOSPHORUS AT NOMINAL 0.035%S, AND (B) SULFUR AT NOMINAL 0.035%P ON THE CHARPY IMPACT TOUGHNESS OF 400°F TEMPERED 4340 CAST STEEL.

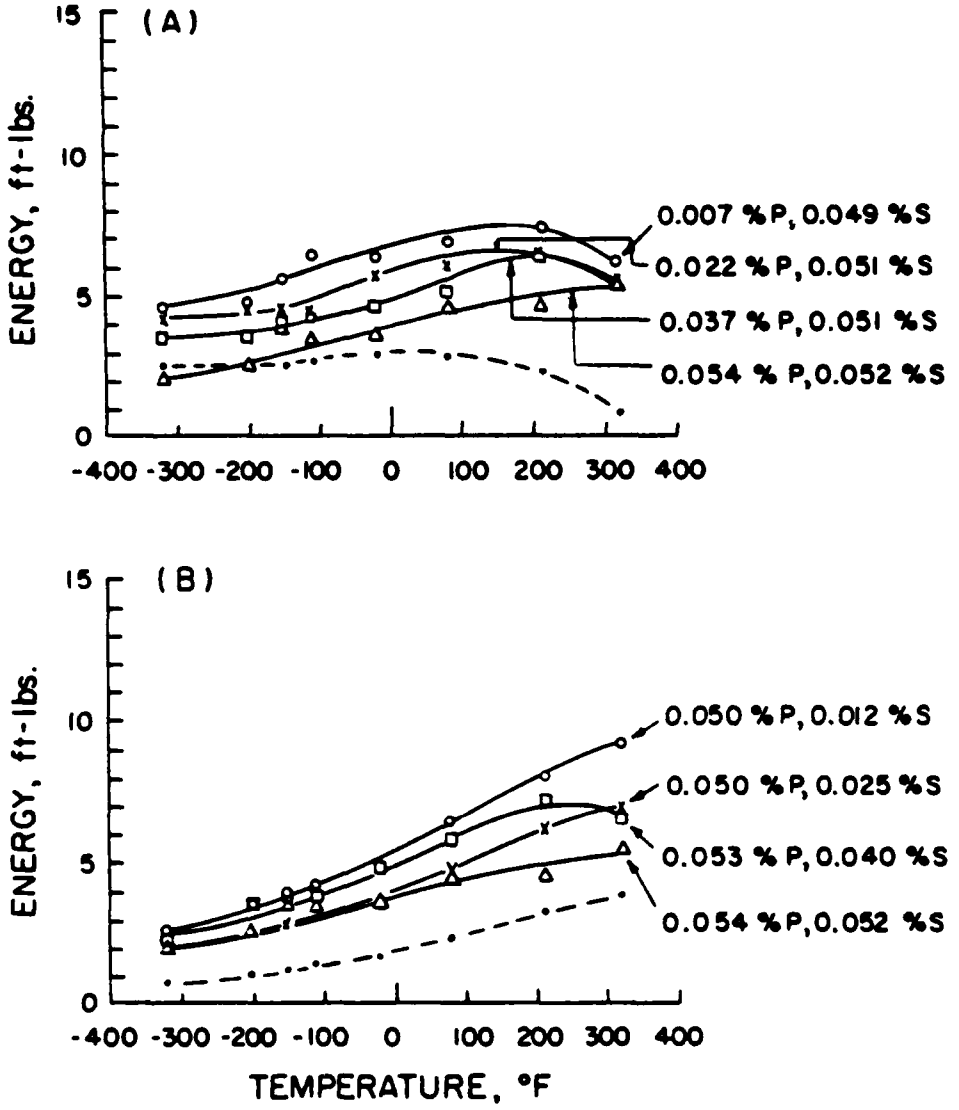

FIGURE 34-4. EFFECT OF INCREASING (A) PHOSPHORUS AT NOMINAL 0.050%S, AND (B) SULFUR AT NOMINAL 0.050%P ON THE CHARPY IMPACT TOUGHNESS OF 400°F TEMPERED 4340 CAST STEEL.

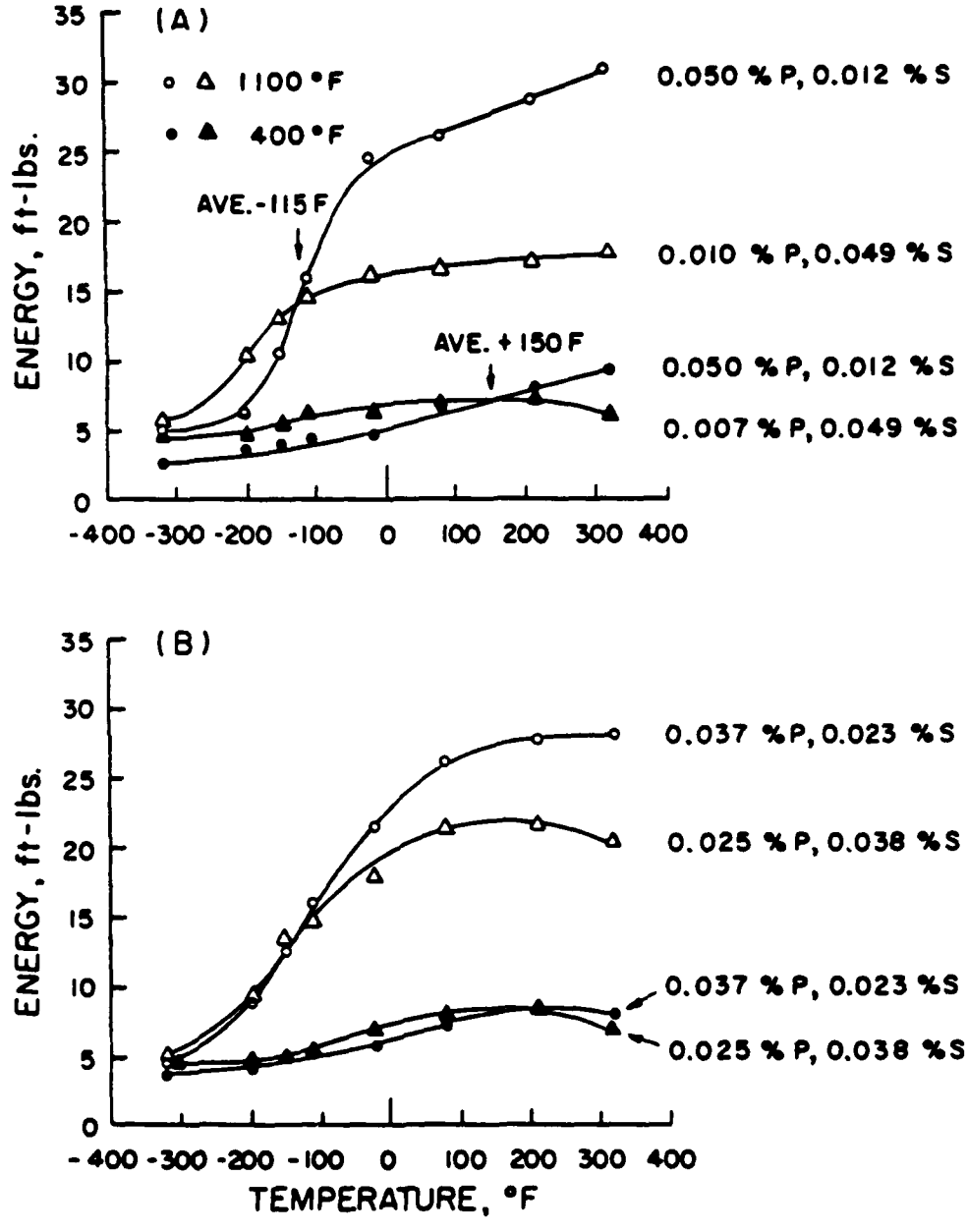

FIGURE 35-1. RELATIVE EFFECT OF PHOSPHORUS AND SULFUR FROM COUNTERPART CASTINGS (A) P AND A, AND (B) K AND F ON THE CHARPY IMPACT BEHAVIOR OF 1100°F AND 400°F TEMPERED 4340 CAST STEEL.

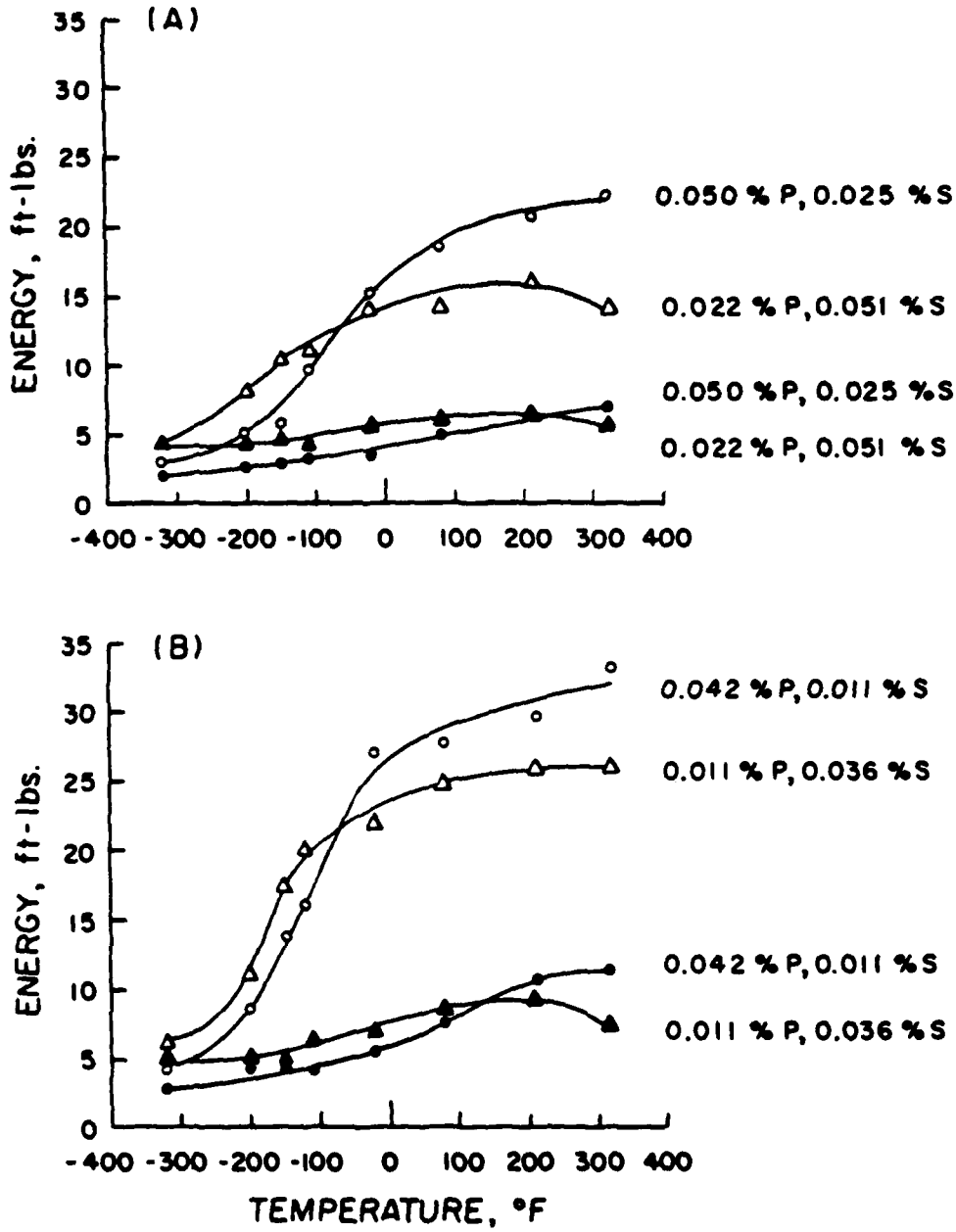

FIGURE 35-2. RELATIVE EFFECT OF PHOSPHORUS AND SULFUR FROM COUNTERPART CASTINGS (A) L AND B, AND (B) O AND E ON THE CHARPY IMPACT BEHAVIOR OF 1100°F AND 400°F TEMPERED 4340 CAST STEEL.

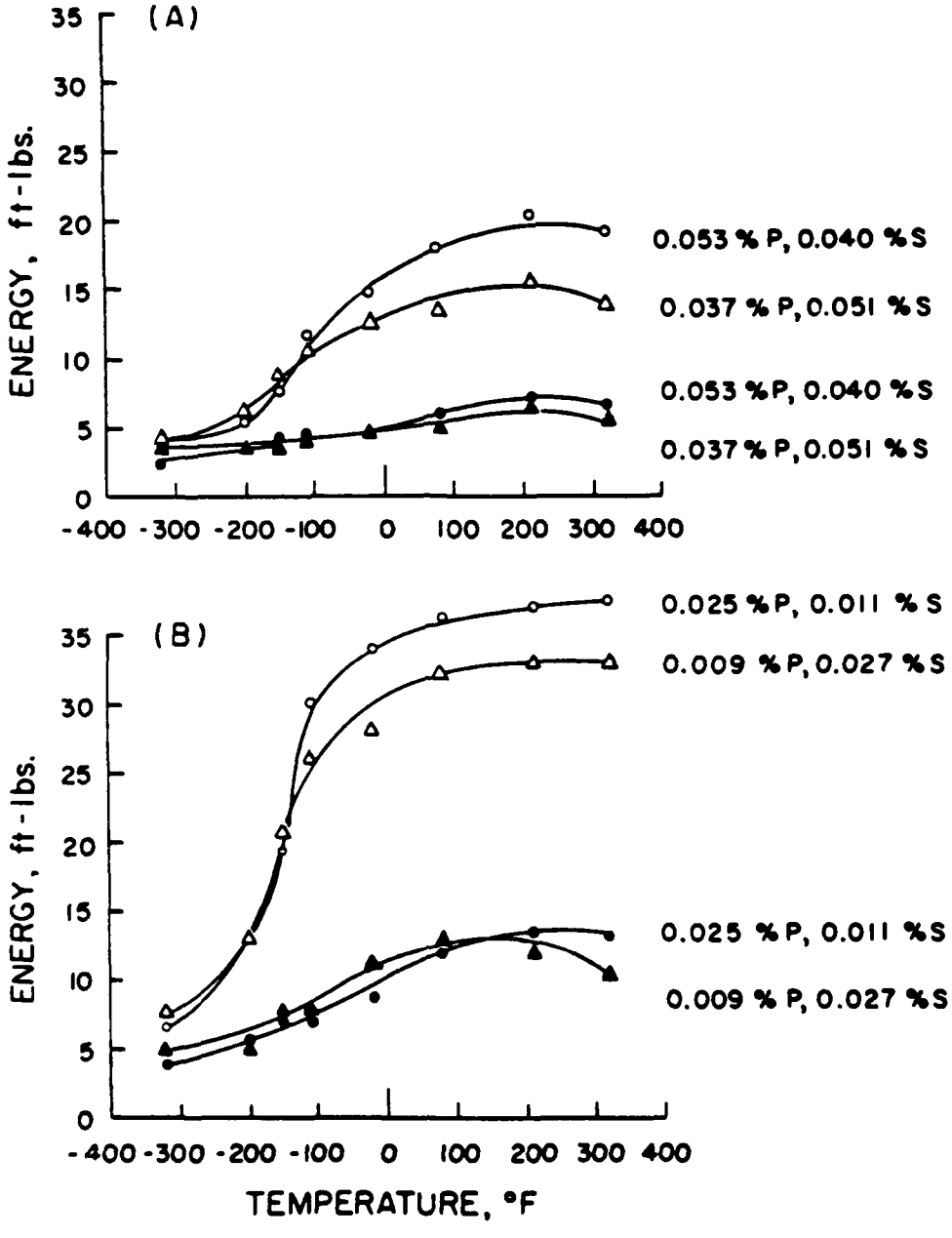

FIGURE 35-3. RELATIVE EFFECT OF PHOSPHORUS AND SULFUR FROM COUNTERPART CASTINGS (A) H AND C, AND (B) N AND I ON THE CHARPY IMPACT BEHAVIOR OF 1100°F AND 400°F TEMPERED 4340 CAST STEEL.

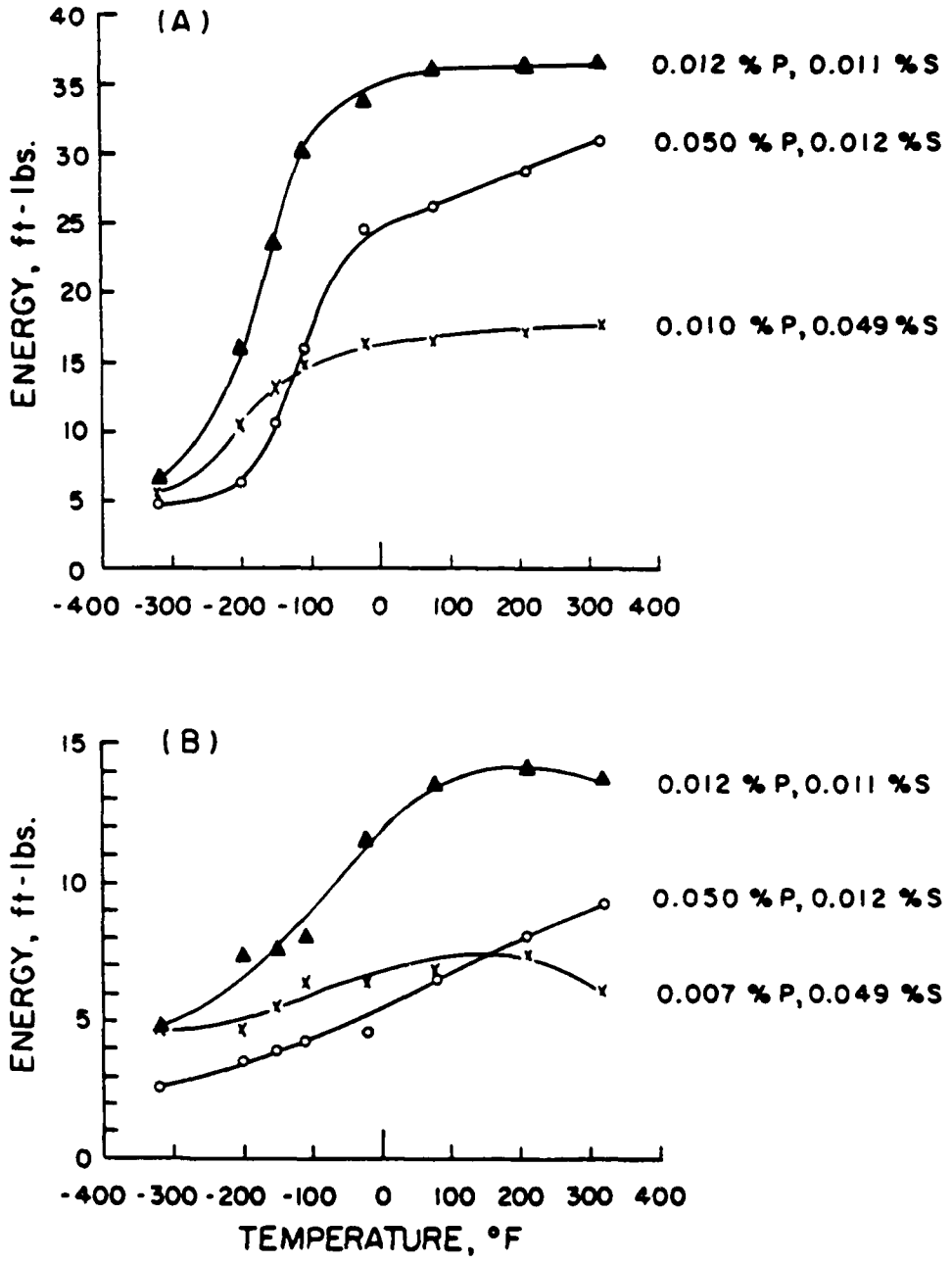

FIGURE 35-4. RELATIVE EFFECT OF PHOSPHORUS AND SULFUR ON THE IMPACT TRANSITION BEHAVIOR OF (A) 1100°F AND (B) 400°F TEMPERED 4340 CAST STEEL.

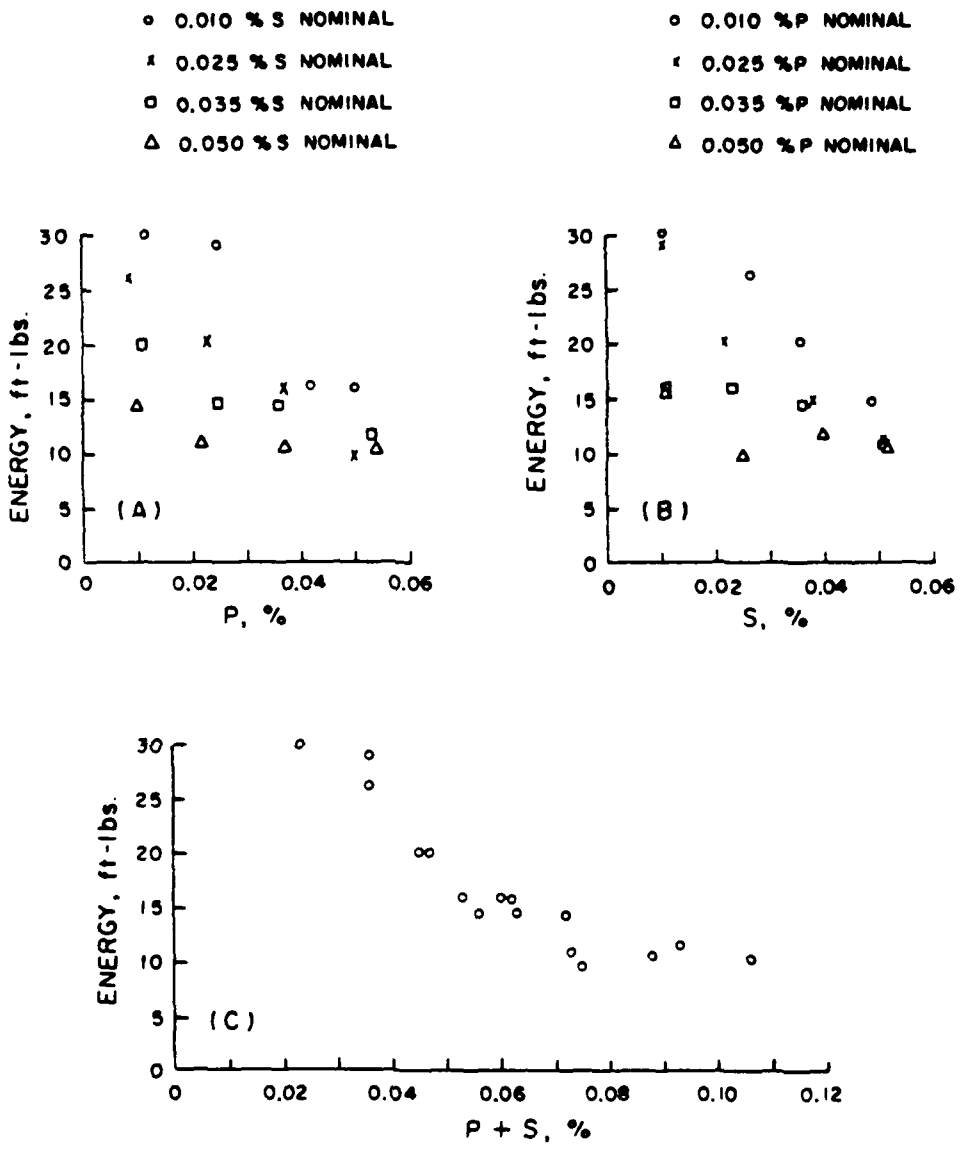

FIGURE 36. EFFECT OF (A) PHOSPHORUS, (B) SULFUR AND (C) PHOSPHORUS PLUS SULFUR CONTENT ON THE -115°F CHARPY IMPACT TOUGHNESS OF 4340 CAST STEEL TEMPERED AT 1100°F.

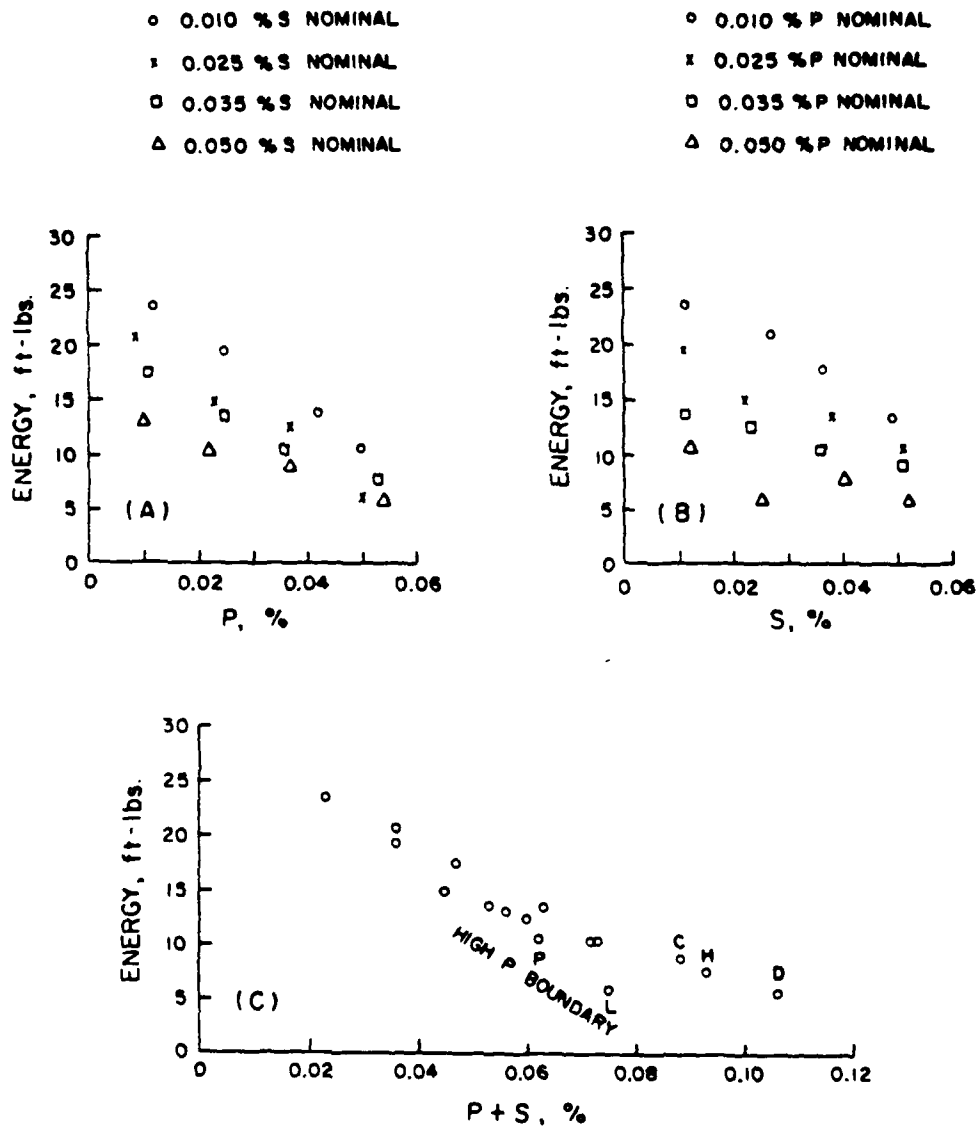

FIGURE 37. EFFECT OF (A) PHOSPHORUS, (B) SULFUR AND (C) PHOSPHORUS PLUS SULFUR CONTENT ON THE -150°F CHARPY IMPACT TOUGHNESS OF 4340 CAST STEEL TEMPERED AT 1100°F.

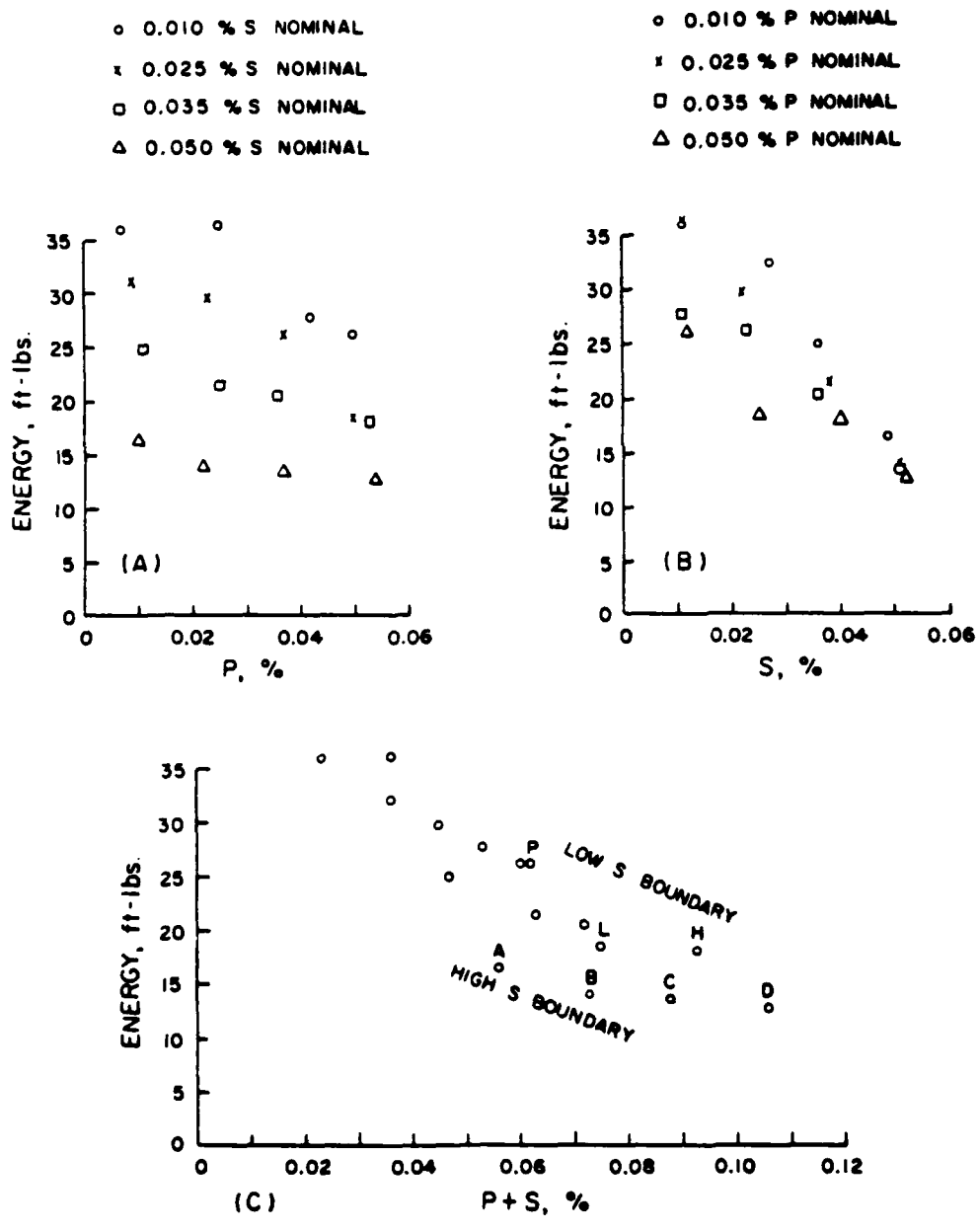

FIGURE 38. EFFECT OF (A) PHOSPHORUS, (B) SULFUR AND (C) PHOSPHORUS PLUS SULFUR CONTENT ON THE ROOM TEMPERATURE CHARPY IMPACT TOUGHNESS OF 4340 CAST STEEL TEMPERED AT 1100°F.

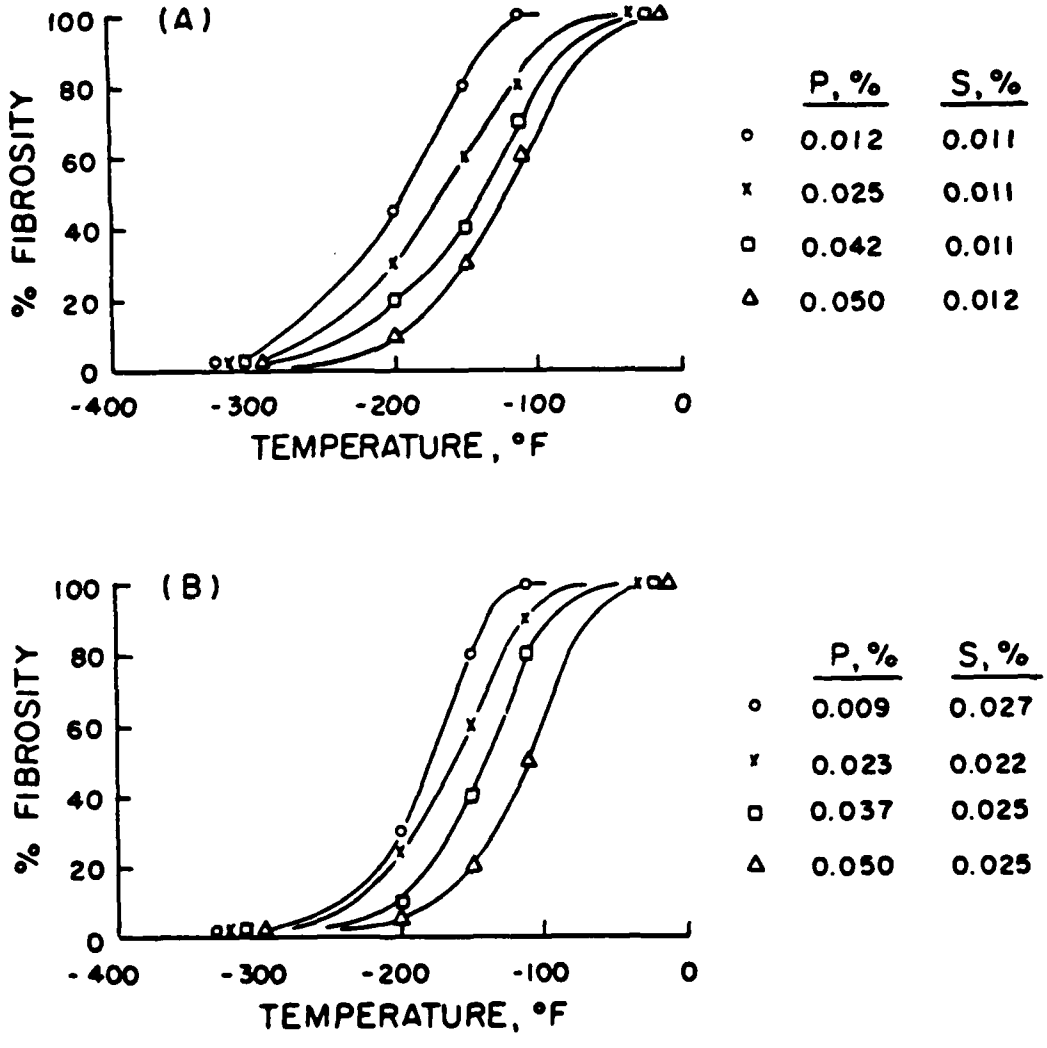

FIGURE 39-1. EFFECT OF INCREASING PHOSPHORUS AT NOMINAL (A) 0.010%S AND (B) 0.025%S ON THE % FIBROSITY TRANSITION BEHAVIOR OF 1100°F TEMPERED 4340 CAST STEEL.

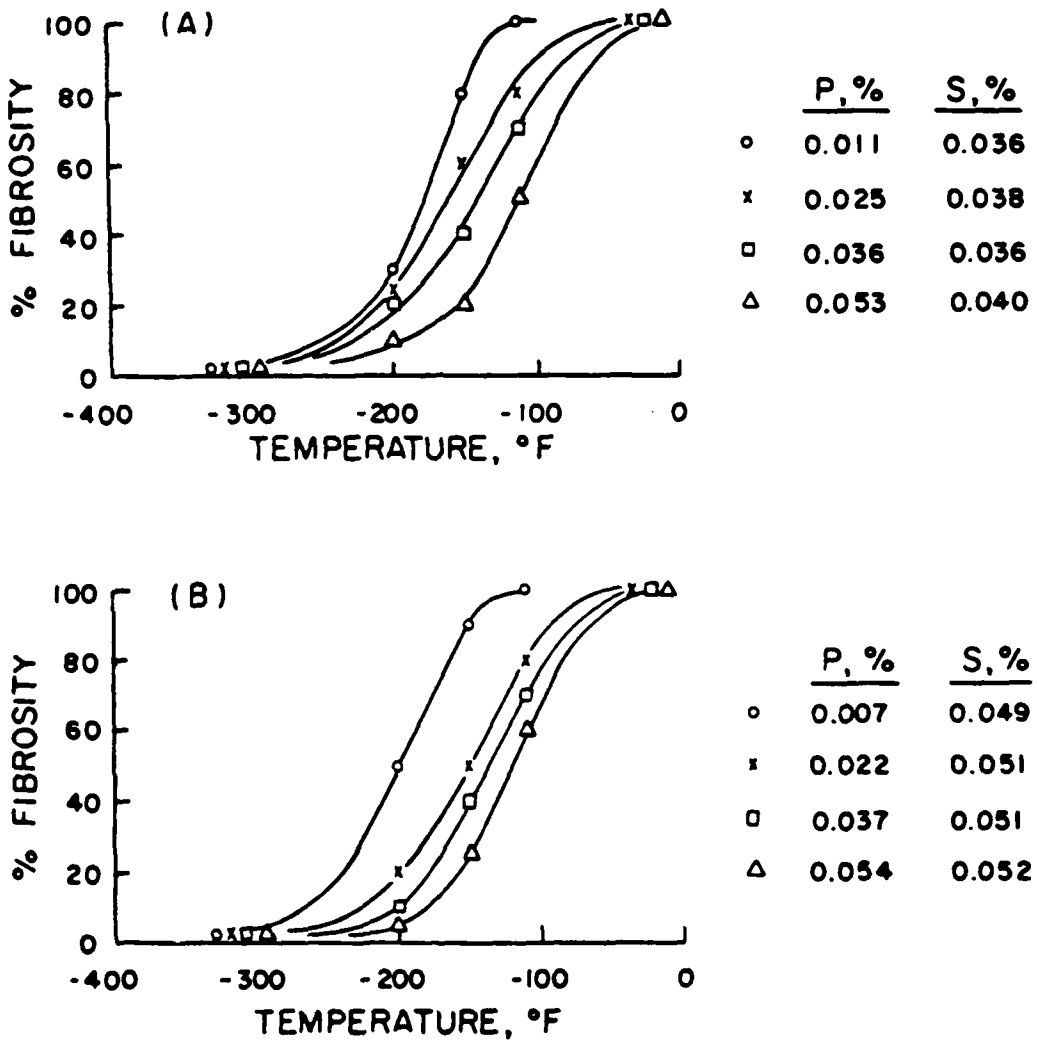

FIGURE 39-2. EFFECT OF INCREASING PHOSPHORUS AT NOMINAL (A) 0.035%S AND (B) 0.050%S ON THE % FIBROSITY TRANSITION BEHAVIOR OF 1100°F TEMPERED 4340 CAST STEEL.

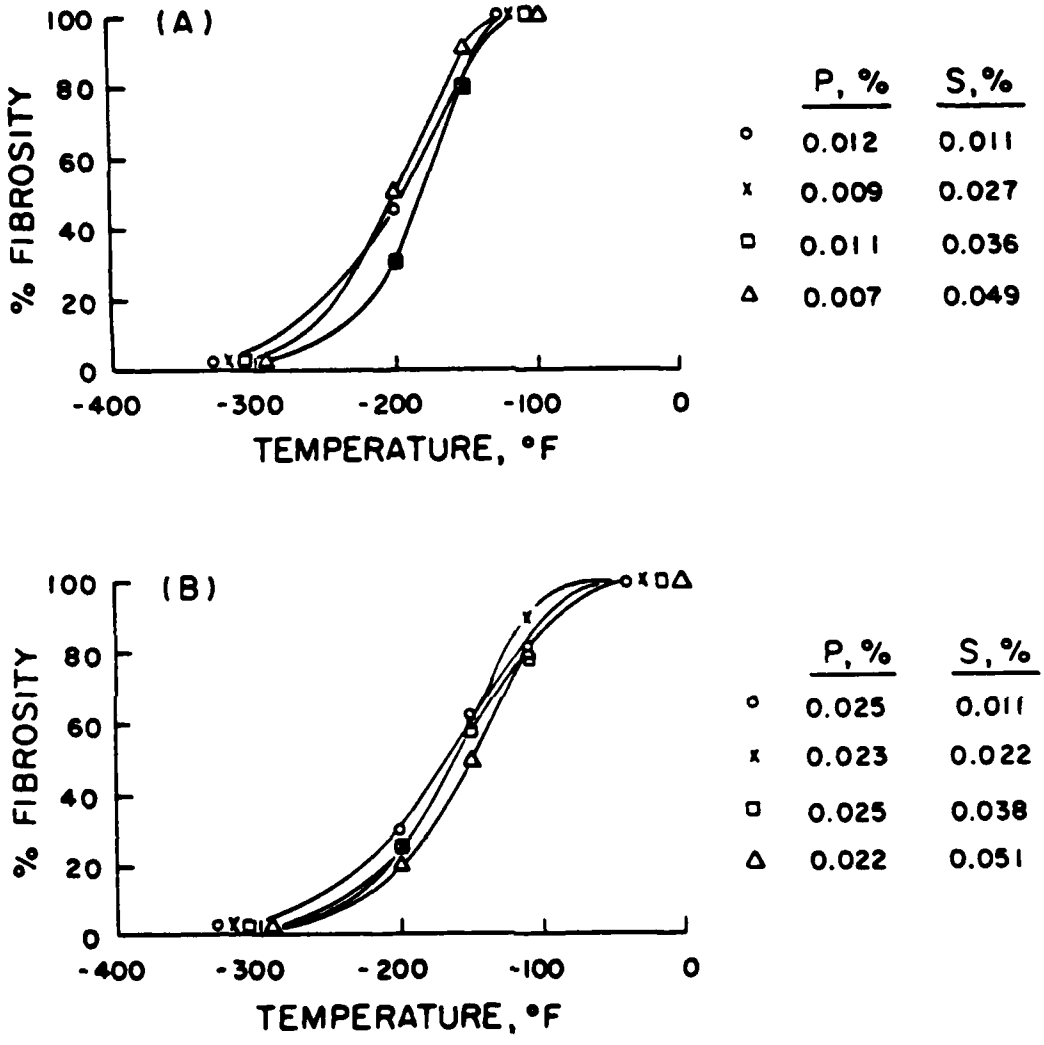

FIGURE 40-1. EFFECT OF INCREASING SULFUR AT NOMINAL (A) 0.010%P AND (B) 0.025%P ON THE % FIBROSITY TRANSITION BEHAVIOR OF 1100°F TEMPERED 4340 CAST STEEL.

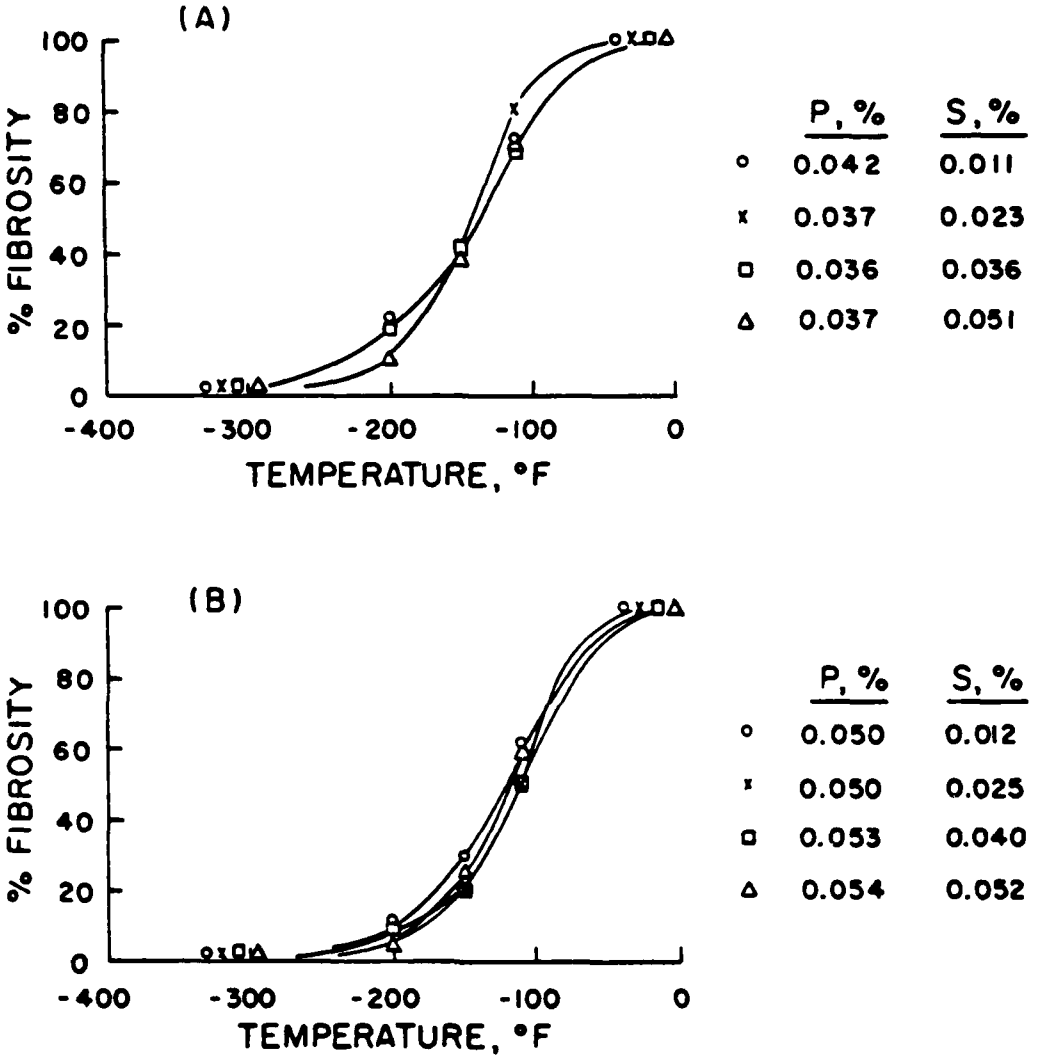

FIGURE 40-2. EFFECT OF INCREASING SULFUR AT NOMINAL (A) 0.035%P AND (B) 0.050%P ON THE %FIBROSITY TRANSITION BEHAVIOR OF 1100°F TEMPERED 4340 CAST STEEL.

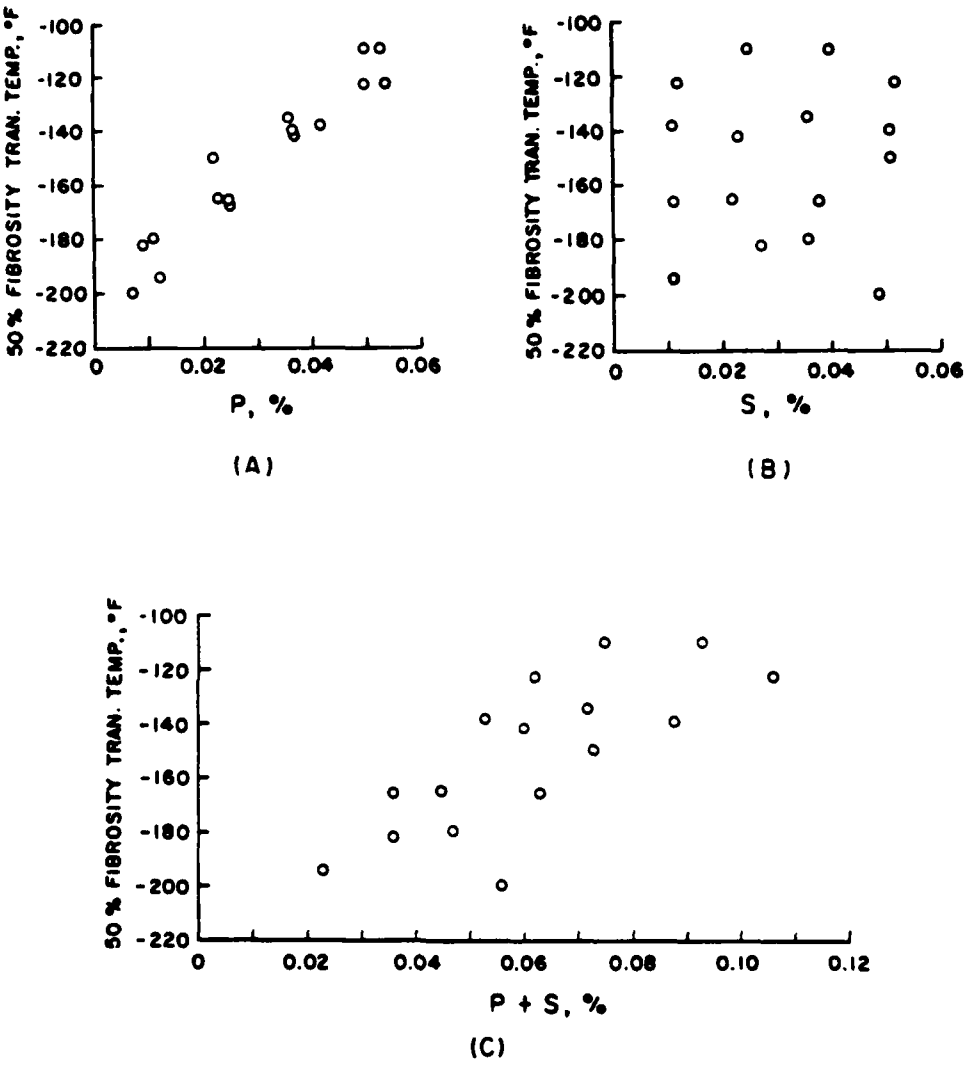

FIGURE 41. EFFECT OF (A) PHOSPHORUS, (B) SULFUR AND (C) PHOSPHORUS PLUS SULFUR CONTENT ON THE 50% FIBROSITY TRANSITION TEMPERATURE OF 1100°F TEMPERED 4340 CAST STEEL.

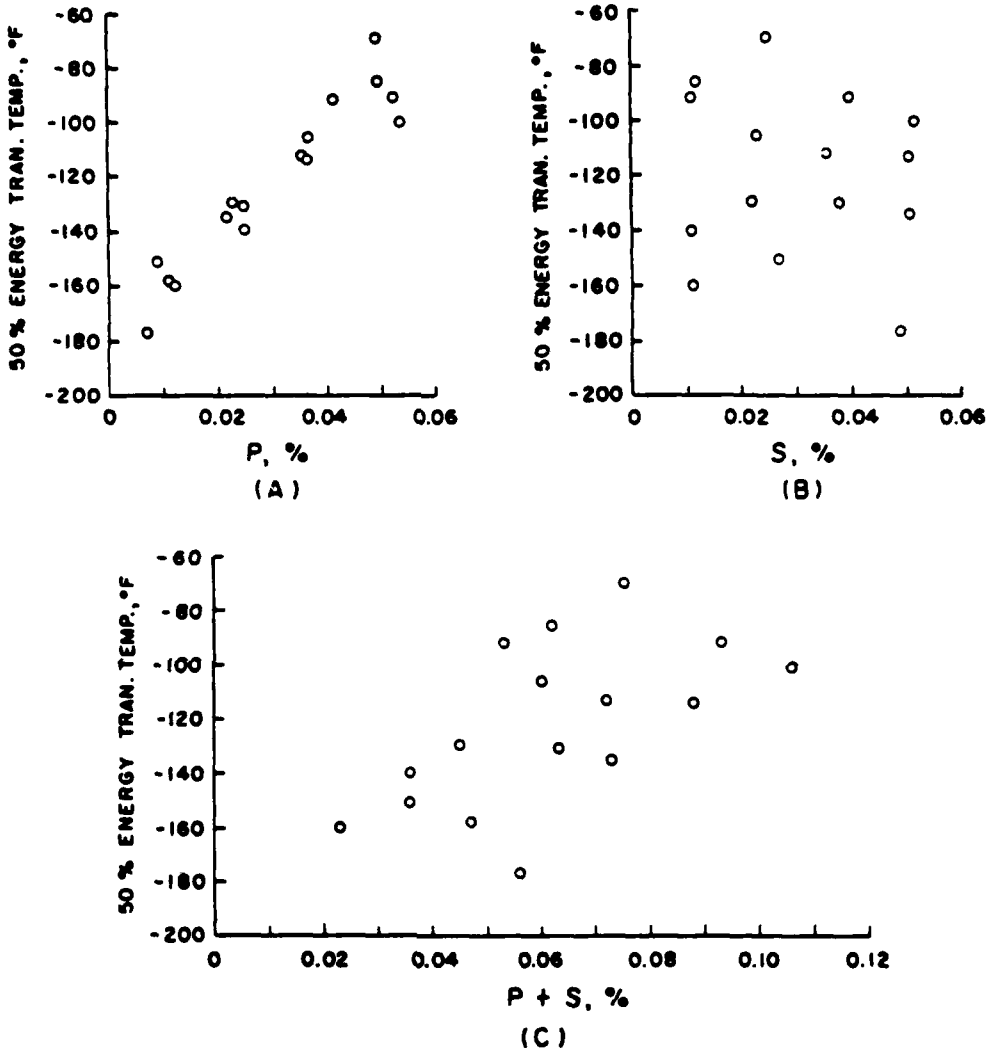

FIGURE 42. EFFECT OF (A) PHOSPHORUS, (B) SULFUR AND (C) PHOSPHORUS PLUS SULFUR CONTENT ON THE 50% ENERGY TRANSITION TEMPERATURE OF 1100°F TEMPERED 4340 CAST STEEL.

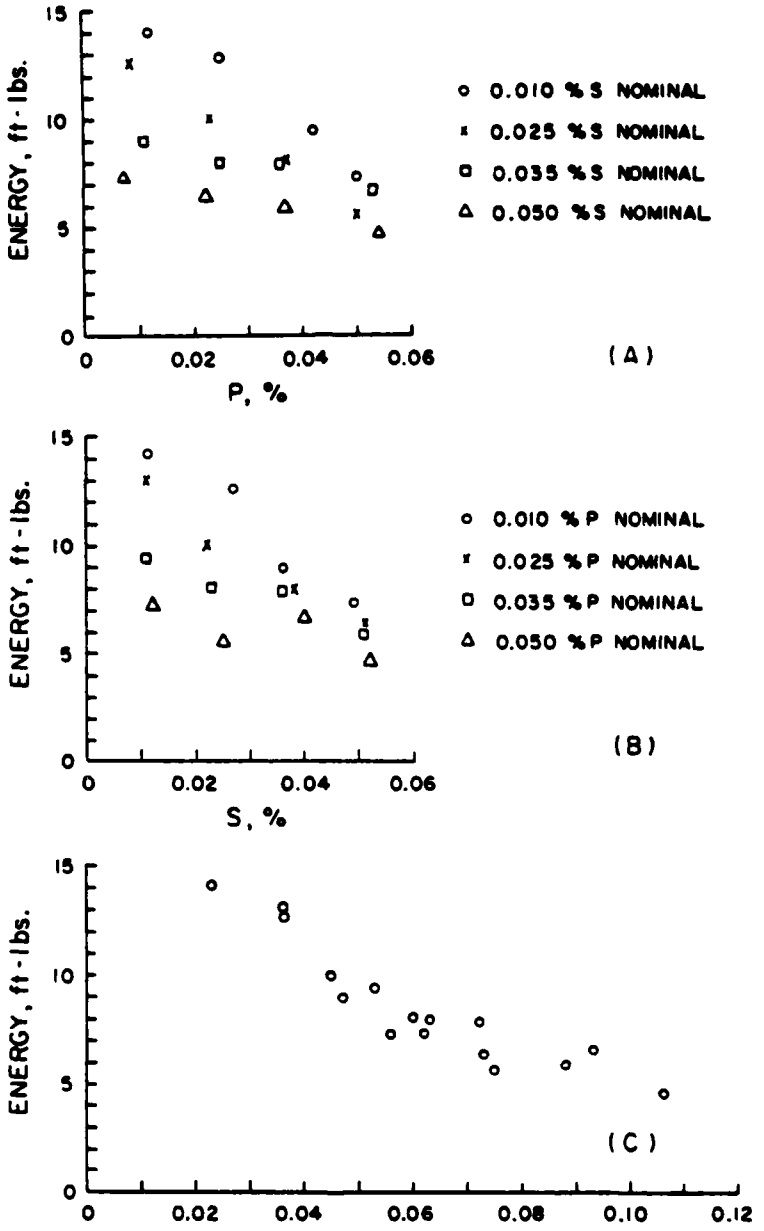

FIGURE 43. EFFECT OF (A) PHOSPHORUS, (B) SULFUR AND (C) PHOSPHORUS PLUS SULFUR CONTENT ON THE 150°F CHARPY IMPACT TOUGHNESS OF 400°F TEMPERED 4340 CAST STEEL.

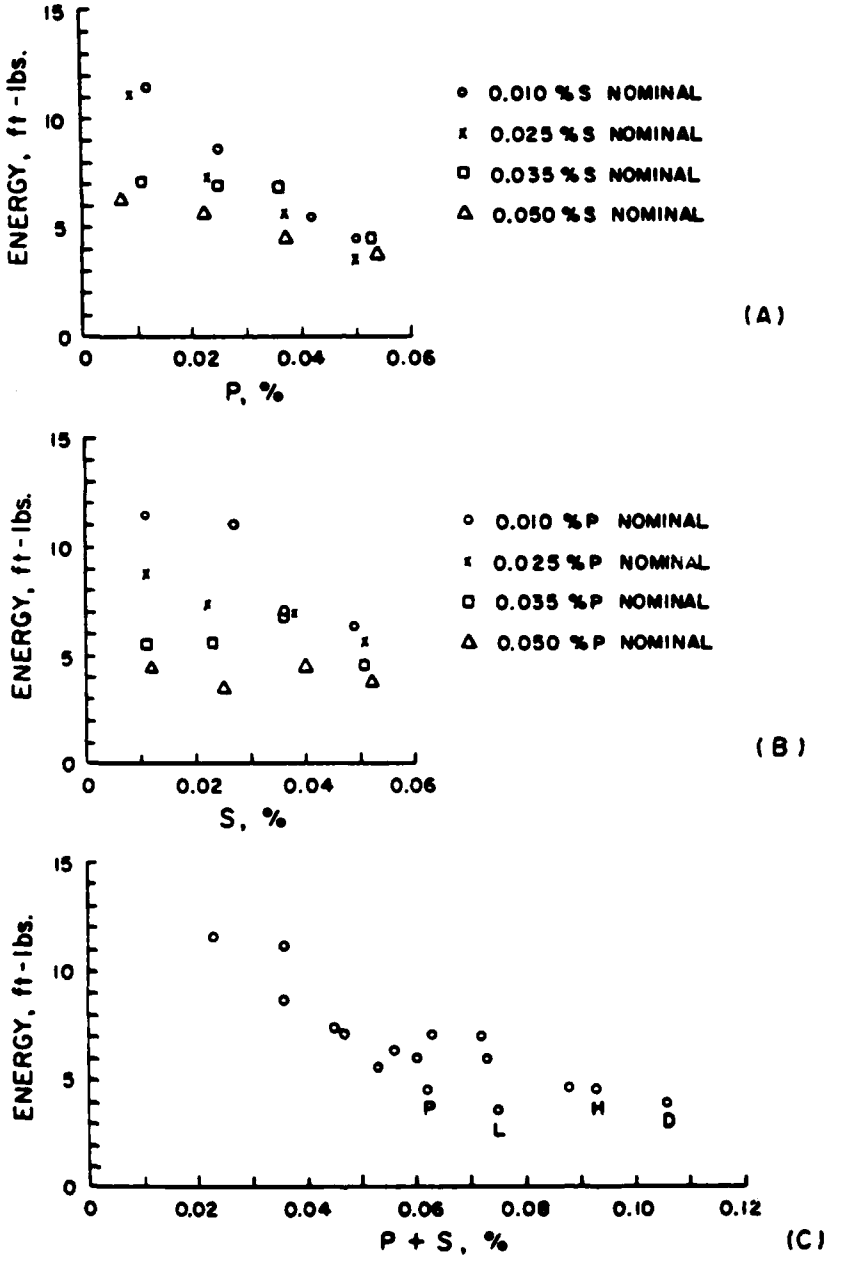

FIGURE 44. EFFECT OF (A) PHOSPHORUS, (B) SULFUR AND (C) PHOSPHORUS PLUS SULFUR CONTENT ON THE -20°F CHARPY IMPACT TOUGHNESS OF 400°F TEMPERED 4340 CAST STEEL.

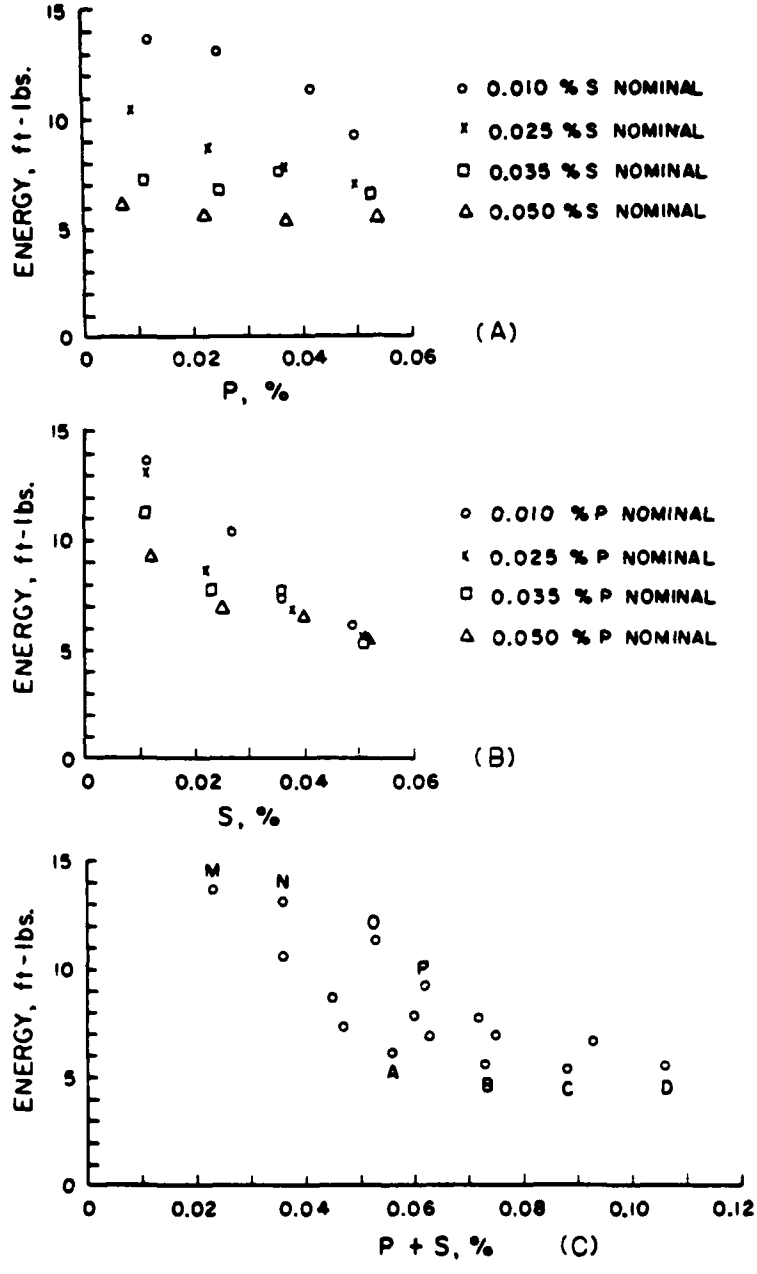

FIGURE 45. EFFECT OF (A) PHOSPHORUS, (B) SULFUR AND (C) PHOSPHORUS PLUS SULFUR CONTENT ON THE 320°F CHARPY IMPACT TOUGHNESS OF 400°F TEMPERED 4340 CAST STEEL.

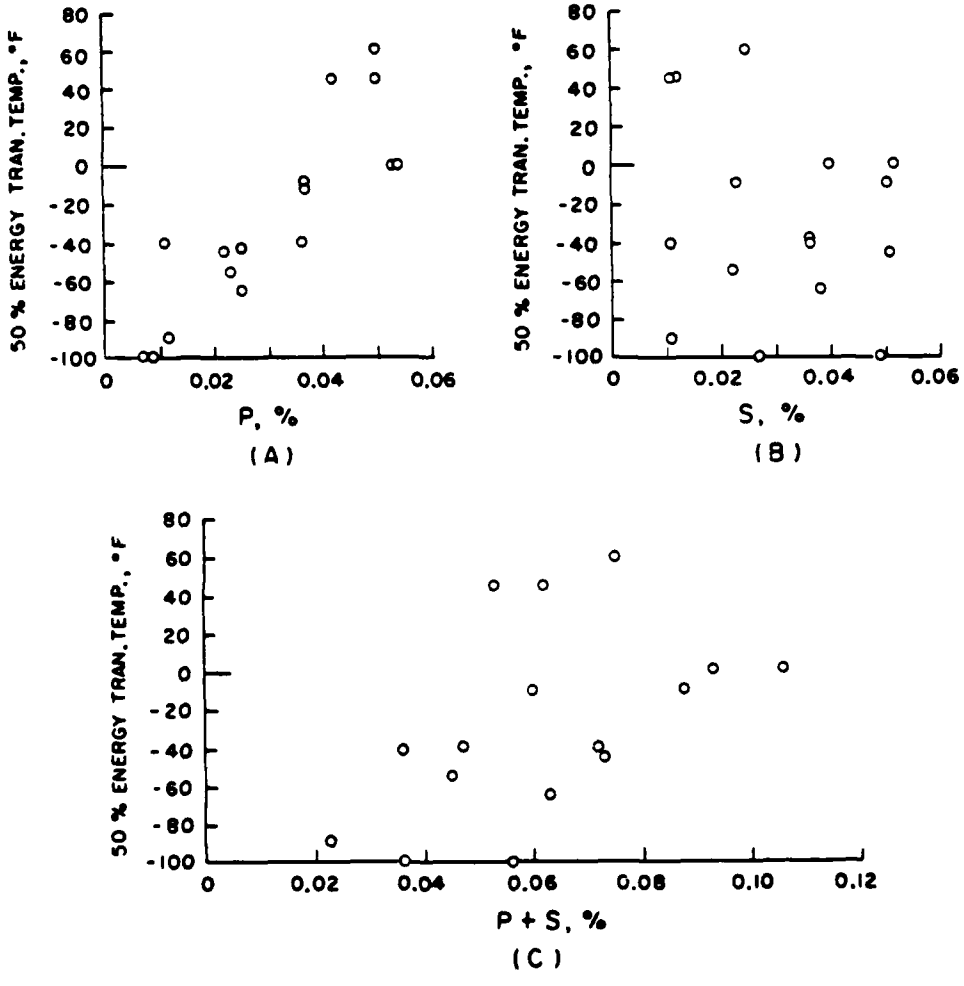

FIGURE 46. EFFECT OF (A) PHOSPHORUS, (B) SULFUR AND (C) PHOSPHORUS PLUS SULFUR CONTENT ON THE 50% ENERGY TRANSITION TEMPERATURE OF 400°F TEMPERED 4340 CAST STEEL.

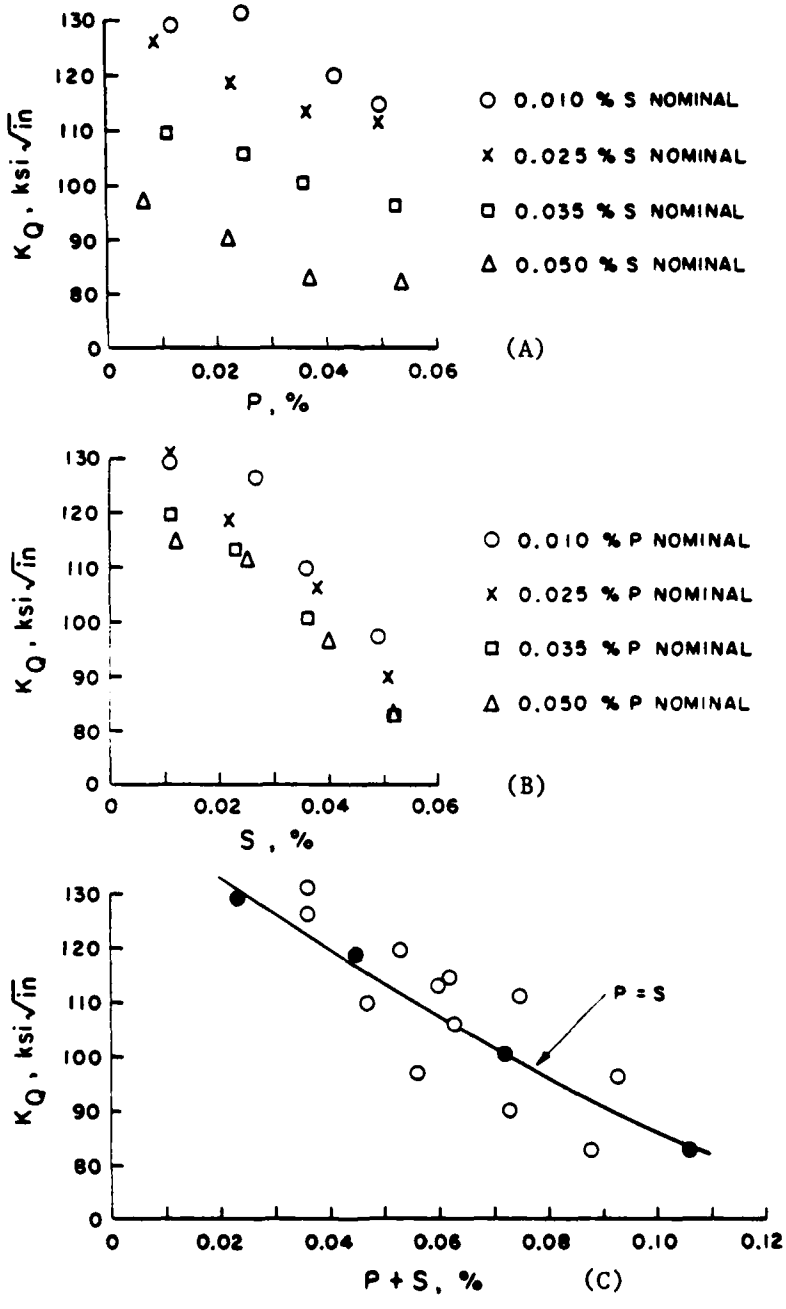

FIGURE 47. EFFECT OF INDIVIDUAL (A) PHOSPHORUS, (B) SULFUR, AND COMBINED (C) PHOSPHORUS PLUS SULFUR CONTENT ON THE ROOM TEMPERATURE PLANE STRAIN FRACTURE TOUGHNESS OF 1100°F TEMPERED 4340 CAST STEEL.

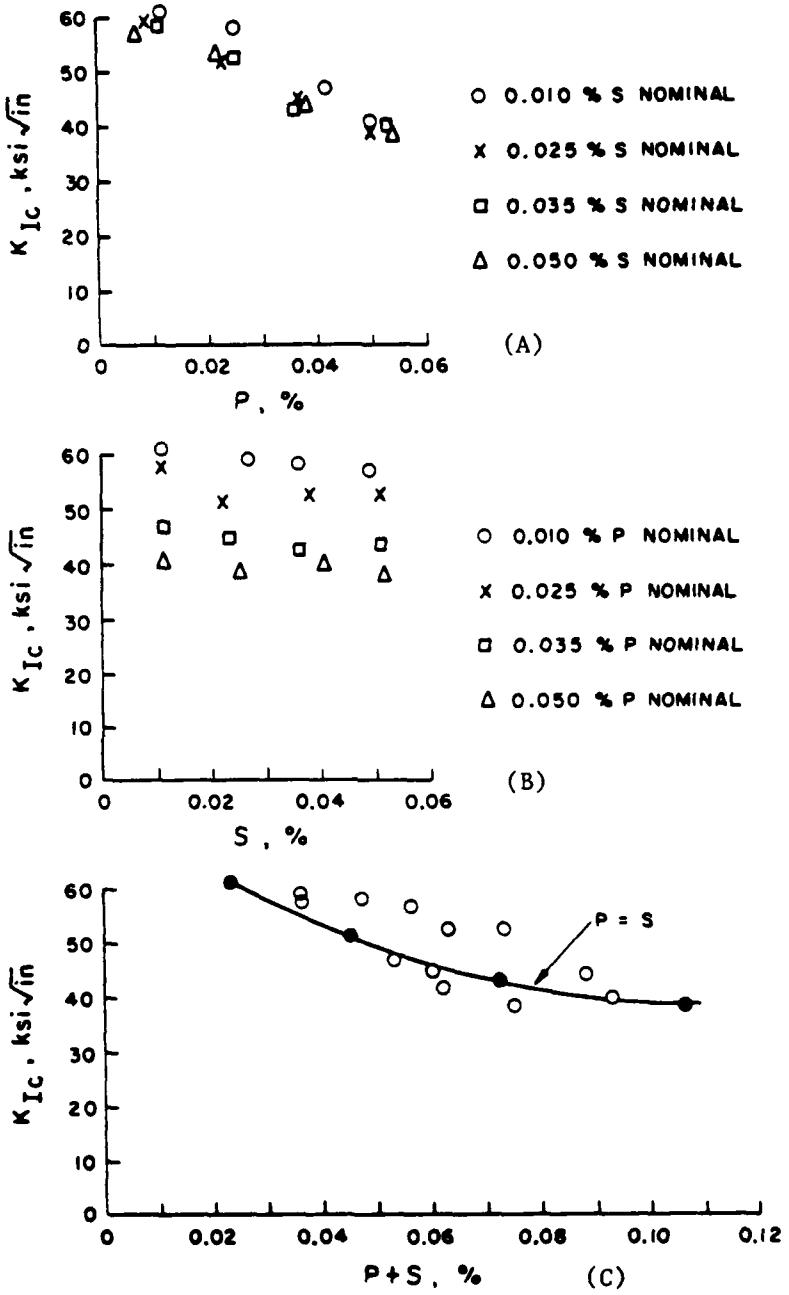

FIGURE 48. EFFECT OF INDIVIDUAL (A) PHOSPHORUS, (B) SULFUR, AND COMBINED (C) PHOSPHORUS PLUS SULFUR CONTENT ON THE ROOM TEMPERATURE PLANE STRAIN FRACTURE TOUGHNESS OF 400°F TEMPERED 4340 CAST STEEL.

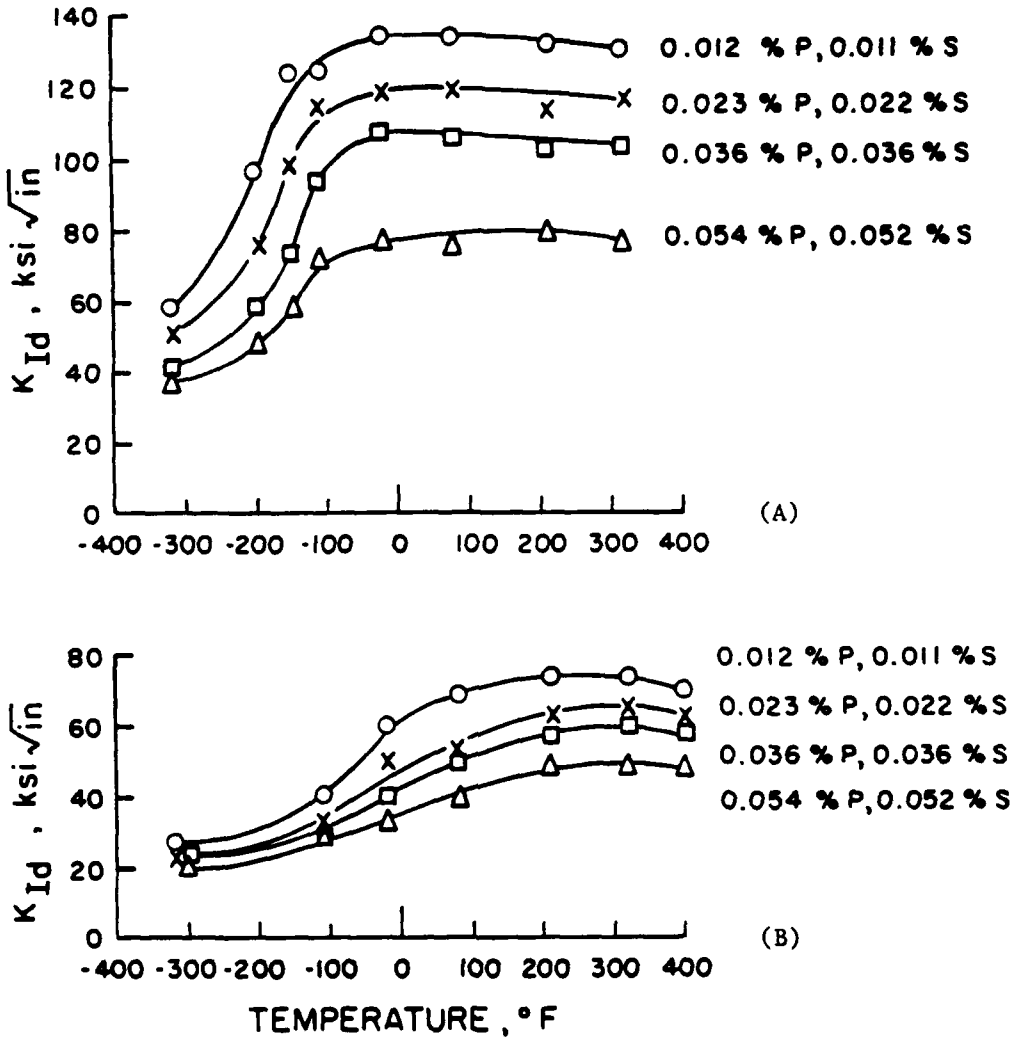

FIGURE 49. COMBINED EFFECT OF PHOSPHORUS AND SULFUR ON THE DYNAMIC FRACTURE TOUGHNESS (K_{Id}) OF (A) 1100°F AND (B) 400°F TEMPERED 4340 CAST STEEL.

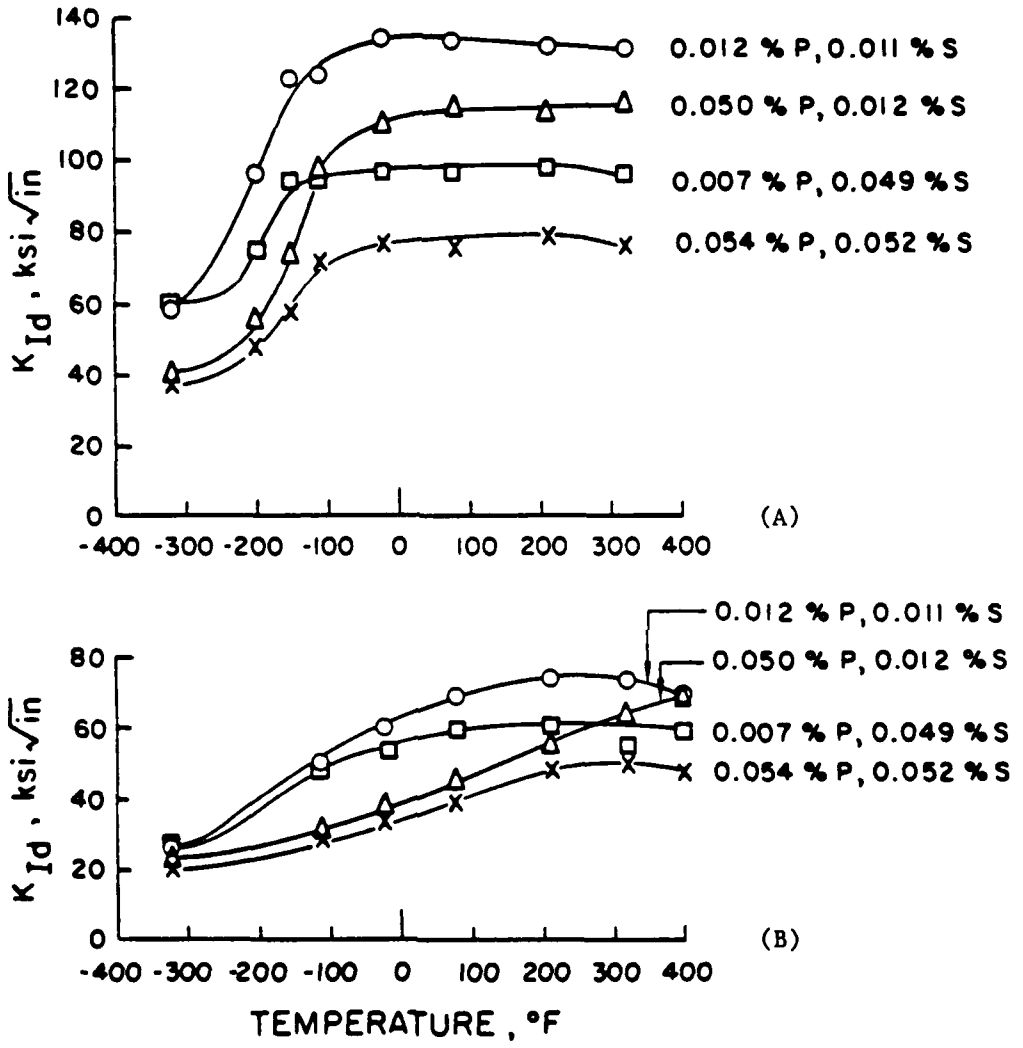

FIGURE 50. INDIVIDUAL AND COMBINED EFFECT OF PHOSPHORUS AND SULFUR ON THE DYNAMIC FRACTURE TOUGHNESS OF (A) 1100°F AND (B) 400°F TEMPERED 4340 CAST STEEL.

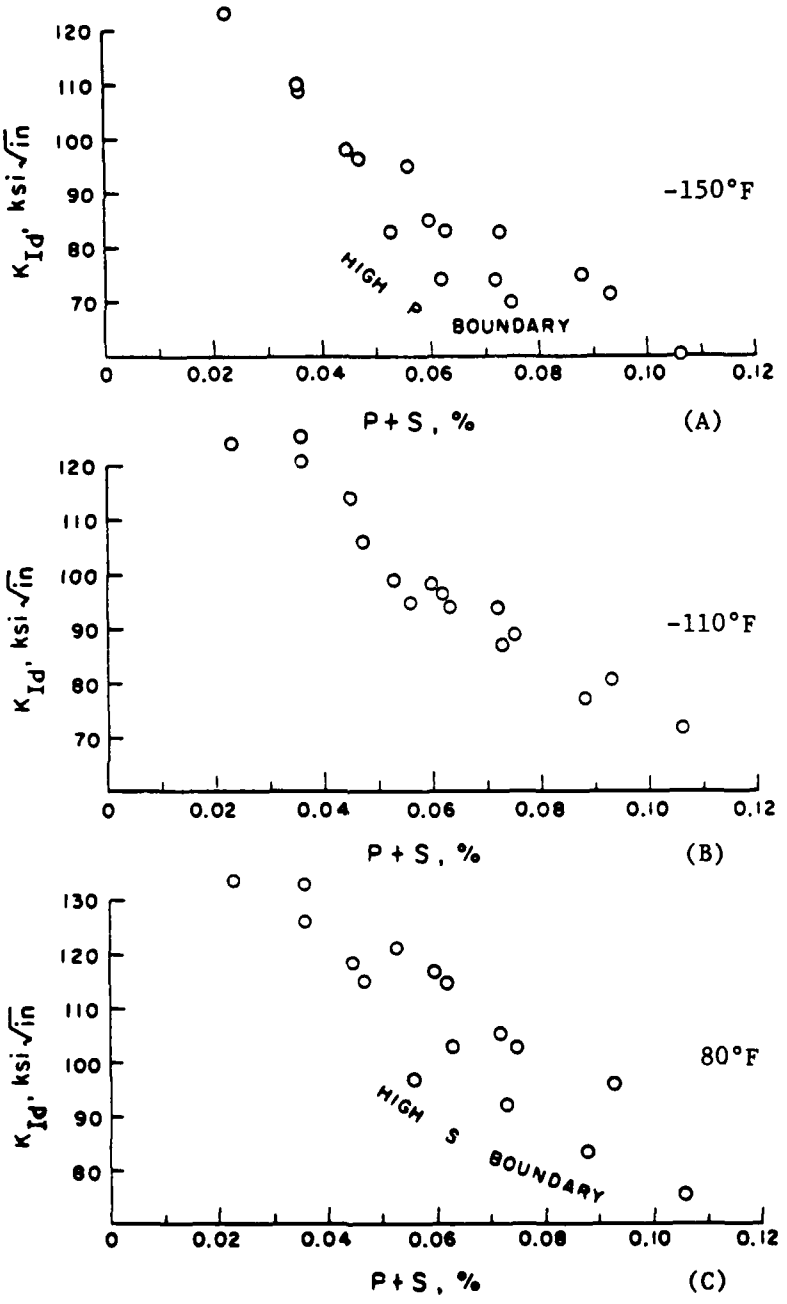

FIGURE 51. EFFECT OF PHOSPHORUS PLUS SULFUR CONTENT ON THE DYNAMIC FRACTURE TOUGHNESS OF 1100°F TEMPERED 4340 CAST STEEL BROKEN AT (A) -150°F (BELOW CROSS OVER TEMP.), (B) -110°F (CROSS OVER TEMP.), AND (C) 80°F (ABOVE CROSS OVER TEMP.).

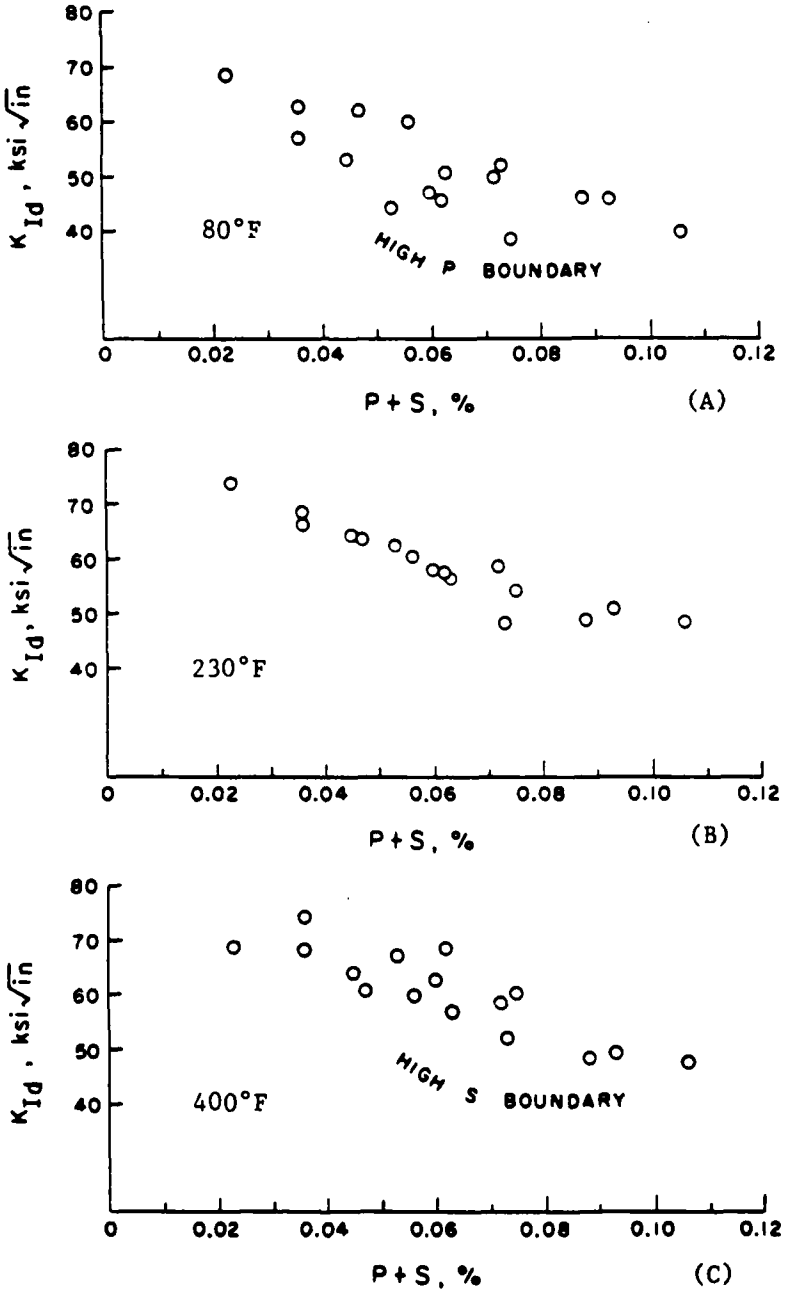

FIGURE 52. EFFECT OF PHOSPHORUS PLUS SULFUR CONTENT ON THE DYNAMIC FRACTURE TOUGHNESS OF 400°F TEMPERED 4340 CAST STEEL BROKEN AT (A) 80°F (BELOW CROSS OVER TEMP.), (B) 230°F (CROSS OVER TEMP.), AND (C) 400°F (ABOVE CROSS OVER TEMP.).

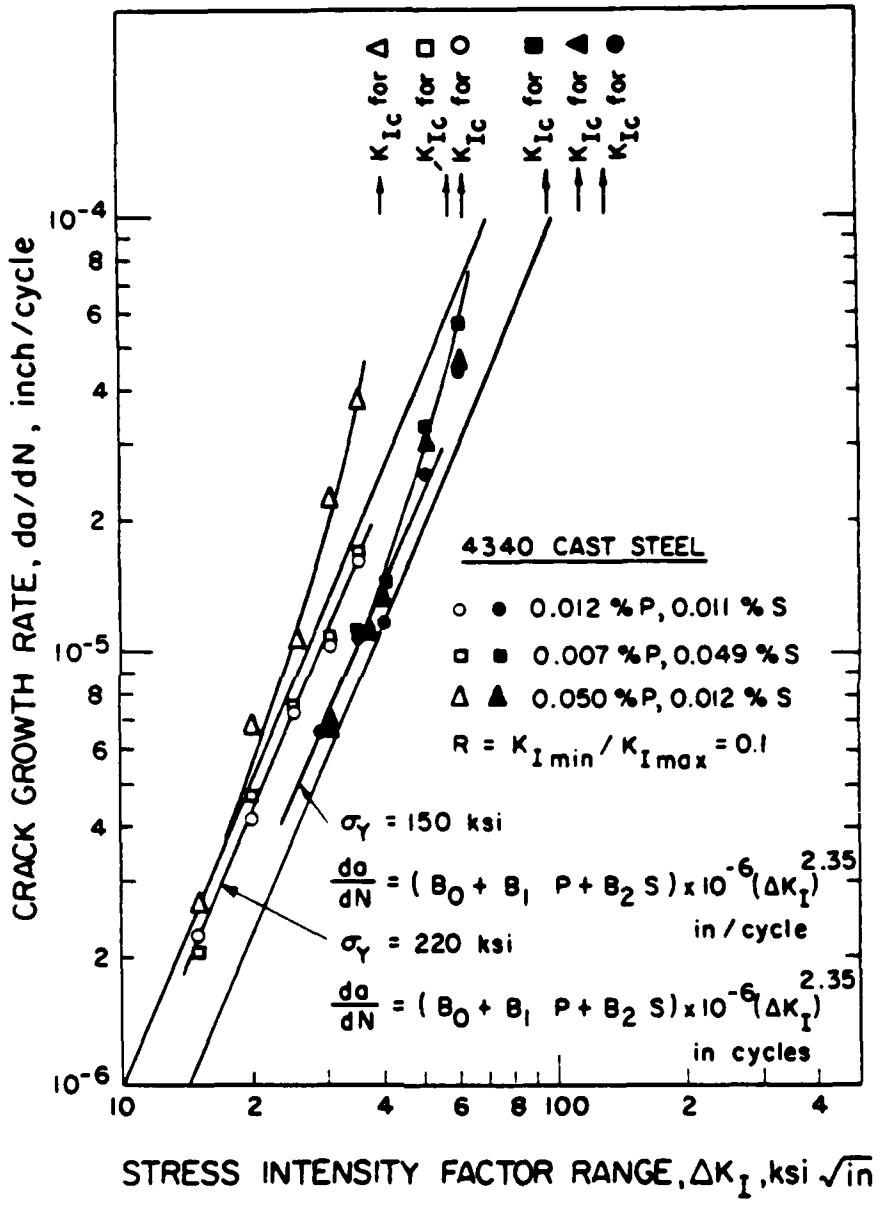

FIGURE 53. VARIATION OF FATIGUE CRACK GROWTH RATE WITH STRESS INTENSITY FACTOR RANGE AS AFFECTED BY PHOSPHORUS AND SULFUR FOR MEDIUM AND HIGH STRENGTH 4340 CAST STEEL.

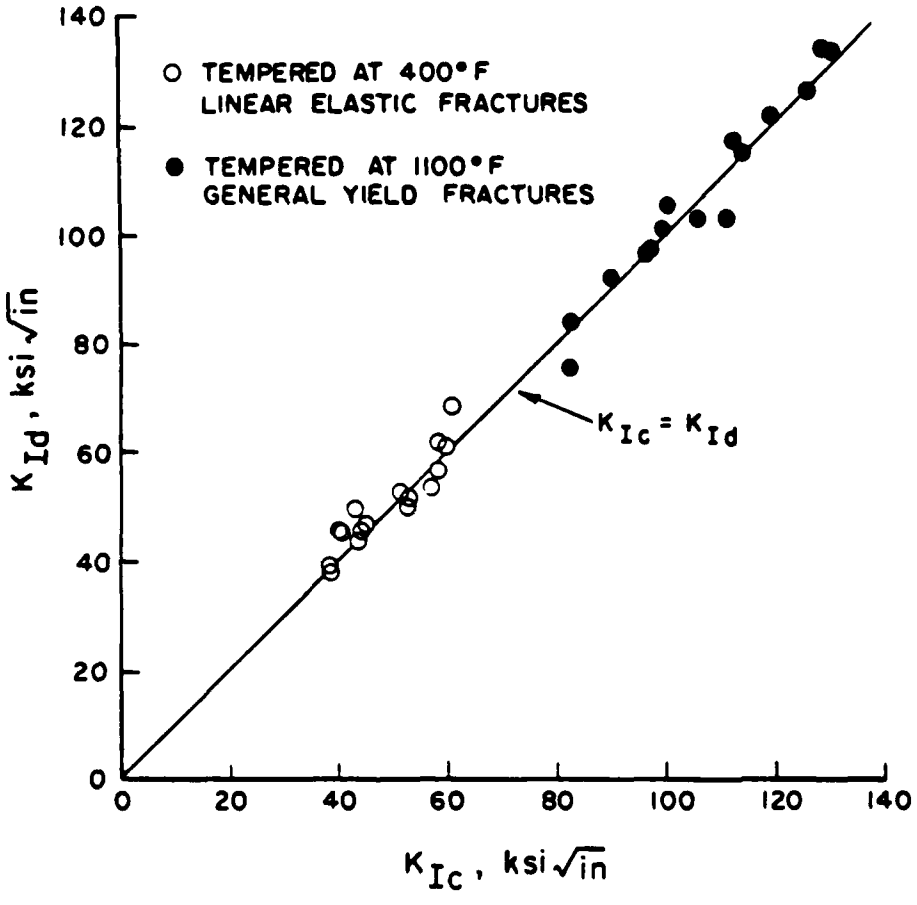

FIGURE 54. DYNAMIC FRACTURE TOUGHNESS (K_{Id}) VS. PLANE STRAIN FRACTURE TOUGHNESS (K_{Ic}) OF 400°F AND 1100°F TEMPERED 4340 CAST STEELS TESTED AT ROOM TEMPERATURE.

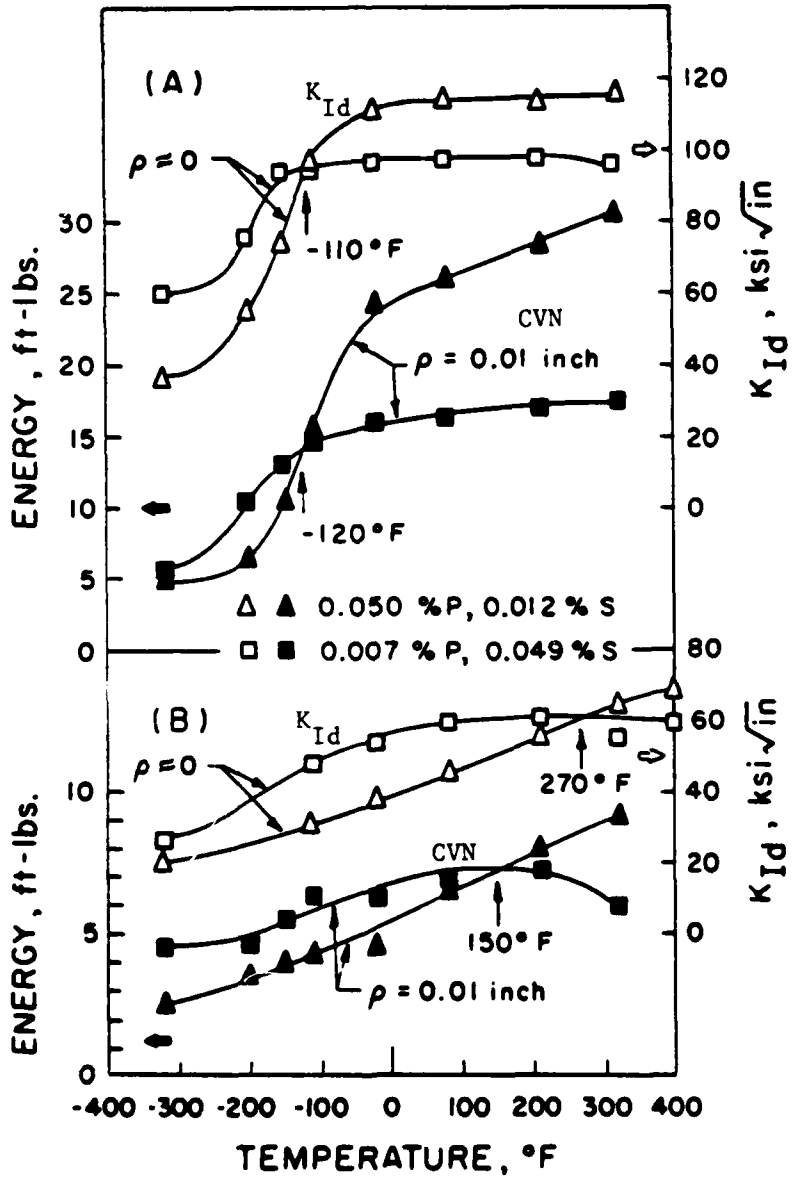

FIGURE 55. RELATIVE NOTCH SENSITIVITY OF HIGH PHOSPHORUS VS. HIGH SULFUR 4340 CAST STEEL TEMPERED AT (A) 1100°F AND (B) 400°F. (ρ IS NOTCH RADIUS)

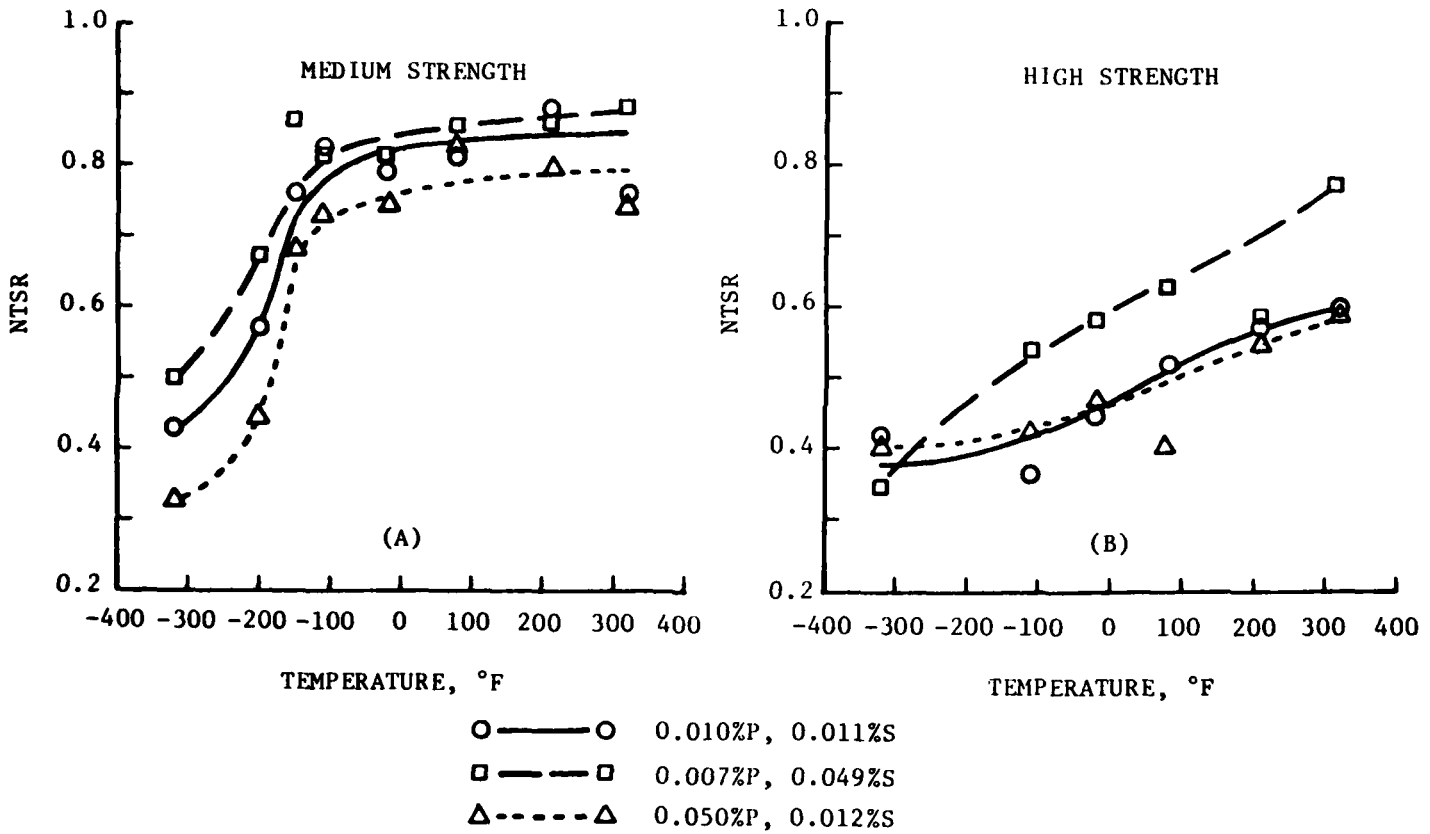

FIGURE 56. EFFECT OF PHOSPHORUS AND SULFUR ON THE NOTCH TOUGHNESS SENSITIVITY RATIO (NTSR) OF (A) MEDIUM AND (B) HIGH STRENGTH 4340 CAST STEEL.

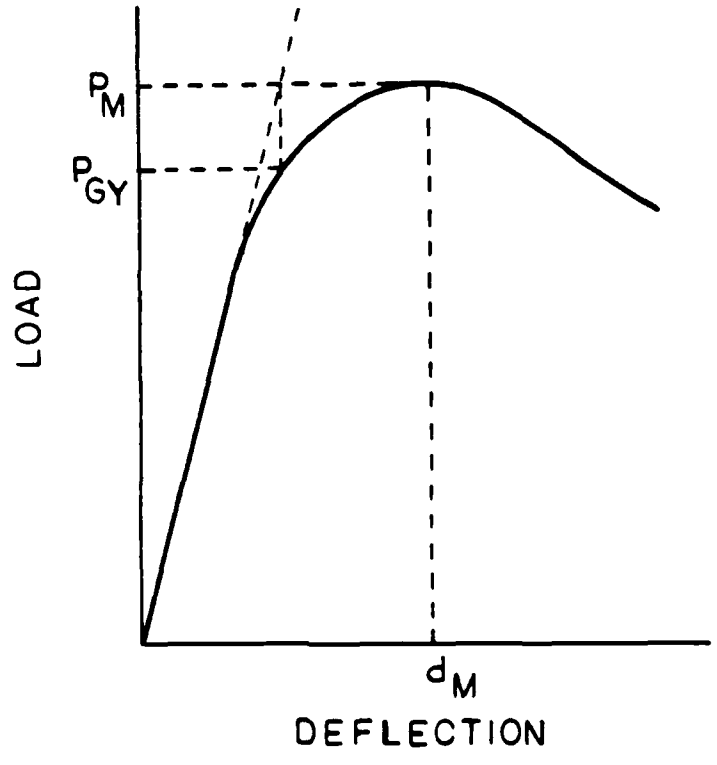

FIGURE 57. METHOD USED TO DEFINE THE GENERAL YIELD LOAD (P_{GY}) OF A ROUND HOUSE TYPE LOAD-DEFLECTION CURVE.

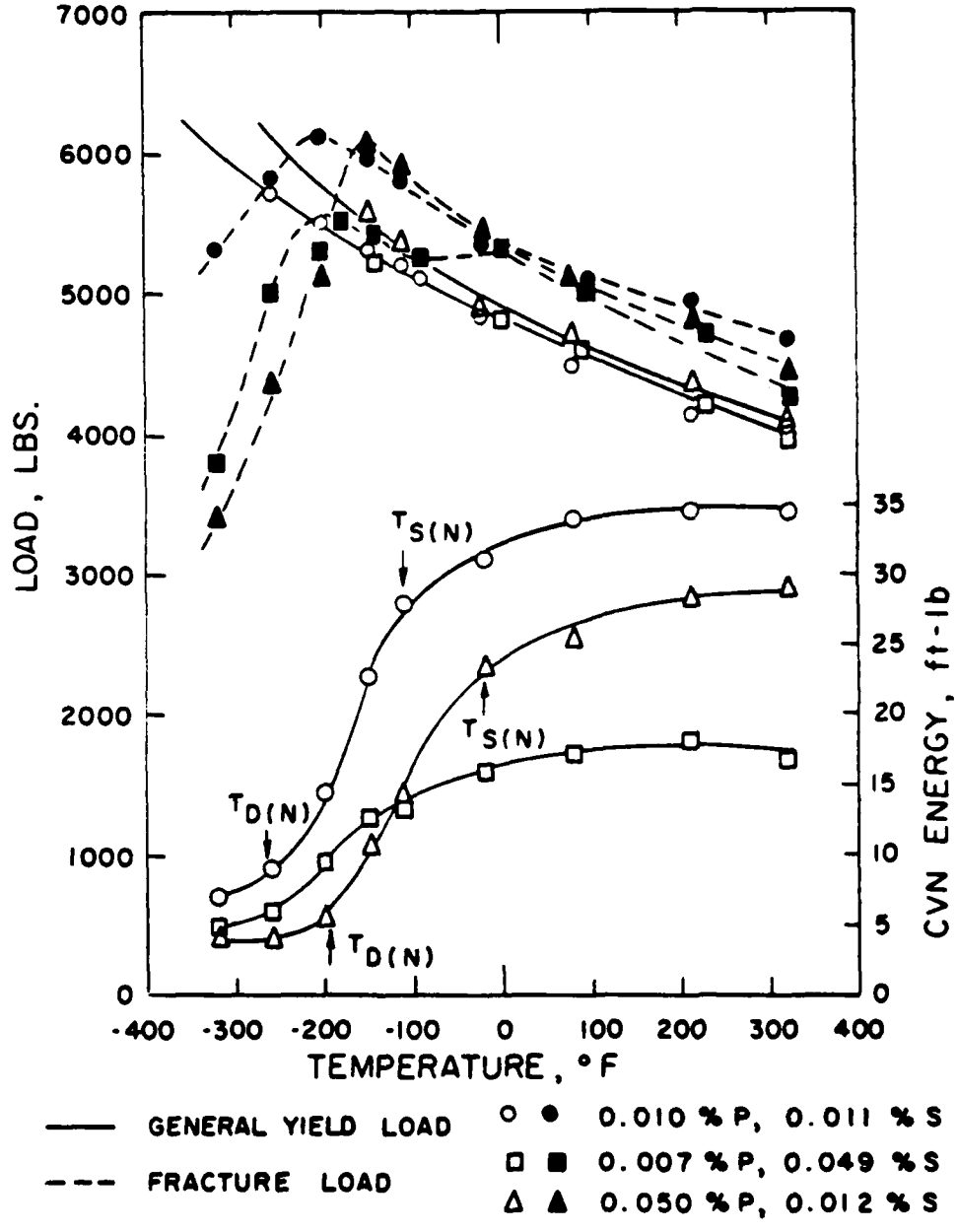

FIGURE 58. EFFECT OF PHOSPHORUS AND SULFUR ON THE IMPACT STRENGTH AND ENERGY OF MEDIUM STRENGTH 4340 CAST STEEL.

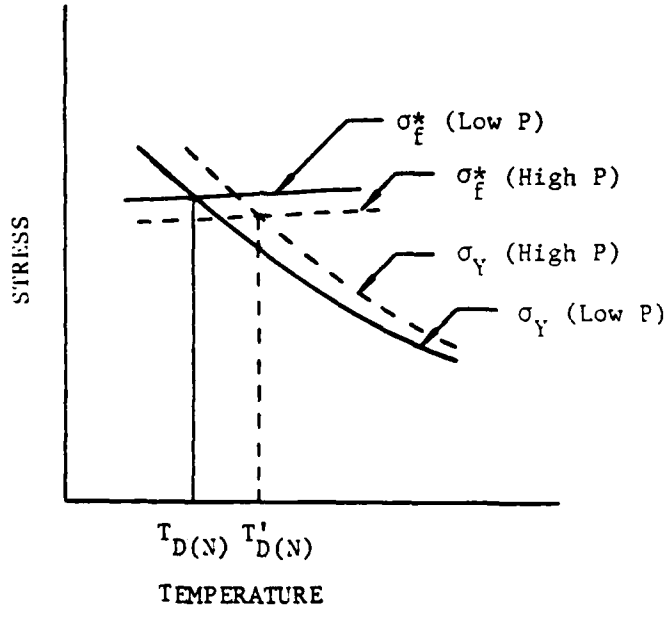

FIGURE 59. AN EXPLANATION OF THE EFFECT OF PHOSPHORUS ON RAISING THE BRITTLENESS TRANSITION TEMPERATURE OF CHARPY V-NOTCH SPECIMEN OF 4340 CAST STEEL.

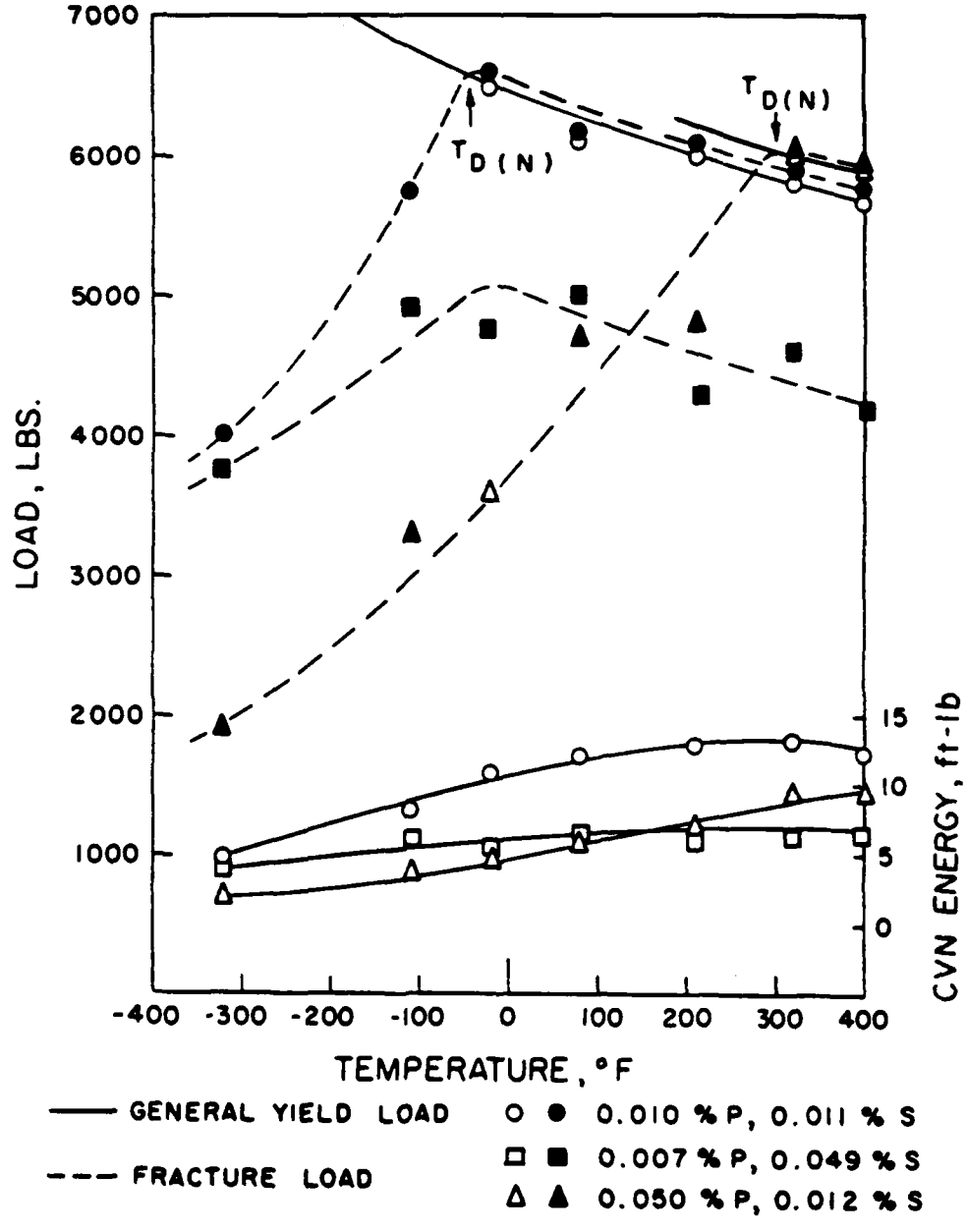

FIGURE 60. EFFECT OF PHOSPHORUS AND SULFUR ON THE IMPACT STRENGTH AND ENERGY OF HIGH STRENGTH 4340 CAST STEEL.

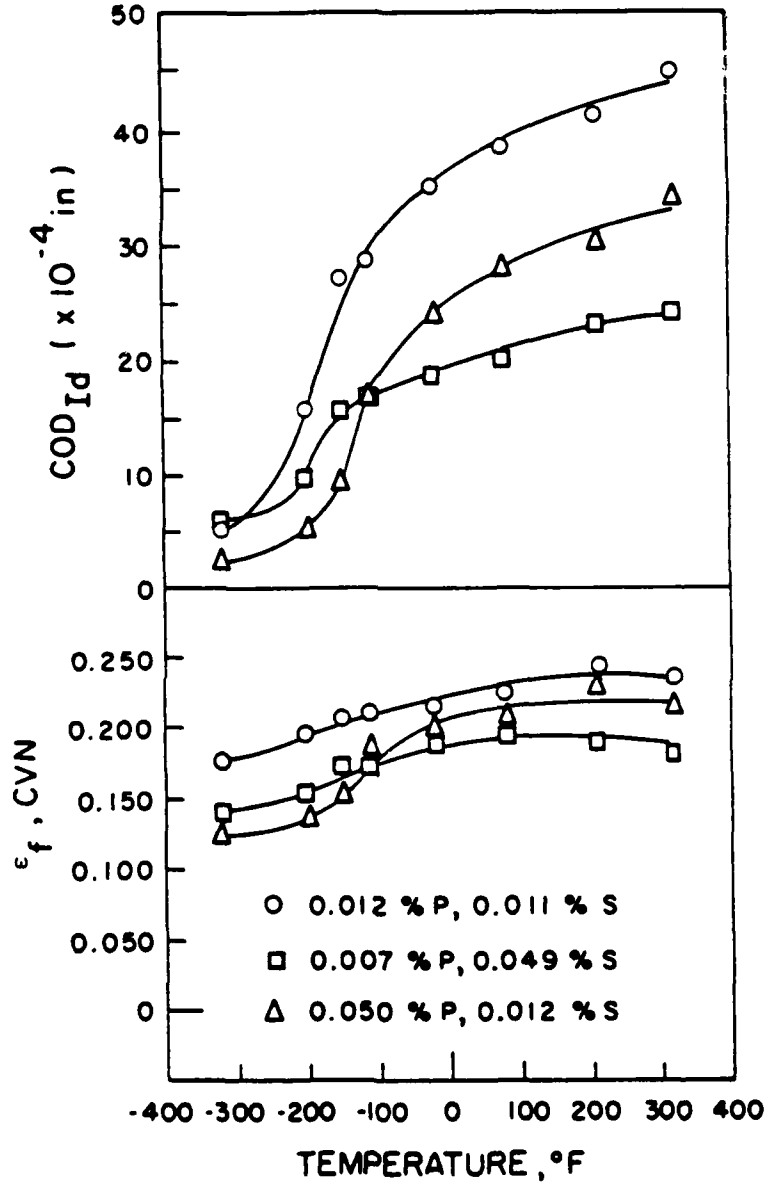

FIGURE 61. EFFECT OF PHOSPHORUS AND SULFUR ON THE (A) CRACK-OPENING DISPLACEMENT, AND (B) TRUE FRACTURE STRAIN IN CVN SPECIMEN OF 1100°F TEMPERED 4340 CAST STEEL.

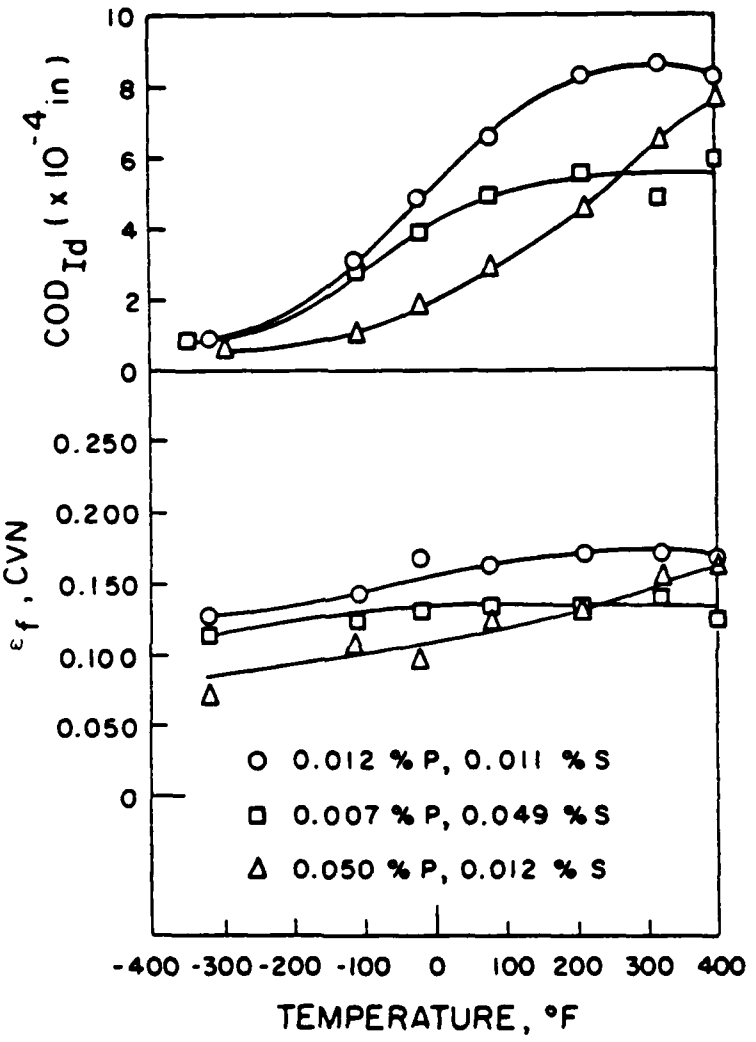

FIGURE 62. EFFECT OF PHOSPHORUS AND SULFUR ON THE (A) CRACK-OPENING DISPLACEMENT, AND (B) TRUE FRACTURE STRAIN IN CVN SPECIMEN OF 400°F TEMPERED 4340 CAST STEEL.

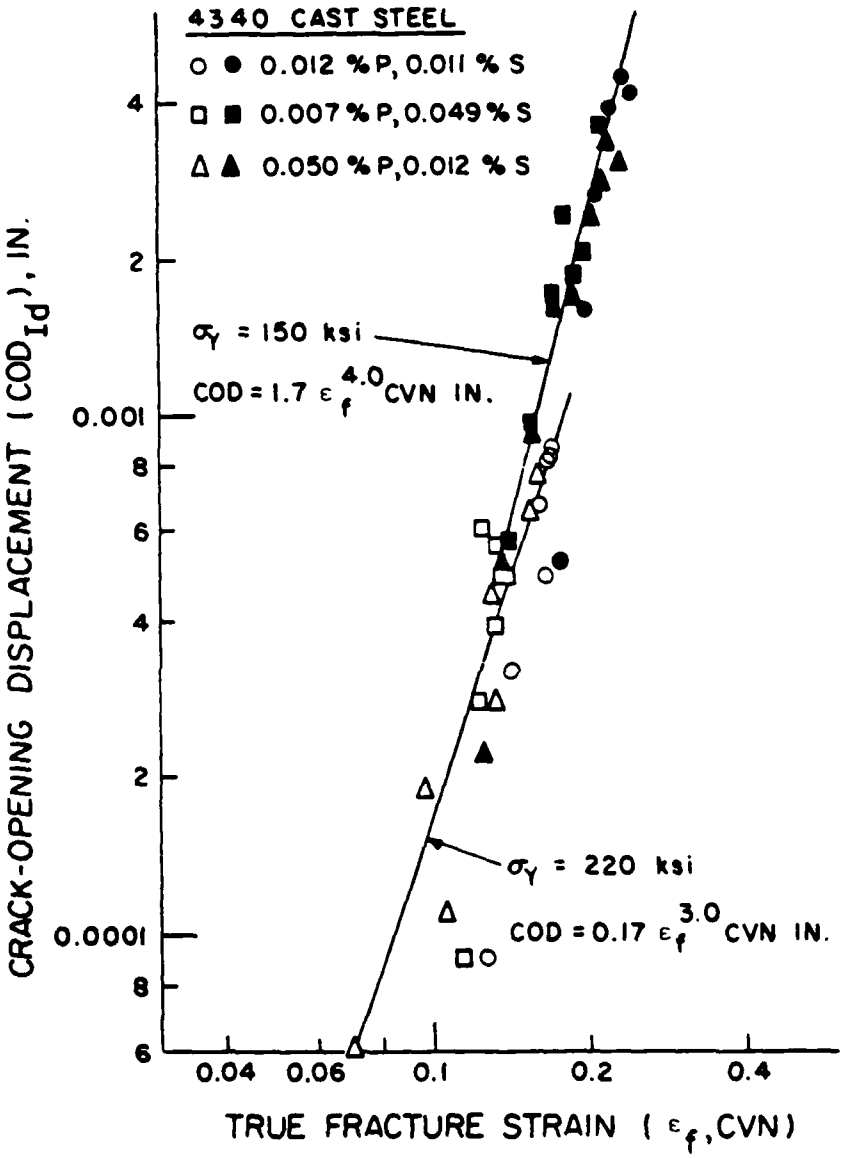

FIGURE 63. RELATION BETWEEN CRITICAL CRACK-OPENING DISPLACEMENT AND TRUE FRACTURE STRAIN IN CVN SPECIMEN FOR MEDIUM AND HIGH STRENGTH 4340 CAST STEEL.

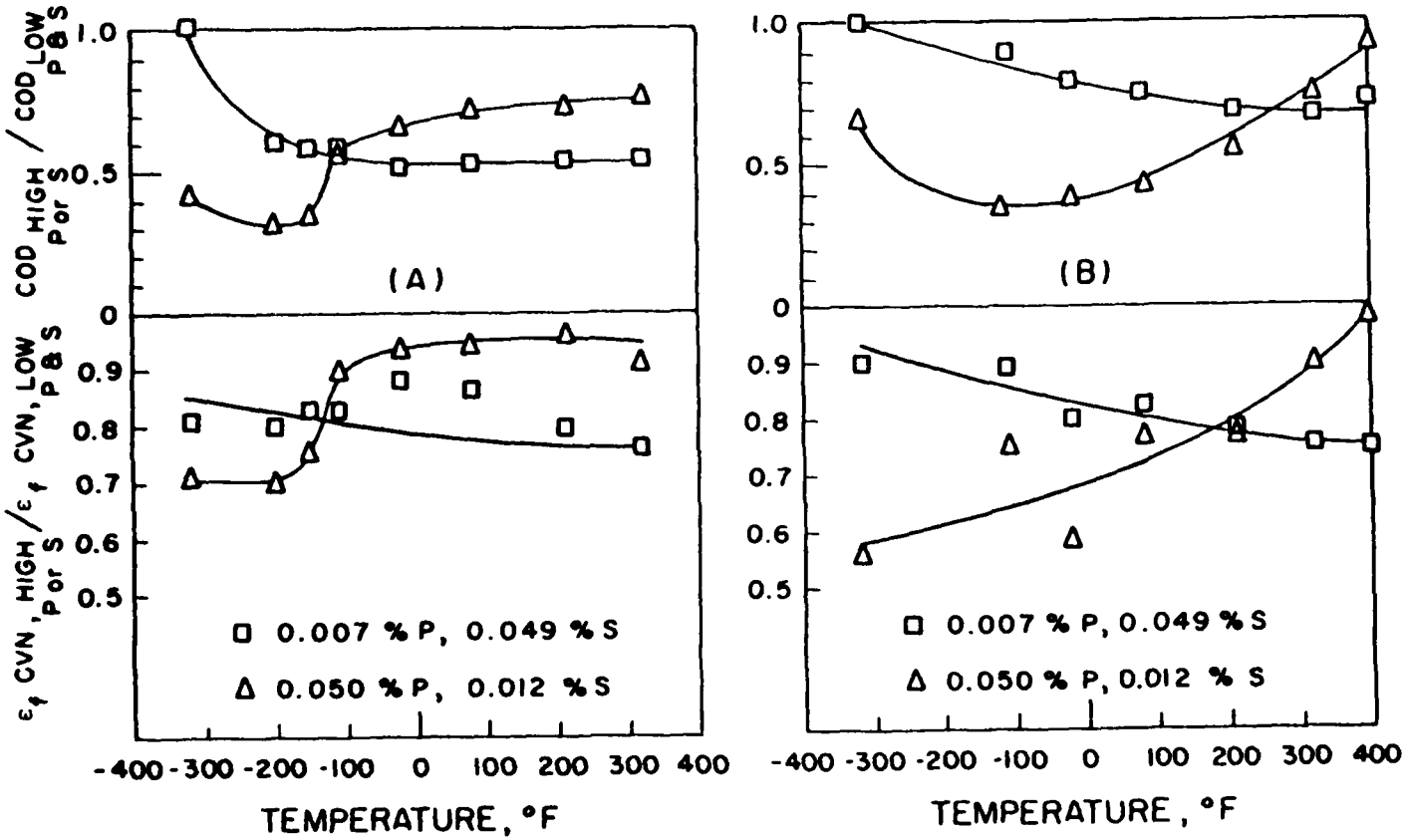

FIGURE 64. EFFECT OF HIGH PHOSPHORUS AND HIGH SULFUR ON THE NORMALIZED COD_{Id} AND $\varepsilon_{f,CVN}$ FOR (A) 1100°F AND (B) 400°F TEMPERED 4340 CAST STEEL. (W. R. T. COD_{Id} AND $\varepsilon_{f,CVN}$ OF LOW PHOSPHORUS AND SULFUR 0.012%P, 0.011%S STEEL)

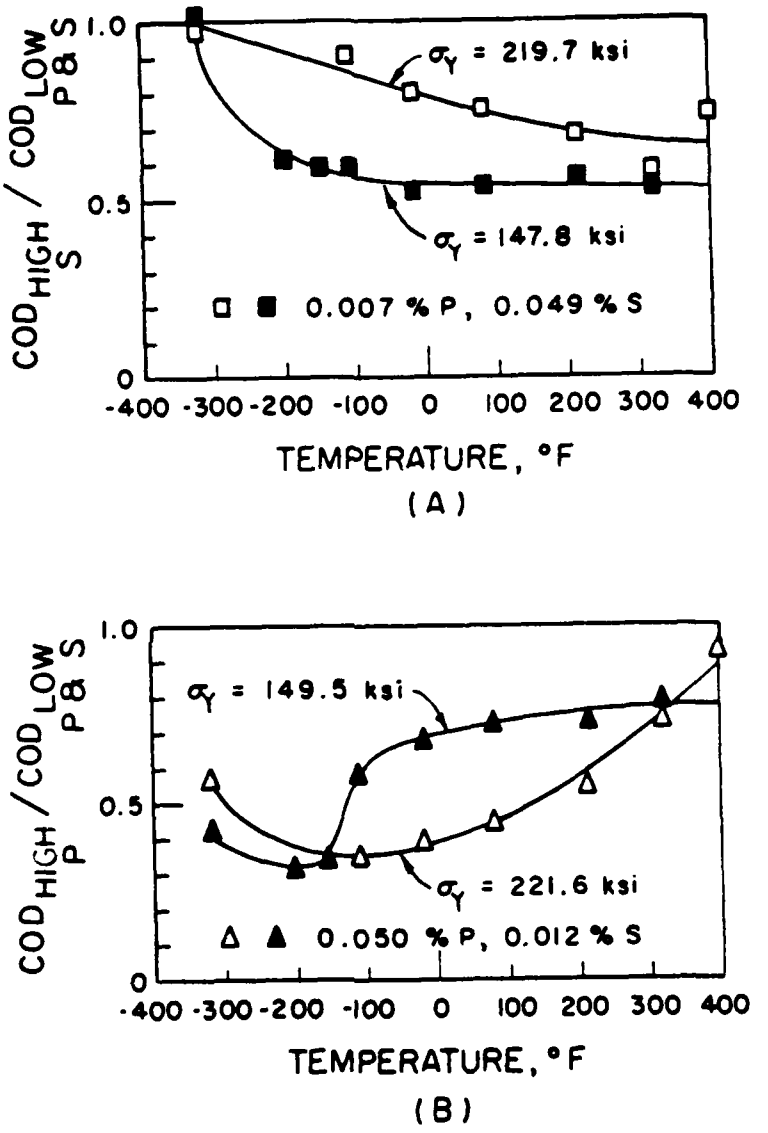

FIGURE 65. EFFECT OF STRENGTH LEVEL ON THE NORMALIZED COD_{Id} OF (A) HIGH SULFUR AND (B) HIGH PHOSPHORUS 4340 CAST STEELS WITH RESPECT TO COD_{Id} OF LOW PHOSPHORUS AND LOW SULFUR 0.012%P, 0.011%S STEEL.

APPENDIX A

A TYPICAL COMPUTER PROGRAM FOR REGRESSION ANALYSIS

```
1.   RUN NAME          MULTIPLE NON-LINEAR REGRESSION
2.   FILE NAME         CORRELATION BETWEEN KIC AND P/
3.                     CORRELATION BETWEEN KIC AND S/
4.                     CORRELATION BETWEEN KIC AND P,S/
5.                     CORRELATION BETWEEN KIC AND P+S/
6.                     DATA FROM GROVES AND WALLACE
7.   VARIABLE LIST     KIC,P,S
8.   VAR LABELS        KIC FRACTURE TOUGHNESS/
9.                     P PHOSPHORUS/
10.                    S SULFUR
11.  COMPUTE           LY=LN(KIC)
12.  COMPUTE           PS=P+S
13.  INPUT FORMATS     FIXED (F5.1,2F7.3)
14.  N OF CASES        8
15.  LIST CASES        CASES=8/VARIABLES=KIC,P,S,PS
16.  PRINT FORMATS     KIC(1), P(3),S(3),PS(3)
17.  REGRESSION        VARIABLES=LY,P/
18.                    REGRESSION=LY WITH P(2)/
19.                    VARIABLES=LY,S/
20.                    REGRESSION-LY WITH S(2)/
21.                    VARIABLES=LY,P,S/
22.                    REGRESSION=LY WITH P,S(2)/
23.                    VARIABLES=LY,PS/
24.                    REGRESSION=LY WITH PS(2)
25.  READ INPUT DATA
```

	KIC	P	S
1.	105.4	.012	.019
2.	81.5	.013	.026
3.	96.0	.015	.024
4.	84.1	.023	.029
5.	66.9	.046	.025
6.	60.6	.044	.040
7.	55.5	.056	.050
8.	47.7	.066	.066

APPENDIX B

DYNAMIC FRACTURE TOUGHNESS CALCULATION

B.1. Elastic Fracture

When the fracture is linear elastic, the dynamic fracture toughness can be determined from the standard linear elastic fracture mechanics relationship:(42,B1)

$$K = \frac{6MYa^{\frac{1}{2}}}{BW} \tag{B1}$$

where M is applied moment, B is specimen thickness, W is specimen depth, a is total crack length, K is stress intensity factor, and

$$Y = 1.93 - 3.07(a/W) + 14.53(a/W)^2 - 25.11(a/W)^3 + 25.8(a/W)^4 \tag{B2}$$

For the Charpy specimen (3 point bending):

$$M = PL/4 \tag{B3}$$

where P is applied load and L is support span = 1.57". Thus, the dynamic plane strain fracture toughness is:

$$K_{id} = \frac{1.5(P_{max})LYa^{\frac{1}{2}}}{BW^2} \tag{B4}$$

where P_{max} is maximum load at fracture.

B.2. General Yield or Elastic-Plastic Fracture

The equivalent-energy method as developed by Witt enables the calculation of a fracture toughness value based on data derived from a specimen which fractures after general yielding.(55,56)

This method assumes that if a sufficiently large specimen had been employed, fracture would have occurred before yielding but at

an energy corresponding to the initiation energy* measured for the smaller specimen. The use of this method is illustrated in Figure B1. The linear portion of the load curve is extended to a value P^* such that the area under the linear portion of the curve is equal to the measured initiation energy of the general yield fracture. This P^* value is then used to calculate K_{Id}:

$$K_{Id} = \frac{1.5(P^*)LYa^{\frac{1}{2}}}{BW^2} \tag{B5}$$

*Note: The initiation energy is taken as the energy to maximum load. It would have been more reasonable to take this value at the load of pop-in; however, this load of the materials studied cannot be sensibly detected by the instrumented impact test.

APPENDIX C

CLEAVAGE FRACTURE STRENGTH CALCULATION

It has been indicated in Sec. B.1. - B.3., Chapter I that the tensile stress distribution ahead of the notch reaches a maximum σ_{yy}^{max} at elastic-plastic interface. The fracture criterion in region II is:

$$\sigma_{yy}^{max} = K_{\sigma(p)}^{max} \sigma_Y^* = \sigma_f^* \tag{C1}$$

For Charpy V-notch specimen of mild steel, Wilshaw and Pratt show that when the applied load (P) reaches 0.8 of the general yield load (P_{GH}), $K_{\sigma(p)}$ reaches a maximum value of 2.18, namely:

$$K_{\sigma(p)}^{max} = 2.18, \text{ at } P/P_{GY} = 0.8 \tag{C2}$$

The relationship between σ_Y and P_{GY} was found from this experiment as:

$$\begin{aligned} \sigma_Y &= 31.6\ P_{GY} \text{ psi, for medium strength 4340 steel} \\ \sigma_Y &= 35.0\ P_{GY} \text{ psi, for high strength 4340 steel} \end{aligned} \tag{C3}$$

where P_{GY} is in pounds and factors 31.6 and 35.0 were calculated by dividing yield strength with general yield load at room temperature, assuming the materials are strain rate insensitive as justified previously. The values of these factors were found in fair agreement with the theoretical value by Green and Hundy for a rigid, perfectly plastic material of CVN specimen loaded in three point bending.(C1)

In the following it is assumed that Eq. (C2) for mild steel can also be applied to 4340 steel, which of course is a rough assumption. Combining Eqs. (C2) and (C3), the cleavage fracture strength (σ^*_f) can be calculated.

For medium strength 4340 cast steel:

(1) 0.012%P, 0.011%S steel

$\sigma^*_f = 69.0\ P_{GY} = 69.0 \times 6380$ psi $= 440.2$ ksi

at $T = -360°F$, where $P/P_{GY} = 0.8$

(2) 0.050%P, 0.012%S steel

$\sigma^*_f = 69.0\ P_{GY} = 69.0 \times 5940$ psi $= 410.0$ ksi

at $T = -235°F$, where $P/P_{GY} = 0.8$

For high strength 4340 cast steel:

(1) 0.012%P, 0.011%S steel

$\sigma^*_f = 76.3\ P_{GY} = 76.3 \times 6880$ psi $= 524.9$ ksi

at $T = -134°F$, where $P/P_{GY} = 0.8$

(2) 0.050%P, 0.012%S steel

$\sigma^*_f = 76.3\ P_{GY} = 76.3 \times 6675$ psi $= 509.3$ ksi

at $T = 180°F$, where $P/P_{GY} = 0.8$

REFERENCES (APPENDICES)

B1. Brown, W.F., Jr. and Srawley, J.E., "Plane Strain Crack Toughness Testing of High Strength Metallic Materials", ASTM STP 410, ASTM, 1966.

C1. Green, A.P. and Hundy, B.B., "Initial Plastic Yielding in Notch Bend Tests", J. of the Mechanics and Physics of Solids, Vol. 4, 1956, pp. 128-144.

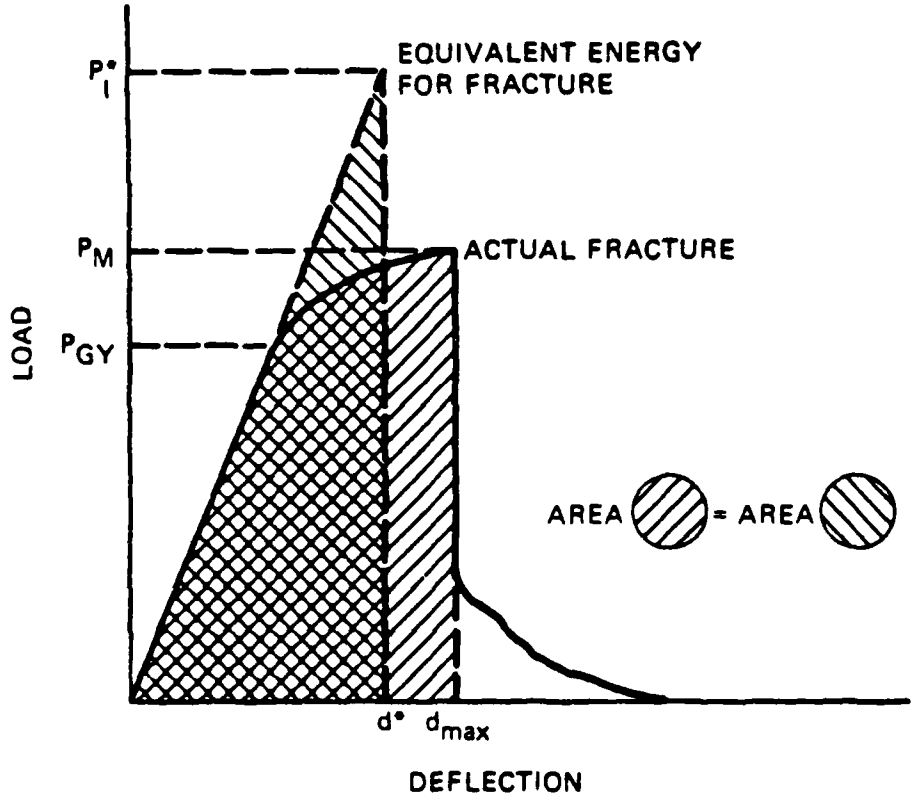

FIGURE B1. SCHEMATIC ILLUSTRATION OF THE DETERMINATION OF THE EQUIVALENT ENERGY FRACTURE LOAD, P*. (42)

DISTRIBUTION LIST

No. of Copies	To
1	Office of the Under Secretary of Defense for Research and Engineering, The Pentagon, Washington, DC 20301
12	Commander, Defense Technical Information Center, Cameron Station, Building 5, 5010 Duke Street, Alexandria, VA 22314
	Metals and Ceramics Information Center, Battelle Columbus Laboratories, 505 King Avenue, Columbus, OH 43201
1	ATTN: J. H. Brown, Jr.
	Deputy Chief of Staff, Research, Development, and Acquisition, Headquarters, Department of the Army, Washington, DC 20310
1	ATTN: DAMA-ARZ
	Commander, Army Research Office, P.O. Box 12211, Research Triangle Park, NC 27709
1	ATTN: Information Processing Office
	Commander, U.S. Army Materiel Development and Readiness Command, 5001 Eisenhower Avenue, Alexandria, VA 22333
1	ATTN: DRCLDC
	Commander, U.S. Army Materiel Systems Analysis Activity, Aberdeen Proving Ground, MD 21005
1	ATTN: DRXSY-MP, Director
	Commander, U.S. Army Missile Command, Redstone Arsenal, AL 35809
1	ATTN: Technical Library
1	DRSMI-CS, R. B. Clem
	Commander, U.S. Army Armament Research and Development Command, Dover, NJ 07801
2	ATTN: Technical Library
1	DRDAR-SCM, J. D. Corrie
1	Dr. J. Waldman
	Commander, U.S. Army Tank-Automotive Research and Development Command, Warren, MI 48090
1	ATTN: DRDTA-RKA
2	DRDTA-UL, Technical Library
1	DRDTA-RCK, Dr. J. Chevalier
	Commander, U.S. Army Foreign Science and Technology Center, 220 7th Street, N.E., Charlottesville, VA 22901
1	ATTN: Military Tech, Mr. Marley
	Director, Eustis Directorate, U.S. Army Air Mobility Research and Development Laboratory, Fort Eustis, VA 23604
1	ATTN: DAVDL-E-MOS
1	DAVDL-EU-TAP

No. of Copies	To
	Commander, U.S. Army Aviation Research and Development Command, 4300 Goodfellow Boulevard, St. Louis, MO 63120
1	ATTN: DRDAV-EGX
1	DRDAV-EX, Mr. R. Lewis
1	DRDAV-EQ, Mr. Crawford
1	DRCPM-AAH-TM, Mr. R. Hubbard
	Naval Research Laboratory, Washington, DC 20375
1	ATTN: Dr. J. M. Krafft - Code 5830
1	Code 2627
	Chief of Naval Research, Arlington, VA 22217
1	ATTN: Code 471
	Commander, U.S. Air Force Wright Aeronautical Laboratories, Wright-Patterson Air Force Base, OH 45433
2	ATTN: AFWAL/MLSE, E. Morrissey
1	AFWAL/MLC
1	AFWAL/MLLP, D. M. Forney, Jr.
1	AFWAL/MLBC, Mr. Stanley Schulman
1	AFWAL/MLXE, A. Olevitch
	National Aeronautics and Space Administration, Washington, DC 20546
1	ATTN: Mr. B. G. Achhammer
1	Mr. G. C. Deutsch - Code RW
	Chief of Naval Operations, Washington, DC 20350
1	ATTN: OP-987, Director
	NASA - Ames Research Center, Mail Stop 223-6, Moffett Field, CA 94035
1	ATTN: SC, J. Parker
	Naval Material Command, Washington, DC 20360
1	ATTN: MAT-0331
	Commander, Rock Island Arsenal, Rock Island, IL 61299
1	ATTN: DRSAR-PPV
	Armament Systems, Inc., 712-F North Valley, Anaheim, CA 92801
1	ATTN: J. Musch
	Calspan Corporation, P.O. Box 235, Buffalo, NY 14221
1	ATTN: Library
	IIT Research Institute, 10 West 35th Street, Chicago, IL 60616
1	ATTN: K. McKee
	Sikorsky Aircraft, A Division of United Aircraft Corporation, Main Street, Stratford, CT 06602
1	ATTN: W. G. Degnan

No. of Copies	To
	Teledyne CAE, 1330 Laskey Road, Toledo, OH 43697
1	ATTN: Librarian, M. Dowdell
	Simonds Steel Division, Guterl Special Steel Corporation, Lockport, NY 14094
1	ATTN: Mr. R. Farrington
	FMC Corporation, Ordnance Engineering Division, 1105 Coleman Avenue, San Jose, CA 95108
1	ATTN: Mr. D. R. Fylling
1	Mr. R. Musante
	Lukens Steel Company, Coatesville, PA 19320
1	ATTN: Dr. R. S. Swift
	Republic Steel Corporation, 410 Oberlin Avenue SW, Massillon, OH 44646
1	ATTN: Mr. R. Sweeney
1	Mr. W. H. Brechtel
1	Mr. B. G. Hughes
	United States Steel Corporation, Research Laboratory, Monroeville, PA 15146
1	ATTN: Dr. Hsun Hu
	METTEC, 1805 E. Carnegie Avenue, Santa Ana, CA 92705
1	ATTN: Dr. L. Raymond
	SRI International, 333 Ravenswood Avenue, Menlo Park, CA 94025
1	ATTN: Dr. D. Shockey
	Director, Army Materials and Mechanics Research Center, Watertown, MA 02172
2	ATTN: DRXMR-PL
1	DRXMR-PR
1	DRXMR-FD
1	DRXMR-K
10	DRXMR-MM, Mr. C. Hickey